PLANT HYDRAULICS UNDER CLIMATE CHANGE

EDITED BY: Dongliang Xiong, Daniel Johnson, Amanda A. Cardoso and Joan Laur

PUBLISHED IN: Frontiers in Plant Science

frontiers Research Topics

frontiers

ISSN 1664-8714
ISBN 978-2-88976-656-7
DOI 10.3389/978-2-88976-656-7

About Frontiers

Frontiers is more than just an open-access publisher of scholarly articles: it is a pioneering approach to the world of academia, radically improving the way scholarly research is managed. The grand vision of Frontiers is a world where all people have an equal opportunity to seek, share and generate knowledge. Frontiers provides immediate and permanent online open access to all its publications, but this alone is not enough to realize our grand goals.

Frontiers Journal Series

The Frontiers Journal Series is a multi-tier and interdisciplinary set of open-access, online journals, promising a paradigm shift from the current review, selection and dissemination processes in academic publishing. All Frontiers journals are driven by researchers for researchers; therefore, they constitute a service to the scholarly community. At the same time, the Frontiers Journal Series operates on a revolutionary invention, the tiered publishing system, initially addressing specific communities of scholars, and gradually climbing up to broader public understanding, thus serving the interests of the lay society, too.

Dedication to Quality

Each Frontiers article is a landmark of the highest quality, thanks to genuinely collaborative interactions between authors and review editors, who include some of the world's best academicians. Research must be certified by peers before entering a stream of knowledge that may eventually reach the public - and shape society; therefore, Frontiers only applies the most rigorous and unbiased reviews.
Frontiers revolutionizes research publishing by freely delivering the most outstanding research, evaluated with no bias from both the academic and social point of view. By applying the most advanced information technologies, Frontiers is catapulting scholarly publishing into a new generation.

What are Frontiers Research Topics?

Frontiers Research Topics are very popular trademarks of the Frontiers Journals Series: they are collections of at least ten articles, all centered on a particular subject. With their unique mix of varied contributions from Original Research to Review Articles, Frontiers Research Topics unify the most influential researchers, the latest key findings and historical advances in a hot research area! Find out more on how to host your own Frontiers Research Topic or contribute to one as an author by contacting the Frontiers Editorial Office: frontiersin.org/about/contact

PLANT HYDRAULICS UNDER CLIMATE CHANGE

Topic Editors:
Dongliang Xiong, Huazhong Agricultural University, China
Daniel Johnson, University of Georgia, United States
Amanda A. Cardoso, North Carolina State University, United States
Joan Laur, Montreal Botanical Garden, Canada

Citation: Xiong, D., Johnson, D., Cardoso, A. A., Laur, J., eds. (2022). Plant Hydraulics Under Climate Change. Lausanne: Frontiers Media SA.
doi: 10.3389/978-2-88976-656-7

Table of Contents

frontiers in Plant Science

ORIGINAL RESEARCH
published: 03 September 2021
doi: 10.3389/fpls.2021.715127

Leaf Shedding and Non-Stomatal Limitations of Photosynthesis Mitigate Hydraulic Conductance Losses in Scots Pine Saplings During Severe Drought Stress

Daniel Nadal-Sala[1], Rüdiger Grote[1], Benjamin Birami[1,2], Timo Knüver[1,3], Romy Rehschuh[1], Selina Schwarz[1] and Nadine K. Ruehr[1]*

[1] Karlsruhe Institute of Technology, Institute of Meteorology and Climate Research - Atmospheric Environmental Research (IMK-IFU), Garmisch-Partenkirchen, Germany, [2] University of Bayreuth, Chair of Plant Ecology, Bayreuth, Germany, [3] Department of Botany, University of Innsbruck, Innsbruck, Austria

OPEN ACCESS

Edited by:
Amanda A. Cardoso, Federal University of Alfenas, Brazil

Reviewed by:
Samuel Cordeiro Vitor Martins, Universidade Federal de Viçosa, Brazil
Virginia Hernandez-Santana, Institute of Natural Resources and Agrobiology of Seville (CSIC), Spain
Alexandria Pivovaroff, Pacific Northwest National Laboratory (DOE), United States

***Correspondence:**
Daniel Nadal-Sala
d.nadal@kit.edu

Specialty section:
This article was submitted to Plant Physiology, a section of the journal Frontiers in Plant Science

Received: *26 May 2021*
Accepted: *08 July 2021*
Published: *03 September 2021*

Citation:
Nadal-Sala D, Grote R, Birami B, Knüver T, Rehschuh R, Schwarz S and Ruehr NK (2021) Leaf Shedding and Non-Stomatal Limitations of Photosynthesis Mitigate Hydraulic Conductance Losses in Scots Pine Saplings During Severe Drought Stress. Front. Plant Sci. 12:715127. doi: 10.3389/fpls.2021.715127

During drought, trees reduce water loss and hydraulic failure by closing their stomata, which also limits photosynthesis. Under severe drought stress, other acclimation mechanisms are trigged to further reduce transpiration to prevent irreversible conductance loss. Here, we investigate two of them: the reversible impacts on the photosynthetic apparatus, lumped as non-stomatal limitations (NSL) of photosynthesis, and the irreversible effect of premature leaf shedding. We integrate NSL and leaf shedding with a state-of-the-art tree hydraulic simulation model (SOX+) and parameterize them with example field measurements to demonstrate the stress-mitigating impact of these processes. We measured xylem vulnerability, transpiration, and leaf litter fall dynamics in *Pinus sylvestris* (L.) saplings grown for 54 days under severe dry-down. The observations showed that, once transpiration stopped, the rate of leaf shedding strongly increased until about 30% of leaf area was lost on average. We trained the SOX+ model with the observations and simulated changes in root-to-canopy conductance with and without including NSL and leaf shedding. Accounting for NSL improved model representation of transpiration, while model projections about root-to-canopy conductance loss were reduced by an overall 6%. Together, NSL and observed leaf shedding reduced projected losses in conductance by about 13%. In summary, the results highlight the importance of other than purely stomatal conductance-driven adjustments of drought resistance in Scots pine. Accounting for acclimation responses to drought, such as morphological (leaf shedding) and physiological (NSL) adjustments, has the potential to improve tree hydraulic simulation models, particularly when applied in predicting drought-induced tree mortality.

Keywords: leaf shedding, non-stomatal limitations of photosynthesis, Scots pine, tree hydraulic simulation models, xylem vulnerability

INTRODUCTION

There is increasing evidence that hydraulic failure is a main trigger of tree death in response to drought and hot drought (Allen et al., 2015; McDowell et al., 2018; Brodribb et al., 2020). While trees are well-adapted to respond to seasonal and short-term increases in soil and atmospheric drought, extreme climatic conditions, e.g., anomalously high summer temperatures coupled with low soil water availability, as experienced, for instance, in central Europe during the summer of 2018 (Hari et al., 2020; Schuldt et al., 2020), can cause substantial hot drought-induced damage. Increasing soil and atmospheric drought result in increasing tree internal water column tensions. As such tensions rise, air bubbles, i.e., emboli, can form in the xylem, reducing xylem hydraulic conductance (Tyree and Ewers, 1991). Reduced xylem conductance limits water transport upward, from soil to the leaves, which may lead to dehydration of cambium and apical meristems, canopy dieback, and ultimately tree death (e.g., Carnicer et al., 2011; Anderegg et al., 2012; Allen et al., 2015; Choat et al., 2018; Reich et al., 2018; Hesse et al., 2019).

It is well-established that stomatal closure is the first and foremost mechanism that limits water loss and buildup of excessive xylem tension (Hall and Kaufmann, 1975; Monteith, 1995; Choat et al., 2018). This comes at a cost of reduced leaf permeability to CO_2, which limits C assimilation (Martorell et al., 2014; Reich et al., 2018). Much research has focused on modeling stomatal conductance (gs) to water deficit (Damour et al., 2010; Mencuccini et al., 2019), as well as tree internal water balance after stomatal closure (e.g., Martin-St. Paul et al., 2017; Cochard et al., 2021). To date, many approaches exist that combine gs responses to decreasing soil water content (SWC) and increasing vapor pressure deficit (VPD). The approaches range from empirical relationships (e.g., Leuning, 1995), to mechanistical descriptions based on optimality theory such as maximizing C gain per unit of transpiration (e.g., Medlyn et al., 2011), maximizing transpiration while reducing conductivity loss (Sperry and Love, 2015), or maximizing C gain while minimizing loss in hydraulic conductivity (e.g., Sperry et al., 2017; Eller et al., 2018; 2020). The success of these models has been mixed, leading to a good representation of broad monthly and annual transpiration and productivity patterns but often failing to capture subtler responses arising when drought stress intensifies (e.g., Drake et al., 2017; Yang et al., 2019; De Kauwe et al., 2020; Bassiouni and Vico, 2021; Mu et al., 2021; Nadal-Sala et al., 2021). Hence, challenges to model tree drought responses and mortality persists albeit increasing developments of optimization-based tree hydraulic models over the recent years. Therefore, further model improvements regarding tree acclimation responses to drought beyond stomatal closure have been recommended (e.g., Keenan et al., 2010; Wolfe et al., 2016; Martin-St. Paul et al., 2017; Sperry et al., 2019; Gourlez de la Motte et al., 2020). To do so, controlled experiments that address specific tree physiological responses to drought provide an opportunity to improve and evaluate the performance of tree hydraulic models (e.g., Hartig et al., 2012; Medlyn et al., 2015; Dietze et al., 2018).

Under sustained drought, stomatal regulation in response to CO_2 demand on the one hand and evaporation demand on the other may not be enough to mitigate hydraulic tension and prevent embolism formation in the xylem. Other responses are, thus, often triggered to reduce water loss, such as metabolic changes or increased internal resistance that then feedback to stomatal conductance, as well as accelerated senescence of various tissues. In particular, many studies report a slowdown of the photosynthetic activity during drought (e.g., Xu and Baldocchi, 2003; Keenan et al., 2010; Yang et al., 2019; Gourlez de la Motte et al., 2020). Such slowdown may have different causes such as increased mesophyll resistance (Flexas et al., 2007, 2012; Evans, 2021), drought-related enzymatic down-regulation (e.g., Flexas et al., 2004; Niinemets and Sack, 2006; Niinemets et al., 2006; Sugiura et al., 2020), and/or decreasing carbon demand (Fatichi et al., 2014). Since all these mechanisms lead to a reduction in water loss, here, we consider them in a lumped manner as non-stomatal limitations of photosynthesis (NSL), thereby enabling the consideration of this additional response process in models that are simulating stand productivity and transpiration in dependence on water availability (Zhou et al., 2013; Drake et al., 2017; Yang et al., 2019).

Another key mechanism of how trees can respond to drought is reducing their leaf area (e.g., Munné-Bosch and Alegre, 2004; Sala et al., 2010; Martin-St. Paul et al., 2013; Wolfe et al., 2016; Hochberg et al., 2017; Li et al., 2020; Schuldt et al., 2020). Drought-induced leaf senescence reduces total tree transpiration, at the expense of growth at mid-term, as rebuilding canopy structure requires extra C investment, either from non-structural carbohydrate reserves or from the assimilation of the remaining or newly grown leaves once drought stress has been released (Yan et al., 2017; Ruehr et al., 2019). Additionally, shedding leaves without full nutrient resorption imply net nutrient losses (Marchin et al., 2010; Chen et al., 2015), which may further limit photosynthesis post-drought with consequences for tree performance in the long term. Leaf shedding tends to occur after stomata closure; hence, it mainly reduces marginal loss in water *via* residual cuticular conductance and incomplete stomatal closure (e.g., Martin-St. Paul et al., 2017; Cardoso et al., 2020; Li et al., 2020). Under sustained drought, such water loss may be critical for tree survival (e.g., Blackman et al., 2016, 2019), especially considering that residual cuticular conductance increases with temperature (Schuster et al., 2016), leading to faster dehydration of plants particularly during heat waves. While leaf shedding, in response to drought, is routine in drought-deciduous trees (e.g., Ichie et al., 2004; Pineda-García et al., 2013; Ruehr et al., 2016), it can be rather seen as an emergency response in temperate conifers, with profound consequences for drought recovery.

Here, we aim to quantify the importance of NSL and leaf shedding mechanisms regarding hydraulic safety. To do so, we measured hydraulic vulnerability, and transpiration and leaf shedding dynamics in potted *P. sylvestris* L. saplings exposed to 2-month severe dry-down. Then, we trained a big-leaf canopy gas exchange simulation model based on the optimization of stomatal conductance as xylem tension increases (SOX model, Eller et al., 2018, 2020). The SOX model assumes that trees regulate stomatal conductance to maximize C uptake while minimizing loss in soil-to-root hydraulic conductance. Once the

model was trained, we evaluated the importance of NSL and leaf shedding for hydraulic regulation. The initial hypotheses were the following: (1) including non-stomatal limitations of photosynthesis will improve the representation of transpiration during drought; (2) seasonal leaf shedding in pine trees is coordinated with stomata closure to reduce dehydration, and (3) according to the "leaf fuse" hypothesis (e.g., Hochberg et al., 2017) leaf shedding will mitigate mid-term losses in hydraulic conductance.

MATERIALS AND METHODS

Experimental Setup

Potted *P sylvestris* L. saplings were grown in Garmisch-Partenkirchen, Germany (708 m above sea level, 47°28′32.9″N, 11°3′44.2″E). Three-year-old Scots pine saplings were purchased from a local tree nursery in 2018 and planted in individual pots (120 l, 55 cm in diameter, 70 cm in height; Brute, Rubbermaid, Atlanta, GA, United States) in a 6:3:1 mixture of potting substrate (No. 170, Klasmann-Deilmann, Geeste, Germany), perlite (Perligran Premium, Knauf Performance Materials GmbH, Dortmund, Germany), and quartz sand (3–6 and 0.1–0.3 mm). Slow-release fertilizer (100 g, Osmocote® Exact Standard 5-6M 15-9-12+2MgO+TE, ICL Specialty Fertilizers Benelux, The Netherlands) was added to the mixture and supplemented by liquid fertilizer (Manna® Wuxal Super; Wilhelm HaugGmbh, Ammerbuch, Germany). From May to October 2019, the saplings were kept inside the adjacent greenhouse and exposed to mild soil water limitation with air temperature ranging between 10 and 35°C, to prime the trees for the upcoming experiment. From October 2019 to July 2020, the saplings were again grown outside and irrigated once a week from May 2020 onwards. After leaf elongation was finished (mid of July), the then 5-year-old saplings ($n = 16$) were transferred to the greenhouse once more and irrigated to field capacity (SWC ∼0.35 m^3 m^{-3}) before the drought experiment was started. To minimize soil evaporation, the top of the soil was covered with an opaque plastic sheet, which was periodically ventilated.

The greenhouse is equipped with special UV-transmissive glass, and incoming light was supplemented with plant growth lamps (T-agro 400 W; Philips, Hamburg, Germany). Air temperature and air humidity were computer-regulated (CC600, RAM Regel- und Messtechnische Apparate GmbH, Herrsching, Germany). Environmental conditions at canopy height such as photosynthetic active radiation (PQS 1, Kipp&Zonen, Delft, The Netherlands), air temperature, and relative humidity (CS215, Campbell Scientific Inc., Logan, UT, United States) were monitored and logged at 10-min intervals (CR1000; Campbell Scientific Inc., Logan, UT, United States). The environmental conditions during the experiment are shown in **Figure 1**.

Soil Water Content and Transpiration

We continuously measured soil water content (SWC) and sap flow in six randomly selected saplings. Measurements started on DOY 206, but the first week was excluded from this analysis because of plant acclimation to the new conditions, and sensor malfunction and re-calibration (data not shown). Therefore, valid measurements started on DOY 212. Volumetric SWC was monitored at 0–10 c and 40–50 cm depth (10HS; Decagon Devices Inc., Pullman, WA, United States, **Supplementary Figure 1**) to cover the entire rooting area. To estimate the water available for each tree, SWC data from the two depths was averaged. Each SWC sensor was pre-calibrated to the potting medium following the recommendation of the manufacturer. Stem sap flow was measured using the heat-balance method (EMS 62, EMS, Brno, Czech Republic). Sap flow sensors were installed in the upper part of the canopy (height ∼1–1.5 m) as the cylindrical build does not support stem diameters >2 cm. The sensors were shielded with aluminum bubble foil to minimize error due to temperature fluctuations. Sap flow measurements were stored in 30-min intervals. Daily whole-tree transpiration was calculated by assuming that transpiration per unit of leaf area (see section Tree Biomass Compartment Measurement) was equal above and below the sensor, as in a homogeneously coupled non-shadowed canopy we expected the environmental drivers to be homogeneous for the leaves above and below. Therefore, transpiration was calculated as the sum of the measured sap flow plus the sap flow needed to supply the transpiration of the leaves below the sensor (Equation 1)

$$Tr = J*(1 + \frac{LA_{below}}{LA_{above}}) \quad (1)$$

where Tr is the daily whole-tree transpiration (in kg day^{-1} $tree^{-1}$), J is the daily sap flow (in kg day^{-1} $tree^{-1}$), and LA_{below}/LA_{above} is the proportion between the leaf area below the sensor in relation to the leaf area above the sensor (in m^{-2} $tree^{-1}$).

Tree Biomass Compartment Measurement

Loss in leaf biomass was assessed once a week as follows. We collected and carefully removed already brown needles from the branches of each individual tree. Leaves were oven-dried at 60°C for 48 h, and the dry weight was measured. Total tree biomass was determined at the end of the experiment and separated into needles, wood, and roots (**Supplementary Table 1**). We separately assessed leaf biomass above and below the sap flow sensor in order to derive total tree transpiration (see section Soil Water Content and Transpiration). As needle elongation was finished before the experiment started, initial leaf biomass per tree was considered as the sum of the remaining needles at the end of the experiment plus leaf biomass shed during the experiment, assuming a constant above-sensor leaf biomass/below-sensor biomass ratio. In order to obtain the actual daily leaf biomass time series, we linearly interpolated cumulative leaf shedding between measurement campaigns and subtracted it from the initial leaf biomass. For each tree, conversion from leaf biomass to leaf area was done based on specific leaf area (SLA, cm^2 g^{-1}), obtained by measuring the width and the length of a representative sub-sample per tree (in total $n = 18$). No significant differences were detected between monitored and not-monitored individuals regarding SLA and tree biomass in different compartments (see **Supplementary Table 1**).

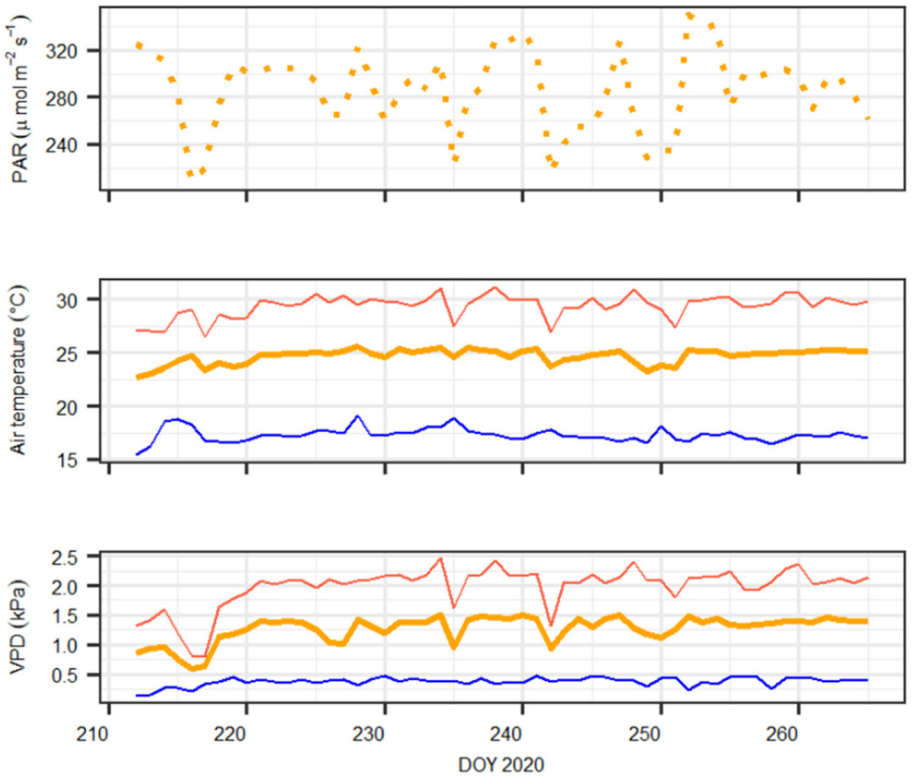

FIGURE 1 | Daily meteorological conditions during the experiment. Upper panel: daylight average photosynthetic active radiation (PAR, in µmol m^{-2} s^{-1}); middle panel: maximum (red), minimum (blue), and average (orange) air temperature (in °C); bottom panel: maximum (red), minimum (blue), and average (orange) atmospheric vapor pressure deficit (VPD, in kPa). Note that on DOY 216–217, vapor pressure deficit (VPD) and temperature conditions were lowest because of a cold weather front that was not compensated by heating the greenhouse.

Xylem Loss in Hydraulic Conductance

We measured xylem vulnerability of branches using the Cavitron technique (Cochard, 2002). Briefly, the centrifugal force of the Cavitron increases the negative pressure in the stem while the hydraulic conductivity and the loss thereof is measured concurrently. At the beginning of the experiment, we sampled the terminal part of the lowest branch (∼33 cm long) in five randomly selected non-monitored trees. Branches were tightly wrapped in cling film and additionally sealed in plastic bags before being transported to Innsbruck where they were kept at 4°C for 2 days. Samples were prepared for the Cavitron as follows: first, side twigs and needles were removed, and branches were re-cut under water several times to relax xylem tension, until a sample length of ∼28 cm was reached and debarked at both ends (∼5 cm) to avoid clogging of tracheids by resin. The cut and debarked ends were cleaned with a sharp razor blade. To remove native embolisms *via* vacuum infiltration, submerged samples were subjected to a low-pressure water flow (0.08 MPa) for 30 min with distilled, filtered (0.22 µm), and degassed water containing 0.005% (v/v) Micropur. Then, branch segments were fixed into a custom-made, honeycomb 28-cm rotor and positioned in a Sorvall RC-5 centrifuge (Thermo Fisher Scientific, Waltham, MA, United States). Distilled, filtered (0.22-µm pore size), and degassed water with 0.005% (v/v) Micropur water purifier (Katadyn Products, Wallisellen, Switzerland) preventing microbial growth, was used for the measurements. Percent loss of conductivity (PLC, in %) measurements started at a force of about −0.5 MPa, which was gradually increased until minimum xylem hydraulic conductivity (K_{xylem}, mol m^{-1} s^{-1} MPa^{-1}) was reached. PLC was recorded at about −0.5 MPa pressure increase steps. We assumed that losses in conductivity reflect losses in xylem conductance (k_{xylem}, in mol m^{-2} s^{-1} MPa^{-1}). In order to model normalized k_{xylem} (k_{norm}, 0–1) responses to xylem water potential increase (Ψ_{xylem}), we evaluated three different response functions: a Weibull function (WB), a sigmoid exponential (SE) function, and the original SOX model function (SOXf)

$$k_{norm,WB} = 1 - (1 - e^{-(\frac{\Psi_{xylem}}{\Psi_{ref}})^{A_{coef}}}) \quad (2)$$

$$k_{norm,SE} = 1 - \frac{1}{(1 + (\exp^{A_{coef}\ (\Psi_{xylem} - \Psi_{50})})} \quad (3)$$

$$k_{norm,SOXf} = (\frac{1}{1 + \left(\frac{\Psi_{xylem}}{\Psi_{50}}\right)^{A_{coef}}}) \quad (4)$$

where $k_{norm,WB}$, $k_{norm,SE}$, and $k_{norm,SOXf}$ are the predicted normalized k_{xylem} of theWB, SE, and SOXf formulations, respectively. Ψ_{xylem} (MPa) is the xylem water potential. In WB,

Ψ_{ref} is the reference xylem water potential (MPa) when $k_{norm,WB}$ is equal to $\exp^{(-1)}$ ~0.37. In SE and SOXf, Ψ_{50} is the xylem water potential at which $k_{norm} = 0.5$. In all the three formulations, A_{coef} is a unit-less shaping parameter. See section Xylem Vulnerability for details about the fitting procedure.

Photosynthesis A_n/C_i Curves

In order to provide estimates for photosynthetic parameters in the FvB model, A_n/C_i curves were measured on trees grown in the greenhouse in June, 2019. Measurements were made on sun-exposed needles, using a portable infrared gas analyzer system (LI-6800, Li-Cor, Inc., Lincoln, NE, United States) with a 6-cm^2 leaf chamber. The measurements were taken at saturating PAR (PAR $\geq$ 1,200 µmol $m^{-2}s^{-1}$). Assimilation in relation to $[CO_2]$ in the intercellular space (A_n/C_i) curves was generated by increasing atmospheric CO_2 concentration (C_a) inside the chamber in five steps, starting at ~400 µmol mol^{-1} and then progressively increasing C_a by ~200 µmol mol^{-1} each step, up to a maximum of ~1,200 µmol mol^{-1}. Leaf temperature (Tleaf, in °C) and other standard variables were also measured. These measurements were taken under prevailing leaf temperature (~25°C) and humidity conditions within the greenhouse. A total of 19 A_n/C_i curves were measured this way. We used these data to determine carboxylation velocity limited by rubisco activity at 25°C ($V_{cmax,25}$ in µmol m^{-2} s^{-1}) and the carboxylation velocity limited by RuBP regeneration rate ($J_{max,25}$ in µmol m^{-2} s^{-1}).

Modeling Approach

The tree hydraulic modeling approach is based on the process-based model SOX (Eller et al., 2018, 2020). We have modified the photosynthetic module, added the possibility to address non-stomatal-limitations of photosynthesis (see below), and included a third conductance node (i.e., the soil-to-root hydraulic conductance, **Figure 2**). In the following, we refer to the modified model version as the SOX+ model. Briefly, the model operates on the assumption that plants regulate stomatal conductance to maximize photosynthesis, while minimizing the loss in root-to-canopy water conductance. The model is relatively simple in terms of parameterization and computational power required and, hence, applicable for a wide range of ecosystem models. The environmental drivers required as an input to run the model are air temperature, PAR, soil water content, and air relative humidity. Here, we describe the main processes involved such as the modification for SOX+, while a more in-depth description of the original SOX model and the analytical solutions for its equations can be found in Eller et al. (2020).

Water flow within the tree is described as a three-step pathway with three different hydraulic conductance nodes: the soil-to-root hydraulic conductance (k_{sr},mol m^{-2} $s^{-1}$$MPa^{-1}$), the root-to-canopy hydraulic conductance (k_{rc}, mol m^{-2} $s^{-1}$$MPa^{-1}$), and the leaf-atmosphere hydraulic conductance (g_s, mol m^{-2} s^{-1}). The model assumes a steady state of tree water status, i.e., it does not account for tree capacitance. The soil-to-root conductance k_{sr} is calculated following Campbell (1985):

$$k_{sr} = k_{sr,\max} * \left(\frac{SWC}{SWC_{FC}}\right)^{\left(2+\frac{3}{b}\right)} \quad (5)$$

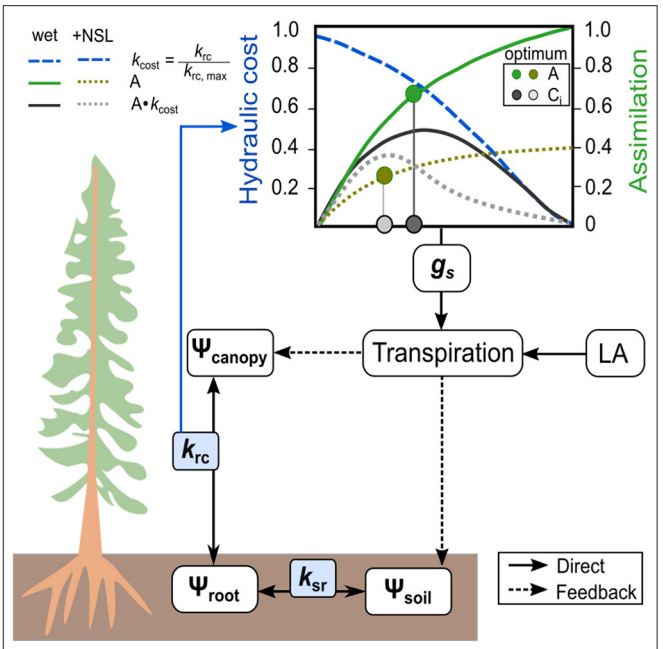

FIGURE 2 | Scheme of the SOX+ model. Soil-to-atmosphere is described as a hydraulic pathway considering three nodes: hydraulic flow from soil to the roots, mediated by soil-to-root conductance (k_{sr}), hydraulic flow from roots to the canopy, mediated by root-to-canopy conductance (k_{rc}), and hydraulic flow from the canopy to the atmosphere, mediated by stomatal conductance (gs). The optimum gs is determined by considering the photosynthetic gain (A) multiplied by the hydraulic cost function (k_{cost}), which describes the decreases in k_{rc} as Ψ_{canopy} becomes more negative. Transpiration is calculated at the tree level by multiplying gs and leaf area, and it has a direct effect on canopy water potential, an indirect effect on soil water content, and therefore on Ψ_{soil}. Non-stomatal limitations of photosynthesis (NSL) decrease optimum stomatal conductance because of limiting A when Ψ_{canopy} declines below a predefined threshold.

where $k_{sr,max}$ is the $k_{sr}$when SWC is at field capacity, SWC is the volumetric soil water content (m^3 m^{-3}), SWC_{FC} is the volumetric SWC at field capacity (m^3 m^{-3}), and b is an empirical coefficient depending on average soil particle size characteristic, calculated as described in Campbell (1985). Using k_{sr} on the one hand, and transpiration per unit of leaf area (E, mol m^{-2} s^{-1}) on the other, the model calculates the water potential within the roots ($\Psi_{root,t}$) based on Darcy's law at hourly time-steps as

$$\Psi_{root,t} = \Psi_{soil,t} - \frac{E_{(t-1)}}{k_{sr(t-1)}} \quad (6)$$

where $\Psi_{soil,t}$ is the soil water potential at time step t (in MPa), calculated according to Campbell (1985) from soil physical properties. Canopy water potential ($\Psi_{canopy,t}$) is closely linked to root water potential, which in turn strongly depends on soil water availability. We assume a simple gravimetrical decline with height, neglecting a potential influence of stored plant water:

$$\Psi_{canopy,t} = \Psi_{root,t} - \frac{E_{(t-1)}}{k_{rc(t-1)}} - h\rho g * 10^{-6} \quad (7)$$

where $k_{rc(t-1)}$ is the hydraulic conductance from the roots to the canopy at t – 1 (mol m^{-2} $s^{-1}MPa^{-1}$) based on the canopy water potential at that time. Therefore, we assume that $\Psi_{canopy,m}$ equals Ψ_{xylem} and that $k_{rc}(\Psi_{canopy,m})$ follows the shape of $k_{norm}(\Psi_{xylem})$, multiplied by the maximum root-to-canopy hydraulic conductance ($k_{rc,max}$, in mol $m^{-2}s^{-1}$ Mpa^{-1}). For representing $k_{norm}(\Psi_{xylem})$, we selected Equation 2, as we found it represented measured data best (see section Leaf Shedding Speed Increased Concurrently With Transpiration Stop). Further, h is the plant height (in m), ρ is the density of water (997 kg m^{-3}), and g is gravity (9.8 m s^{-2}). The 10^{-6} multiplier transforms Pa to MPa. For each day, we calculated pre-dawn canopy water potential ($\Psi_{canopy,PD}$, MPa) using equation 7 but assuming $E_{(t-1)} \approx 0$, which results in $\Psi_{canopy,PD}$ being dependent on Ψ_{soil} minus the gravimetric component. As in the previous SOX model iterations (Eller et al., 2018, 2020), SOX+ represents the water potential in the xylem with a dampened canopy water potential ($\Psi_{canopy,m}$, MPa), calculated as $\frac{\Psi_{canopy,t}+\Psi_{canopy,PD}}{2}$ for all the hourly calculations to account for the gradual decline in water potential along the plant hydraulic pathway. Such assumption greatly simplifies the calculation of water potential drop within the tree (e.g., Sperry and Love, 2015; Sperry et al., 2017).

The core assumption in SOX+ is that stomatal conductance (gs, mol m^{-2} s^{-1}) is regulated to maximize photosynthetic net assimilation (A_n, μmol m^{-2} s^{-1}) while minimizing the decrease in xylem hydraulic conductance, represented by root-to-canopy conductance (k_{rc}) here. Eller et al. (2020) solved for gs using an analytical approximation based on the partial derivatives of A_n with respect to CO_2 concentration in the chloroplast (C_i, μmol mol^{-1}) and k_{rc} with respect to $\Psi_{canopy,m}$.

$$gs_{SOX} = 0.5\frac{\partial A_n}{\partial C_i}\left(\sqrt{\left(\frac{4\xi}{\partial A_n/\partial C_i}+1\right)}-1\right) \quad (8)$$

where $\delta A_n/\delta C_i$ represents the gain in net photosynthesis per unit of C_i increase, i.e., the positive effect of opening the stomata on A_n, solved numerically as in Eller et al. (2020), while ξ represents the cost in terms of loss in hydraulic conductance of opening the stomata as canopy water potential declines and/or vapor pressure deficit increases (Equation 9). Specifically, the lower the ξ, the lower the stomatal conductance projected by SOX+. If estimates of gs_{SOX} are lower than a predefined minimum leaf conductance, representing leaf leakiness once stomata are fully closed (g_{min}, in mmol m^{-2} s^{-1}; here 2 mmol m^{-2} s^{-1}), we considered gs equal to g_{min}, otherwise gs = gs_{SOX}, following Duursma et al. (2019). Note that in the approach, g_{min} integrates leaf water losses both because of imperfect stomatal closure and leaf cuticular conductance, considering a well-coupled canopy and low wind speed conditions (e.g., Cochard et al., 2021).

$$\xi = \frac{2}{\frac{1}{k_{norm,rc}} * \frac{\delta k_{norm,rc}}{\delta \Psi_{canopy,m}} * rplant_{\min,\ \Psi} * 1.6 * VPD} \quad (9)$$

$$rplant_{\min,\Psi} = \frac{rplant_{\min}}{k_{norm,r,c}(\Psi_{canopy,m})} \quad (10)$$

where VPD is the vapor pressure deficit at leaf level (kPa) and $\frac{\delta k_{norm,rc}}{\delta \Psi_{canopy,m}}$ represents the decrease in conductance as mean canopy water potential increases, solved numerically as described in Eller et al. (2020). $rplant_{,min}$ is the minimum plant resistance (in MPa m^2 s mol^{-2}), a parameter used to describe the increase in whole tree resistance with decreasing $\Psi_{canopy,m}$.

Net assimilation (A_n) is calculated according to the Farquhar, von Caemmerer, and Bell photosynthesis model (FvCB, Farquhar et al., 1980; De Pury and Farquhar, 1997). Briefly, the FvCB assumes that A_n is limited by either rubisco carboxylation velocity ($_{Avc}$) or RuBP regeneration (A_j), and is calculated considering dark respiration (R_d). All of these processes depend on leaf temperature (Farquhar et al., 1980; Harley et al., 1992; Bernacchi et al., 2001), which we assume to equal air temperature.

$$A_n = argmin\left(A_{vc}, A_j\right) - R_d \quad (11)$$

As novelty compared with the original SOX model, SOX+ accounts for non-stomatal limitations (NSL) in photosynthesis, as have been repeatedly found important to properly represent reductions of transpiration and productivity under drought stress (e.g., Keenan et al., 2010; Duursma and Medlyn, 2012; Drake et al., 2017; Yang et al., 2019, Gourlez de la Motte et al., 2020). NSL assume that additional constrains on A_n arise with decreasing Ψ_{canopy} from mesophyll conductance reductions, biochemical limitations, or other indirect effects (e.g., Fatichi et al., 2014). Here, note that in SOX+ and according to Equation 8, NSL will result in a reduction in $\delta An/\delta C_i$, thus also indirectly leading to reduced gs_{SOX}. In SOX+, declining $\Psi_{canopy,m}$[$f(\Psi_{canopy,m})$, unit-less, its value ranging between 1 (no limitation) and 0 (complete limitation)] is calculated based on Tuzet et al. (2003) as follows:

$$f\left(\Psi_{canopy,m}\right) = \left(\frac{1+\exp^{\left(a^*_{Tuz}\Psi_{ref,Tuz}\right)}}{1+\exp^{\left[a^*_{Tuz}\left(\Psi_{ref,Tuz}-\Psi_{canopy,m}\right)\right]}}\right) \quad (12)$$

where $\Psi_{ref,Tuz}$ and a_{Tuz} are two empirically determined parameters, $\Psi_{ref,Tuz}$ being a reference canopy water potential (in MPa), as defined in Tuzet et al. (2003), and a_{Tuz} being a unit-less coefficient that determines the sensitivity of the sigmoid curve to $\Psi_{canopy,m}$reductions. After simulating f ($\Psi_{canopy,m}$), apparent V_{cmax} and apparent J_{max} are computed as

$$X_{apparent} = X^*_{\max,25} f\left(\Psi_{canopy,m}\right) \quad (13)$$

where the $X_{apparent}$ (μmol m^{-2} s^{-1}) is the apparent kinetic parameter value for either V_{cmax} or J_{max} for a $X_{max,25}$ (μmol m^{-2} s^{-1}) reference value (see **Table 2**) multiplied by the NSL (Equation 12), represented by the unit-less stress term f ($\Psi_{canopy,m}$). These new kinetic parameters accounting for direct impacts of Ψ_{canopy} decline on photosynthesis are then used to calculate A_{vc} and A_j in Equation 11.

Because of the feedback mechanism between A_n and gs, SOX+ solves both processes iteratively for the equilibrium C_i.

Model Parameterization and Calibration

Photosynthesis in the FvCB Model

Temperature dependencies of rubisco kinetics were obtained from Bernacchi et al. (2001). Temperature dependencies for

TABLE 1 | Fixed, not previously calibrated parameters used in the SOX+ model.

Parameter	Units	Value	Source
EaV_{cmax}	J mol^{-1}	52,750	Wang et al. (1996)
EdV_{cmax}	J mol^{-1}	202,600	Wang et al. (1996)
SV_{cmax}	J mol^{-1} K^{-1}	669	Wang et al. (1996)
EaJ_{max}	J mol^{-1}	61,750	Wang et al. (1996)
EdJ_{max}	J mol^{-1}	185,600	Wang et al. (1996)
SJ_{max}	J mol^{-1}K^{-1}	621	Wang et al. (1996)
Rd_{25}	μmol m^{-2} s^{-1}	0.5	Calculated as $V_{cmax,25}$ * 0.015
Q_{10}	unitless	2	This study
Γ^*_{25}	μmol mol^{-1}	42.2	Bernacchi et al. (2001)
$Ea\Gamma^*$	J mol^{-1}	37,830	Bernacchi et al. (2001)
$K_{c,25}$	μmol mol^{-1}	404	Bernacchi et al. (2001)
EaK_c	J mol^{-1}	84,200	Bernacchi et al. (2001)
$K_{O,25}$	μmol mol^{-1}	278,000	Bernacchi et al. (2001)
EaK_O	J mol^{-1}	15,200	Bernacchi et al. (2001)
g_{min}	mmol m^{-2} s^{-1}	2	This study
LA	m^{-2}	1.35	This study
Height	M	2	This study
SoilDensity	g cm^{-3}	1.3	This study
FieldCapacity	cm^{-3}cm^{-3}	0.35	This study

EaV_{cmax}, EdV_{cmax}, and SV_{cmax} are the activation energy, deactivation energy, and entropy for the V_{cmax} temperature response, respectively. EaJ_{max}, EdJ_{max}, and SJ_{max} are the activation energy, deactivation energy, and entropy for the J_{max} temperature response. Rd_{25} is the dark respiration at 25°C, calculated from $V_{cmax,25}$ according to Collatz et al. (1991), and Q_{10} is the increase rate of R_d as temperature increases. Γ^*_{25} and $Ea\Gamma^*$ are the CO_2 compensation point at 25°C and the activation energy of the compensation point. $K_{O,25}$ and $K_{c,25}$ are the kinetic constants of oxidase and carboxylase activity for rubisco at 25°C, respectively. EaK_O and EaK_c are the energy activation for the oxidase and carboxylase activity of rubisco, respectively. g_{min} is the minimum leaf conductance, which integrates both residual stomatal conductance because of imperfect stomatal closure and leaf cuticular conductance. LA is the average tree leaf area on day 1 of the experiment. Height is the average tree height. Soil density and field capacity are the dry soil weight per unit of soil volume and the volumetric soil water content at saturation, respectively. Given are parameter names, units, values, and reference.

the FvCB model were obtained for *P. sylvestris* from Wang et al. (1996), see **Table 1** for the parameter values. To obtain the carboxylation velocity limited by rubisco activity at 25°C ($V_{cmax,25}$ in μmol m^{-2} s^{-1}) and the carboxylation velocity limited by RuBP regeneration rate ($J_{max,25}$ in μmol m^{-2} s^{-1}), we used measured A_n/C_i curves under no drought stress to calibrate the FvCB model for each curve individually, using the package "DEOptim" (Mullen et al., 2011). The algorithm obtains the most likely parameters providing the observations, a parameter distribution and a likelihood function, by performing differential evolution optimization (see below for more details). We used the default three-chain settings to establish non-informative priors within the biological meaningful range (**Table 2**). The objective function for optimization was a Gaussian log-likelihood distribution. This provided a $V_{cmax,25}$ and a $J_{max,k25}$ value for each curve. To summarize the average photosynthesis kinetics of the *P. sylvestris* population, we used the median calibrated values of $V_{cmax,25}$ and $J_{max,25}$ to run the SOX+ model (**Table 2**). We calculated the dark respiration rate at 25°C ($R_{d,25}$ in μmol m^{-2} s^{-1}) as $R_{d,25} = 0.015^* V_{cmax,25}$, according to Collatz et al. (1991). After FvCB model optimization, $A_n$estimates were very close to observations [**Figure 3**, slope not significantly different than 1($p > 0.1$) and intercept not significantly different than zero ($p > 0.1$)]. The median $J_{max,25}$ to $V_{cmax,25}$ ratio was ∼1.7, with $V_{cmax,25}$ values of 33.3[27.7–38.9] μmol m^{-2} s^{-1} (median [95% CI]), and $J_{max,25}$ values of 51[45.1–56.8] μmol m^{-2} s^{-1} (**Table 2**). To run the SOX+ model, we used the median values of $V_{cmax,25}$ and $J_{max,25}$.

Xylem Vulnerability

In order to decide for an appropriate response function and define the respective parameters describing $k_{xylem}(\Psi_{xylem})$, we first inversely calibrated each of the proposed equations (Equations 2–4) with the $k_{xylem}(\Psi_{xylem})$ observations. Independent of the equation we proceeded as follows: we calibrated one vulnerability curve per sample using each of the three equations, using broadly set but biologically meaningful priors (**Table 2**) and a Gaussian likelihood function. The sampler used was a differential evolution Markov Monte-Carlo Chain (MCMC) with memory and a snooker update (DEzs, terBraak and Vrugt, 2008), implemented in the "BayesianTools" R package (Hartig et al., 2017). We ran each calibration for 50 k iterations, and then the first 30 k where discarded as a burn-in. For initial trials, we ran tree calibrations for each vulnerability curve and addressed between-chain convergence *via* Gelman-Rubin convergence diagnosis (Gelman and Rubin, 1992). As running the model this way is time-consuming and the initial trials provided very low Gelman–Rubin scores for all the three equations (G-R < 1.02, $n = 2$ for each model), which indicates fast convergence, we visually inspected the MCMC to confirm convergence afterward. Once all individual curves were calibrated, we merged the five posteriors to obtain the average response by sampling with replacement 1 k times the posterior distribution for each curve. We then merged the samples together into a new combined posterior distribution. From this combined posterior distribution, we obtained the median parameter value ±95% confidence intervals. Model predictions were performed by sampling 1 k samples from the combined posterior. Goodness of fit was assessed for each run through the root mean square error (RMSE) and a pseudo-R^2 calculated from Spearman's correlation coefficient as pseudo-R^2 = [cor (Observed, Modeled)]^2. Finally, SOX+ was run with the median parameters of the equation that presented the best fit (i.e., the Weibull equation, Equation 2).

SOX+ Model

We calibrated the SOX+ model based on average daily transpiration rates of the tree population (n = 6). To do so, we performed Bayesian inverse model calibration (e.g., Ellison, 2004; Hartig et al., 2012) selecting the parameters $k_{sr,max}$, $k_{rc,max}$, $rplant_{min}$, $\Psi_{ref,Tuz}$, and a_{Tuz}. Since we were primarily interested in the initial transpiration response to decreasing soil water content to see if SOX+ was able to capture the dry-down phase, we only used the initial 19 days (DOY 212–230) for calibration, further excluding days 216 and 217 because of low VPD and PAR conditions in the greenhouse (**Figure 1**). As including or

TABLE 2 | Results of the three-step SOX+ model parameterization.

				Prior		Parameters ($n = 19$)					
Model	**Parameter**	**Units**	**Distribution**	**Min**	**Max**	**Median**	**95%CI**				
FvCB (Optimization)	$V_{cmax,25}$	μmol m^{-2} s^{-1}	Uniform	10	80	33.3	[26.8–38.8]				
	$J_{max,25}$	μmol m^{-2} s^{-1}	Uniform	30	140	51	[45.1–56.8]				
k_{xylem} (Ψ_{xylem}),$_{WB}$				Prior		Combined posterior ($n = 5$)					
(Calibration)	**Parameter**	**Units**	**Distribution**	**Min**	**Max**	**Q2.5%**	**Median**	**Q97.5%**			
	Ψ_{ref}	MPa	Uniform	−1.5	−3.5	−3.21	−3.01	−2.12			
	A_{coef}	unitless	Uniform	1	8	2.03	2.85	3.16			
				Prior		Posterior (Hydraulic + NSL)			Posterior (Hydraulic)		
SOX+ (Calibration)	**Parameter**	**Units**	**Distribution**	**Min**	**Max**	**Q2.5%**	**Median**	**Q97.5%**	**Q2.5%**	**Median**	**Q97.5%**
	$k_{sr,max}$	mol m^{-2} s^{-1} MPa^{-1}	Uniform	0.01	1	0.36	0.77	0.99	0.01	0.01	0.01
				Mean	SD						
	$k_{rc,max}$	mol m^{-2} s^{-1} MPa^{-1}	Gaussian	0.025	0.01	0.024	0.035	0.043	0.033	0.042	0.045
	$Rplant_{min}$	m^2 s MPa mol^{-1}	Gaussian	10	3	4.75	4.87	4.92	4.75	4.77	4.8
	Ref_{Tuz}	MPa	Gaussian	−1.5	0.5	−1.75	−1.72	−1.71	NA	NA	NA
	A_{Tuz}	unitless	Gaussian	3	0.5	2.75	2.92	2.97	NA	NA	NA

For the FvCB photosynthesis model, the prior assumed for each individual A_n/C_i curve ($n = 19$) for $V_{cmax,25}$ and $J_{max,25}$ is provided, together with the median and 95%CI parameter value calculated from the 19 individual optimizations. For the Weibull (WB) xylem vulnerability model kyxlem(Ψ_{xylem}),$_{WB}$ calibration, the prior parameter distribution assumed for each individual curve ($n = 5$) is provided for Ψ_{ref} and A_{coef} parameters. The median and the 95% credible interval are reported from the combined posterior distribution for the five curves. Two different SOX+ model calibrations were performed, one accounting for non-stomatal limitations (NSL, Hydraulic + NSL) and one not accounting for NSL (Hydraulic). SOX+ model calibrations are reported as median posterior parameter estimates ± 95% credible interval for the five (three) parameters included in the calibration for the Hydraulic + NSL (Hydraulic). For each model and parameter, assumed prior parameter distributions are also reported.

not a given process changes the whole structure of the model, and because we wanted to run SOX+ with and without accounting for NSL, we performed two different calibrations (hereafter referred as "Hydraulic," i.e., SOX + model without including NSL, and "Hydraulic+NSL," i.e., SOX + model including NSL). The procedure was the same in both cases, though the "Hydraulic" calibration did not include the $\Psi_{ref,Tuz}$and a_{Tuz} parameters. Again, we used broadly set, biologically meaningful priors (**Table 2**), a Gaussian likelihood function, and the differential evolution MCMC with memory and a snooker update (DEzs, terBraak and Vrugt, 2008) as implemented in the "BayesianTools" R package (Hartig et al., 2017). We ran each calibration three times, 30 k iterations each, and then we discarded the first 20 k iterations as a burn-in. Between-MCMC convergence was addressed by the Gelman–Rubin convergence diagnosis (G-R < 1.1 for both calibrations, G-R < 1.1 considered being a conservative threshold; Brooks and Gelman, 1998). To assess the calibrated SOX+ performance, we ran for 500 times both the "Hydraulic" and "Hydraulic+NSL" model formulations for the entire time series (DOY 212–265), by sampling resulting posterior parameter distribution. For each run, we compared projected daily cumulated transpiration with the observations using a linear model accounting for temporal autocorrelation with an auto-regressive [corAR()] correlation structure centered in DOY. This was done with the package "nlme" (Pinheiro et al., 2021). Goodness of fit was assessed through the RMSE and a pseudo-R^2 [R^2_{cs}; Cox and Snell, 1989), based on the deviance from the regressive model with respect to the null model and reported as the median RMSE and R^2_{cs} for the 500 runs.

Simulation Scenarios

NSL and Leaf Shedding Importance in Preventing Loss in Hydraulic Conductance

To quantify the importance of non-stomatal limitations (NSL) of photosynthesis and leaf shedding in preventing k_{rc} decline, we ran the calibrated SOX+model for 54 days (DOYs 212–265) under the following scenarios: (1) hydraulic limitations with observed leaf shedding dynamics, i.e., accounting for the daily leaf area reduction (Hydraulic scenario, ran with the "Hydraulic" calibration); (2) Hydraulic limitations and NSL, but considering leaf area constant at the initial value during the entire simulation (Hydraulic + NSL scenario, ran with the "Hydraulic+NSL" calibration); and (3) Hydraulic limitations and NSL plus observed leaf shedding dynamics (Hydraulic + NSL + leaf shedding scenario, ran with the "Hydraulic+NSL" calibration). This setup enabled to assess the importance of NSL and leaf shedding on k_{rc}loss separately. To obtain model projections for each scenario, we sampled 500 times the posterior parameter distribution. We report the daily evolution of percent loss in k_{rc}(PLk$_{rc}$, in %), calculated as $100^{*}k_{rc}(\Psi_{canopy,PD})/k_{rc,max}$, as the median ± 95% CI of the 500 runs.

Importance of Leaf Shedding at Different Degrees of Leaf Leakiness

We tested the sensitivity of the model to variations in minimum leaf conductance (g_{min}). This highly uncertain parameter is assumed to vary strongly between plants, while being extremely important for water loss and leaf shedding under extreme drought stress (e.g., Vilagrosa et al., 2003; Hochberg et al., 2017;

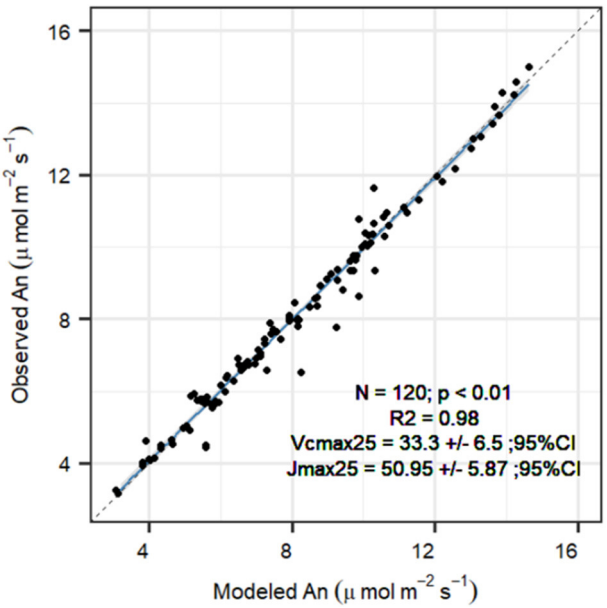

FIGURE 3 | Comparison between FvCB model net assimilation (An, μmol m^{-2} s^{-1}) projections with observations after parameter optimization for each A_n/C_i curve ($n = 19$), for the *P. sylvestris* saplings grown in the greenhouse in year 2019. Reported are the fit (R^2), the median optimum $V_{cmax,25}$ ± 95% confidence interval, and the median optimum $J_{max,25}$ ± 95% confidence interval. The solid line indicates the trend between observed and modeled An ($p < 0.01$), with the gray area representing the 95% CI. The slope was not significantly different than 1 ($p > 0.1$), and intercept was not significantly different than 0 ($p > 0.1$) based on a *t*-test. Dashed line represents the 1:1 fit.

Duursma et al., 2019; Li et al., 2020). It is assumed that plants with higher g_{min} will likely benefit more from leaf shedding, as the reduction in water loss per unit of leaf shed will be higher. The model formulation "Hydraulic+NSL" was run with two different g_{min} values ($g_{min} = 2$ mmol m^{-2} s^{-1} and $g_{min} = 3$ mmol m^{-2} s^{-1}, a 50% increase), considering either constant leaf area, i.e., no leaf shedding, or observed leaf dynamics, i.e., observed leaf shedding. Again, posterior parameter sampling with replacement was carried out for 500 model runs for each of the 2 × 2 scenarios (leaf dynamics × g_{min} assumption). Then, for each g_{min} scenario, we calculated the daily average cumulative benefits of leaf shedding as

$$Benefit_{LS,i} = \frac{\sum_{i=1}^{i} PLk_{rc,NoShed,i} - PLk_{rc,Shed,i}}{i} \quad (14)$$

where $Benefit_{LS,i}$ is the daily average cumulative reduction in percent loss of k_{rc} if trees dynamically shed their leaves relative to the same trees in the absence of leaf shedding, "i" is the day since the beginning of the experiment, and $PLk_{rc,NoShed,i}$ and $PLk_{rc,Shed,i}$ are the percent loss in k_{rc} on day "i" in the absence or presence of leaf shedding, respectively. For this and all the other statistical analyses described before, as well as to develop and implement the SOX+ model, we used the R statistical program (R Core Team, 2021, Version 3.6.1).

RESULTS

Calibration of Xylem Vulnerability Models

All the three equations to describe hydraulic vulnerability [Weibull (WB); sigmoid exponential (SE), and original SOX+ formulation (SOXf)] provided similar, overlapping results. The median xylem water potentials at which 50% of loss in hydraulic conductivity occurred were: WB −2.53 MPa, SE −2.6 MPa, and SOXf−2.6 MPa. The WB function described the observed trends slightly better than the other functions while also maintaining the assumption in the original SOX model that loss of hydraulic conductivity does not occur at Ψ_{xylem} values ≈ 0 (**Figure 4**). Therefore, WB was selected to run SOX+ for *P. sylvestris* in this experiment. Parameter values describing prior and the posterior parameters are listed in **Table 2**.

Leaf Shedding Speed Increased Concurrently With Transpiration Stop

After starting the drought experiment at DOY 212, transpiration of all six measured *P. sylvestris* saplings decreased from 1–2.6 kg tree^{-1} day^{-1} to about 10% of the starting value within 2 weeks (DOY 226). Within this period, transpiration was strongly reduced for 2 days (DOY 216–217), most likely because of exceptionally cloudy days with low temperature conditions outside the greenhouse that were not compensated (see **Supplementary Figure 2**). From DOY 227 onward, tree transpiration almost stopped, with median [95% CI] values of 0.034 [0.001–0.19] kg tree^{-1} day^{-1} (**Figure 5**). At the same time, leaf shedding increased, which was only marginal during the initial phase of the experiment (0.2 [0.02–0.2] % day^{-1} between DOY 212 and 225). Once transpiration was close to zero, litterfall tripled to 0.55[0.03–0.9] % day^{-1}. At the end of the experiment (DOY 265), the trees had lost 30.2% [16.9–37.8] of the initial leaves. We observed that only 2 and 3 year-old needles were shed but never current year needles.

SOX+ Performance Improved When Including Non-Stomatal Limitations of Photosynthesis

SOX+ model calibration accounting for non-stomatal limitations (Hydraulic + NSL) outperformed the standard SOX+ model (**Figure 6**) during the entire experiment. It also provided a more realistic set of posterior parameter estimates, especially regarding $k_{sr,max}$ (**Table 2**). For the calibration period (DOY 212–230), the standard "Hydraulic" model setup led to 27.8 ± 17% (Median ± SE) overestimation of daily transpiration, while with "Hydraulic+NSL," the error reduced to 2.5 ± 16.9% (**Figure 6C**). Such differences were especially important during the dry-down phase (DOY 220–228). The differences in accuracy between the two model simulations strongly declined during the second half of the experiment, when both model setups resulted in full stomatal closure ($gs = g_{min}$, DOY 240–265).

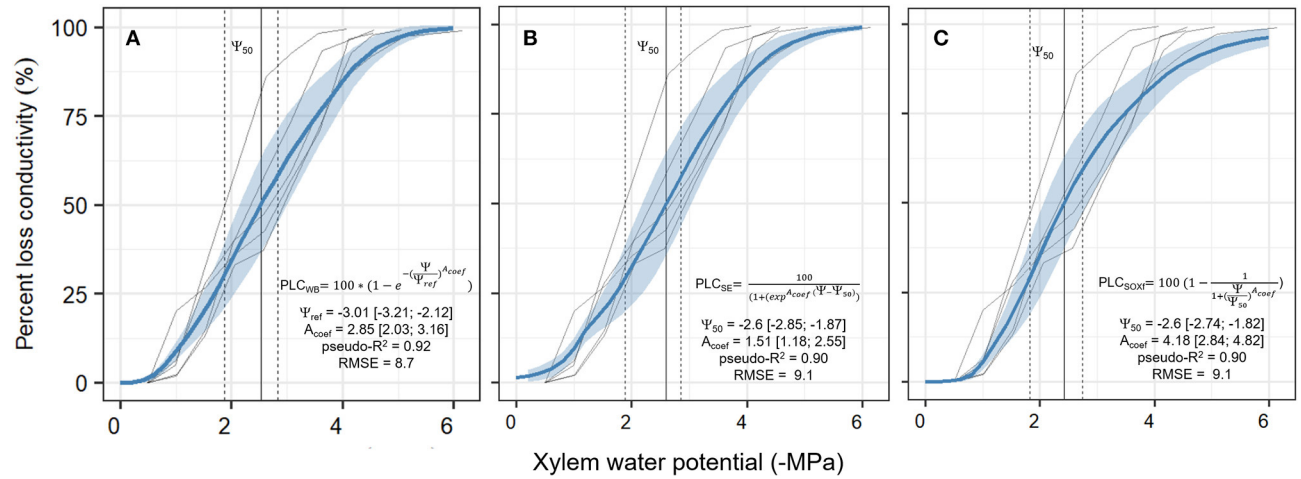

FIGURE 4 | Calibration of the three different xylem vulnerability models [Weibull model (WB, **A**), the Sigmoid Exponential (SE, **B**), and the original SOX formulation (SOXf, **C**)] for the *P. sylvestris* saplings. Solid transparent lines are the five measured curves of the observed percent loss in xylem conductivity (PLC, in %) in relation to xylem water potential decrease (Ψ_{xylem}, in -MPa). Solid blue line ± shadowed blue area is the median ± 95 CI obtained from 1 k model runs sampling the combined posterior parameter estimate, resulting from curve-individual calibrations for each model, as described in section Xylem Vulnerability. The vertical solid line shows the Ψ_{50} value; this is when xylem has lost 50% of its conductivity (±95% CI, vertical dashed lines). For each model, formulation and median ± 95% CI values for each parameter are provided. Note that in the WB model Ψ_{ref} parameter meaning is not equivalent to the Ψ_{50} parameter from the other two models. Goodness of fit is given as the median pseudo-R^2 and the median root mean square error (RMSE) of all model runs.

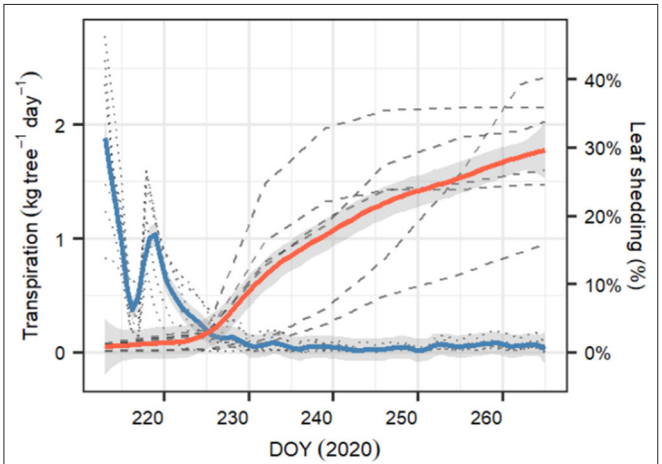

FIGURE 5 | Temporal evolution of whole-tree transpiration (in kg tree^{-1} day^{-1}) and percent of leaf shed for the six monitored *P. sylvestris* saplings growing in the greenhouse during the whole length of the experiment (DOY 212–265). Blue line represents the average daily transpiration ±1 SD, whereas red line represents the daily cumulated percent of leaf shed since the beginning of the experiment ±1 SD. Transparent dotted lines are the observed daily transpiration for each tree, and transparent dashed lines are the cumulated percent of leaf shed for each tree.

NSL and Leaf Shedding Reduce Projected Loss in Root-To-Canopy Hydraulic Conductance

Compared to the original "Hydraulic" SOX+ setup, projected percent loss in root-to-canopy conductance (PLk_{rc}, in %) at the end of the experiment when accounting for NSL (Hydraulic + NSL) was smaller by 6.3 ± 0.2%. Including observed leaf shedding (Hydraulic + NSL + leaf shedding scenario) further reduced projected PLk_{rc} by a 13 ± 0.2 % (**Figure 7**). Interestingly, with NSL and leaf shedding considered, the median simulated PLk_{rc}after 54 days of water shortage was below 80%, an important threshold for pine mortality (Hammond et al., 2019). Leaf shedding speed drastically increased between DOYs 225 and 231, when trees had lost between 44 and 53% of their root-to-canopy conductance, according to the SOX+ model (**Figure 8**) and their stomata were fully closed (daily maximum gs < 10% of maximum simulated gs). After full stomatal closure, tree water losses were highly dependent on leaf leakiness, here summarized as g_{min}. Increasing g_{min} by 50% resulted in shedding of leaves that was significantly beneficial in reducing k_{rc} losses compared with no shedding leaves 6 days earlier than assuming g_{min} = 2 mmol m^{-2} s^{-1} (DOY 244 vs. DOY 250). The benefits of leaf shedding were significantly higher at g_{min} = 3 mmol m^{-2} s^{-1} than at g_{min} = 2 mmol m^{-2} s^{-1} after DOY 232 ($p < 0.05$, after a Kolmogorov–Smirnov non-parametric test), and for the rest of the period simulated (**Figure 9**).

DISCUSSION

The findings suggest that non-stomatal limitations (NSL) of photosynthesis and leaf shedding processes play an important role as hydraulic safety mechanisms in *P. sylvestris*, as they reduce losses in root-to-canopy conductance during severe drought stress (**Figure 7**). Drought-induced leaf shedding in

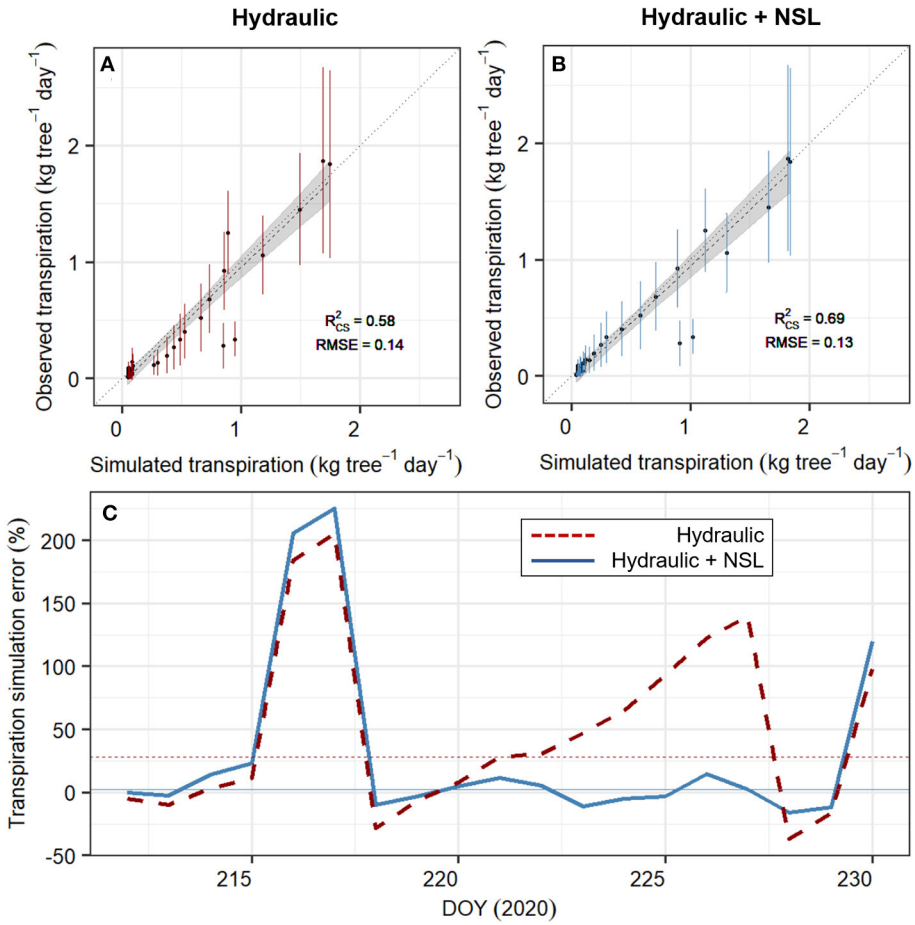

FIGURE 6 | Performance of the SOX+ model calibrated without ("Hydraulic," **A**, in red) and with ("Hydraulic + NSL," **B**, in blue) non-stomatal limitations of photosynthesis. **(A,B)** show the comparison between simulated and observed transpiration (in kg tree^{-1}day^{-1}, points ± SD error bars), during the experiment (DOY 212–265). Daily simulated transpiration is the projected median by sampling 500 times each of the SOX+ model formulation posterior parameter estimates. Noted is the generalized linear model accounting for temporal autocorrelation, model fit (R^2_{cs}), and the RMSE. In both formulations, the slope was not significantly different than 1 ($p < 0.01$), and the intercept was not significantly different than 0 ($p < 0.01$). **(C)** represents the SOX+ error in transpiration estimates for the calibration period (DOY 212–230), and for the Hydraulic (red, dashed lines) and Hydraulic + NSL (blue, continuous lines) formulations. Simulation error was calculated as $\frac{Tr_{sim} - Tr_{obs}}{Tr_{obs}}$, where Tr_{sim} is the daily median transpiration from the 500 model, and Tr_{obs} is the daily observed transpiration, both in kg tree^{-1} day^{-1}. Horizontal lines represent the median simulated error for each SOX+ formulation.

P. sylvestris saplings started when predicted loss of root-to-canopy hydraulic conductance was close to 50%. This is in accordance with the "hydraulic fuse" hypothesis, which states that cavitation in leaves would occur earlier than xylem cavitation to avoid irreversible xylem conductance losses (e.g., Hochberg et al., 2017, Choat et al., 2018), as leaves are cheaper to rebuild than new vessels in the xylem (Tyree and Ewers, 1991). The results also concur with previous observations of leaf shedding delaying the time to reach lethal dehydration thresholds (Blackman et al., 2019) while also identifying g_{min} as a key trait involved in plant dehydration processes (Duursma et al., 2019; Cochard, 2020). These findings highlight the importance of including non-stomatal processes (i.e., NSL and leaf area adjustments) into simulation models in order to account for tree physiological feedback responses to drought stress.

Non-Stomatal Limitations of Photosynthesis as a Hydraulic Safety Mechanism

Including NSL to restrict photosynthesis improved the SOX+ model representation of observed transpiration reductions during the dehydration phase, especially when stomata were not fully closed. Model improvements based on similar observations have been reported previously (e.g., Yang et al., 2019; Gourlez de la Motte et al., 2020). Including NSL reduced projected losses in root-to-canopy conductance by overall 6% after 54 days without irrigation. It also delayed reaching 80% of PLk_{rc}, an important threshold for pine mortality (Hammond et al., 2019), by 8 days. As plants dehydrate, considering NSL led to lower optimum stomatal conductance per photosynthetic gain (i.e., it led to decreased $\delta An/\delta C_i$ in Equation 8). We identified a Ψ_{canopy}

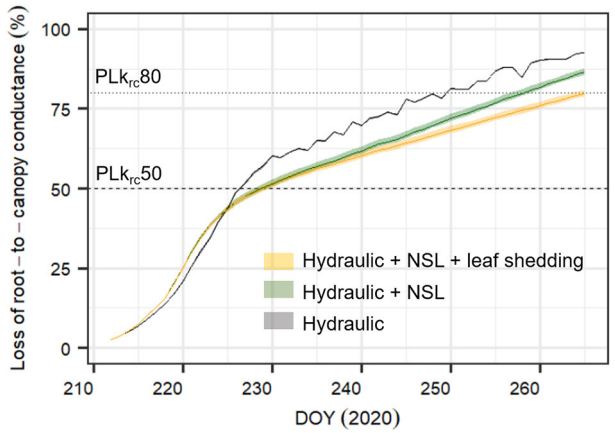

FIGURE 7 | Simulated percent loss in root-to-canopy conductance during the experiment (PLk_{rc}, in %) with three different SOX+ model formulations. Only hydraulic constraints on stomatal conductance (Hydraulic, in gray); hydraulic constrains on stomatal conductance and non-stomatal limitations of photosynthesis accounting for equal leaf area during the whole experiment (Hydraulic + NSL, in green); and hydraulic constraints on stomatal conductance, non-stomatal limitations of photosynthesis, and observed leaf shedding (Hydraulic + NSL + leaf shedding, in orange). Posterior parameter distributions are different for (Hydraulic) and (Hydraulic + NSL, Hydraulic + NSL + leaf shedding), see **Table 2**. For each model formulation, the figure shows the daily pre-dawn median ± 95% CI PLk_{rc}, obtained from running the simulation by sampling 500 times the posterior parameter distribution. Horizontal lines indicate when $k_{rc} = 0.5 * k_{rc,max}$ ($PLk_{rc}50$, dashed line), and when $k_{rc} = 0.2 * k_{rc,max}$ ($PLk_{rc}80$, dotted line), a threshold that has been found to be critical for pine survival probability (Hammond et al., 2019).

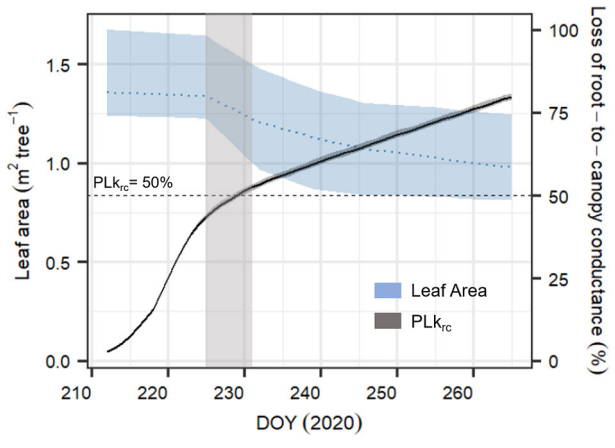

FIGURE 8 | Time series of averaged leaf area (in m^2 tree^{-1}, blue dashed line) for the six monitored *Pinus sylvestris* saplings and simulated dynamics in percent loss in root-to-canopy conductance (PLk_{rc}, in %, black continuous line) according to the complete SOX+ model scheme (Hydraulic + NSL + leaf shedding). Daily leaf area is represented as the mean ± SD. Daily simulated PLk_{rc} is represented as the median ± 95% CI after 500 model simulation runs by sampling the posterior parameter estimate. The horizontal line indicates when $k_{rc} = 0.5 * k_{rc,max}$ ($PLk_{rc}50$, dashed line), while the light gray area represents the uncertainty of when the leaf shedding rate accelerated. Because of weekly sampling campaigns, the area is relatively broad.

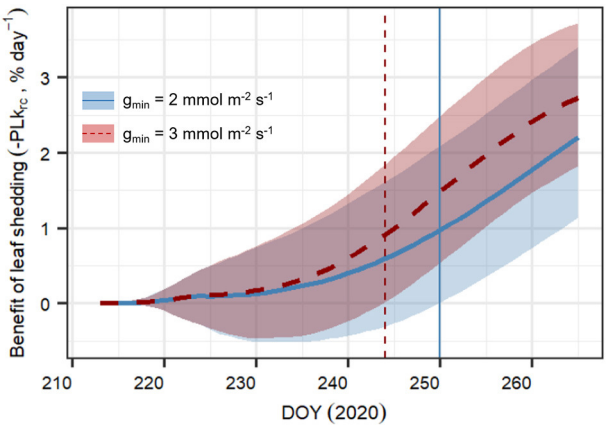

FIGURE 9 | Daily averaged cumulated benefit of observed leaf shedding in preventing loss in root-to-canopy conductance (PLk_{rc}, in %) for minimum leaf conductance (g_{min}) = 2 mmol m^{-2} s^{-1} (blue continuous line), and g_{min} = 3 mmol m^{-2} s^{-1} (red dashed line). Results represent the median ± 95% CI of 500 model simulations obtained by randomly sampling the posterior parameter distribution for each of the following scenarios and their combination:with and without leaf shedding, and the two g_{min} values considered. The daily average cumulated difference in PLk_{rc} between shedding and no shedding is calculated according to Equation 14. The vertical lines for both scenarios indicate the DOY at which the benefit of leaf shedding is significantly >0.

reference value of −1.7 MPa for a 50% strength of the NSL limitation, this value being lower than the observed $\Psi_{xylem,50}$ (−2.6 MPa). This implies that NSL mechanisms are acting at the onset of embolism formation, which may be indicative of an active hydraulic safety mechanism (Choat et al., 2018).

We acknowledge that simulating NSL as a decline in apparent V_{cmax} and J_{max} summarizes the effects from a multiplicity of interacting plant physiological responses to drought, which might be better considered separately. For example, water and carbon transport in the mesophyll might be described as a function of aquaporin expression in dependence on cell water potential (Flexas et al., 2012; Paudel et al., 2019), and the effects on photosynthesis could be separated into suppression of rubisco regeneration (Rizhsky et al., 2002; Pilon et al., 2018), and reduction in rubisco activity. Also, reduced sink strength of tissue experiencing drought limitations (Hsiao et al., 1976; Fatichi et al., 2014) could eventually be used to describe the down-regulation of photosynthesis explicitly, e.g., *via* higher leaf sugar concentration due to reduced phloem load (Riesmeier et al., 1994; Sevanto, 2014). These mechanisms, however, have not been sufficiently resolved to be used in general models.

Shedding Leaves After Stomatal Closure Buffered Projected Loss in Conductance

Reducing leaf area is a well-known phenomenon that decreases whole tree transpiration (e.g., Whitehead et al., 1984; Martínez-Vilalta et al., 2014; Wolfe et al., 2016). During the first phase of the dry-down, leaf shedding was only marginal, but it increased after full stomatal closure (**Figures 5**, **8**), when reducing leaf

area was the only possibility to further reduce leaf leakiness and leaf C maintenance cost. We found that leaf shedding reduced projected k_{rs} losses by 7% at the end of the experiment. Also, when including leaf shedding dynamics, the pines did not reach the lethal $PLk_{rc}80$ threshold. Interestingly, increasing g_{min} by 50% further underscored the benefits of leaf shedding, which then even started earlier during the dry-down. Since g_{min} seems to depend on environmental conditions during leaf development (Duursma et al., 2019) and also increases with leaf temperature (e.g., Schuster et al., 2016; Cochard, 2020), leaf shedding may represent an acclimation strategy to counteract leaf leakiness during later growth stages (Blackman et al., 2019) and heat waves. This is supported by findings that less sclerophyllous trees (i.e., those with higher g_{min}) are likely to shed more leaves earlier during heat-drought stress development (e.g., Ogaya and Penuelas, 2004; Montserrat-Marti et al., 2009).

In accordance with recent findings (Wolfe et al., 2016; Cardoso et al., 2020; Li et al., 2020), Scots pine shed its 2 and 3 year-old needles once k_{rs} was halved and leaf conductance was strongly reduced (approximately $gs = g_{min}$). This implies that in *P. sylvestris,* leaf shedding has likely been triggered as a last-chance hydraulic safety mechanism, as pines do not re-grow shed leaves until the next growing season. This may lead to severe C uptake reductions after drought release, especially if the drought occurs early during the growing season (Eilmann et al., 2013), with consequences that may extend up to 4 years after drought (e.g., Galiano et al., 2011). In the experiment, the trees shed about 30% of their leaves, which may imply an equivalent loss in photosynthesis capacity after re-watering. Such C uptake reductions may still have severe implications for post-drought xylem and canopy recovery (e.g., Yan et al., 2017; Ruehr et al., 2019; Kannenberg et al., 2020). However, negative impacts of leaf losses are probably less severe because mostly the older leaves, which are less efficient in terms of photosynthesis, were shed first (Escudero and Mediavilla, 2003; Niinemets et al., 2005, but see Poyatos et al., 2013). Also, the C balance during drought is less negative because of reduced maintenance respiration; thus, lower depletion of non-structural carbohydrates reserves is expected. The inclusion of the SOX+ model in a whole-tree dynamics simulation model may shed more light upon the benefits and drawbacks of leaf shedding in terms of whole tree C balance and growth.

Uncertainties and Lines to Proceed Further

Trees may respond to soil drought with various physiological reactions in order to save water and protect their conductive tissue. Besides stomatal regulation of evaporation demand and potential photosynthesis, additional processes are involved that affect the relationship between stomatal opening and photosynthesis activity, particularly under drought as has been described, e.g., by Eller et al. (2018, 2020). In this study, we have accounted for these processes in a lumped way by training a process-based tree hydraulic model (SOX+) from "*in situ*" observations (e.g., Medlyn et al., 2015; Dietze et al., 2018). However, we acknowledge that the experimental basis for this new mechanism is still poor, based on a small number of repetitions and a relatively high variability in individual plants. Also, it would be more convincing that loss in xylem conductance is a driving force for drought responses if it would have been directly measured instead of indirectly calculated from water potential and transpiration. It should also be noted that the additional parameters required to describe the new model features are yet uncertain with respect to their generality; thus, further studies are needed to evaluate their precision, species-dependency, or relationship to wood or leaf anatomical traits (Schumann et al., 2019, Velikova et al., 2020).

Similar caution needs to be applied to the second investigated process of leaf shedding. It seems that there is a clear threshold of loss in root-to-canopy hydraulic conductance at which leaf shedding began. Therefore, we suggest a generalization of drought-induced leaf shedding dynamics that may be included in simulation models accounting for tree hydraulics. This is based on a basal leaf turnover rate and a drought-induced leaf shedding rate that is considered after a given threshold of loss in hydraulic conductanceis reached:

$$LA_i = LA_{(i-1)} - basal_{LS} LA_{(i-1)} if PLk_{rc} < x \quad (15a)$$

$$LA_i = LA_{(i-1)} - drougth_{LS} LA_{(i-1)} if PLk_{rc} \geq x \quad (15b)$$

where LA_i is the whole tree leaf area on day "i" (in m^2 $tree^{-1}$), $basal_{LS}$ is the basal rate of leaf shedding without drought stress, $drought_{LS}$ is the leaf shedding rate under drought stress, and x is the threshold of conductance loss at which drought-induced leaf shedding occurs. For instance, in the experiment (Section Leaf Shedding Speed Increased Concurrently With Transpiration Stop), $basal_{LS}$ would equal to 0.002, $drought_{LS}$ to 0.0055, and x to 50%. According to recent observations, 50% loss in hydraulic conductance seems to be a realistic threshold, occurring within a wide range of environments and plant types (e.g., Wolfe et al., 2016; Cardoso et al., 2020; Li et al., 2020). Nonetheless, we acknowledge that depending on the species-specific strategies to face hydraulic stress, such threshold may vary (e.g., Ruehr et al., 2016). We hypothesize further that this strategy may be linked to differences in g_{min}, as the benefits of leaf shedding appear earlier and to a larger degree when leaf leakiness is higher.

The suggested model modifications account for non-stomatal acclimation mechanisms affecting canopy conductance, which are commonly accepted as an important driver of plant water use regulation but are still poorly tested in simulation models. Nevertheless, we are aware that other potential acclimation processes such as changes in rooting depth, root distribution, or soil-to-root conductance (e.g., Mu et al., 2021), as well as changes in leaf distribution or traits, such as leaf thickness and stomatal density, affect whole plant conductance. Also, short-term responses, such as an increase in leaf cuticular conductance (g_{min}) in response to rising temperature (e.g., Cochard et al., 2021), are not addressed in this version of SOX+, which leaves room for model improvement. Furthermore, the SOX+ model has, so far, been tested only for small trees growing under controlled conditions. Thus, model performance should be assessed under field conditions, particularly for trees of different sizes and species. Still, the inclusion of NSL and leaf shedding processes enhanced model transpiration estimates, which were identified as key mechanisms that trees trigger to buffer conductance losses under drought stress.

Relevance for Climate-Change Scenario Analyses

Including the proposed processes into ecosystem models would improve water consumption estimates during drought and hot drought events. Because heat waves alongside increased VPD are supposed to increase in intensity and frequency (Basarin et al., 2020), this may potentially improve model projections of forest drought responses. Parametrizing species in order to consider tradeoffs between elongating carbon gain and reducing hydraulic stress *via* leaf shedding will also enable to better represent the differences in competition strength between tree species under future environmental conditions. This is particularly useful in ecosystem models addressing the interactive impacts of increased atmospheric CO_2 and a hotter and drier climate on forests. In addition, the mechanistic simulation of loss in xylem conductance also considering feedback responses may lead to an improvement in tree mortality process description (Bugmann et al., 2019). In contrast to empirical approaches, it allows to consider species- and environmental-specific adaptation strategies, represented by species traits that indicate different hydraulic vulnerabilities. Since tree mortality is an underrepresented but highly important process when addressing forest dynamics under global warming (Meir et al., 2015), incorporating leaf area acclimation to drought and non-stomatal limitations of photosynthesis in larger-scale forest simulation models will likely improve climate change scenario assessments.

DATA AVAILABILITY STATEMENT

The datasets presented in this study can be found in online repositories. The names of the repository/repositories and accession number(s) can be found at: Code and data available at: https://zenodo.org/badge/latestdoi/381126647.

AUTHOR CONTRIBUTIONS

DN-S wrote the initial version of the manuscript, implemented SOX+ model formulation, and analyzed the data. DN-S, NR, and BB designed and implemented the experiment. RG and NR assisted with manuscript writing and research design and supervised the data analysis. TK analyzed the xylem vulnerability curves. BB, TK, RR, and SS collaborated for the manuscript content and collected field data. All the authors contributed to manuscript editing and writing.

FUNDING

This study was supported by the German Research Foundation through its Emmy Noether Program (RU 1657/2-1).

ACKNOWLEDGMENTS

We would like to thank Andreas Gast and Martha Lutzenberger for their helpful assistance during the experiment. We also would like to thank the three reviewers for their insightful comments on a previous version of the manuscript.

SUPPLEMENTARY MATERIAL

The Supplementary Material for this article can be found online at: https://www.frontiersin.org/articles/10.3389/fpls.2021.715127/full#supplementary-material

REFERENCES

Allen, C. D., Breshears, D. D., and McDowell, N. G. (2015). On underestimation of global vulnerability to tree mortality and forest die-off from hotter drought in the Anthropocene. *Ecosphere* 6, 1–55. doi: 10.1890/ES15-00203.1

Anderegg, W. R., Berry, J. A., Smith, D. D., Sperry, J. S., Anderegg, L. D., and Field, C. B. (2012). The roles of hydraulic and carbon stress in a widespread climate-induced forest die-off. *Proc. Nat. Acad. Sci.* 109, 233–237. doi: 10.1073/pnas.1107891109

Basarin, B., Lukić, T., and Matzarakis, A. (2020). Review of biometeorology of heatwaves and warm extremes in Europe. *Atmosphere* 11:1276. doi: 10.3390/atmos11121276

Bassiouni, M., and Vico, G. (2021). Parsimony versus predictive and functional performance of three stomatal optimization principles in a big-leaf framework. *New Phytol.* 228, 1796–1810. doi: 10.1111/nph.17392

Bernacchi, C. J., Singsaas, E. L., Pimentel, C., Portis, A. R. Jr., and Long, S. P. (2001). Improved temperature response functions for models of Rubisco-limited photosynthesis. *Plant Cell Environ.* 24, 253–259. doi: 10.1111/j.1365-3040.2001.00668.x

Blackman, C. J., Li, X., Choat, B., Rymer, P. D., De Kauwe, M. G., Duursma, R. A., et al. (2019). Desiccation time during drought is highly predictable across species of Eucalyptus from contrasting climates. *New Phytol.* 224, 632–643. doi: 10.1111/nph.16042

Blackman, C. J., Pfautsch, S., Choat, B., Delzon, S., Gleason, S. M., and Duursma, R. A. (2016). Toward an index of desiccation time to tree mortality under drought. *Plant Cell Environ.* 39, 2342–2345. doi: 10.1111/pce.12758

Brodribb, T. J., Powers, J., Cochard, H., and Choat, B. (2020). Hanging by a thread? *For. Drought. Sci.* 368, 261–266. doi: 10.1126/science.aat7631

Brooks, S. P., and Gelman, A. (1998). General methods for monitoring convergence of iterative simulations. *J. Comput. Graph. Stat.* 7, 434–455. doi: 10.1080/10618600.1998.10474787

Bugmann, H., Seidl, R., Hartig, F., Bohn, F., Bruna, J., Cailleret, M., et al. (2019). Tree mortality submodels drive simulated long-term forest dynamics: assessing 15 models from the stand to global scale. *Ecosphere* 10:e02616. doi: 10.1002/ecs2.2616

Campbell, G. S. (1985). *Soil Physics With BASIC*: *Transport Models for Soil-Plant Systems*. Amsterdam: Elsevier.

Cardoso, A. A., Batz, T. A., and McAdam, S. A. (2020). Xylem embolism resistance determines leaf mortality during drought in Persea americana. *Plant Physiol.* 182, 547–554. doi: 10.1104/pp.19.00585

Carnicer, J., Coll, M., Ninyerola, M., Pons, X., Sanchez, G., and Penuelas, J. (2011). Widespread crown condition decline, food web disruption, and amplified tree mortality with increased climate change-type drought. *Proc. Nat. Acad. Sci.* 108, 1474–1478. doi: 10.1073/pnas.1010070108

Chen, D., Wang, S., Xiong, B., Cao, B., and Deng, X. (2015). Carbon/nitrogen imbalance associated with drought-induced leaf senescence in Sorghum bicolor. *PLoS ONE* 10:e0137026. doi: 10.1371/journal.pone.0137026

Choat, B., Brodribb, T. J., Brodersen, C. R., Duursma, R. A., Lopez, R., and Medlyn, B. E. (2018). Triggers of tree mortality under drought. *Nature* 558, 531–539. doi: 10.1038/s41586-018-0240-x

Cochard, H. (2002). A technique for measuring xylem hydraulic conductance under high negative pressures. *Plant Cell Environ.* 25, 815–819. doi: 10.1046/j.1365-3040.2002.00863.x

Cochard, H. (2020). A new mechanism for tree mortality due to drought and heatwaves. *Peer Commun. Forest Wood Sci.* 17. doi: 10.1101/531632

Cochard, H., Pimont, F., Ruffault, J., and Martin-St. Paul, N. (2021). SurEau: a mechanistic model of plant water relations under extreme drought. *Ann. For. Sci.* 78, 1–23. doi: 10.1007/s13595-021-01067-y

Collatz, G. J., Ball, J. T., Grivet, C., and Berry, J. A. (1991). Physiological and environmental regulation of stomatal conductance, photosynthesis and transpiration: a model that includes a laminar boundary layer. *Agric. For. Meteorol.* 54, 107–136. doi: 10.1016/0168-1923(91)90002-8

Damour, G., Simonneau, T., Cochard, H., and Urban, L. (2010). An overview of models of stomatal conductance at the leaf level. *Plant Cell Environ.* 33, 1419–1438. doi: 10.1111/j.1365-3040.2010.02181.x

De Kauwe, M. G., Medlyn, B. E., Ukkola, A. M., Mu, M., Sabot, M. E., Pitman, A. J., et al. (2020). Identifying areas at risk of drought-induced tree mortality across South-Eastern Australia. *Glob. Chang. Biol.* 26, 5716–5733. doi: 10.1111/gcb.15215

De Pury, D. G. G., and Farquhar, G. D. (1997). Simple scaling of photosynthesis from leaves to canopies without the errors of big-leaf models. *Plant Cell Environ.* 20, 537–557. doi: 10.1111/j.1365-3040.1997.00094.x

Dietze, M. C., Fox, A., Beck-Johnson, L. M., Betancourt, J. L., Hooten, M. B., Jarnevich, C. S., et al. (2018). Iterative near-term ecological forecasting: needs, opportunities, and challenges. *Proc. Nat. Acad. Sci.* 115, 1424–1432. doi: 10.1073/pnas.1710231115

Drake, J. E., Power, S. A., Duursma, R. A., Medlyn, B. E., Aspinwall, M. J., Choat, B., et al. (2017). Stomatal and non-stomatal limitations of photosynthesis for four tree species under drought: a comparison of model formulations. *Agric. For. Meteorol.* 247, 454–466. doi: 10.1016/j.agrformet.2017.08.026

Duursma, R. A., Blackman, C. J., Lopéz, R., Martin-StPaul, N. K., Cochard, H., and Medlyn, B. E. (2019). On the minimum leaf conductance: its role in models of plant water use, and ecological and environmental controls. *New Phytol.* 221, 693–705. doi: 10.1111/nph.15395

Duursma, R. A., and Medlyn, B. E. (2012). MAESPA: a model to study interactions between water limitation, environmental drivers and vegetation function at tree and stand levels, with an example application to [CO 2]× drought interactions. *Geosci. Model Dev.* 5, 919–940. doi: 10.5194/gmd-5-919-2012

Eilmann, B., Dobbertin, M., and Rigling, A. (2013). Growth response of Scots pine with different crown transparency status to drought release. *Ann. For. Sci.* 70, 685–693. doi: 10.1007/s13595-013-0310-z

Eller, C. B., Rowland, L., Mencuccini, M., Rosas, T., Williams, K., Harper, A., et al. (2020). Stomatal optimization based on xylem hydraulics (SOX) improves land surface model simulation of vegetation responses to climate. *New Phytol.* 226, 1622–1637. doi: 10.1111/nph.16419

Eller, C. B., Rowland, L., Oliveira, R. S., Bittencourt, P. R., Barros, F. V., da Costa, A. C., et al. (2018). Modelling tropical forest responses to drought and El Niño with a stomatal optimization model based on xylem hydraulics. *Philos. Transac. R. Soc. B Biol. Sci.* 373:20170315. doi: 10.1098/rstb.2017.0315

Ellison, A. M. (2004). Bayesian inference in ecology. *Ecol. Lett.* 7, 509–520. doi: 10.1111/j.1461-0248.2004.00603.x

Escudero, A., and Mediavilla, S. (2003). Decline in photosynthetic nitrogen use efficiency with leaf age and nitrogen resorption as determinants of leaf life span. *J. Ecol.* 91, 880–889. doi: 10.1046/j.1365-2745.2003.00818.x

Evans, J. R. (2021). Mesophyll conductance: walls, membranes and spatial complexity. *New Phytol.* 229, 1864–1876. doi: 10.1111/nph.16968

Farquhar, G. D., von Caemmerer, S. V., and Berry, J. A. (1980). A biochemical model of photosynthetic CO_2 assimilation in leaves of C 3 species. *Planta* 149, 78–90. doi: 10.1007/BF00386231

Fatichi, S., Leuzinger, S., and Körner, C. (2014). Moving beyond photosynthesis: from carbon source to sink-driven vegetation modeling. *New Phytol.* 201, 1086–1095. doi: 10.1111/nph.12614

Flexas, J., Barbour, M. M., Brendel, O., Cabrera, H. M., Carriquí, M., Diaz-Espejo, A., et al. (2012). Mesophyll diffusion conductance to CO_2: an unappreciated central player in photosynthesis. *Plant Sci.* 193, 70–84. doi: 10.1016/j.plantsci.2012.05.009

Flexas, J., Bota, J., Cifre, J., Mariano Escalona, J., Galmés, J., Gulías, J., et al. (2004). Understanding down-regulation of photosynthesis under water stress: future prospects and searching for physiological tools for irrigation management. *Ann. Appl. Biol.* 144, 273–283. doi: 10.1111/j.1744-7348.2004.tb00343.x

Flexas, J., Diaz-Espejo, A., Galmes, J., Kaldenhoff, R., Medrano, H., Ribas-Carbo, M., et al. (2007). Rapid variations of mesophyll conductance in response to changes in CO2 concentration around leaves. *Plant Cell Environ.* 30, 1284–1298. doi: 10.1111/j.1365-3040.2007.01700.x

Galiano, L., Martínez-Vilalta, J., and Lloret, F. (2011). Carbon reserves and canopy defoliation determine the recovery of Scots pine 4 yr after a drought episode. *New Phytol.* 190, 750–759. doi: 10.1111/j.1469-8137.2010.03628.x

Gelman, A., and Rubin, D. B. (1992). Inference from iterative simulation using multiple sequences. *Stat. Sci.* 7, 457–472. doi: 10.1214/ss/1177011136

Gourlez de la Motte, L., Beauclaire, Q., Heinesch, B., Cuntz, M., Foltýnová, L., Šigut, L., et al. (2020). Non-stomatal processes reduce gross primary productivity in temperate forest ecosystems during severe edaphic drought. *Philos. Transac. R. Soc. B* 375:20190527. doi: 10.1098/rstb.2019.0527

Hall, A. E., and Kaufmann, M. R. (1975). Stomatal response to environment with *Sesamum indicum*. L. *Plant Physiol.* 55, 455–459. doi: 10.1104/pp.55.3.455

Hammond, W. M., Yu, K., Wilson, L. A., Will, R. E., Anderegg, W. R., and Adams, H. D. (2019). Dead or dying? Quantifying the point of no return from hydraulic failure in drought-induced tree mortality. *New Phytol.* 223, 1834–1843. doi: 10.1111/nph.15922

Hari, V., Rakovec, O., Markonis, Y., Hanel, M., and Kumar, R. (2020). Increased future occurrences of the exceptional 2018–2019 Central European drought under global warming. *Sci. Rep.* 10, 1–10. doi: 10.1038/s41598-020-68872-9

Harley, P. C., Thomas, R. B., Reynolds, J. F., and Strain, B. R. (1992). Modelling photosynthesis of cotton grown in elevated CO2. *Plant Cell Environ.* 15, 271–282. doi: 10.1111/j.1365-3040.1992.tb00974.x

Hartig, F., Dyke, J., Hickler, T., Higgins, S. I., O'Hara, R. B., Scheiter, S., et al. (2012). Connecting dynamic vegetation models to data–an inverse perspective. *J. Biogeogr.* 39, 2240–2252. doi: 10.1111/j.1365-2699.2012.02745.x

Hartig, F., Minunno, F., and Paul, S. (2017). BayesianTools: general-purpose MCMC and SMC samplers and tools for Bayesian statistics, R package version 0.1.3. Available online at: https://cran.r-project.org/web/packages/BayesianTools/vignettes/BayesianTools.html

Hesse, B. D., Goisser, M., Hartmann, H., and Grams, T. E. (2019). Repeated summer drought delays sugar export from the leaf and impairs phloem transport in mature beech. *Tree Physiol.* 39, 192–200. doi: 10.1093/treephys/tpy122

Hochberg, U., Windt, C. W., Ponomarenko, A., Zhang, Y. J., Gersony, J., Rockwell, F. E., et al. (2017). Stomatal closure, basal leaf embolism, and shedding protect the hydraulic integrity of grape stems. *Plant Physiol.* 174, 764–775. doi: 10.1104/pp.16.01816

Hsiao, T. C., Acevedo, E., Fereres, E., and Henderson, D. W. (1976). Water stress, growth and osmotic adjustment. *Philos. Transac. R. Soc. Lond. B Biol. Sci.* 273, 479–500. doi: 10.1098/rstb.1976.0026

Ichie, T., Hiromi, T., Yoneda, R., Kamiya, K., Kohira, M., Ninomiya, I., et al. (2004). Short-term drought causes synchronous leaf shedding and flushing in a lowland mixed dipterocarp forest, Sarawak, Malaysia. *J. Trop. Ecol.* 697–700. doi: 10.1017/S0266467404001713

Kannenberg, S. A., Schwalm, C. R., and Anderegg, W. R. (2020). Ghosts of the past: how drought legacy effects shape forest functioning and carbon cycling. *Ecol. Lett.* 23, 891–901. doi: 10.1111/ele.13485

Keenan, T., Sabate, S., and Gracia, C. (2010). Soil water stress and coupled photosynthesis–conductance models: bridging the gap between conflicting reports on the relative roles of stomatal, mesophyll conductance and biochemical limitations to photosynthesis. *Agric. For. Meteorol.* 150, 443–453. doi: 10.1016/j.agrformet.2010.01.008

Leuning, R. (1995). A critical appraisal of a combined stomatal-photosynthesis model for C3 plants. *Plant Cell Environ.* 18, 339–355. doi: 10.1111/j.1365-3040.1995.tb00370.x

Li, X., Smith, R., Choat, B., and Tissue, D. T. (2020). Drought resistance of cotton (Gossypium hirsutum) is promoted by early stomatal closure and leaf shedding. *Funct. Plant Biol.* 47, 91–98. doi: 10.1071/FP19093

Marchin, R., Zeng, H., and Hoffmann, W. (2010). Drought-deciduous behavior reduces nutrient losses from temperate deciduous trees under severe drought. *Oecologia* 163, 845–854. doi: 10.1007/s00442-010-1614-4

Martínez-Vilalta, J., Poyatos, R., Aguadé, D., Retana, J., and Mencuccini, M. (2014). A new look at water transport regulation in plants. *New Phytol.* 204, 105–115. doi: 10.1111/nph.12912

Martin-St. Paul, N., Delzon, S., and Cochard, H. (2017). Plant resistance to drought depends on timely stomatal closure. *Ecol. Lett.* 20, 1437–1447. doi: 10.1111/ele.12851

Martin-St. Paul, N. K., Limousin, J. M., Vogt-Schilb, H., Rodríguez-Calcerrada, J., Rambal, S., Longepierre, D., et al. (2013). The temporal response to drought in a Mediterranean evergreen tree: comparing a regional precipitation gradient and a throughfall exclusion experiment. *Glob. Chang. Biol.* 19, 2413–2426. doi: 10.1111/gcb.12215

Martorell, S., Diaz-Espejo, A., Medrano, H., Ball, M. C., and Choat, B. (2014). Rapid hydraulic recovery in *Eucalyptus pauciflora* after drought: linkages between stem hydraulics and leaf gas exchange. *Plant Cell Environ.* 37, 617–626. doi: 10.1111/pce.12182

McDowell, N., Allen, C. D., Anderson-Teixeira, K., Brando, P., Brienen, R., Chambers, J., et al. (2018). Drivers and mechanisms of tree mortality in moist tropical forests. *New Phytol.* 219, 851–869. doi: 10.1111/nph.15027

Medlyn, B. E., Duursma, R. A., Eamus, D., Ellsworth, D. S., Prentice, I. C., Barton, C. V., et al. (2011). Reconciling the optimal and empirical approaches to modelling stomatal conductance. *Glob. Chang. Biol.* 17, 2134–2144. doi: 10.1111/j.1365-2486.2010.02375.x

Medlyn, B. E., Zaehle, S., De Kauwe, M. G., Walker, A. P., Dietze, M. C., Hanson, P. J., et al. (2015). Using ecosystem experiments to improve vegetation models. *Nat. Clim. Chang.* 5, 528–534. doi: 10.1038/nclimate2621

Meir, P., Mencuccini, M., and Dewar, R. C. (2015). Drought-related tree mortality: addressing the gaps in understanding and prediction. *New Phytol.* 207, 28–33. doi: 10.1111/nph.13382

Mencuccini, M., Manzoni, S., and Christoffersen, B. (2019). Modelling water fluxes in plants: from tissues to biosphere. *New Phytol.* 222, 1207–1222. doi: 10.1111/nph.15681

Monteith, J. L. (1995). A reinterpretation of stomatal responses to humidity. *Plant Cell Environ.* 18, 357–364. doi: 10.1111/j.1365-3040.1995.tb00371.x

Montserrat-Marti, G., Camarero, J. J., Palacio, S., Pérez-Rontomé, C., Milla, R., Albuixech, J., et al. (2009). Summer-drought constrains the phenology and growth of two coexisting Mediterranean oaks with contrasting leaf habit: implications for their persistence and reproduction. *Trees* 23, 787–799. doi: 10.1007/s00468-009-0320-5

Mu, M., De Kauwe, M. G., Ukkola, A. M., Pitman, A. J., Gimeno, T. E., Medlyn, B. E., et al. (2021). Evaluating a land surface model at a water-limited site: implications for land surface contributions to droughts and heatwaves. *Hydrol. Earth Syst. Sci.* 25, 447–471. doi: 10.5194/hess-25-447-2021

Mullen, K., Ardia, D., Gil, D. L., Windover, D., and Cline, J. (2011). DEoptim: an R package for global optimization by differential evolution. *J. Stat. Softw.* 40, 1–26. doi: 10.18637/jss.v040.i06

Munné-Bosch, S., and Alegre, L. (2004). Die and let live: leaf senescence contributes to plant survival under drought stress. *Funct. Plant Biol.* 31, 203–216. doi: 10.1071/FP03236

Nadal-Sala, D., Grote, R., Birami, B., Lintunen, A., Mammarella, I., Preisler, Y., and Ruehr, N. K. (2021). Assessing model performance via the most limiting environmental driver in two differently stressed pine stands. *Ecol. Appl.* 31:e02312. doi: 10.1002/eap.2312

Niinemets, Ü., Cescatti, A., Rodeghiero, M., and Tosens, T. (2006). Complex adjustments of photosynthetic potentials and internal diffusion conductance to current and previous light availabilities and leaf age in Mediterranean evergreen species Quercus ilex. *Plant Cell Environ.* 29, 1159–1178. doi: 10.1111/j.1365-3040.2006.01499.x

Niinemets, Ü., and Sack, L. (2006). "Structural determinants of leaf light-harvesting capacity and photosynthetic potentials," in *Progress in Botany* (Berlin; Heidelberg: Springer), 385–419.

Niinemets, Ü. L. O., Cescatti, A., Rodeghiero, M., and Tosens, T. (2005). Leaf internal diffusion conductance limits photosynthesis more strongly in older leaves of Mediterranean evergreen broad-leaved species. *Plant Cell Environ.* 28, 1552–1566. doi: 10.1111/j.1365-3040.2005.01392.x

Ogaya, R., and Penuelas, J. (2004). Phenological patterns of Quercus ilex, Phillyrea latifolia, and Arbutus unedo growing under a field experimental drought. *Ecoscience* 11, 263–270. doi: 10.1080/11956860.2004.11682831

Paudel, I., Gerbi, H., Zisovich, A., Sapir, G., Ben-Dor, S., Brumfeld, V., et al. (2019). Drought tolerance mechanisms and aquaporin expression of wild vs. cultivated pear tree species in the field. *Environ. Exp. Bot.* 167:103832. doi: 10.1016/j.envexpbot.2019.103832

Pilon, C., Snider, J. L., Sobolev, V., Chastain, D. R., Sorensen, R. B., Meeks, C. D., et al. (2018). Assessing stomatal and non-stomatal limitations to carbon assimilation under progressive drought in peanut (*Arachishypogaea* L.). *J. Plant Physiol.* 231, 124–134. doi: 10.1016/j.jplph.2018.09.007

Pineda-García, F., Paz, H., and Meinzer, F. C. (2013). Drought resistance in early and late secondary successional species from a tropical dry forest: the interplay between xylem resistance to embolism, sapwood water storage and leaf shedding. *Plant Cell Environ.* 36, 405–418. doi: 10.1111/j.1365-3040.2012.02582.x

Pinheiro, J., Bates, D., DebRoy, S., and Sarkar, D. (2021). nlme: Linear and Nonlinear Mixed Effects Models. R package version 3. 1–152.

Poyatos, R., Aguadé, D., Galiano, L., Mencuccini, M., and Martínez-Vilalta, J. (2013). Drought-induced defoliation and long periods of near-zero gas exchange play a key role in accentuating metabolic decline of Scots pine. *New Phytol.* 200, 388–401. doi: 10.1111/nph,0.12278

R Core Team (2021). *R: A Language and Environment for Statistical Computing*. Vienna: R Foundation for Statistical Computing. Available online at: https://www.R-project.org/

Reich, P. B., Sendall, K. M., Stefanski, A., Rich, R. L., Hobbie, S. E., and Montgomery, R. A. (2018). Effects of climate warming on photosynthesis in boreal tree species depend on soil moisture. *Nature* 562, 263–267. doi: 10.1038/s41586-018-0582-4

Riesmeier, J. W., Willmitzer, L., and Frommer, W. B. (1994). Evidence for an essential role of the sucrose transporter in phloem loading and assimilate partitioning. *EMBO J.* 13, 1–7. doi: 10.1002/j.1460-2075.1994.tb06229.x

Rizhsky, L., Liang, H., and Mittler, R. (2002). The combined effect of drought stress and heat shock on gene expression in tobacco. *Plant Physiol.* 130, 1143–1151. doi: 10.1104/pp.006858

Ruehr, N. K., Gast, A., Weber, C., Daub, B., and Arneth, A. (2016). Water availability as dominant control of heat stress responses in two contrasting tree species. *Tree Physiol.* 36, 164–178. doi: 10.1093/treephys/tpv102

Ruehr, N. K., Grote, R., Mayr, S., and Arneth, A. (2019). Beyond the extreme: recovery of carbon and water relations in woody plants following heat and drought stress. *Tree Physiol.* 39, 1285–1299. doi: 10.1093/treephys/tpz032

Sala, A., Piper, F., and Hoch, G. (2010). Physiological mechanisms of drought-induced tree mortality are far from being resolved. *New Phytol.* 186, 274–281. doi: 10.1111/j.1469-8137.2009.03167.x

Schuldt, B., Buras, A., Arend, M., Vitasse, Y., Beierkuhnlein, C., Damm, A., et al. (2020). A first assessment of the impact of the extreme 2018 summer drought on Central European forests. *Basic Appl. Ecol.* 45, 86–103. doi: 10.1016/j.baae.2020.04.003

Schumann, K., Leuschner, C., and Schuldt, B. (2019). Xylem hydraulic safety and efficiency in relation to leaf and wood traits in three temperate *Acer* species differing in habitat preferences. *Trees Struct. Funct.* 33. 1475–1490. doi: 10.1007/s00468-019-01874-x

Schuster, A. C., Burghardt, M., Alfarhan, A., Bueno, A., Hedrich, R., Leide, J., et al. (2016). Effectiveness of cuticular transpiration barriers in a desert plant at controlling water loss at high temperatures. *AoB Plants* 8:plw027. doi: 10.1093/aobpla/plw027

Sevanto, S. (2014). Phloem transport and drought. *J. Exp. Bot.* 65, 1751–1759. doi: 10.1093/jxb/ert467

Sperry, J. S., and Love, D. M. (2015). What plant hydraulics can tell us about responses to climate-change droughts. *New Phytol.* 207, 14–27. doi: 10.1111/nph.13354

Sperry, J. S., Venturas, M. D., Anderegg, W. R., Mencuccini, M., Mackay, D. S., Wang, Y., et al. (2017). Predicting stomatal responses to the environment from the optimization of photosynthetic gain and hydraulic cost. *Plant Cell Environ.* 40, 816–830. doi: 10.1111/pce.12852

Sperry, J. S., Venturas, M. D., Todd, H. N., Trugman, A. T., Anderegg, W. R., Wang, Y., et al. (2019). The impact of rising CO_2 and acclimation on the response of US forests to global warming. *Proc. Nat. Acad. Sci.* 116, 25734–25744. doi: 10.1073/pnas.1913072116

Sugiura, D., Terashima, I., and Evans, J. R. (2020). A decrease in mesophyll conductance by cell-wall thickening contributes to photosynthetic downregulation. *Plant Physiol.* 183, 1600–1611. doi: 10.1104/pp.20.00328

terBraak, C. J., and Vrugt, J. A. (2008). Differential evolution Markov chain with snooker updater and fewer chains. *Stat. Comput.* 18, 435–446. doi: 10.1007/s11222-008-9104-9

Tuzet, A., Perrier, A., and Leuning, R. (2003). A coupled model of stomatal conductance, photosynthesis and transpiration. *Plant Cell Environ*. 26, 1097–1116. doi: 10.1046/j.1365-3040.2003.01035.x

Tyree, M. T., and Ewers, F. W. (1991). The hydraulic architecture of trees and other woody plants. *New Phytol*. 119, 345–360. doi: 10.1111/j.1469-8137.1991.tb00035.x

Velikova, V., Arena, C., Izzo, L. G., Tsonev, T., Koleva, D., Tattini, M., et al. (2020). Functional and structural leaf plasticity determine photosynthetic performances during drought stress and recovery in two *Platanusorientalis*populations from contrasting habitats. *Int. J. Mol. Sci.* 21:3912. doi: 10.3390/ijms21113912

Vilagrosa, A., Bellot, J., Vallejo, V. R., and Gil-Pelegrín, E. (2003). Cavitation, stomatal conductance, and leaf dieback in seedlings of two co-occurring Mediterranean shrubs during an intense drought. *J. Exp. Bot*. 54, 2015–2024. doi: 10.1093/jxb/erg221

Wang, K. Y., Kellomäki, S., and Laitinen, K. (1996). Acclimation of photosynthetic parameters in Scots pine after three years exposure to elevated temperature and CO2. *Agric. For. Meteorol*. 82, 195–217. doi: 10.1016/0168-1923(96)02329-5

Whitehead, D., Edwards, W. R. N., and Jarvis, P. G. (1984). Conducting sapwood area, foliage area, and permeability in mature trees of Piceasitchensis and Pinus contorta. *Can. J. For. Res*. 14, 940–947. doi: 10.1139/x84-166

Wolfe, B. T., Sperry, J. S., and Kursar, T. A. (2016). Does leaf shedding protect stems from cavitation during seasonal droughts? A test of the hydraulic fuse hypothesis. *New Phytol*. 212, 1007–1018 doi: 10.1111/nph.14087

Xu, L., and Baldocchi, D. D. (2003). Seasonal trends in photosynthetic parameters and stomatal conductance of blue oak (*Quercus douglasii*) under prolonged summer drought and high temperature. *Tree Physiol*. 23, 865–877. doi: 10.1093/treephys/23.13.865

Yan, W., Zhong, Y., and Shangguan, Z. (2017). Rapid response of the carbon balance strategy in Robinia pseudoacacia and Amorphafruticosa to recurrent drought. *Environ. Exp. Bot*. 138, 46–56. doi: 10.1016/j.envexpbot.2017.03.009

Yang, J., Duursma, R. A., De Kauwe, M. G., Kumarathunge, D., Jiang, M., Mahmud, K., et al. (2019). Incorporating non-stomatal limitation improves the performance of leaf and canopy models at high vapour pressure deficit. *Tree Physiol*. 39, 1961–1974. doi: 10.1093/treephys/tpz103

Zhou, S., Duursma, R. A., Medlyn, B. E., Kelly, J. W., and Prentice, I. C. (2013). How should we model plant responses to drought? An analysis of stomatal and non-stomatal responses to water stress. *Agric. For. Meteorol*. 182, 204–214. doi: 10.1016/j.agrformet.2013.05.009

Conflict of Interest: The authors declare that the research was conducted in the absence of any commercial or financial relationships that could be construed as a potential conflict of interest.

Publisher's Note: All claims expressed in this article are solely those of the authors and do not necessarily represent those of their affiliated organizations, or those of the publisher, the editors and the reviewers. Any product that may be evaluated in this article, or claim that may be made by its manufacturer, is not guaranteed or endorsed by the publisher.

frontiers in Plant Science

ORIGINAL RESEARCH
published: 14 October 2021
doi: 10.3389/fpls.2021.722954

Arbuscular Mycorrhiza Symbiosis Enhances Water Status and Soil-Plant Hydraulic Conductance Under Drought

Mohanned Abdalla[1,2]* *and Mutez Ali Ahmed*[1]

[1]Chair of Soil Physics, Bayreuth Center of Ecology and Environmental Research (BayCEER), University of Bayreuth, Bayreuth, Germany, [2]Department of Horticulture, Faculty of Agriculture, University of Khartoum, Khartoum North, Sudan

Recent studies have identified soil drying as a dominant driver of transpiration reduction at the global scale. Although Arbuscular Mycorrhiza Fungi (AMF) are assumed to play a pivotal role in plant response to soil drying, studies investigating the impact of AMF on plant water status and soil-plant hydraulic conductance are lacking. Thus, the main objective of this study was to investigate the influence of AMF on soil-plant conductance and plant water status of tomato under drought. We hypothesized that AMF limit the drop in matric potential across the rhizosphere, especially in drying soil. The underlying mechanism is that AMF extend the effective root radius and hence reduce the water fluxes at the root-soil interface. The follow-up hypothesis is that AMF enhance soil-plant hydraulic conductance and plant water status during soil drying. To test these hypotheses, we measured the relation between transpiration rate, soil and leaf water potential of tomato with reduced mycorrhiza colonization (RMC) and the corresponding wild type (WT). We inoculated the soil of the WT with *Rhizophagus irregularis* spores to potentially upsurge symbiosis initiation. During soil drying, leaf water potential of the WT did not drop below −0.8 MPa during the first 6 days after withholding irrigation, while leaf water potential of RMC dropped below −1 MPa already after 4 days. Furthermore, AMF enhanced the soil-plant hydraulic conductance of the WT during soil drying. In contrast, soil-plant hydraulic conductance of the RMC declined more abruptly as soil dried. We conclude that AMF maintained the hydraulic continuity between root and soil in drying soils, hereby reducing the drop in matric potential at the root-soil interface and enhancing soil-plant hydraulic conductance of tomato under edaphic stress. Future studies will investigate the role of AMF on soil-plant hydraulic conductance and plant water status among diverse plant species growing in contrasting soil textures.

Keywords: Soil drying, AMF, rhizosphere, root water uptake, biostimulant, plant microbiome, abiotic stress

OPEN ACCESS

Edited by:
Amanda A. Cardoso, Federal University of Alfenas, Brazil

Reviewed by:
Alice Gauthey, Western Sydney University, Australia
Thiago Corrêa Souza, Federal University of Alfenas, Brazil

***Correspondence:**
Mohanned Abdalla
mohanned.abdalla-ali-abdalla@uni-bayreuth.de

Specialty section:
This article was submitted to Plant Physiology, a section of the journal Frontiers in Plant Science

Received: *09 June 2021*
Accepted: *20 September 2021*
Published: *14 October 2021*

Citation:
Abdalla M and Ahmed MA (2021) Arbuscular Mycorrhiza Symbiosis Enhances Water Status and Soil-Plant Hydraulic Conductance Under Drought. Front. Plant Sci. 12:722954. doi: 10.3389/fpls.2021.722954

INTRODUCTION

Water scarcity in soil and atmosphere escalates stress on vegetation and threatens future agricultural production and forest survival, especially in the face of climate change (Madadgar et al., 2017; Brodribb et al., 2020). Recent studies have identified soil drying as a primary cause of transpiration reduction globally, which is a greater stress factor than vapor pressure

deficit (VPD; Liu et al., 2020). Thus, detailed knowledge of water flow processes, particularly belowground, is required to fully understand and predict plant behavior under drought episodes and future climate conditions.

Water flow across the soil-plant-atmosphere continuum is driven by gradients in water potential between the atmosphere and soil. Water evaporation at the leaf surface (i.e., due to the increase in the vapor pressure deficit) creates a tension that propagates down to the roots and the soil. The leaf water potential (ψ_{leaf}) depends on both water potential in the soil (ψ_{soil}) and the hydraulic conductivities of the different elements (soil, root-soil interface, root, xylem, and leaf) composing the soil-plant continuum. Sperry and Love (2015) used a hydraulic model of water flow to propose that stomata regulation allows plants not to exceed the water supply function determined by soil-plant hydraulics. In other words, downregulation of stomata in dry conditions avoids an excessive decline in leaf water potential before approaching a critical transpiration rate. This hypothesis implies that the leaf water potentials at which stomata close depend also on belowground hydraulic properties (root, soil, and their interface). Despite their importance, studies investigating the impact of belowground traits on plant water status and soil-plant hydraulic conductance remain limited.

In wet soils, the hydraulic conductivity of soil is much higher than that of roots and hence, water flow is mainly controlled by root hydraulic conductivity (Draye et al., 2010). However, as soil dries, its conductivity drops by a few orders of magnitude, limiting the water flow toward the root surface (Passioura, 1980; Draye et al., 2010). Indeed, Carminati and Javaux (2020) combined a soil-plant hydraulic model with meta-analysis to elucidate that the loss in soil conductivity, especially at the root-soil interface, controls stomatal response during water deficit. Similarly, we have recently showed that, in tomato, the decline in soil-root hydraulic conductance was the main driver of stomatal closure (Abdalla et al., 2021). Rodriguez-Dominguez and Brodribb (2020) used a novel rehydration technique to demonstrate that the loss in hydraulic conductivity at the root-soil interface occurred in parallel with stomatal closure. In a follow-up study, Bourbia et al. (2021) showed that a decline in root hydraulic conductivity was concomitant with a stomatal closure in both herbaceous and woody species. Plants developed various strategies to deal with the drop of conductivity at the root-soil interface (Carminati et al., 2016; Ahmed et al., 2018a). For instance, in barley, root hairs were not only documented to soften the gradients in matric potential at the root-soil interface (Carminati et al., 2017) but also enhance plant water status and yield during water deficit (Marin et al., 2020). Another example is mucilage, a gel exuded at the root tip, which was shown to facilitate water uptake in drying soils (Ahmed et al., 2014). Furthermore, root-microbiome interactions (e.g., Arbuscular mycorrhiza fungi) provide fitness advantages to the host plant to mitigate water stress conditions [reviewed in Trivedi et al. (2020)].

Arbuscular mycorrhiza fungi (AMF) symbiosis, which occurs naturally between fungal and most plant species, is documented to play a positive role in plant water relations, especially under water deficit (Augé, 2001; Augé et al., 2015; Ouledali et al., 2018). For instance, Bitterlich et al. (2018b) showed that, in tomato, AMF facilitated higher transpiration rates in dry soils. Similarly, Chitarra et al. (2016) demonstrated that AMF enhanced tomato performance under water stress. The authors showed that AMF improved plant biomass and water use efficiency (Chitarra et al., 2016). In maize, Quiroga et al. (2019) reported that AMF symbiosis enabled higher stomatal conductance under soil water deficit. Furthermore, it was also suggested that AMF increase root hydraulic conductivity (Aroca et al., 2007; Quiroga et al., 2019) and alter soil hydraulic properties (Bitterlich et al., 2018a; Pauwels et al., 2020). However, the impact of AMF on soil-plant hydraulic conductance, especially in drying soil, remains unknown. Note that this would be crucial to improve our current understanding of plant response to drought (Carminati et al., 2020; Hayat et al., 2020; Rodriguez-Dominguez and Brodribb, 2020; Abdalla et al., 2021). Thus, there is an urgent need to investigate the influence of AMF on soil-plant hydraulic conductance during soil drying.

We hypothesize that AMF increase the root-soil contact and hence the effective root radius, especially in dry soil. This would reduce the flow velocity at the root surface and soften the drop in matric potential at the root-soil interface (**Figure 1**). This, in turn, would facilitate higher (less negative) leaf water potential and enhance soil-plant hydraulic conductance during soil drying.

We tested this hypothesis in tomato plants inoculated with *Rhizophagus irregularis* spores. We utilized mutant variety with highly reduced AMF symbiosis and the corresponding wild type. We measured transpiration rate, soil water content, water potentials in soil and leaf during soil drying. We used the relation between transpiration rate and leaf water potential to infer the hydraulic conductance of the soil-plant system for both genotypes during soil drying.

MATERIALS AND METHODS

Plant Preparation

We used two tomato genotypes (*Solanum lycopersicum* L.): a mutant with highly reduced AMF symbiosis (RMC) and its wild-type counterpart (WT; Barker et al., 1998). Growth was shown to be very similar in both genotypes, suggesting no pleiotropic effects of the mutation (Cavagnaro et al., 2004). Seeds were sterilized in 30% H_2O_2 for 90 s and thereafter washed and germinated on Petri dishes. The seeds were then planted in PVC columns of 30 cm in height and 9 cm in diameter. The columns had small five holes on the side, which were used for soil water content measurements during the experiment. The columns were filled with sandy soil through a 1-mm sieve. The hydraulic properties and fertilization of the soil are reported in Vetterlein et al. (2021) and in supplementary information (**Supplementary Figure S1**). To potentially upsurge AMF colonization of the WT, the soil was inoculated with commercial *R. irregularis* spores (BIOFA AG, Münstingen, Germany) in a ratio of 50 spore kg^{-1}.

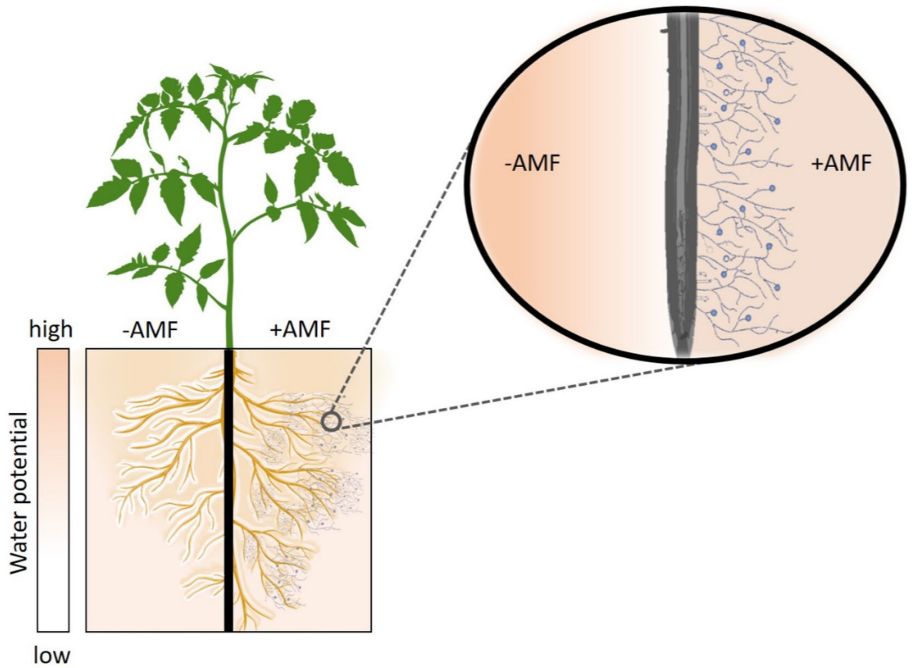

FIGURE 1 | Hypothetical role of Arbuscular Mycorrhiza Fungi (AMF) in enhancing plant water status and soil-plant hydraulic conductance. During soil drying, AMF increase the root-soil contact and extend the effective root radius hereby reducing the water fluxes at the root-soil interface and softening the drop in matric potential across the rhizosphere. The follow-up hypothesis is that AMF enhance soil-plant hydraulic conductance and plant water status during soil drying. Plants without AMF symbiosis (-AMF) require larger gradients in matric potential around their roots to sustain similar transpiration rates.

Growth Conditions

Twenty plants (10 per genotype) were placed in a climate-controlled chamber with a day/night temperature of 29/19°C, a day/night relative humidity of 51/79%, 14 h of photoperiod, and light intensity of 1,000 µmol m^{-2} s^{-1}. Plants were randomized inside the chamber. The soil surface was covered with polyolefin to prevent evaporation. We measured shoot fresh weight at the end of the experiment.

Transpiration Rate

Plants were placed into wireless balances that automatically recorded the changes in weight every 10 mins. Transpiration rate was obtained gravimetrically by calculating the difference in weight over time. We extracted the transpiration rate for predawn (no light and low VPD) and midday. Plants were irrigated daily until the start of measurements.

Leaf Water Potential Measurements

After withholding irrigation, leaf water potential was measured on daily basis at midday. A leaflet was covered with a plastic bag and lined with aluminum foil for at least 20 mins before measurement. Covered leaves were cut and placed inside a Scholander-type pressure chamber (MODEL 3115, Soil Moisture Equipment Corp, Santa Barbara, CA, Unites States) to obtain stem water potential, which was used as a proxy for leaf water potential (One leaflet was measured per plant).

Soil Dryness Assessment

Soil water content (θ) was measured daily using time-domain refractometer that encompasses two rods (spacing: 0.5 cm; length: 6 cm) connected to a data logger (E-Test, Lublin, Poland). Soil water potential was computed from the soil water content using the soil water retention curve (**Supplementary Figure S1**).

Soil-Plant Hydraulic Conductance

During soil drying, soil-plant hydraulic conductances of RMC and WT were obtained using Equation (1) as follow:

$$Ksp = E / \Delta\psi \quad (1)$$

where Ksp is soil-plant hydraulic conductance (cm^3 s^{-1} MPa^{-1}), E is transpiration rate (cm^3 s^{-1}), and $\Delta\psi$ is the difference between absolute values of leaf and soil water potentials (MPa).

AMF Abundance Assessment

Roots were collected at the end of the experiments and stored in 60% ethanol. Root samples of both genotypes were washed with distilled water, cleared with 5% KOH, and stained in 5% ink-vinegar solution to visualize AMF colonization in roots [after Vierheilig et al. (1998)]. The percentage of colonized root length was determined by recording 150 root-intersects per sample using the light microscopy (Olympus BX40) and the attached digital camera (Olympus SC50).

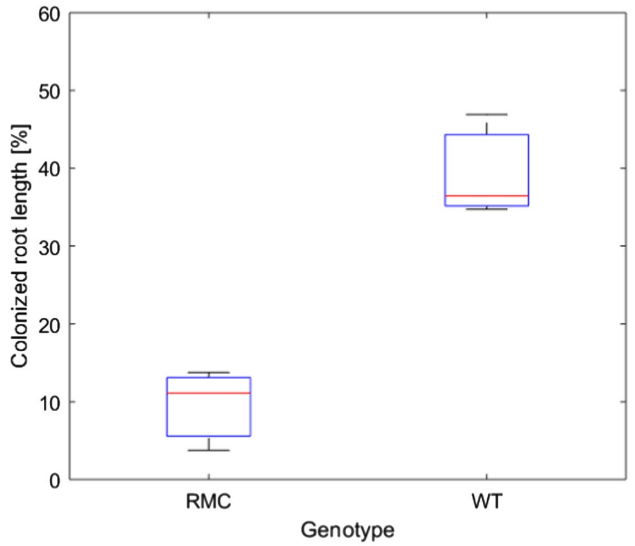

FIGURE 2 | AMF abundance assessment in roots of reduced mycorrhiza colonization (RMC) and wild-type counterpart (WT). AMF colonization was four times higher in WT compare to RMC (value of $p < 0.05$).

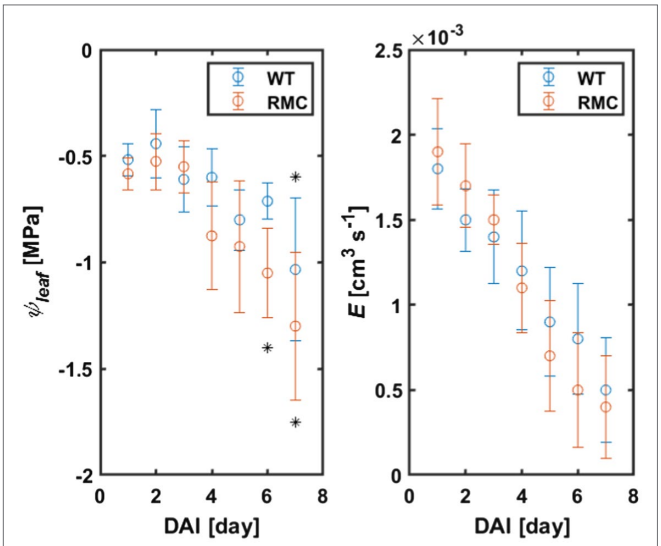

FIGURE 3 | Leaf water potential (ψ_{leaf}) and transpiration rate (E) of RMC and WT tomato during soil drying. ψ_{leaf} declined markedly in the absence of AMF, which nicely support our initial hypothesis. Asterisks denote significance decline of ψ_{leaf} (value of $p < 0.01$), on top for WT and bottom for RMC. DAI, day after last irrigation. $n = 10$.

Statistical Analysis

ANOVA was used to identify significant differences in transpiration rates, leaf water potential, and soil-plant hydraulic conductance of WT and RMC. T-test was applied to evaluate the differences in root colonization between the WT and RMC mutant. MATLAB (R2019) was used to perform the statistical analysis.

RESULTS AND DISCUSSION

We investigated the impact of AMF on plant water status and soil-plant hydraulic conductance in two tomato genotypes, reduced mycorrhiza colonization (RMC) and its wild type counterpart (WT). Plant biomass of both genotypes was similar (**Supplementary Figure S2**). Shoot fresh weight was 30.2 ± 8.2 g and 28.4 ± 7.9 g for the WT and RMC, respectively (**Supplementary Figure S2**). The root colonization of the WT was four times higher than RMC (value of $p < 0.05$; **Figure 2**). This finding is consistent with results of Zhou et al. (2020), who assessed AMF root colonization in same tomato genotypes and observed significantly higher AMF abundance in roots of WT compared to RMC.

Leaf water potential of the WT plants did not drop below −0.8 MPa 6 days after withholding irrigation, while leaf water potential of the RMC dropped below −1.0 MPa already after 4 days (value of $p < 0.01$; **Figure 3**; **Supplementary Table S1**). These results are in line with previous findings in maize, soybean, and barley (Subramanian et al., 1997; Porcel, 2004; Khalvati et al., 2005). The authors showed that, under water deficit, plants with AMF colonization exhibited higher (less negative) leaf water potential compared to plants without AMF.

Transpiration declined in both treatments as a consequence of water deficit (**Figure 3**). During soil drying, we observed, surprisingly, no differences in transpiration rate between the two genotypes (value of $p = 0.5$, **Supplementary Table S2**). These results are in line with the findings of Chitarra et al. (2016), who reported similar stomatal conductance of tomato inoculated with different AMF species and the control [see Figure 1B in Chitarra et al. (2016)]. Despite the absence of difference in transpiration rate, the authors compared the water use efficiency and demonstrated that AMF improved tomato performance under water deficit (Chitarra et al., 2016). Similar transpiration rate was also observed in inoculated and not inoculated common bean (Aroca et al., 2007). On the other hand, Bitterlich et al. (2018b) showed that, in tomato, AMF facilitate higher transpiration in dry soil. Similarly, Hallett et al. (2009) used the same genotypes and reported a significant increase in transpiration of the wild type compared to RMC mutant. These apparently contradicting findings on the impact of AMF on transpiration rate clearly suggest that the role of AMF on transpiration (and stomatal conductance) is soil, species, and environment specific. Hence, the impact of AMF on transpiration on some of these studies might have been masked out as a result of species × environment interactions, which is well known to impact transpiration (Vadez et al., 2013, 2021). Indeed, an improved performance of AMF treatment was shown in field experiments compare to greenhouse and climate-controlled experiments (where normally plants are grown in pots; Poorter et al., 2012; Augé et al., 2015). The fact that the two genotypes exhibited no significant difference in transpiration in the present study could be explained by the limited soil volume. Hence, plants and AMF had to share a limited amount of water (and nutrients) within the pot (Chitarra et al., 2016). Moreover, this explanation can potentially justify the drop in leaf water

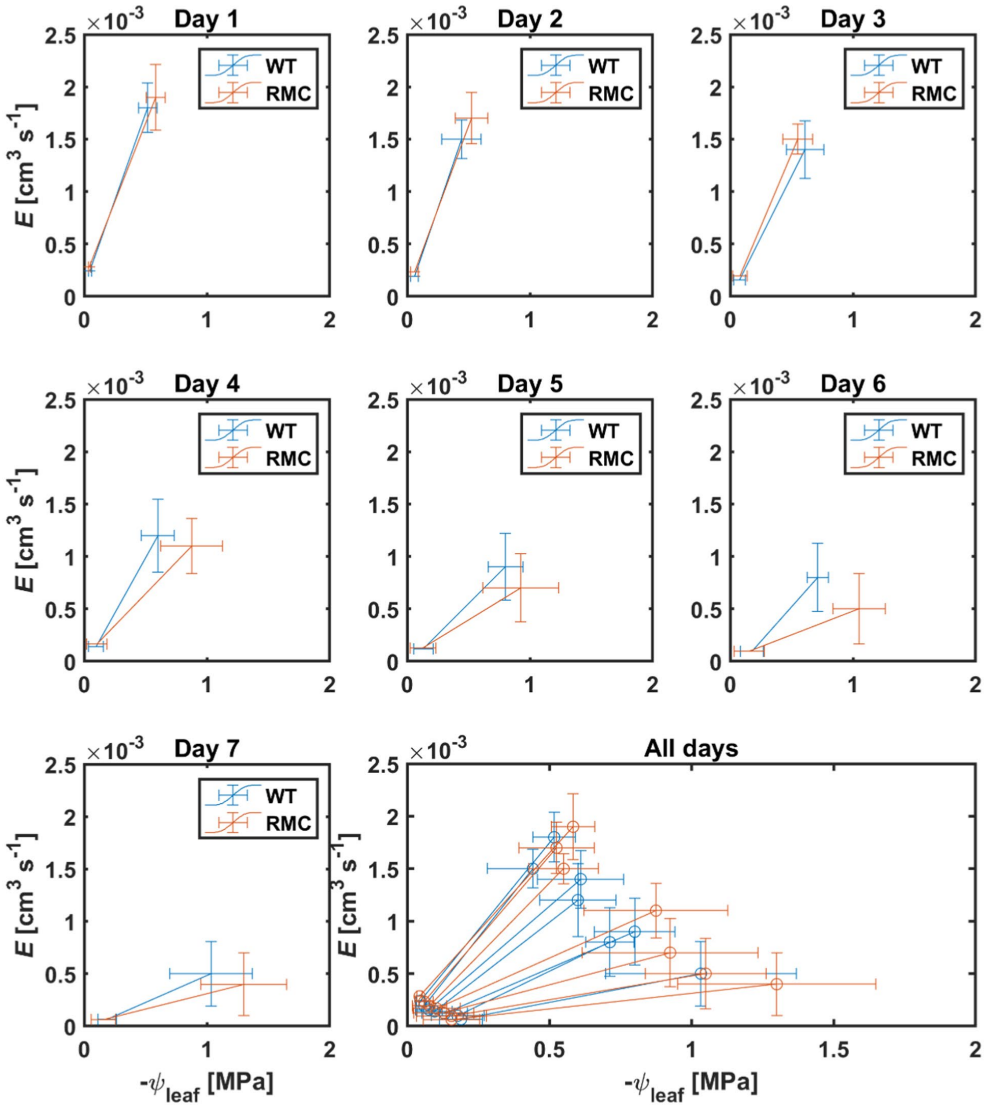

FIGURE 4 | Relation between transpiration rate (E) and leaf water potential (ψ_{leaf}) during soil drying. Subplots show the relation on daily basis after last irrigation. As soil progressively dried, the RMC plants showed lower E and more negative ψ_{leaf} on the same day compare to WT. $n = 10$.

potential in both genotypes on the seventh day after withholding irrigation (**Figure 3**).

In previous studies, simultaneous measurements of transpiration rate and leaf water potential with high temporal resolution revealed that leaf water potential drops rapidly when a critical transpiration rate is reached at a given soil water potential (Carminati et al., 2017; Abdalla et al., 2021; Cai et al., 2021). In other words, at a specific transpiration rate, leaf water potential can vary based on belowground hydraulic conductance [see Cai et al. (2021)]. In this study, we observed a decoupling in the relation between transpiration and leaf water potential (**Figure 3**). We explain this by the fact that RMC plants require larger gradients in soil water potential at the root-soil interface to sustaining a similar transpiration rate to the WT. The underlying mechanisms is that AMF extends the root surface active in water uptake, which reduces the flow velocity and attenuate the drop in matric potential at the root surface (see **Figure 1**). Hence, RMC plants exhibited more negative leaf water potential to sustain a similar transpiration rate as in WT. This would explain why RMC plants displayed more negative leaf water potential while maintaining similar transpiration rate as WT plants. These results demonstrate that the relation between transpiration rate and leaf water potential is not unique and depends on belowground hydraulics. Moreover, our data show that AMF clearly affect this relation. More work would be needed to test the impact of AMF on this relation among diverse plant species, contrasting soil types, and climatic conditions.

Another possible explanation for similar transpiration rate is that AMF colonization might influence the stomatal density.

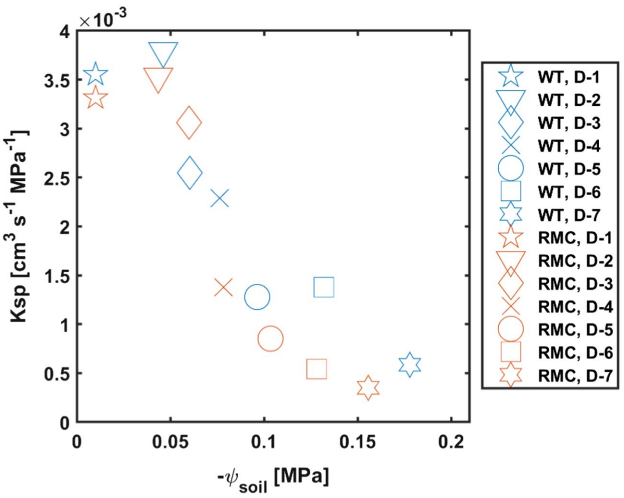

FIGURE 5 | Soil-plant hydraulic conductance (*Ksp*) decreases as soil water potential (ψ_{soil}) declines. Plants with mycorrhiza symbiosis (WT) show higher *Ksp* during soil drying (similar symbols and diverse colors) compare to RMC mutants. D, day after last irrigation. $n = 10$.

Chitarra et al. (2016) demonstrated that inoculation with *Rhizophagus intraradices* induced two times stomatal density compared to un-inoculated tomato plants or inoculated with *Funneliformis mosseae*. However, a different AMF species was used in this study, namely, *R. irregularis*, and its influences on stomatal density in tomato are yet to be explored. Nevertheless, our data on leaf water potential suggest that AMF could contribute positively, allowing tomato plants to mitigate water stress conditions.

During soil drying, the relation between transpiration and leaf water potential was affected by AMF colonization (**Figure 4**). In wet conditions, i.e., day one, both genotypes showed high transpiration and leaf water potential (**Figure 4**). As soil progressively dried, RMC showed relatively lower transpiration and more negative leaf water potential than the WT (**Figure 4**). Soil-plant hydraulic conductance (*Ksp*) was obtained from the relation between transpiration rate and leaf water potential at a given soil water potential (**Figure 5**). **Figure 5** shows that, during soil drying, WT plants exhibited a higher *Ksp* compared to RMC (**Figure 5**; value of $p = 0.06$; **Supplementary Table S3**). Note that *Ksp* is highly dependent on both transpiration rate and leaf water potential [see Equation (1)]. The marginal difference in *Ksp* is a reflection of the similar transpiration rate and the significantly different leaf water potential between the two genotypes. This finding supports our hypothesis that AMF maintain soil-root hydraulic conductance. Further, *Ksp* of RMC plants declined at less negative soil water potential compare to WT (**Figure 5**). The absence of AMF in the RMC plants entailed a severe reduction in leaf water potential as soil water potential declined, possibly due to loss of contact between root and soil (Carminati et al., 2009, 2013). On the other hand, AMF presence in the WT facilitated higher leaf water potential despite declining soil water potential (**Figure 3**). AMF could play a central role in sustaining the hydraulic continuity between root and soil, as it not only improves the unsaturated hydraulic conductivity (Bitterlich et al., 2018a; Pauwels et al., 2020), but also avoids excessive drop of soil water potential around roots.

Taken together, we have demonstrated the direct influence of AMF on soil-plant hydraulic conductance and plant water status during soil drying. WT plants exhibited higher soil-plant hydraulic conductance and leaf water potential compared to RMC plants during soil drying. We conclude that AMF extended the effective root radius hereby reducing the water fluxes at the root-soil interface and softening the drop in matric potential across the rhizosphere. This would result in an enhanced soil-plant hydraulic conductance and plant water status in drying soil. Further research is needed to directly measure the effects of AMF on water fluxes under contrasting soil textures and nutrient availabilities. The latter could be achieved using the combination of isotopes and neutron imaging (Ahmed et al., 2016, 2018b). Our data suggest that AMF could play an essential role in achieving sustainable agricultural production with greater importance in regions faced by water scarcity conditions worldwide.

DATA AVAILABILITY STATEMENT

The original contributions presented in the study are included in the article/**Supplementary Material**, and further inquiries can be directed to the corresponding author.

AUTHOR CONTRIBUTIONS

MoA and MuA designed the study and wrote the manuscript. MoA conducted the experiments and analyzed the data. All authors contributed to the article and approved the submitted version.

FUNDING

The German Academic Exchange Service (DAAD) is acknowledged for funding the doctoral position of MoA. This publication was funded by the University of Bayreuth Open Access Publishing Fund.

ACKNOWLEDGMENTS

We acknowledge Gaochao Cai, Anna Sauer, Asegid Akale, and Osman Mustafa for their help during the experiments. We thank Johanna Pausch for providing seeds of two genotypes.

SUPPLEMENTARY MATERIAL

The Supplementary Material for this article can be found online at: https://www.frontiersin.org/articles/10.3389/fpls.2021.722954/full#supplementary-material

REFERENCES

Abdalla, M., Carminati, A., Cai, G., Javaux, M., and Ahmed, M. A. (2021). Stomatal closure of tomato under drought is driven by an increase in soil–root hydraulic resistance. *Plant Cell Environ.* 44, 425–431. doi: 10.1111/pce.13939

Ahmed, M. A., Kroener, E., Holz, M., Zarebanadkouki, M., and Carminati, A. (2014). Mucilage exudation facilitates root water uptake in dry soils. *Funct. Plant Biol.* 41, 1129–1137. doi: 10.1071/FP13330

Ahmed, M. A., Passioura, J., and Carminati, A. (2018a). Hydraulic processes in roots and the rhizosphere pertinent to increasing yield of water-limited grain crops: a critical review. *J. Exp. Bot.* 69, 3255–3265. doi: 10.1093/jxb/ery183

Ahmed, M. A., Zarebanadkouki, M., Kaestner, A., and Carminati, A. (2016). Measurements of water uptake of maize roots: the key function of lateral roots. *Plant Soil* 398, 59–77. doi: 10.1007/s11104-015-2639-6

Ahmed, M. A., Zarebanadkouki, M., Meunier, F., Javaux, M., Kaestner, A., and Carminati, A. (2018b). Root type matters: measurement of water uptake by seminal, crown, and lateral roots in maize. *J. Exp. Bot.* 69, 1199–1206. doi: 10.1093/jxb/erx439

Aroca, R., Porcel, R., and Ruiz-Lozano, J. M. (2007). How does arbuscular mycorrhizal symbiosis regulate root hydraulic properties and plasma membrane aquaporins in *Phaseolus vulgaris* under drought, cold or salinity stresses? *New Phytol.* 173, 808–816. doi: 10.1111/j.1469-8137.2006.01961.x

Augé, R. M. (2001). Water relations, drought and vesicular-arbuscular mycorrhizal symbiosis. *Mycorrhiza* 11, 3–42. doi: 10.1007/s005720100097

Augé, R. M., Toler, H. D., and Saxton, A. M. (2015). Arbuscular mycorrhizal symbiosis alters stomatal conductance of host plants more under drought than under amply watered conditions: a meta-analysis. *Mycorrhiza* 25, 13–24. doi: 10.1007/s00572-014-0585-4

Barker, S. J., Stummer, B., Gao, L., Dispain, I., O'Connor, P. J., and Smith, S. E. (1998). A mutant in *Lycopersicon esculentum* Mill. with highly reduced VA mycorrhizal colonization: isolation and preliminary characterisation. *Plant J.* 15, 791–797. doi: 10.1046/j.1365-313X.1998.00252.x

Bitterlich, M., Franken, P., and Graefe, J. (2018a). Arbuscular mycorrhiza improves substrate hydraulic conductivity in the plant available moisture range under root growth exclusion. *Front. Plant Sci.* 9:301. doi: 10.3389/fpls.2018.00301

Bitterlich, M., Sandmann, M., and Graefe, J. (2018b). Arbuscular mycorrhiza alleviates restrictions to substrate water flow and delays transpiration limitation to stronger drought in tomato. *Front. Plant Sci.* 9:154. doi: 10.3389/fpls.2018.00154

Bourbia, I., Pritzkow, C., and Brodribb, T. J. (2021). Herb and conifer roots show similar high sensitivity to water deficit. *Plant Physiol.* 186, 1908–1918. doi: 10.1093/plphys/kiab207

Brodribb, T. J., Powers, J., Cochard, H., and Choat, B. (2020). Hanging by a thread? Forests and drought. *Science* 368, 261–266. doi: 10.1126/science.aat7631

Cai, G., Carminati, A., Abdalla, M., and Ahmed, M. A. (2021). Soil textures rather than root hairs dominate water uptake and soil-plant hydraulics under drought. *Plant Physiol.* doi: 10.1093/plphys/kiab271, [Epub ahead of print]

Carminati, A., Ahmed, M. A., Zarebanadkouki, M., Cai, G., Lovric, G., and Javaux, M. (2020). Stomatal closure prevents the drop in soil water potential around roots. *New Phytol.* 226, 1541–1543. doi: 10.1111/nph.16451

Carminati, A., and Javaux, M. (2020). Soil rather than xylem vulnerability controls stomatal response to drought. *Trends Plant Sci.* 25, 868–880. doi: 10.1016/j.tplants.2020.04.003

Carminati, A., Passioura, J. B., Zarebanadkouki, M., Ahmed, M. A., Ryan, P. R., Watt, M., et al. (2017). Root hairs enable high transpiration rates in drying soils. *New Phytol.* 216, 771–781. doi: 10.1111/nph.14715

Carminati, A., Vetterlein, D., Koebernick, N., Blaser, S., Weller, U., and Vogel, H.-J. (2013). Do roots mind the gap? *Plant Soil* 367, 651–661. doi: 10.1007/s11104-012-1496-9

Carminati, A., Vetterlein, D., Weller, U., Vogel, H.-J., and Oswald, S. E. (2009). When roots lose contact. *Vadose Zone J.* 8, 805–809. doi: 10.2136/vzj2008.0147

Carminati, A., Zarebanadkouki, M., Kroener, E., Ahmed, M. A., and Holz, M. (2016). Biophysical rhizosphere processes affecting root water uptake. *Ann. Bot.* 118, 561–571. doi: 10.1093/aob/mcw113

Cavagnaro, T. R., Smith, F. A., Hay, G., Carne-Cavagnaro, V. L., and Smith, S. E. (2004). Inoculum type does not affect overall resistance of an arbuscular mycorrhiza-defective tomato mutant to colonisation but inoculation does change competitive interactions with wild-type tomato. *New Phytol.* 161, 485–494. doi: 10.1111/j.1469-8137.2004.00967.x

Chitarra, W., Pagliarani, C., Maserti, B., Lumini, E., Siciliano, I., Cascone, P., et al. (2016). Insights on the impact of arbuscular mycorrhizal symbiosis on tomato tolerance to water stress. *Plant Physiol.* 171, 1009–1023. doi: 10.1104/pp.16.00307

Draye, X., Kim, Y., Lobet, G., and Javaux, M. (2010). Model-assisted integration of physiological and environmental constraints affecting the dynamic and spatial patterns of root water uptake from soils. *J. Exp. Bot.* 61, 2145–2155. doi: 10.1093/jxb/erq077

Hallett, P. D., Feeney, D. S., Bengough, A. G., Rillig, M. C., Scrimgeour, C. M., and Young, I. M. (2009). Disentangling the impact of AM fungi versus roots on soil structure and water transport. *Plant Soil* 314, 183–196. doi: 10.1007/s11104-008-9717-y

Hayat, F., Ahmed, M. A., Zarebanadkouki, M., Javaux, M., Cai, G., and Carminati, A. (2020). Transpiration reduction in maize (*Zea mays* L) in response to soil drying. *Front. Plant Sci.* 10:1695. doi: 10.3389/fpls.2019.01695

Khalvati, M. A., Hu, Y., Mozafar, A., and Schmidhalter, U. (2005). Quantification of water uptake by arbuscular mycorrhizal hyphae and its significance for leaf growth, water relations, and gas exchange of barley subjected to drought stress. *Plant Biol.* 7, 706–712. doi: 10.1055/s-2005-872893

Liu, L., Gudmundsson, L., Hauser, M., Qin, D., Li, S., and Seneviratne, S. I. (2020). Soil moisture dominates dryness stress on ecosystem production globally. *Nat. Commun.* 11:4892. doi: 10.1038/s41467-020-18631-1

Madadgar, S., AghaKouchak, A., Farahmand, A., and Davis, S. J. (2017). Probabilistic estimates of drought impacts on agricultural production. *Geophys. Res. Lett.* 44, 7799–7807. doi: 10.1002/2017GL073606

Marin, M., Feeney, D. S., Brown, L. K., Naveed, M., Ruiz, S., Koebernick, N., et al. (2020). Significance of root hairs for plant performance under contrasting field conditions and water deficit. *Ann. Bot.* 128, 1–16. doi: 10.1093/aob/mcaa181

Ouledali, S., Ennajeh, M., Zrig, A., Gianinazzi, S., and Khemira, H. (2018). Estimating the contribution of arbuscular mycorrhizal fungi to drought tolerance of potted olive trees (*Olea europaea*). *Acta Physiol. Plant.* 40:81. doi: 10.1007/s11738-018-2656-1

Passioura, J. B. (1980). The transport of water from soil to shoot in wheat seedlings. *J. Exp. Bot.* 31, 333–345. doi: 10.1093/jxb/31.1.333

Pauwels, R., Jansa, J., Püschel, D., Müller, A., Graefe, J., Kolb, S., et al. (2020). Root growth and presence of *Rhizophagus irregularis* distinctly alter substrate hydraulic properties in a model system with *Medicago truncatula*. *Plant Soil* 457, 131–151. doi: 10.1007/s11104-020-04723-w

Poorter, H., Bühler, J., Dusschoten, D.van, Climent, J., Postma, J. A., Poorter, H., et al. (2012). Pot size matters: a meta-analysis of the effects of rooting volume on plant growth. *Funct. Plant Biol.* 39, 839–850. doi:10.1071/FP12049.

Porcel, R. (2004). Arbuscular mycorrhizal influence on leaf water potential, solute accumulation, and oxidative stress in soybean plants subjected to drought stress. *J. Exp. Bot.* 55, 1743–1750. doi: 10.1093/jxb/erh188

Quiroga, G., Erice, G., Ding, L., Chaumont, F., Aroca, R., and Ruiz-Lozano, J. M. (2019). The arbuscular mycorrhizal symbiosis regulates aquaporins activity and improves root cell water permeability in maize plants subjected to water stress. *Plant Cell Environ.* 42, 2274–2290. doi: 10.1111/pce.13551

Rodriguez-Dominguez, C. M., and Brodribb, T. J. (2020). Declining root water transport drives stomatal closure in olive under moderate water stress. *New Phytol.* 225, 126–134. doi: 10.1111/nph.16177

Sperry, J. S., and Love, D. M. (2015). What plant hydraulics can tell us about responses to climate-change droughts. *New Phytol.* 207, 14–27. doi: 10.1111/nph.13354

Subramanian, K. S., Charest, C., Dwyer, L. M., and Hamilton, R. I. (1997). Effects of arbuscular mycorrhizae on leaf water potential, sugar content, and P content during drought and recovery of maize. *Can. J. Bot.* 75, 1582–1591.

Trivedi, P., Leach, J. E., Tringe, S. G., Sa, T., and Singh, B. K. (2020). Plant–microbiome interactions: from community assembly to plant health. *Nat. Rev. Microbiol.* 18, 607–621. doi: 10.1038/s41579-020-0412-1

Vadez, V., Choudhary, S., Kholová, J., Hash, C. T., Srivastava, R., Kumar, A. A., et al. (2021). Transpiration efficiency: insights from comparisons of C4 cereal species. *J. Exp. Bot.* 72, 5221–5234. doi: 10.1093/jxb/erab251

Vadez, V., Kholova, J., Zaman-Allah, M., and Belko, N. (2013). Water: the most important 'molecular' component of water stress tolerance research. *Funct. Plant Biol.* 40, 1310–1322. doi: 10.1071/FP13149

Vetterlein, D., Lippold, E., Schreiter, S., Phalempin, M., Fahrenkampf, T., Hochholdinger, F., et al. (2021). Experimental platforms for the investigation of spatiotemporal patterns in the rhizosphere—laboratory and field scale. *J. Plant Nutr. Soil Sci.* 184, 35–50. doi: 10.1002/jpln.202000079

Vierheilig, H., Coughlan, A. P., Wyss, U., and Piché, Y. (1998). Ink and vinegar, a simple staining technique for arbuscular-mycorrhizal fungi. *Appl. Environ. Microbiol.* 64, 5004–5007. doi: 10.1128/AEM.64.12.5004-5007.1998

Zhou, J., Zang, H., Loeppmann, S., Gube, M., Kuzyakov, Y., and Pausch, J. (2020). Arbuscular mycorrhiza enhances rhizodeposition and reduces the rhizosphere priming effect on the decomposition of soil organic matter. *Soil Biol. Biochem.* 140:107641. doi: 10.1016/j.soilbio.2019.107641

Conflict of Interest: The authors declare that the research was conducted in the absence of any commercial or financial relationships that could be construed as a potential conflict of interest.

Publisher's Note: All claims expressed in this article are solely those of the authors and do not necessarily represent those of their affiliated organizations, or those of the publisher, the editors and the reviewers. Any product that may be evaluated in this article, or claim that may be made by its manufacturer, is not guaranteed or endorsed by the publisher.

frontiers in Plant Science

ORIGINAL RESEARCH
published: 25 October 2021
doi: 10.3389/fpls.2021.693815

High Leaf Vein Density Promotes Leaf Gas Exchange by Enhancing Leaf Hydraulic Conductance in *Oryza sativa* L. Plants

Miao Ye[1,2], *Meng Wu*[1], *Hao Zhang*[1], *Zuolin Zhang*[2] *and Zujian Zhang*[1]*

[1] Key Laboratory of Crop Genetics and Physiology of Jiangsu Province, Jiangsu Key Laboratory of Crop Cultivation and Physiology, Co-innovation Center for Modern Production Technology of Grain Crops, Yangzhou University, Yangzhou, China, [2] Ministry of Agriculture Key Laboratory of Crop Ecophysiology and Farming System in the Middle Reaches of the Yangtze River, College of Plant Science and Technology, Huazhong Agricultural University, Wuhan, China

Six cultivated rice genotypes showing different stomatal conductance (g_s) values were used to investigate the influence of leaf vein traits on leaf gas exchange and leaf hydraulics. The results showed that g_s was the main determinant of the varietal difference in the net photosynthetic rate (P_N), whereas the area-based leaf nitrogen content (N_{area}) and mesophyll conductance (g_m) were not main factors. g_s and P_N were both positively correlated with leaf hydraulic conductance (K_{leaf}). A high density of leaf veins (vein length per leaf area, VLA), especially minor leaf veins (VLA_{minor}), was of benefit for improving the K_{leaf}. The proportion of the minor leaf vein length to the total leaf vein length did not impact the leaf hydraulics or leaf gas exchange. Overall, these findings suggested that a high density of leaf veins, especially minor leaf veins, enhances K_{leaf} and promotes g_s and P_N in cultivated rice genotypes and a high VLA can be regarded as a high photosynthetic capacity trait in rice plants.

Keywords: cultivated rice (*Oryza sativa* L.), leaf gas exchange, stomatal conductance, leaf hydraulics, leaf vein density

OPEN ACCESS

Edited by:
Joan Laur,
Montreal Botanical Garden, Canada

Reviewed by:
Elizabeth Van Volkenburgh,
University of Washington,
United States
Debabrata Panda,
Central University of Orissa,
Koraput, India
Yusuke Mizokami,
Tokyo University of Pharmacy and Life Sciences, Japan

***Correspondence:**
Zujian Zhang
zzj@yzu.edu.cn

Specialty section:
This article was submitted to Plant Physiology, a section of the journal Frontiers in Plant Science

Received: *12 April 2021*
Accepted: *20 September 2021*
Published: *25 October 2021*

Citation:
Ye M, Wu M, Zhang H, Zhang Z and Zhang Z (2021) High Leaf Vein Density Promotes Leaf Gas Exchange by Enhancing Leaf Hydraulic Conductance in Oryza sativa L. Plants. Front. Plant Sci. 12:693815. doi: 10.3389/fpls.2021.693815

INTRODUCTION

Under the current ambient atmospheric conditions, CO_2 diffusional conductance from air to carboxylation sites is regarded as one of the main limiting factors of net photosynthetic rate (P_N) in C_3 plants (Evans et al., 2009; Li et al., 2009; Yamori et al., 2011; Flexas et al., 2012; Adachi et al., 2013; Gago et al., 2019). To reach carboxylation sites, CO_2 in the air must first overcome the air–leaf boundary resistance to reach the surroundings of the stomata, and it then enters the stomatal pores to reach the substomatal cavity, diffuses to the surroundings of the cell wall, and successively passes through the cell wall, cell membrane, cytoplasm, chloroplast envelope, and the stroma (Terashima et al., 2011; Tholen et al., 2012). The CO_2 diffusional resistance from air to the surface of the leaf is called boundary layer resistance, the CO_2 diffusional resistance from air to the substomatal cavity is called stomatal resistance, and the CO_2 diffusional resistance from the substomatal cavity to the carboxylation sites is called mesophyll resistance. Mesophyll resistance can be as important as stomatal resistance under many conditions (Terashima et al., 2011), although it was ignored in earlier studies (Farquhar et al., 1980; Kodama et al., 2011). The reciprocals of stomatal resistance and mesophyll resistance are called stomatal conductance (g_s) and mesophyll conductance (g_m),

respectively. Many previous studies have shown that P_N is positively correlated with both g_s and g_m (Giuliani et al., 2013; Carriquí et al., 2015; Liu and Li, 2016).

Stomatal pores are the common pathway for CO_2 entering the leaf and H_2O evaporating from the leaf. g_s is mainly determined by the stomatal size, stomatal density and distribution, and especially by the stomatal aperture (Xu and Zhou, 2008; Ocheltree et al., 2012; Ouyang et al., 2017). g_s has been found to be closely linked to plant hydraulics (Hirasawa et al., 1992; Brodribb et al., 2007; Xiong and Nadal, 2020). Tabassum et al. (2016) reported that the P_N, g_s, and the transpiration rate (E) values in *Oryza sativa* L. plants were all positively correlated with whole-plant hydraulic conductance.

As leaf hydraulic conductance (K_{leaf}) is one of the key components of whole-plant hydraulic conductance (Sack et al., 2003; Sack and Holbrook, 2006), it is vitally important for determining leaf gas exchange parameters. Brodribb et al. (2007) found that P_N was positively correlated with K_{leaf} across diverse terrestrial plants. Hirasawa et al. (1992) found that g_s was positively correlated with K_{leaf} in rice plants across different light and chemical treatments. Taylaran et al. (2011) found that the P_N of the high-yield rice cultivar Takanari was higher than that of the other common rice cultivars, which was partly due to its higher K_{leaf}. In higher plants, transpiration drives water from the stem into the petiole, and then, the water enters the midrib, flows in an orderly fashion to different vein branches, passes through the vascular bundle sheath, enters the mesophyll tissue, evaporates into the intercellular airspace, and finally diffuses out of the leaf from stomatal pores (Rockwell et al., 2014; Xiong et al., 2017). Thus, leaf hydraulic transport can be divided into xylem hydraulic transport and outside-xylem hydraulic transport.

According to the water transport route inside leaves, K_{leaf} is mainly determined by the leaf vein traits such as the leaf vein density, the size of the xylem conduits within the bundle sheath (Flexas et al., 2013), and the leaf anatomical traits such as the fraction of intercellular airspace (Xiong et al., 2017). Many recent studies have focused on the relationships between K_{leaf} and leaf vein density (vein length per leaf area, VLA) (Xiong et al., 2015; Tabassum et al., 2016). Although a few studies have demonstrated that K_{leaf} showed no or even negative relationships with VLA, most studies illustrated that a high VLA is beneficial for improving K_{leaf} and promoting g_s and P_N (Sack and Frole, 2006; Brodribb et al., 2007; Boyce et al., 2009; Brodribb and Field, 2010; McKown et al., 2010; Field et al., 2011; Walls, 2011; Nardini et al., 2012; Flexas et al., 2013). High VLA can improve the parallel transport pathways per leaf area, thus improving the xylem hydraulic conductance (K_x), and it can also shorten the distance from veins to evaporating sites, thus improving the outside-xylem hydraulic conductance (K_{ox}) (Sack and Frole, 2006; Brodribb et al., 2007; Sack et al., 2013; Buckley et al., 2015).

Nevertheless, VLA was found to affect K_x but not K_{ox} or K_{leaf} across *Oryza* species, including cultivated and wild genotypes (Xiong et al., 2015, 2017). The irrelevance of K_{ox} and K_{leaf} with VLA may be due to the low ratio of xylem hydraulic resistance (R_x) to leaf hydraulic resistance (R_{leaf}), which is only 40% (Xiong et al., 2017). Thus, although a high VLA improved K_x, the improvement in K_x contributed to K_{leaf} very slightly. Although the average R_x/R_{leaf} in *Oryza* species was only 40%, the ratios in cultivated rice genotypes were much higher than 40% (Xiong et al., 2017), which may be due to the increase in VLA during domestication. Thus, although no correlations were found between K_{leaf} and VLA across *Oryza* species, these correlations may exist when only considering cultivated rice genotypes because cultivated genotypes have relatively high R_x/R_{leaf} (Xiong et al., 2017). Therefore, we hypothesized that in cultivated rice genotypes in which R_x/R_{leaf} is relatively high, high VLA can enhance K_{leaf} and promote leaf gas exchange.

In fact, the correlations among leaf gas exchange, leaf hydraulics, and leaf vein traits have already attracted a lot of attention. For example, Brodribb et al. (2007) reported that leaf maximum photosynthetic rate and venation are linked by hydraulics across 43 species. Brocious and Hacke (2016) found that stomatal conductance was positively correlated with the transport capacity of the petiole, estimated from the diameter and number of xylem vessels, whereas the variation in stomatal conductance and leaf hydraulic conductance was not linked to vein density or other anatomical lamina properties across different *populus* genotypes. However, most previous studies were done in wood species, and rare studies were done in cereal species, especially in rice.

In the present study, six rice genotypes that showed different g_s values in a previous study (Ye et al., 2019) were selected to verify the hypothesis that high VLA can enhance K_{leaf} and promote leaf gas exchange in cultivated rice genotypes. The results may provide insights for high photosynthetic capacity rice breeding.

MATERIALS AND METHODS

Plant Materials

A pot experiment was conducted at the Huazhong Agricultural University (114.37°E, 30.48°N), Wuhan, Hubei Province, China. Six cultivated rice genotypes (*O. sativa* L.) found worldwide were used, including Kirmizi Celtik, Huayou 675, Teqing, Huanghuazhan, Champa, and N22. The g_s of these six genotypes varied greatly in the study by Ye et al. (2019), thus indicating feasibility for studying the underlying mechanisms for different g_s and P_N values in rice. Rice plants were grown from September to December 2014. After germination on moist filters, seeds were transferred to nursery plates. When the seedlings had developed an average of three leaves, they were transplanted to 11 L pots with a density of three hills per pot and two seedlings per hill. There were five pots per genotype, and each pot was filled with 10 kg of soil. The soil used for the experiment had a clay loam texture, with pH 6.63, organic matter 6.42 g/kg, total nitrogen (N) 0.07 mg/kg, available phosphorus (P) 8.21 mg/kg, and available potassium (K) 126.95 mg/kg. P and K were applied as basal fertilizers at an amount of 1.5 g/pot. N was applied at an amount of 2.0 g(N)/pot, with 40% applied as a basal fertilizer, and 60% applied at the mid-tillering stage. Plants were watered daily, and a minimum 2 cm water layer was maintained to avoid drought stress. Pests were intensively controlled using chemical pesticides.

Rice plants were grown outdoors. All genotypes were arranged in a random design with five replicates. The radiation

intensity, average temperature, and relative humidity during rice growth were 12.6 ± 5.7 MJ/m^2/d, 23.3 ± 3.4°C, and 74.4 ± 10.4%, respectively. Gas exchange measurements were conducted in a growth chamber (Conviron GR48, Controlled Environments Limited, Winnipeg, MB, Canada) [photosynthetic photon flux density (PPFD), 1,000 μmol(photo)/m^2/s at the leaf level; temperature, 28°C; relative humidity, 60%; and CO_2 concentration, 400 μmol/mol] to avoid the influence of a changing environment on gas exchange parameters. The vapor pressure deficit between leaf and air ($VPD_{leaf-air}$) of the six rice genotypes during the measurements is shown in **Supplementary Table 1**. The measurements were conducted 2 weeks after mid-tillering fertilization, and all measurements were conducted on the newly expanded leaves from three different pots of each genotype.

Gas Exchange and Chlorophyll Fluorescence Measurements

A portable photosynthesis system (LI-6400XT, LI-CORInc., Lincoln, NE, United States) with an integrated fluorescence leaf chamber (Li-6400-40; Li-Cor) was used to measure gas exchange and chlorophyll fluorescence on leaves between 08:00 and 16:00. Measurements began after the plants had acclimatized to the chamber for ∼2 h. In the LI-6400XT cuvette, the ambient CO_2 concentration was controlled and set to 400 μmol/mol, the leaf temperature was maintained at 28°C, the PPFD was 1,500 μmol(photo)/m^2/s, and the flow rate was 500 μmol/s. After reaching a steady state, which usually takes 25 min, the gas exchange parameters, steady-state fluorescence (F_s), and maximum fluorescence (F_m') were recorded with a light saturating pulse of 8,000 μmol(photo)/m^2/s. The actual photochemical efficiency of photosystem II (Φ_{PSII}) was calculated as follows:

$$\Phi_{PSII} = \frac{(F_m' - F_s)}{F_m'} \quad (1)$$

The electron transport rate (J) was calculated as follows:

$$J = PPFD \times \alpha\beta \times \Phi_{PSII} \quad (2)$$

where α is the leaf absorptance and β is the partitioning of absorbed quanta between photosystem II and photosystem I. The product $\alpha\beta$ was determined from the slope of the relationship between Φ_{PSII} and the quantum efficiency of CO_2 uptake (Φ_{CO2}), which was obtained by varying the light intensity under non-photorespiratory conditions at <2% O_2 (Valentini et al., 1995).

The variable J method described by Harley et al. (1992) was used to calculate the chloroplastic CO_2 concentration (C_c) and g_m. C_c and g_m were calculated as follows:

$$C_c = \frac{\Gamma^* \times [J + 8 \times (P_N + R_d)]}{J - 4 \times (P_N + R_d)} \quad (3)$$

$$g_m = \frac{P_N}{C_i - C_c} \quad (4)$$

where Γ* represents the CO_2 compensation point in chloroplasts without day respiration. The day respiration (R_d) and the apparent CO_2 photocompensation point (C_i^*) were determined using the Laisk method (Brooks and Farquhar, 1985). Briefly, A/C_i (A, net photosynthetic rate; C_i, intercellular CO_2 concentration) curves were measured over the linear portion of the response curve (at 100, 80, 50, and 25 μmol CO_2/mol air) over three PPFDs (150, 300, and 600 μmol/m^2/s) with an LI 6400-02B chamber (Li-Cor), and then linear regressions to the responses for each PPFD were fitted for individual leaves. The intersection point of three A/C_i curves was considered as C_i^* (x-axis) and R_d (y-axis) (von Caemmerer et al., 1994). Γ* was calculated as follows:

$$\Gamma^* = C_i^* + R_d/g_m \quad (5)$$

The Γ* and R_d of the six rice genotypes are shown in **Supplementary Table 2**.

Leaf Hydraulic Conductance

The evaporative flux method (EFM) was used to determine the K_{leaf} (Sack et al., 2002; Brodribb et al., 2007; Guyot et al., 2012; Sack and Scoffoni, 2012; Tabassum et al., 2016). A leaf of each genotype was excised in water, and the base of the leaf was placed in a test tube filled with distilled water under favorable conditions for transpiration (in a growth chamber under a PPFD of 1,000 μmol(photo)/m^2/s and air temperature of 28°C). Immediately after placing the leaf in a test tube filled with distilled water, the leaf was attached to a Li-COR 6400XT portable infrared gas analyzer (IRGA) (LI-COR, NE, United States) to record the leaf transpiration rate (E). A Dewpoint Potential Meter WP4C (Decagon, Pullman, WA, United States) was used to measure the leaf water potential (Ψ_{leaf}) of the leaf that was used to measure E. K_{leaf} was calculated as follows (Taylaran et al., 2011):

$$K_{leaf} = \frac{E}{0 - \Psi_{leaf}} \quad (6)$$

Leaf Morphological Traits

Leaf width was measured *in vivo*, and leaves were excised to count the major veins (midrib vein and large veins) and minor veins separately under 40× magnification using a light microscope (SA3300, Beijing Tech Instrument Co., Ltd, Beijing, China). Four leaves were counted for each genotype. As rice leaf veins are parallel to each other, the major leaf vein density (VLA_{major}), minor leaf vein density (VLA_{minor}), and total leaf vein density (VLA) were calculated as follows:

$$VLA_{major} = \frac{\text{Numbers of leaf major veins} \times \text{leaf Length}}{\text{Leaf width} \times \text{leaf length}} \quad (7)$$

$$VLA_{minor} = \frac{\text{Numbers of leaf minor veins} \times \text{leaf Length}}{\text{Leaf width} \times \text{leaf length}} \quad (8)$$

$$VLA = VLA_{major} + VLA_{minor} \quad (9)$$

Leaf Nitrogen Content

The leaf used for gas exchange measurements was detached, and another two leaves were also detached, then the leaf

TABLE 1 | Gas exchange parameters and area-based leaf nitrogen content (N_{area}) of the six rice genotypes.

Genotype	P_N (μmol/m²/s)	N_{area}(g/m²)	g_s (mol/m²/s)	g_m (mol/m²/s)
Champa	36.2 ± 0.5 a	1.80 ± 0.01 b	0.46 ± 0.03 a	0.31 ± 0.05 a
Huayou 675	35.3 ± 1.2 a	1.64 ± 0.13 b	0.45 ± 0.07 a	0.26 ± 0.05 ab
Teqing	27.7 ± 2.7 bc	1.69 ± 0.08 b	0.22 ± 0.01 c	0.33 ± 0.04 a
Huanghuazhan	30.0 ± 2.0 b	1.75 ± 0.11 b	0.31 ± 0.04 b	0.27 ± 0.02 ab
Kirmizi Celtik	25.6 ± 1.9 c	2.06 ± 0.08 a	0.22 ± 0.03 c	0.23 ± 0.02 b
N22	21.2 ± 3.6 d	1.23 ± 0.05 c	0.18 ± 0.05 c	0.31 ± 0.08 a
ANOVA				
Average	29.3	1.69	0.31	0.29
Genotype	***	***	***	ns

*Data are shown as the means ± SD of three replicates. *** indicates significance at the 0.001 level; ns indicates not significant at the 0.05 level. Within a column, different letters represent data that are significantly different from each other in the LSD (0.05).*

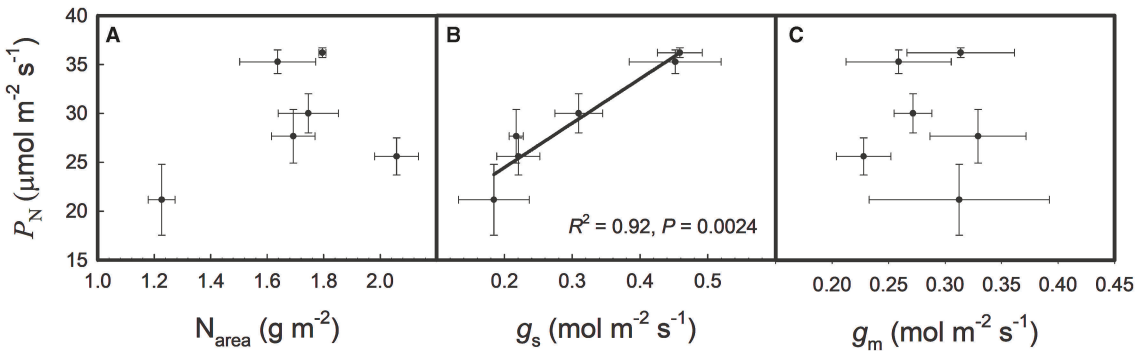

FIGURE 1 | Relationships of net photosynthetic rate (P_N) with: **(A)** area-based leaf nitrogen content (N_{area}), **(B)** stomatal conductance (g_s), and **(C)** mesophyll conductance (g_m) across the six rice genotypes. Data are shown as the means ± SD of three replicates.

area of these three leaves was measured using a LI-Cor 3000C (LI-COR Inc., Lincoln, NE, United States) leaf area analyzer. Leaves were then oven-dried at 80°C until they achieved a constant weight. Afterward, the leaf dry mass was weighed and the leaf mass per area (LMA) was calculated as the ratio of the leaf dry mass to leaf area. The leaf N content based on leaf mass (N_{mass}, %) was measured with an Elementar Vario MAX CN analyzer (Elementar Analysesysteme GmbH, Hanau, Germany), and the area-based leaf N content (N_{area}) was calculated by multiplying N_{mass} with LMA.

Statistical Analysis

One-way analysis of variance (ANOVA) was used to assess the effects of the genotypes on each parameter using Statistix 9.0 software (Analytical Software, Tallahassee, FL, United States). Parameters were compared between genotypes based on the least significant difference (LSD) test level at the 0.05 probability level. Graphs were created, and a linear regression analysis was performed to test the correlations between the parameters using SigmaPlot 10.0 (Systat Software Inc., CA, United States).

RESULTS

Varietal Differences in Leaf Gas Exchange Parameters and N_{area}

As shown in **Table 1**, P_N, N_{area}, and g_s showed significant varietal differences among the six rice genotypes. P_N ranged from 21.2 to 36.2 μmol/m²/s, and the highest and the lowest values were found in Champa and N22, respectively. Kirmizi Celtik showed the highest N_{area} of 2.03 g/m² and N22 showed the lowest N_{area} of 1.23 g/m². g_s ranged from 0.18 to 0.46 mol/m²/s and the highest and lowest values were found in Champa and N22, respectively. g_m showed no significant varietal difference among the six rice genotypes. The highest g_m was 0.33 mol/m²/s, which was found in Teqing, whereas the lowest g_m was 0.23 mol/m²/s, which was found in Kirmizi Celtik. As shown in **Figure 1**, P_N was not correlated with N_{area} or g_m but was positively correlated with g_s across the six rice genotypes.

Varietal Differences in the Leaf Morphological Traits and Leaf Hydraulics

As shown in **Table 2**, leaf width showed significant varietal differences. Champa possessed the widest leaf of 14.2 mm, whereas Kirmizi Celtik possessed the narrowest leaf of 9.4 mm.

TABLE 2 | Leaf morphological traits and leaf hydraulics of the six rice genotypes.

Genotype	Leaf width (mm)	VLA (mm/ mm^2)	VLA_{major} (mm/mm^2)	VLA_{minor} (mm/mm^2)	Proportion of minor leaf vein length to total leaf vein length (%)	E (mmol/m^2/s)	Ψ_{leaf} (MPa)	K_{leaf} (mmol/m^2/s/MPa)
Champa	14.2 ± 0.8 a	4.98 ± 0.19 a	0.81 ± 0.09 a	4.16 ± 0.17 a	83.6 ± 1.5 a	8.95 ± 0.21 a	−0.69 ± 0.03 a	13.0 ± 0.9 a
Huayou 675	11.2 ± 0.1 cd	4.94 ± 0.32 ab	0.82 ± 0.05 a	4.11 ± 0.36 a	83.2 ± 2.2 a	8.31 ± 1.90 a	−0.64 ± 0.09 a	12.9 ± 2.6 a
Teqing	13.4 ± 2.7 ab	4.58 ± 0.46 ab	0.80 ± 0.13 a	3.77 ± 0.38 a	82.5 ± 1.9 a	7.66 ± 1.28 a	−0.73 ± 0.22 a	10.6 ± 1.8 ab
Huanghuazhan	10.8 ± 1.2 cd	4.55 ± 0.21 ab	0.72 ± 0.05 ab	3.83 ± 0.20 a	84.1 ± 1.0 a	8.04 ± 1.09 a	−0.68 ± 0.03 a	11.7 ± 1.1 ab
Kirmizi Celtik	9.4 ± 0.8 d	4.34 ± 0.83 b	0.72 ± 0.09 ab	3.62 ± 0.82 a	82.9 ± 3.8 a	7.05 ± 0.93 a	−0.74 ± 0.15 a	9.6 ± 1.2 b
N22	11.8 ± 1.5 bc	4.32 ± 0.14 b	0.66 ± 0.04 b	3.66 ± 0.14 a	84.7 ± 0.9 a	7.86 ± 2.30 a	−0.81 ± 0.09 a	9.7 ± 2.4 b
ANOVA								
Average	11.8	4.62	0.76	3.86	83.5	7.98	−0.71	11.3
Genotype	**	ns	*	ns	ns	ns	ns	ns

*Data are shown as the means ± SD. There were four replicates for leaf morphological traits and three replicates for E, Ψ_{leaf}, and K_{leaf}. * and ** indicate significance at the 0.05 and 0.01 levels, respectively; ns indicates non-significant at the 0.05 level. Within a column, different letters represent data that are significantly different from each other in the LSD (0.05). VLA, vein length per leaf area.*

VLA, VLA_{minor}, and the proportion of minor leaf vein length to the total leaf vein length all showed no significant varietal differences. VLA_{major} showed significant varietal differences. Huayou 675 had the largest VLA_{major} of 0.82 mm/mm^2, and N22 had the smallest VLA_{major} of 0.66 mm/mm^2. E, Ψ_{leaf}, and K_{leaf} all showed no significant varietal differences.

Relationships Among the Leaf Gas Exchange Parameters, Leaf Hydraulics, and Leaf Morphological Traits

As shown in **Figure 2**, g_s was positively correlated with both E and K_{leaf} across the six rice genotypes and P_N was positively correlated with K_{leaf} but had no relationship with E across the six rice genotypes. As shown in **Figure 3**, E, K_{leaf}, g_s, and P_N were all positively correlated with VLA and VLA_{minor} across the six rice genotypes; P_N was positively correlated with VLA_{major}, but E, K_{leaf}, and g_s had no relationship with VLA_{major} across the six rice genotypes.

DISCUSSION

In the present study, P_N was not correlated with N_{area} and g_m but was correlated with g_s and K_{leaf}. VLA and VLA_{minor} showed no varietal differences in the present study, which was perhaps due to the few genotypes used, and their vein traits ranged very narrowly. Rice leaf veins are distributed in parallel, and the leaf vein density is strongly affected by the leaf width (Baird et al., 2021). For example, Tabassum et al. (2016) reported that polyethylene glycol–induced water deficit caused rice leaf narrowing and led to an increase in leaf density. Xiong et al. (2015) investigated the leaf morphological traits of 11 rice genotypes, including seven wild genotypes and four cultivated genotypes, and found that leaf morphological traits showed great varietal differences because the leaf area showed ∼seven times the variation, ranging from 18.4 to 127.3 cm^2, and leaf width showed ∼six times the variation, ranging from 0.38 to 2.20 cm. The leaf width in the present study only showed 1.5 times the variation, ranging from 9.4 to 14.2 mm. Thus, leaf vein densities in the present study did not vary greatly. More genotypes and varying environmental conditions should be included in future studies to investigate the varietal differences in rice leaf vein traits and their impacts on leaf gas exchange.

In the present study, K_{leaf}, E, g_s, and P_N all substantially increased with VLA and VLA_{minor} across the six cultivated rice genotypes, thus verifying the hypothesis that high VLA can enhance K_{leaf} and promote leaf gas exchange in cultivated rice genotypes in which R_x/R_{leaf} is relatively high. By sorting the correlations between leaf gas exchange parameters, leaf hydraulic parameters, and leaf vein densities, we drew the conclusion that leaf vein density affected leaf gas exchange parameters by regulating leaf water transport. However, we still lack the analyses of many other vein traits such as the diameter of xylem conduits and the outside xylem anatomical traits on leaf hydraulics and gas exchange. More studies should be done to explore the coordination between the physiological and structural traits of the leaf.

Furthermore, VLA and K_{leaf} data from other studies (Xiong et al., 2015, 2017) were extracted to verify our hypothesis. As shown in **Figure 4**, K_{leaf} was positively correlated with VLA and VLA_{minor} across the cultivated rice genotypes, whereas these correlations disappeared across the wild rice genotypes. Therefore, we conclude that in cultivated rice genotypes, high VLA and high VLA_{minor} can enhance K_{leaf} and promote leaf gas exchange, and a high VLA can be regarded as a feature of rice materials having high photosynthetic capacity. Variations in VLA drove the correlation between K_{leaf} and VLA, which was probably due to the determining role of VLA on K_{leaf}, as other features of hydraulic architecture may vary slightly in cultivated rice genotypes. However, this correlation may be

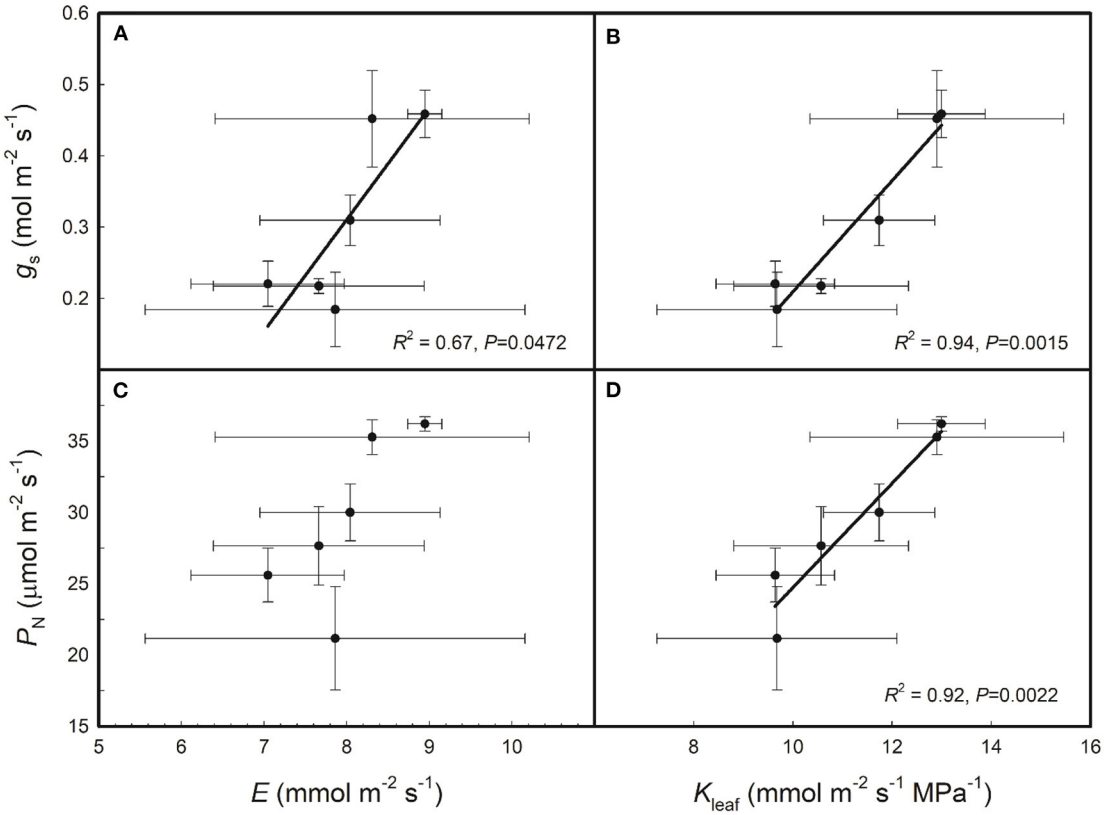

FIGURE 2 | Relationships of stomatal conductance (g_s) and net photosynthetic rate (P_N) with leaf transpiration rate (E) **(A,C)** and leaf hydraulic conductance (K_{leaf}) **(B,D)** across the six rice genotypes. Data are shown as the means ± SD of three replicates.

obscured when other features of hydraulic architecture vary. For example, the positive effects of high VLA on K_{leaf} may be attenuated by the negative effects of small xylem conduits in a plant. Besides, as one of the few studies on cereal crops, the present study showed different results with previous studies on wood species, for example, *populus* plants in Brocious and Hacke's (Brocious and Hacke, 2016) study. A positive correlation was found between K_{leaf} and VLA in the present study but not in Brocious and Hacke (2016) may also be attributed to the different importance of VLA to K_{leaf} in the species. The comprehensive effects of hydraulic architecture on leaf hydraulics should be summarized.

Correlations between K_{leaf} and VLA existing in cultivated but not wild rice genotypes illustrate the importance of leaf vein traits during rice domestication or genetic improvement. For example, Wu et al. (2020) revealed that an increase in leaf vein dimensions during rice genetic improvement enhanced leaf gas exchange. In addition to leaf vein traits, leaf morphological traits associated with leaf gas exchange, such as stomatal density and stomatal size in rice, have also been improved during crop genetic improvement (Panda et al., 2018; Wu et al., 2020). There is a need for establishing the underlying morphological and physiological changes for crop improvement.

A previous study (Venturas et al., 2017) illustrated that minor leaf vein length accounts for more than 80% of the total leaf vein length in higher plants. In the present study, minor leaf vein length accounted for 83.5% of the total leaf vein length on average (**Table 2**). Xiong et al. (2015) reported that the proportion of minor leaf vein length to total leaf vein length but not leaf vein density is the critical factor determining K_{leaf}. However, in the present study, neither E, K_{leaf}, g_s, nor P_N showed significant correlations with the proportion of minor leaf vein length to total leaf vein length (data not shown).

Except for the leaf vein density, other vein traits also greatly impacted K_{leaf}. Previous studies documented that short distance from minor veins to stomata and large diameters of xylem conduit accompanied by thin xylem conduit walls were beneficial for improving K_{leaf} (Brodribb et al., 2007; Sack and Scoffoni, 2013; Venturas et al., 2017; Xiong and Nadal, 2020). Nardini et al. (2014) found that large leaves tend to have higher VLA_{major} than small leaves and can promote K_{leaf}. Simonin et al. (2012) demonstrated that K_{leaf} increased with

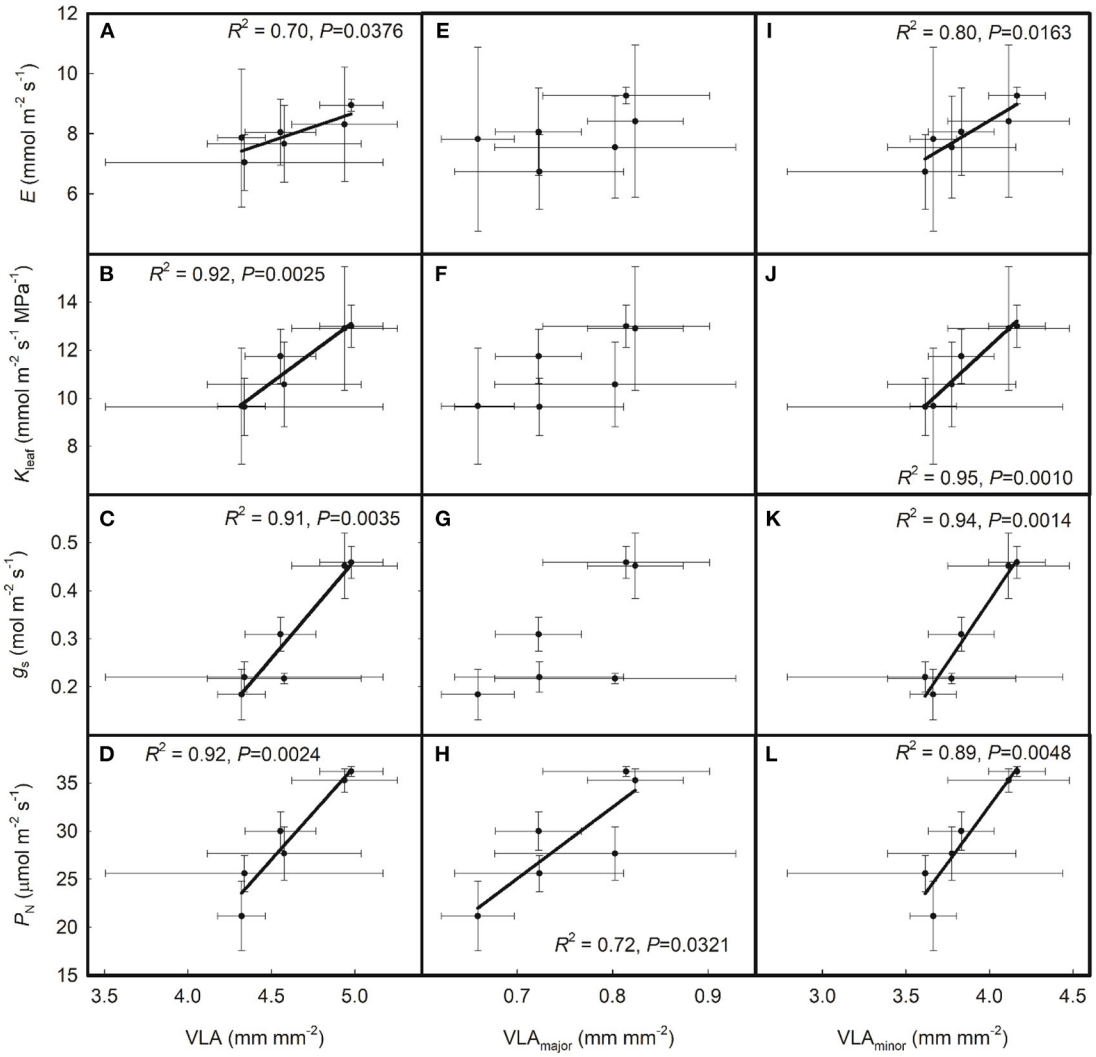

FIGURE 3 | Relationships of the leaf hydraulics and leaf gas exchange parameters with **(A–D)** total leaf vein density (VLA), **(E–H)** major leaf vein density (VLA$_{minor}$), and **(I–L)** minor leaf vein density (VLA$_{minor}$) across the six rice genotypes. Data are shown as the means ± SD. There were four replicates for leaf vein densities and three replicates for P_N, g_s, K_{leaf}, and E.

leaf area. However, a recent study exploring the development and biophysical determinations of grass leaf size worldwide revealed that small leaves have hydraulic benefits due to their higher VLA$_{major}$ (Baird et al., 2021). Optimal leaf morphological and anatomical traits for improving K_{leaf} and P_N should be defined to provide theories for high photosynthetic capacity rice breeding.

K_x is mainly determined by leaf vein traits, whereas K_{ox} is mainly determined by leaf anatomical traits. Xiong et al. (2017) found that K_{ox} is positively correlated with the fraction of intercellular airspace, the mesophyll cell surface area exposed to intercellular airspace per leaf area, and the surface area of chloroplasts exposed to intercellular airspace per leaf area, whereas it is negatively correlated with cell wall thickness. g_m has been reported to be positively correlated with g_s in recent years (Flexas et al., 2013). One reason for the positive relationship between g_s and g_m is that they are both positively correlated with K_{leaf} (Xiong and Nadal, 2020). g_s is positively correlated with K_{leaf} due to the close relationship between stomatal opening and leaf water transport; g_m is positively correlated with K_{leaf} and K_{ox} because g_m and K_{ox} are mediated by leaf anatomical traits (Xiong et al., 2017). However, K_x, K_{ox}, and leaf anatomical traits were not measured in the present study, and more studies should be done to investigate and explain the coordination among leaf gas exchange, leaf hydraulics, and leaf anatomy.

In addition, the water transport pathways inside leaves, i.e., where the evaporating sites occur, are currently unclear. Rockwell et al. (2014) reported that water dominantly evaporated from the vascular bundle sheath and its surroundings to

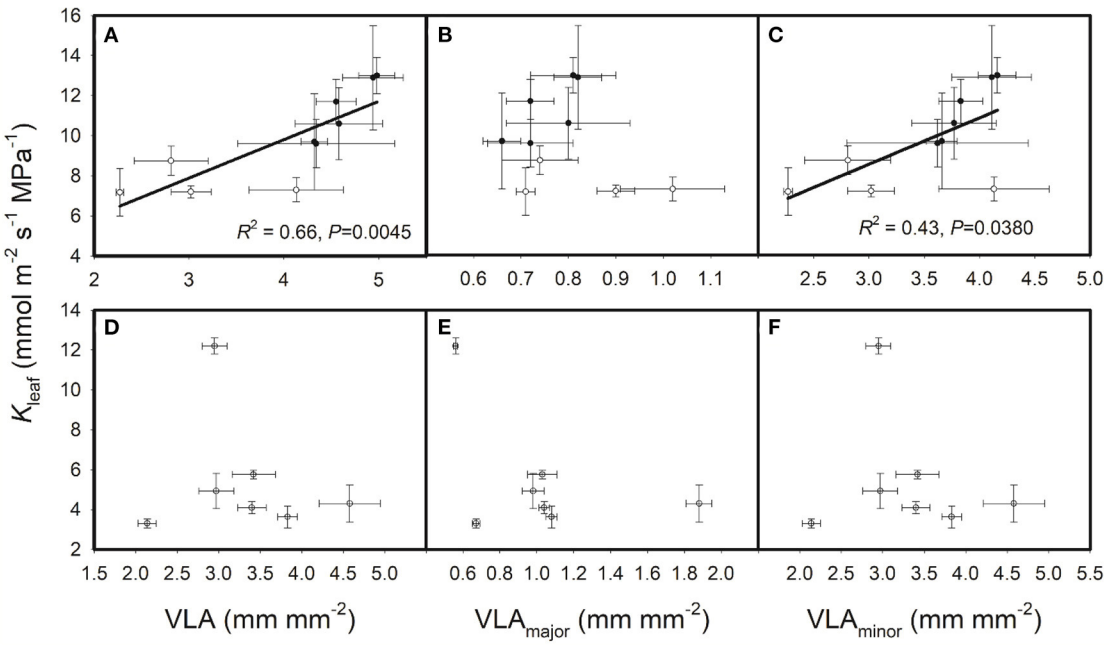

FIGURE 4 | Relationships of leaf hydraulic conductance (K_{leaf}) with leaf vein densities across **(A–C)** cultivated rice genotypes and **(D–F)** wild rice genotypes. The solid circles are data for the six cultivated rice genotypes in the present study, and the empty circles are data from Xiong et al. (2015, 2017) studies.

the intercellular airspace in *Quercus rubra*. Moreover, the conversion of water between the vapor and liquid phases is unknown. For example, Buckley et al. (2015) found that vapor phase transport contributed 39.25–44.00% to K_{ox} when the temperature difference between the xylem and leaf epidermis reached 0.2 K, suggesting that temperature greatly affects leaf hydraulic status. Evaporating sites and leaf hydraulic status inside rice leaves need more investigation.

CONCLUSIONS

In the present study, VLA$_{major}$ showed great varietal differences among cultivated rice genotypes, whereas VLA, VLA$_{minor}$, and the proportion of minor leaf vein length to total leaf vein length showed no varietal differences. E, K_{leaf}, g_s, and P_N were all positively correlated with VLA and VLA$_{minor}$, and P_N was positively correlated with VLA$_{major}$. We concluded that high VLA and high VLA$_{minor}$ can enhance K_{leaf} and promote leaf gas exchange in the cultivated rice genotypes and high VLA can be regarded as a high photosynthetic capacity trait in rice plants.

DATA AVAILABILITY STATEMENT

The original contributions presented in the study are included in the article/**Supplementary Material**, further inquiries can be directed to the corresponding author.

AUTHOR CONTRIBUTIONS

MY designed the research and wrote the paper. MY and ZuoZ conducted the experiments. MY and MW analyzed the data. HZ and ZujZ commented and revised the paper. All authors contributed to the article and approved the submitted version.

FUNDING

This research was funded by the National Natural Science Foundation of China, grant nos. 31871532 and 31871559, the National Key Research and Development Program of China, grant nos. 2016YFD0300102 and 2016YFD0300502, and the Priority Academic Program Development of Jiangsu Higher Education Institutions.

ACKNOWLEDGMENTS

We thank Ms. Xi Liu from Huazhong Agricultural University for helping to measure the leaf gas exchange parameters. We also thank Professor Yong Li from Huazhong Agricultural University for revising and commenting on this manuscript.

SUPPLEMENTARY MATERIAL

The Supplementary Material for this article can be found online at: https://www.frontiersin.org/articles/10.3389/fpls.2021.693815/full#supplementary-material

REFERENCES

Adachi, S., Nakae, T., Uchida, M., Soda, K., Takai, T., Oi, T., et al. (2013). The mesophyll anatomy enhancing CO_2 diffusion is a key trait for improving rice photosynthesis. *J. Exp. Bot.* 64, 1061–1072. doi: 10.1093/jxb/ers382

Baird, A. S., Taylor, S. H., Pasquet-Kok, J., Vuong, C., Zhang, Y., Watcharamongkol, T., et al. (2021). Developmental and biophysical determinants of grass leaf size worldwide. *Nature* 592, 242–247. doi: 10.1038/s41586-021-03370-0

Boyce, C. K., Brodribb, T. J., Field, T. S., and Zwieniecki, M. J. (2009). Angiosperm leaf vein evolution was physiologically and environmentally transformative. *Proc.. R. Soc. B. Biol. Sci.* 276, 1771–1776. doi: 10.1098/rspb.2008.1919

Brocious, C. A., and Hacke, U. G. (2016). Stomatal conductance scales with petiole xylem traits in *populus* genotypes. *Funct. Plant Biol.* 43, 553–562. doi: 10.1071/FP15336

Brodribb, T. J., and Field, T. S. (2010). Leaf hydraulic evolution led a surge in leaf photosynthetic capacity during early angiosperm diversification. *Ecol. Lett.* 13, 175–183. doi: 10.1111/j.1461-0248.2009.01410.x

Brodribb, T. J., Field, T. S., and Jordan, G. J. (2007). Leaf maximum photosynthetic rate and venation are linked by hydraulics. *Plant Physiol.* 144, 1890–1898. doi: 10.1104/pp.107.101352

Brooks, A., and Farquhar, G. D. (1985). Effect of temperature on the CO_2/O_2 specificity of ribulose-1, 5-bisphosphate carboxylase/oxygenase and the rate of respiration in the light. *Planta* 165, 397–406. doi: 10.1007/BF00392238

Buckley, T. N., John, G. P., Scoffoni, C., and Sack, L. (2015). How does leaf anatomy influence water transport outside the xylem? *Plant Physiol.* 168, 1616–1635. doi: 10.1104/pp.15.00731

Carriquí, M., Cabrera, H. M., Conesa, M. À., Coopman, R. E., Douthe, C., Gago, J., et al. (2015). Diffusional limitations explain the lower photosynthetic capacity of ferns as compared with angiosperms in a common garden study. *Plant Cell Environ.* 38, 448–460. doi: 10.1111/pce.12402

Evans, J. R., Kaldenhoff, R., Genty, B., and Terashima, I. (2009). Resistances along the CO_2 diffusion pathway inside leaves. *J. Exp. Bot.* 60, 2235–2248. doi: 10.1093/jxb/erp117

Farquhar, G. D., von Caemmerer, S., and Berry, J. A. (1980). A biochemical model of photosynthetic CO_2 assimilation in leaves of C_3 species. *Planta* 149, 78–90. doi: 10.1007/BF00386231

Field, T. S., Brodribb, T. J., Iglesias, A., Chatelet, D. S., Baresch, A., Upchurch, G. R. Jr., et al. (2011). Fossil evidence for Cretaceous escalation in angiosperm leaf vein evolution. *Proc. Natl. Acad. Sci. U. S. A.* 108, 8363–8366. doi: 10.1073/pnas.1014456108

Flexas, J., Barbour, M. M., Brendel, O., Cabrera, H. M., Carriqu,í, M., Díaz-Espejo, A., et al. (2012). Mesophyll diffusion conductance to CO_2: an unappreciated central player in photosynthesis. *Plant Sci.* 193, 70–84. doi: 10.1016/j.plantsci.2012.05.009

Flexas, J., Scoffoni, C., Gago, J., and Sack, L. (2013). Leaf mesophyll conductance and leaf hydraulic conductance: an introduction to their measurement and coordination. *J. Exp. Bot.* 64, 3965–3981. doi: 10.1093/jxb/ert319

Gago, J., Carriquí, M., Nadal, M., Clemente-Moreno, M. J., Coopman, R. E., Fernie, A. R., et al. (2019). Photosynthesis optimized across land plant phylogeny. *Trends Plant Sci.* 24, 947–958. doi: 10.1016/j.tplants.2019.07.002

Giuliani, R., Koteyeva, N., Voznesenskaya, E., Evans, M. A., Cousins, A. B., and Edwards, G. E. (2013). Coordination of leaf photosynthesis, transpiration, and structural traits in rice and wild relatives (genus *Oryza*). *Plant Physiol.* 162, 1632–1651. doi: 10.1104/pp.113.217497

Guyot, G., Scoffoni, C., and Sack, L. (2012). Combined impacts of irradiance and dehydration on leaf hydraulic conductance: insights into vulnerability and stomatal control. *Plant Cell Environ.* 35, 857–871. doi: 10.1111/j.1365-3040.2011.02458.x

Harley, P. C., Loreto, F., Di Marco, G., and Sharkey, T. D. (1992). Theoretical considerations when estimating the mesophyll conductance to CO_2 flux by analysis of the response of photosynthesis to CO_2. *Plant Physiol.* 98, 1429–1436. doi: 10.1104/pp.98.4.1429

Hirasawa, T., Tsuchida, M., and Ishihara, K. (1992). Relationship between resistance to water transport and exudation rate and the effect of the resistance on the midday depression of stomatal aperture in rice plants. *Jap. J. Crop Sci.* 61, 145–152. doi: 10.1626/jcs.61.145

Kodama, N., Wada, R., Nakayama, T., Takemura, K., and Matsumi, Y. (2011). "*High precision and continuous measurements of mesophyll and stomatal conductance to CO2 diffusion during photosynthesis* using QCL," in AGU Fall Meeting Abstracts (San Francisco, CA).

Li, Y., Gao, Y., Xu, X., Shen, Q., and Guo, S. (2009). Light-saturated photosynthetic rate in high-nitrogen rice (*Oryza sativa* L.) leaves is related to chloroplastic CO_2 concentration. *J. Exp. Bot.* 60, 2351–2360. doi: 10.1093/jxb/erp127

Liu, X., and Li, Y. (2016). Varietal difference in the correlation between leaf nitrogen content and photosynthesis in rice (*Oryza sativa* L.) plants is related to specific leaf weight. *J. Integr. Agr.* 15, 2002–2011. doi: 10.1016/S2095-3119(15)61262-X

McKown, A. D., Cochard, H., and Sack, L. (2010). Decoding leaf hydraulics with a spatially explicit model: principles of venation architecture and implications for its evolution. *Am. Nat.* 175, 447–460. doi: 10.1086/650721

Nardini, A., Õunapuu-Pikas, E., and Savi, T. (2014). When smaller is better: leaf hydraulic conductance and drought vulnerability correlate to leaf size and venation density across four *Coffea arabica* genotypes. *Funct. Plant Biol.* 41, 972–982. doi: 10.1071/FP13302

Nardini, A., Ped,à, G., and Rocca, N. L. (2012). Trade-offs between leaf hydraulic capacity and drought vulnerability: morpho-anatomical bases, carbon costs and ecological consequences. *New Phytol.* 196, 788–798. doi: 10.1111/j.1469-8137.2012.04294.x

Ocheltree, T. W., Nippert, J. B., and Prasad, P. V. V. (2012). Changes in stomatal conductance along grass blades reflect changes in leaf structure. *Plant Cell Environ.* 35, 1040–1049. doi: 10.1111/j.1365-3040.2011.02470.x

Ouyang, W., Struik, P. C., Yin, X., and Yang, J. (2017). Stomatal conductance, mesophyll conductance, and transpiration efficiency in relation to leaf anatomy in rice and wheat genotypes under drought. *J. Exp. Bot.* 68, 5191–5205. doi: 10.1093/jxb/erx314

Panda, D., Mahakhud, A., Mohanty, B., Mishra, S. S., and Barik, J. (2018). Genotypic variation of photosynthetic gas exchange and stomatal traits in some traditional rice (*Oryza sativa* L.) landraces from Koraput, India for crop improvement. *Physiol. Mol. Biol. Plants* 24, 973–983. doi: 10.1007/s12298-018-0542-3

Rockwell, F. E., Holbrook, N. M., and Stroock, A. D. (2014). The competition between liquid and vapor transport in transpiring leaves. *Plant Physiol.* 164, 1741–1758. doi: 10.1104/pp.114.236323

Sack, L., Cowan, P. D., Jaikumar, N., and Holbrook, N. M. (2003). The 'hydrology' of leaves: co-ordination of structure and function in temperate woody species. *Plant Cell Environ.* 26, 1343–1356. doi: 10.1046/j.0016-8025.2003.01058.x

Sack, L., and Frole, K. (2006). Leaf structural diversity is related to hydraulic capacity in tropical rain forest trees. *Ecology* 87, 483–491. doi: 10.1890/05-0710

Sack, L., and Holbrook, N. M. (2006). Leaf hydraulics. *Annu. Rev. Plant Biol.* 57, 361–381. doi: 10.1146/annurev.arplant.56.032604.144141

Sack, L., Melcher, P. J., Zwieniecki, M. A., and Holbrook, N. M. (2002). The hydraulic conductance of the angiosperm leaf lamina: a comparison of three measurement methods. *J. Exp. Bot.* 53, 2177–2184. doi: 10.1093/jxb/erf069

Sack, L., and Scoffoni, C. (2012). Measurement of leaf hydraulic conductance and stomatal conductance and their responses to irradiance and dehydration using the Evaporative Flux Method (EFM). *J. Vis. Exp.* 70:e4179. doi: 10.3791/4179

Sack, L., and Scoffoni, C. (2013). Leaf venation: structure, function, development, evolution, ecology and applications in the past, present and future. *New Phytol.* 198, 983–1000. doi: 10.1111/nph.12253

Sack, L., Scoffoni, C., John, G. P., Poorter, H., Mason, C. M., Mendez-Alonzo, R., et al. (2013). How do leaf veins influence the worldwide leaf economic spectrum? Review and synthesis. *J. Exp. Bot.* 64, 4053–4080. doi: 10.1093/jxb/ert316

Simonin, K. A., Limm, E. B., and Dawson, T. E. (2012). Hydraulic conductance of leaves correlate with leaf lifespan: implications for lifetime carbon gain. *New Phytol.* 193, 939–947. doi: 10.1111/j.1469-8137.2011.04014.x

Tabassum, M. A., Ye, Y., Yu, T., Zhu, G., Rizwan, M. S., Wahid, M. A., et al. (2016). Rice (*Oryza sativa* L.) hydraulic conductivity links to leaf venation architecture under well-watered condition rather than PEG-induced water deficit. *Acta. Physiol. Plant.* 38:92. doi: 10.1007/s11738-016-2109-7

Taylaran, R. D., Adachi, S., Ookawa, T., Usuda, H., and Hirasawa, T. (2011). Hydraulic conductance as well as nitrogen accumulation plays a role in the higher rate of leaf photosynthesis of the most productive variety of rice in Japan. *J. Exp. Bot.* 62, 4067–4077. doi: 10.1093/jxb/err126

Terashima, I., Hanba, Y. T., Tholen, D., and Niinemets, Ü. (2011). Leaf functional anatomy in relation to photosynthesis. *Plant Physiol.* 155, 108–116. doi: 10.1104/pp.110.165472

Tholen, D., Boom, C., and Zhu, X. G. (2012). Opinion: Prospects for improving photosynthesis by altering leaf anatomy. *Plant Sci.* 197, 92–101. doi: 10.1016/j.plantsci.2012.09.005

Valentini, R., Epron, D., De Angelis, P., Matteucci, G., and Dreyer, E. (1995). *In situ* estimation of net CO2 assimilation, photosynthetic electron flow and photorespiration in Turkey oak (*Q. cerris L.*) leaves: diurnal cycles under different levels of water supply. *Plant Cell Environ.* 18, 631–640. doi: 10.1111/j.1365-3040.1995.tb00564.x

Venturas, M. D., Sperry, J. S., and Hacke, U. G. (2017). Plant xylem hydraulics: what we understand, current research, and future challenges. *J. Integr. Plant Biol.* 59, 356–389. doi: 10.1111/jipb.12534

von Caemmerer, S., Evans, J. R., Hudson, G. S., and Andrews, T. J. (1994). The kinetics of ribulose-1, 5-bisphosphate carboxylase/oxygenase *in vivo* inferred from measurements of photosynthesis in leaves of transgenic tobacco. *Planta* 195, 88–97. doi: 10.1007/BF00206296

Walls, R. L. (2011). Angiosperm leaf vein patterns are linked to leaf functions in a global scale data set. *Am. J. Bot.* 98, 244–253. doi: 10.3732/ajb.1000154

Wu, L., Boer, H. J., Zhang, Z., Chen, X., Shi, Y., Peng, S., et al. (2020). The coordinated increase in stomatal density and vein dimensions during genetic improvement in rice. *Agron. J.* 112, 2791–2804. doi: 10.1002/agj2.20180

Xiong, D., Flexas, J., Yu, T., Peng, S., and Huang, J. (2017). Leaf anatomy mediates coordination of leaf hydraulic conductance and mesophyll conductance to CO_2 in *Oryza*. *New Phytol.* 213, 572–583. doi: 10.1111/nph.14186

Xiong, D., and Nadal, M. (2020). Linking water relations and hydraulics with photosynthesis. *Plant J.* 101, 800–815. doi: 10.1111/tpj.14595

Xiong, D., Yu, T., Zhang, T., Li, Y., Peng, S., and Huang, J. L. (2015). Leaf hydraulic conductance is coordinated with leaf morpho-anatomical traits and nitrogen status in the genus *Oryza*. *J. Exp. Bot.* 66, 741–748. doi: 10.1093/jxb/eru434

Xu, Z., and Zhou, G. (2008). Responses of leaf stomatal density to water status and its relationship with photosynthesis in a grass. *J. Exp. Bot.* 59, 3317–3325. doi: 10.1093/jxb/ern185

Yamori, W., Nagai, T., and Makino, A. (2011). The rate-limiting step for CO_2 assimilation at different temperatures is influenced by the leaf nitrogen content in several C_3 crop species. *Plant Cell Environ.* 34, 764–777. doi: 10.1111/j.1365-3040.2011.02280.x

Ye, M., Peng, S., and Li, Y. (2019). Intraspecific variation in photosynthetic nitrogen-use efficiency is positively related to photosynthetic rate in rice (*Oryza sativa* L.) plants. *Photosynthetica* 57, 311–319. doi: 10.32615/ps.2019.011

Conflict of Interest: The authors declare that the research was conducted in the absence of any commercial or financial relationships that could be construed as a potential conflict of interest.

Publisher's Note: All claims expressed in this article are solely those of the authors and do not necessarily represent those of their affiliated organizations, or those of the publisher, the editors and the reviewers. Any product that may be evaluated in this article, or claim that may be made by its manufacturer, is not guaranteed or endorsed by the publisher.

frontiers in Plant Science

ORIGINAL RESEARCH
published: 21 December 2021
doi: 10.3389/fpls.2021.786593

Tracheid and Pit Dimensions Hardly Vary in the Xylem of *Pinus sylvestris* Under Contrasting Growing Conditions

Magdalena Held[1,2†], Andrea Ganthaler[1†], Anna Lintunen[2†], Walter Oberhuber[1†] and Stefan Mayr[1†]*

[1] Department of Botany, University of Innsbruck, Innsbruck, Austria, [2] Institute for Atmospheric and Earth System Research (INAR)/Forest Sciences, University of Helsinki, Helsinki, Finland

OPEN ACCESS

Edited by:
Dongliang Xiong, Huazhong Agricultural University, China

Reviewed by:
Patrick Fonti, Swiss Federal Institute for Forest, Snow and Landscape Research (WSL), Switzerland
Marcin Klisz, Forest Research Institute (IBL), Poland

***Correspondence:**
Magdalena Held
magdalena.held@helsinki.fi

†ORCID:
Magdalena Held
orcid.org/0000-0001-5555-1385
Andrea Ganthaler
orcid.org/0000-0002-8670-6199
Anna Lintunen
orcid.org/0000-0002-1077-0784
Walter Oberhuber
orcid.org/0000-0002-5197-7044
Stefan Mayr
orcid.org/0000-0002-3319-4396

Specialty section:
This article was submitted to Plant Physiology, a section of the journal Frontiers in Plant Science

Received: *30 September 2021*
Accepted: *16 November 2021*
Published: *21 December 2021*

Citation:
Held M, Ganthaler A, Lintunen A, Oberhuber W and Mayr S (2021) Tracheid and Pit Dimensions Hardly Vary in the Xylem of Pinus sylvestris Under Contrasting Growing Conditions. Front. Plant Sci. 12:786593. doi: 10.3389/fpls.2021.786593

Maintaining sufficient water transport *via* the xylem is crucial for tree survival under variable environmental conditions. Both efficiency and safety of the water transport are based on the anatomical structure of conduits and their connections, the pits. Yet, the plasticity of the xylem anatomy, particularly that of the pit structures, remains unclear. Also, trees adjust conduit dimensions to the water transport distance (i.e., tree size), but knowledge on respective adjustments in pit dimensions is scarce. We compared tracheid traits [mean tracheid diameter d, mean hydraulic diameter d_h, cell wall reinforcement $(t/b)^2$], pit dimensions (diameters of pit aperture D_a, torus D_t, margo D_m, and pit border D_p), and pit functional properties (margo flexibility F, absolute overlap O_a, torus overlap O, and valve effect V_{ef}) of two Scots pine (*Pinus sylvestris* L.) stands of similar tree heights but contrasting growth rates. Furthermore, we analyzed the trends of these xylem anatomical parameters across tree rings. Tracheid traits and pit dimensions were similar on both sites, whereas O_a, O, and F were higher at the site with a lower growth rate. On the lower growth rate site, d_h and pit dimensions increased across tree rings from pith to bark, and in trees from both sites, d_h scaled with pit dimensions. Adjusted pit functional properties indicate slightly higher hydraulic safety in trees with a lower growth rate, although a lack of major differences in measured traits indicated overall low plasticity of the tracheid and pit architecture. Mean hydraulic diameter and pit dimension are well coordinated to increase the hydraulic efficiency toward the outer tree rings and thus with increasing tree height. Our results contribute to a better understanding of tree hydraulics under variable environmental conditions.

Keywords: xylem anatomy, water transport, interconduit pit, *Pinus sylvestris*, tracheid, plasticity

INTRODUCTION

To cope with variable water availability, trees must maintain sufficient water transport (McDowell et al., 2008; Adams et al., 2017). Water transport is, besides mechanical support and storage, the main function of the xylem and is based on the xylem's anatomical structures (Kramer and Kozlowski, 1960; Zimmermann, 1983). Xylem conduits transport water from roots to leaves based

on a water potential gradient (negative pressure or tension) induced by transpiration from the stomata (Dixon and Joly, 1895). Water flow is restricted by resistances along the entire pathway and the cumulative resistance thus increases with pathway length (Ryan and Yoder, 1997). Resistance of single xylem elements decreases approximately with the fourth power of conduit lumen diameter (Hagen-Poiseuille's law; Zimmermann, 1983), and trees counteract pathway length resistance by, respectively, widening their conduits with distance to the treetop (or branch tip; Anfodillo et al., 2013; Carrer et al., 2015; Lazzarin et al., 2016; Olson et al., 2021). However, with increasing conduit lumen diameter, the risk of hydraulic failure can increase (e.g., Rosner et al., 2016).

Larger conduits may have a higher probability of vulnerable pits (interconduit connections) as more pits are embedded in their cell walls (Hargrave et al., 1994; Jacobsen et al., 2019). Bordered pits are crucial structures regarding both hydraulic efficiency (by representing the main resistance within the xylem; Domec et al., 2006) and hydraulic safety (i.e., resistance against hydraulic failure; Zimmermann, 1983). Both water flow between conduits and the probability of air seeding, which may cause embolism and block water transport, increase with a pore size of pit membranes (e.g., Zimmermann, 1983; Tyree et al., 1994; Hacke and Sperry, 2001; Choat et al., 2008). In conifers, valve-like structured pits counteract this trade-off: their pit membrane, formed by the primary wall, consists of an outer microfibril web (margo), and a central thickening (torus). The secondary cell wall protrudes to form a border with an aperture on each side of the membrane (toward both adjacent tracheids). If neighboring conduits are functional, the membrane is in a relaxed, central position, exposing both margo pores and pit apertures to water flow. If one conduit is air filled (i.e., embolized; Zimmermann, 1983), the pressure difference between the adjacent conduits causes the torus to seal the pit aperture, covering large margo pores to prevent air seeding (Bailey, 1916; Zimmermann, 1983; Sperry and Tyree, 1990). However, under critically high tensions pits may fail. Several air-seeding mechanisms have been proposed for this process (Sperry and Tyree, 1990; Domec and Gartner, 2002; Hacke et al., 2004; Cochard, 2006; Cochard et al., 2009; Delzon et al., 2010), which imply that dimensions of the pit border, margo, torus, and aperture, and particularly the ratios of these dimensions play a crucial role concerning the resistance against air seeding (e.g., Cochard, 2006; Hacke and Jansen, 2009; Delzon et al., 2010; Jansen et al., 2012; Schulte and Hacke, 2021). Hacke et al. (2004) found both smaller margo and pit aperture to respond to higher resistance to embolism. Furthermore, Hacke and Jansen (2009) reported that the ratio of torus and pit membrane area to pit aperture increase with resistance to embolism. According to Schulte et al. (2015), a high total area of margo pores and pit diameter reduce the hydraulic resistance of pits, while margo pore size and number also influence the hydraulic efficiency (Hacke et al., 2004). Thus, an optimized pit architecture and torus–margo ratio is important for hydraulics of length-limited tracheids in conifers (Hacke et al., 2004). The potential plasticity of xylem anatomical structures may be relevant for tree survival and is the subject of several studies. For example, Castagneri et al. (2015) found temperature and precipitation to influence conduit dimensions in *Picea abies* (L.) Karst. In contrast, Olson et al. (2018, 2021) suggested that trees hardly adjust their conduit dimensions to environmental conditions and that different conduit dimensions at the commonly sampled breast height can occur as a secondary effect due to different tree heights (or branch lengths). Furthermore, knowledge concerning the potential plasticity in conifer pit dimensions and the coordination of pit and conduit dimensions remains poor (e.g., Lazzarin et al., 2016; Losso et al., 2018).

In our study, we analyzed xylem anatomical traits in *Pinus sylvestris* L. sampled on two sites with contrasting growth rates but similar tree heights (tree-ring width 727 ± 15 μm *vs.* 2,724 ± 135 μm; tree height 17.4 ± 0.4 m *vs.* 16.9 ± 0.3 m) to reveal if trees adjust these traits to growing conditions independently from the distance to the treetop. Measured tracheid traits were mean tracheid lumen area (a), mean tracheid lumen diameter (d), mean hydraulic diameter (d_h), and cell wall reinforcement [$(t/b)^2$; Hacke et al., 2001]. From the pits, we measured border diameter (D_p), margo diameter (D_m), torus diameter (D_t), and aperture diameter (D_a), with which we calculated the following functional properties according to Delzon et al. (2010) and Domec et al. (2008): margo flexibility (F), absolute overlap (O_a), torus overlap (O), and valve effect (V_{ef}). Our study aimed to (a) explore differences in these tracheid and pit traits between trees that are of similar height but have experienced different growing conditions, and (b) to better understand the within-tree variation and coordination of tracheid and pit characteristics. We hypothesized that (1) trees on the limited site have a higher hydraulic safety than trees on the favorable site thanks to adjusted tracheid and pit characteristics, particularly D_m, D_t, D_a, and resulting functional properties, and (2) trees adjust their tracheid and pit characteristics according to the distance from the treetop. Thus, at breast height we expected anatomical adjustments increasing the hydraulic efficiency from the inner to the outer tree rings.

MATERIALS AND METHODS

Site Description

This study was performed in the Eastern Alps, on two forest sites situated in the Inn valley west of Innsbruck (Tyrol, Austria). Tree growth was limited on one site, whereas the other site had more favorable conditions. The limited sampling site (Tschirgant; N47°13.922′, E10°50.886′) lies at 745 m asl. Its rock bed consists of post-glacial rockfall material (Patzelt and Poscher, 1993) classified as dolomite (Land Tirol, 2021) and has a low water-holding capacity due to shallow, stony soils, and low nutrient availability (Oberhuber et al., 2014). A weather station close to the site (Haiming) measured a mean annual temperature of 7.4°C and mean annual precipitation of 716.7 mm (ZAMG, 2021). *P. sylvestris* dominated this site with *P. abies* and *Larix decidua* Mill., occurring occasionally in the understory. The natural forest types in the sampled area are *Erico-Pinetum dorycnietosum germanici* (dominated by *P. sylvestris*) and *Carici albae-Tilietum*

cordatae typicum (broad-leaf dominated), of which the latter has a higher water and nutrient demand (Land Tirol, 2021).

The favorable site (Mieming; N47°18.542′, E11°01.019′) lies at 825 m asl on a gravel terrace, which is partly covered by scree material (von Klebelsberg, 1935), which is siliceous but rich in carbonates (Land Tirol, 2021). As the favorable site lies about 10 km northeast of the limited site, the climatic conditions are similar; however, due to a precipitation gradient toward the west, the favorable site may experience a slightly higher mean annual precipitation. Here, *P. sylvestris* grew mixed with *P. abies*. The natural forest type in the sampled area is *Carici albae-Tilietum cordatae typicum* (Land Tirol, 2021). Sampled trees on the limited site were 17.4 ± 0.4 m high, with an average cambial age at breast height of 160 ± 7 years, whereas, trees on the favorable site were 16.9 ± 0.3 m high (difference between sites non-significant; $p = 0.162$), with a cambial age at breast height of 32 ± 1 years (mean ± SE).

Sampling

On each site, we selected ten *P. sylvestris* trees of similar height and sampled them using a tree increment borer (5.15 mm diameter, 400 mm length; Haglöf, Mora 400). We extracted two cores per tree at breast height (1.25–1.35 m) from the south-facing side of the trunk in November 2017 (limited site) and March 2018 (favorable site) for tree-ring and anatomical analysis *via* light and scanning electron microscopy. We also recorded tree circumference at breast height and tree height, the latter using a laser rangefinder (TruPulse 200 Series, Laser Inc. Technology, Centennial, CO, United States).

Tree-Ring Analysis

One core per tree was used for the tree-ring analysis. Using a measuring table (LINTAB 6, RINNTECH, Heidelberg, Germany) connected to the tree-ring program TSAPwin Scientific (ver. 4.80e RINNTECH), earlywood and latewood widths were measured (resolution 1 μm). The boundary between earlywood and latewood was set to a point where double cell wall thickness was equal or larger than the tracheid lumen area (both in radial direction). In *P. sylvestris*, the transition from earlywood to latewood is abrupt (Schweingruber, 1993), allowing for a relatively accurate determination of the boundary. Total tree-ring width was calculated as the sum of earlywood and latewood width. We checked the quality of cross-dating using the COFECHA software (Holmes, 1986).

Xylem Anatomical Analysis

For tracheid analysis, we extracted selected tree rings (tree-ring samples) from the cores of five trees per site (randomly selected; previously used for tree-ring analysis). In tree cores from the limited site, we selected every 20th tree ring starting from the outermost tree ring (2017) to compare the measured tracheid traits between sites (to sample the whole life span with regular intervals as on the limited site). To analyze trends in tracheid traits from the inner to the outer tree rings, we used the same tree-ring samples as for the site comparison but added additional tree-ring samples to make the trends better visible. From one of the trees, we selected every 10th tree ring throughout the whole life span, and from the remaining trees, we selected every 10th tree ring within the innermost 50 tree rings (because trees grow usually faster while they are young; Baker, 1950). In tree cores from the favorable site, we selected every 10th tree ring for site comparison and trend analysis. Also, we compared the tracheid traits of the outermost tree ring separately, as this tree ring was formed when the trees on both sites reached similar heights. For pit analysis, we used the second tree core of all ten trees per site and selected tree rings according to the same scheme as for tracheid analysis (**Supplementary Table 1**).

For tracheid analysis, tree-ring samples were soaked in ethanol/glycerol/water solution (1:1:1, v/v/v) for at least 5 days (Losso et al., 2018), before cross-sections (around 30 μm thickness to avoid breaking and to get a good contrast) were produced using a sliding microtome (Sledge Microtome G.S.L. 1, Schenkung Dapples, Zurich, Switzerland). The sections were stained with Etzold's solution for at least 15 min. Images were taken with a light microscope (Olympus BX41, Olympus Austria, Wien, Austria), connected to a digital camera (ProgRes CT3, Jenoptik, Jena, Germany) at 10 × magnification and with a resolution of 2,048 × 1,536 pixels (see **Supplementary Figures 1A–F** for an example tree ring from the limited and favorable site, respectively). With the ImageJ 1.45 software (National Institutes of Health, Bethesda, MD, United States), we measured the cross-sectional tracheid lumen area in both earlywood and latewood in at least five radial files, whereby we differentiated tracheid lumina from walls by applying a threshold value on gray-scale images and edited the images manually where necessary. From each image, we cropped the area of interest manually. In tree rings covering several images, we analyzed each image separately. The mean tracheid lumen area was calculated for each tree-ring sample. The lumen diameter was calculated for each tracheid assuming square-shaped lumina and then averaged (mean tracheid lumen diameter, d). Tracheid diameter distribution based on 2-μm classes was calculated for each site. Furthermore, the mean hydraulic diameter (d_h), which weighs conduit diameters with respect to the theoretical hydraulic conductance (Sperry et al., 1994), was calculated according to Sperry and Hacke (2004) as $\Sigma d^5 / \Sigma d^4$, where d_t is the diameter of each analyzed tracheid. For calculating cell wall reinforcement $[(t/b)^2]$ according to Hacke et al. (2001), tracheid lumen diameter (b) and wall thickness (t) were manually measured (therefore $b \neq d$) on 10 selected tracheids per tree-ring sample with a hydraulic diameter of $d_h \pm 6$ μm. The $(t/b)^2$ is typically measured on tracheids within a certain diameter range around d_h. The diameter range applied here was necessary for small tree rings to reach the sample number of 10.

For pit analysis, tree-ring samples were soaked in 50% ethanol for at least one night. Using a sliding microtome (see tracheid analysis), the samples were radially cut to produce woodblocks of approximately 5 mm × 5 mm × 2 mm, which were dried at 70°C for at least one night. Next, they were fixed on object stages and dried again at 40°C overnight. Finally, they were sputtered with gold using Leica EM SCD050 (Leica Microsystem, Wetzlar, Germany). A scanning electron microscope (SEM model XL 20, Philips, Amsterdam, Netherlands) was used to measure the dimensions of ten pits per sample, which were randomly

cut open by the microtome. The entire selected tree ring was searched for measurable pits (i.e., opened pit chamber, all pit structures visible, horizontal orientation). When the number of measurable pits was insufficient, pits of adjacent tree rings were included in the measurements. Most of the measurable pits were found in the earlywood (as the pits of larger tracheids are more likely to be cut open). Measured dimensions were the diameter of pit aperture (D_a), torus (D_t), margo (D_m), and pit border (D_p). From these dimensions (**Figure 1**), functional properties were calculated for each pit: the absolute torus overlap ($O_a = D_t/D_a$) was calculated according to Domec et al. (2008), and the margo flexibility [$F = (D_m - D_t)/D_m$], torus overlap [$O = (D_t - D_a)/D_t$], and valve effect ($V_{ef} = F \times O$) were calculated according to Delzon et al. (2010).

Data Analysis and Statistics

All values are given as mean ± standard error (SE). For statistical analyses, R (version 4.0.1, R Core Team, 2020) was used in RStudio (version 1.3.959, RStudio Team, 2020) by applying the packages tidyverse (version 1.3.0, Wickham et al., 2019) and Hmisc (version 4.4-1, Harrell and Dupont, 2020). The Shapiro–Wilk Normality tests were carried out before further analyses. To analyze differences between sites, parameters were averaged per tree and tested with Welch's *t*-test if normally distributed, otherwise the Mann–Whitney *U* tests were carried out. For correlations, parameters were averaged per year and site. Correlations were tested using either the Pearson product–moment coefficient or Spearman's rank correlation coefficient (in the case of non-normally distributed data).

RESULTS

Radial Growth

Trees on the limited site were older than those on the favorable site. On average, tree cores from the limited site contained 160 ± 7 tree rings, whereas those from the favorable site contained 32 ± 1 ($p < 0.001$; all values given as mean ± SE). No false or missing rings were observed in any tree individual. However, the pith was missing in some cores, and thus, the cambial age at breast height was underestimated by approximately 3 years in some trees. Trees on the limited site had larger circumferences at breast height (93.0 ± 5.3 cm) than those on the favorable site (70.6 ± 3.7 cm; $p = 0.003$). The

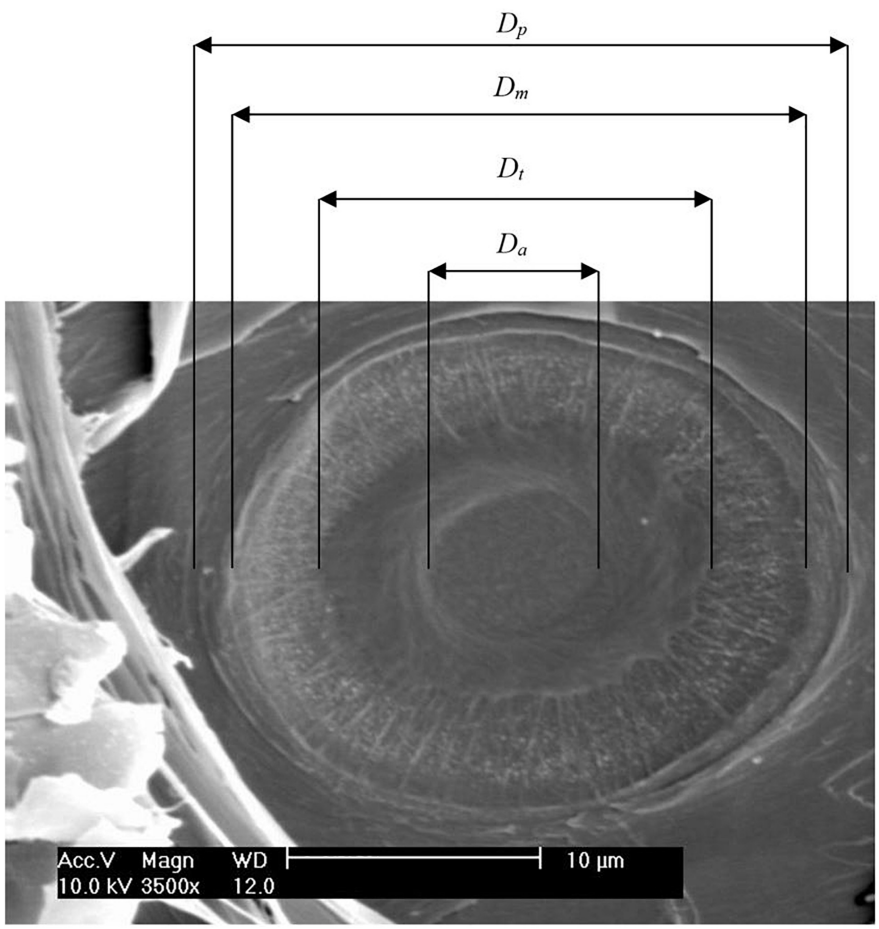

FIGURE 1 | A dissected pit is viewed *via* a scanning electron microscope. Diameter of pit (D_p), margo (D_m), torus (D_t), and pit aperture (D_a) are indicated.

average earlywood width was 515 ± 12 μm *vs.* 2,099 ± 156 μm ($p < 0.001$) and latewood width was 212 ± 5 μm *vs.* 625 ± 36 μm ($p < 0.001$) on the limited *vs.* favorable sites, respectively, resulting in an average tree-ring width of 727 ± 15 μm on the limited and 2,724 ± 135 μm on the favorable site ($p < 0.001$). The ring width chronology of the limited site covered a time span (i.e., maximum number of tree rings) of 192 years. Tree-ring width and earlywood width exhibited a decreasing trend from pith to bark ($p = 0.002$ and $p < 0.001$), whereas latewood width remained constant. The ring width chronology of the favorable site covered a time span of 37 years. While tree-ring width and earlywood width exhibited a decreasing trend, an increasing trend in latewood width was observed (each $p < 0.001$; **Supplementary Figure 2**). Thus, the earlywood–latewood ratio decreased with cambial age on both sites.

Tracheid Traits

We found no differences in the analyzed tracheid traits between the study sites (**Table 1**), both when considering tree rings representing the entire life span or only the outermost tree ring. Tracheid diameter frequency distribution calculated from the entire life span (**Supplementary Figure 3**) exhibited two peaks at both sites, representing latewood and earlywood tracheids. Tracheids between 2 and 4 μm, 4 and 6 μm, and 6 and 8 μm in diameter were more frequent on the limited site ($p < 0.05$), while those between 12 and 14 μm, 14 and 16 μm, and 16 and 18 μm in diameter were more frequent at the favorable site ($p < 0.01$). Tracheids wider than 48 μm only occurred in trees from the limited site. Considering the outermost tree ring, 6–8-μm tracheids were more frequent on the limited site ($p = 0.047$), while 10–12 μm, 12–14 μm, 14–16 μm, and 16–18 μm tracheids were more frequent on the favorable site ($p < 0.05$). Tracheids wider than 40 μm only occurred in trees on the limited site. In trees on the limited site, d_h increased toward the outer tree rings (**Figure 2**). On the favorable site, d decreased and $(t/b)^2$ increased toward the outer tree rings.

TABLE 1 | Comparison of analyzed tracheid traits, pit dimensions, and pit functional properties between study sites [d = mean tracheid diameter, d_h = mean hydraulic diameter, $(t/b)^2$ = cell wall reinforcement, D_p = pit border diameter, D_m = margo diameter, D_t = torus diameter, D_a = aperture diameter, F = margo flexibility, O_a = absolute overlap, O = torus overlap, V = valve effect].

	All analyzed tree rings		Outermost tree ring	
	Limited site	**Favorable site**	**Limited site**	**Favorable site**
Tracheid traits				
d (μm)	17.20 ± 0.9[a]	19.65 ± 1.0[a]	18.09 ± 1.2[a]	16.38 ± 1.1[a]
d_h (μm)	29.04 ± 1.1[a]	29.29 ± 1.1[a]	31.53 ± 1.5[a]	27.33 ± 1.9[a]
$(t/b)^2$	0.040 ± 0.004[a]	0.026 ± 0.004[a]	0.040 ± 0.007[a]	0.043 ± 0.011[a]
Pit dimensions				
D_p (μm)	19.92 ± 0.26[a]	19.14 ± 0.33[a]	20.53 ± 0.44[a]	19.86 ± 0.50[a]
D_m (μm)	18.38 ± 0.26[a]	17.91 ± 0.30[a]	19.03 ± 0.43[a]	18.59 ± 0.49[a]
D_t (μm)	10.63 ± 0.20[a]	10.08 ± 0.20[a]	11.21 ± 0.32[a]	10.74 ± 0.31[a]
D_a (μm)	5.28 ± 0.10[a]	5.71 ± 0.12[b]	5.74 ± 0.16[a]	5.91 ± 0.21[a]
Pit functional properties				
F	0.422 ± 0.005[a]	0.437 ± 0.003[b]	0.410 ± 0.006[a]	0.423 ± 0.006[a]
O_a	2.05 ± 0.02[a]	1.78 ± 0.02[b]	1.95 ± 0.03[a]	1.83 ± 0.03[b]
O	0.503 ± 0.004[a]	0.433 ± 0.005[b]	0.519 ± 0.035[a]	0.447 ± 0.006[b]
V_{ef}	0.212 ± 0.003[a]	0.188 ± 0.001[b]	0.211 ± 0.013[a]	0.188 ± 0.003[b]

Different letters indicate significant differences ($p < 0.05$) between sites. Mean ± SE.

Pit Dimensions and Functional Properties

Comparing pits from tree rings representing the entire life span, D_a was lower on the limited site than on the favorable site ($p = 0.002$; **Table 1**). In the outermost tree ring, pit dimensions were similar on both sites. Functional properties indicated several differences between the study sites: F was lower on the limited site than on the favorable site ($p = 0.007$). O_a, O, and V_{ef} were higher on the limited than on the favorable site ($p < 0.001$). This was also observed in the outermost tree ring: O_a, O, and V_{ef} differed ($p < 0.05$). On the limited site, D_p, D_m, D_t, and D_a increased toward the outer tree rings (**Figure 3**). On the favorable site, no trends for the analyzed pit dimensions were observed from the inner to the outer tree rings, however, D_t tended to be larger in the outer tree rings. No trend was found in trees from the limited site for F, whereas O_a, O, and V_{ef} were higher in the inner compared to the outer tree ring. On the favorable site, F tended to be and V_{ef} was lower in the outer than the inner tree rings. Furthermore, pit dimensions D_p, D_m, D_t, and D_a scaled positively with d_h among the tree rings (**Figure 4**).

DISCUSSION

Tracheid traits and pit dimensions were similar in trees of both sites (in contrast to our hypothesis). However, at a similar distance to the treetop, pit functional properties O_a, O, and V_{ef} were higher in trees from the limited site, indicating higher hydraulic safety. Furthermore, d_h and pit dimensions increased toward the outer tree rings in trees from the limited site, indicating higher hydraulic efficiency with increasing distance from the treetop.

Slightly Higher Hydraulic Safety on the Limited Site

Although trees on the limited site were older than those on the favorable site, both sampled stands had similar tree heights because trees on the favorable site were growing faster (tree rings were on average 3.75 times wider; see also **Supplementary Figure 2**). The higher growth rate was most probably caused by higher nutrient and water availability due to different soil properties.

Despite the striking difference in radial growth between the sites, tracheid dimensions were similar (**Table 1**). Accordingly, Kiorapostolou et al. (2018) found no difference in conduit lumen area in *P. sylvestris* saplings exposed to different water availability and sampled at the same distance from the treetop. Generally, the allometric scaling with distance from the treetop (or branch

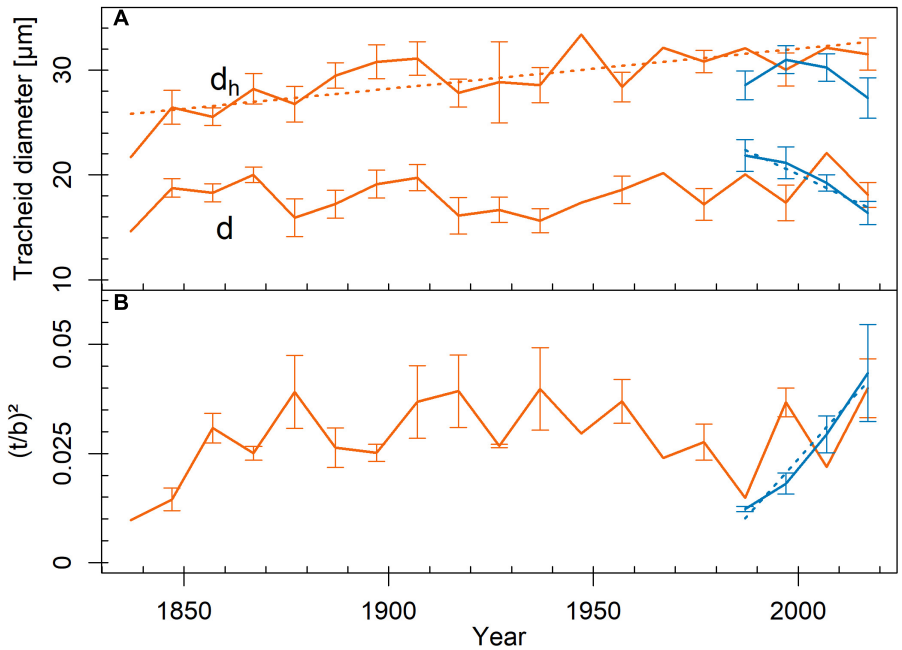

FIGURE 2 | Trends in tracheid traits across tree rings from pith to bark (red = limited site, blue = favorable site). **(A)** mean tracheid diameter (d; $r^2_{favorable}$ = 0.94, p = 0.032) and mean hydraulic diameter (d_h; $r^2_{limited}$ = 0.57, $p < 0.001$), **(B)** cell wall reinforcement [$(t/b)^2$; $r^2_{favorable}$ = 0.97, p = 0.015]. Mean ± SE. Measurement points without SE bars represent tree rings, which were sampled only in one tree individual. Given r^2- and p-values resulted from Pearson product–moment coefficient or Spearman's rank correlation coefficient. Significant trends are marked with regression lines.

tip) seems to be the main driver of conduit diameters, whereas environmental conditions have low influence (Olson et al., 2018, 2021). Deviating from the optimal scaling pattern may decrease a plant's fitness by pushing hydraulic efficiency and hydraulic safety out of balance (Olson et al., 2021). For example, Kiorapostolou et al. (2020) found larger tracheid diameters in *P. sylvestris* trees declining from drought stress than in non-declining trees at the same distance from the treetop.

In addition to conduits, pits are crucial for hydraulic efficiency and safety. Pit functional properties O_a, O, and V_{ef}, which were higher in trees on the limited study site compared to those on the favorable site (**Table 1**), indicated slightly higher hydraulic safety, as these properties play a crucial role in various air-seeding mechanisms (Domec et al., 2008; Delzon et al., 2010). Seal capillary seeding, occurring when the torus–aperture seal is insufficiently airtight, is the most probable air-seeding mechanism in *P. sylvestris* (Bouche et al., 2014), possibly due to the uneven surface of the pit border (**Figure 4**). A larger torus relative to the pit aperture (i.e., O_a or O) increases resistance against air seeding by this mechanism (Delzon et al., 2010). However, with increasing torus diameter, hydraulic efficiency decreases, which Roskilly et al. (2019) suggested to be contributing to the trade-off between longevity and fast growth in conifers.

Pit dimensions change with tracheid size within tree rings, and even small variations in pit dimensions affect the tracheid hydraulic functions (Sviderskaya et al., 2021). Our selection of randomly cut open pits, which mainly occurred in large earlywood conduits, may have led to a small overestimation of pit dimensions in tree rings with a higher proportion with large conduits. However, the potential bias, particularly concerning the pit functional properties, is small, as the proportions of large earlywood tracheids were similar on both sites (**Supplementary Figure 3**).

Increasing Hydraulic Efficiency From Inner to Outer Tree Rings

In trees from the limited site, d_h and pit dimensions increased from the inner to the outer tree rings (**Figures 2**, **5**), leading to increased hydraulic efficiency at breast height as the trees grew. Trees, therefore, adjusted their tracheids and pits to the increasing distance from the treetop to counteract the increasing pathway length resistance (compare Lintunen and Kalliokoski, 2010; Anfodillo et al., 2013; Lazzarin et al., 2016; Losso et al., 2018; Christof et al., 2020). Existing deviation from the linear regression may on the one hand result from unknown height growth dynamics of the tree individuals. On the other hand, it may indicate, that other factors besides the distance from the treetop may have some influence on tracheid and pit dimensions. Castagneri et al. (2015) found the mean tracheid lumen area in *P. abies* to be sensitive to summer precipitation and suggested that water availability could influence tracheid enlargement.

Simultaneously with increasing pit dimensions, functional properties O_a, O, and V_{ef} decreased toward the outer tree rings (**Figure 2**), which indicates a trade-off between hydraulic efficiency and safety at the pit level (Domec et al., 2006). However, as trees grow, they develop an increasingly efficient

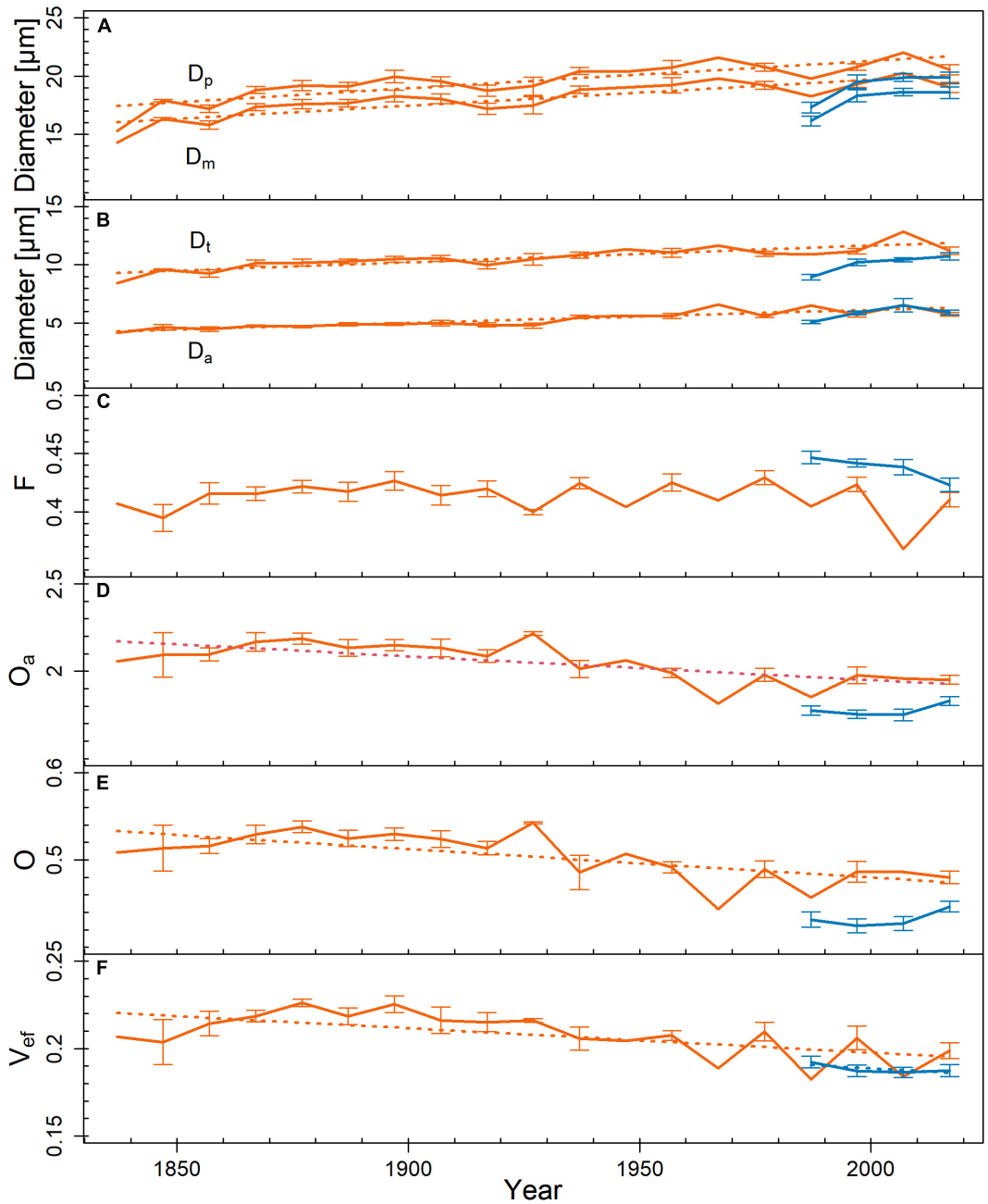

FIGURE 3 | Trends in pit dimensions and functional properties across tree rings from pith to bark (red = limited site, blue = favorable site). **(A)** pit diameter (D_p; $r^2_{limited}$ = 0.71, $p < 0.001$), margo diameter (D_m; $r^2_{limited}$ = 0.72, $p < 0.001$), **(B)** torus diameter (D_t; $r^2_{limited}$ = 0.74, $p < 0.001$), pit aperture diameter (D_a; $r^2_{limited}$ = 0.85, $p < 0.001$), **(C)** margo flexibility (F), **(D)** absolute overlap (O_a; $r^2_{limited}$ = 0.48, $p < 0.001$), **(E)** torus overlap (O; $r^2_{limited}$ = 0.48, p = 0.001), and **(F)** valve effect (V_{ef}; $r^2_{limited}$ = 0.4, p = 0.004; $r^2_{favorable}$ = 0.54, p = 0.027). Mean ± SE. Measurement points without SE bars represent tree rings, which were sampled only in one tree individual. Given r^2- and p-values resulted from Pearson product–moment coefficient or Spearman's rank correlation coefficient. Significant trends are marked with regression lines.

root system (Brodribb et al., 2010), and the improving water supply may allow a slightly decreasing hydraulic safety in favor of increasing hydraulic efficiency at breast height. On the contrary, Domec et al. (2008) and Losso et al. (2018) found O_a to increase with tree height in *Pseudotsuga menziesii*, *P. abies*, and *Pinus cembra*.

Trees on the favorable site showed a decreasing trend from the inner to the outer tree rings in V_{ef}, similar to the trees from the limited site (**Figure 2**). For the short time span of 37 years, the sampling interval of every 10th tree ring was possibly insufficient to show trends in d_h, pit dimensions, and functional properties. The deviation due to height growth dynamics or

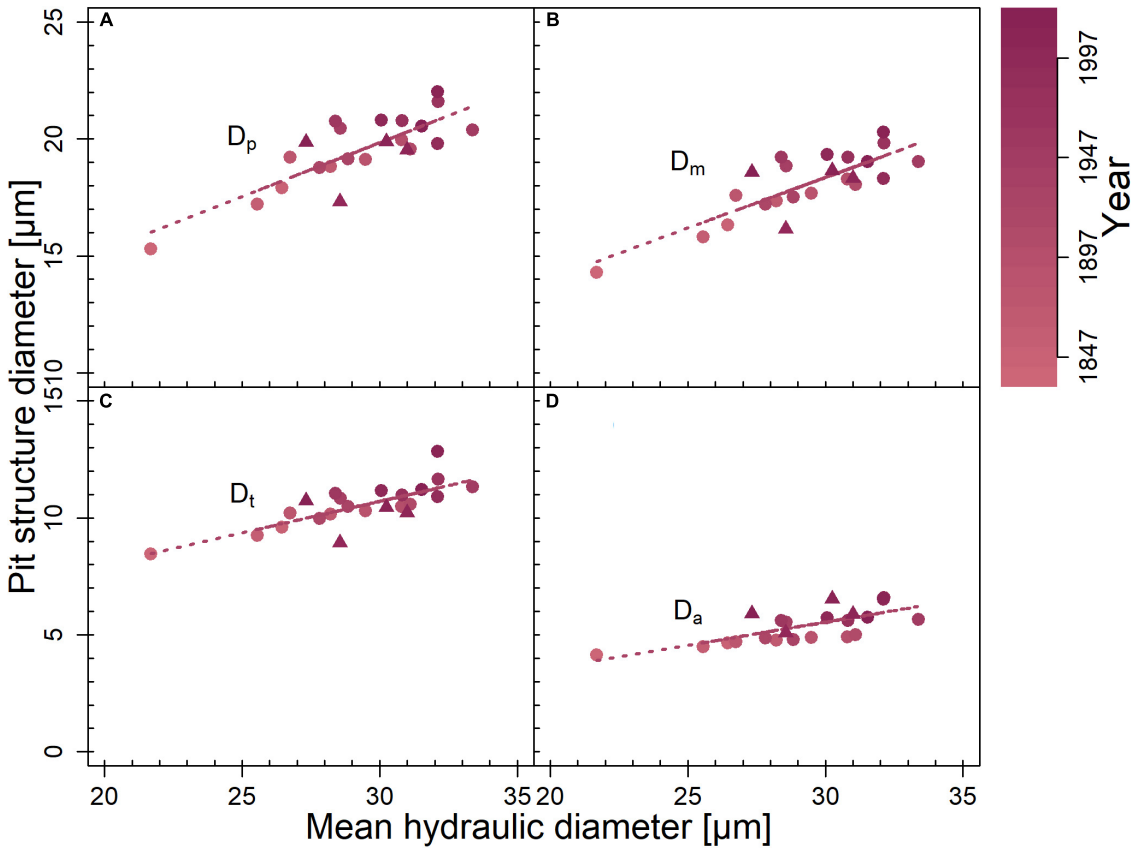

FIGURE 4 | Correlation of mean hydraulic diameter with diameter of **(A)** pit border (D_p; $r^2 = 0.8$, $p < 0.001$), **(B)** margo (D_m; $r^2 = 0.81$, $p < 0.001$), **(C)** torus (D_t; $r^2 = 0.77$, $p < 0.001$), and **(D)** aperture (D_a; $r^2 = 0.72$, $p < 0.001$). Averaged per year for each site (circles = limited site, triangles = favorable site). Correlations were calculated for both sites together. Given r^2- and p-values resulted from Pearson product–moment coefficient. Significant correlations are marked with regression lines. Color gradient indicates year.

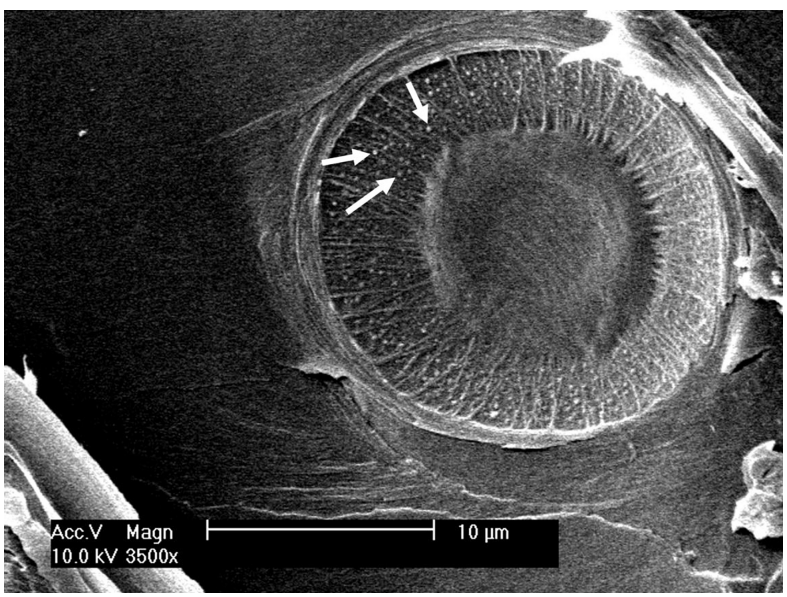

FIGURE 5 | Uneven surface structure (white arrows) of a pit border visible through an aspirated margo.

possibly due to external influences (as mentioned above for the trees from the limited site) may blur the trends. According to Anfodillo et al. (2013) and Kiorapostolou et al. (2020), the adjustment of hydraulic efficiency to transport distance (i.e., distance from the treetop) is independent of environmental conditions. An increasing proportion of latewood in the tree rings due to the opposite trends of earlywood width and latewood width (**Supplementary Figure 2**) explains the negative trend in d toward the outer tree rings.

Because pits can contribute $\geq$ 50% to the xylem's total hydraulic resistance (Domec et al., 2006; Choat et al., 2008), trees under any condition need to coordinate d_h and pit dimensions (**Figure 3**; Hacke et al., 2004; Lazzarin et al., 2016) to optimally adjust hydraulic efficiency.

CONCLUSION

Despite the contrasting growth rates due to different environmental conditions, *P. sylvestris* trees of similar height formed similar-sized tracheids. Only the pit architecture differed, indicating slightly higher hydraulic safety on the limited site and higher efficiency on the favorable site. This suggests that maintaining efficient xylem transport is necessary for tree survival under any condition, whereas the importance of hydraulic safety increases under stressful conditions. The distinctly older trees on the limited site adjusted their d_h and pit dimensions during their lifetime according to the growing distance from the treetop and clearly coordinated these traits with each other to increase their hydraulic efficiency at breast height. Our results provide evidence that under contrasting growing conditions, intra-specific variation in tracheid and pit traits is mainly driven by the distance from the treetop. However, even at a similar distance from the treetop, small but significant variations in pit traits occur, which may affect tree hydraulic safety and efficiency under drought.

DATA AVAILABILITY STATEMENT

The raw data supporting the conclusions of this article will be made available by the authors, without undue reservation.

AUTHOR CONTRIBUTIONS

MH conducted the practical work, analyzed the data, prepared the figures, and wrote the text. SM and WO designed the study and supervised the work. AG outlined the figure concept. SM, WO, AG, and AL revised and commented on the text and figures. All authors contributed to the article and approved the submitted version.

FUNDING

We acknowledge the University of Helsinki Doctoral School in Atmospheric Sciences and the Jane and Aatos Erkko Foundation for financial support during the writing process of the article.

ACKNOWLEDGMENTS

We would like to thank Birgit Dämon and Werner Kofler for their excellent help. The content of the manuscript has previously appeared online as a master thesis (Held, 2019). Also, we would like to thank two reviewers, who helped to improve the manuscript.

SUPPLEMENTARY MATERIAL

The Supplementary Material for this article can be found online at: https://www.frontiersin.org/articles/10.3389/fpls.2021.786593/full#supplementary-material

REFERENCES

Adams, H. D., Zeppel, M. J. B., Anderegg, W. R. L., Hartmann, H., Landhäusser, S. M., Tissue, D. T., et al. (2017). A multi-species synthesis of physiological mechanisms in drought-induced tree mortality. *Nat. Ecol. Evol.* 1, 1285–1291. doi: 10.1038/s41559-017-0248-x

Anfodillo, T., Petit, G., and Crivellaro, A. (2013). Axial conduit widening in woody species: a still neglected anatomical pattern. *IAWA J.* 34, 352–364. doi: 10.1163/22941932-00000030

Bailey, I. W. (1916). The structure of the bordered pits of conifers and its bearing upon the tension hypothesis of the ascent of sap in plants. *Bot. Gaz.* 62, 133–142.

Baker, F. S. (1950). *Principles of Silviculture*. New York: McGraw-Hill Book company, Inc.

Bouche, P. S., Larter, M., Domec, J. C., Burlett, R., Gasson, P., Jansen, S., et al. (2014). A broad survey of hydraulic and mechanical safety in the xylem of conifers. *J. Exp. Bot.* 65, 4419–4431. doi: 10.1093/jxb/eru218

Brodribb, T. J., Bowman, D. J., Nichols, S., Delzon, S., and Burlett, S. (2010). Xylem function and growth rate interact to determine recovery rates after exposure to extreme water deficit. *New Phytol.* 188, 533–542. doi: 10.1111/j.1469-8137.2010.03393.x

Carrer, M., von Arx, G., Castagneri, D., and Petit, G. (2015). Distilling allometric and environmental information from time series of conduit size: the standardization issue and its relationship to tree hydraulic architecture. *Tree Physiol.* 35, 27–33. doi: 10.1093/treephys/tpu108

Castagneri, D., Petit, G., and Carrer, M. (2015). Divergent climate response on hydraulic-related xylem anatomical traits of *Picea abies* along a 900-m altitudinal gradient. *Tree Physiol.* 35, 1378–1387. doi: 10.1093/treephys/tpv085

Choat, B., Cobb, A. R., and Jansen, S. (2008). Structure and function of bordered pits: new discoveries and impacts on whole-plant hydraulic function. *New Phytol.* 177, 608–626. doi: 10.1111/j.1469-8137.2007.02317.x

Christof, A., Ræbild, A., and Thygesen, L. G. (2020). Pit and pit aperture dimensions in plantation-grown Douglas fir as affected by local growth conditions and height in stem. *IAWA J.* 41, 131–140. doi: 10.1163/22941932-bja10003

Cochard, H. (2006). Cavitation in trees. *C. R. Phys.* 7, 1018–1026.

Cochard, H., Hölttä, T., Herbette, S., Delzon, S., and Mencuccini, M. (2009). New insights into the mechanisms of water-stress-induced cavitation in conifers. *Plant Physiol.* 151, 949–954. doi: 10.1104/pp.109.138305

Delzon, S., Douthe, C., Sala, A., and Cochard, H. (2010). Mechanism of water-stress induced cavitation in conifers: bordered pit structure and function support

the hypothesis of seal capillary-seeding. *Plant Cell Environ.* 33, 2101–2111. doi: 10.1111/j.1365-3040.2010.02208.x

Dixon, H. H., and Joly, J. (1895). On the ascent of sap. *Philos. Trans. R. Soc. Lond. Ser. B* 186, 563–576.

Domec, J.-C., and Gartner, B. L. (2002). How do water transport and water storage differ in coniferous earlywood and latewood? *J. Exp. Bot.* 53, 2369–2379. doi: 10.1093/jxb/erf100

Domec, J.-C., Lachenbruch, B., and Meinzer, F. C. (2006). Bordered pit structure and function determine spatial patterns of air-seeding thresholds in xylem of douglas-fir (*Pseudotsuga menziesii*; Pinaceae) trees. *Am. J. Bot.* 93, 1588–1600. doi: 10.3732/ajb.93.11.1588

Domec, J.-C., Lachenbruch, B., Meinzer, F. C., Woodruff, D. R., Warren, J. M., and McCulloh, K. A. (2008). Maximum height in a conifer is associated with conflicting requirements for xylem design. *Proc. Natl. Acad. Sci. U. S. A.* 105, 12069–12074. doi: 10.1073/pnas.0710418105

Hacke, U. G., and Jansen, S. (2009). Embolism resistance of three boreas conifer speices varies with pit structure. *New Phytol.* 182, 675–686. doi: 10.1111/j.1469-8137.2009.02783.x

Hacke, U. G., and Sperry, J. S. (2001). Functional and ecological xylem anatomy. *Perspect. Plant Ecol. Evol. Syst.* 4, 97–115. doi: 10.1078/1433-8319-00017

Hacke, U. G., Sperry, J. S., and Pittermann, J. (2004). Analysis of circular bordered pit function II. Gymnosperm tracheids with torus-margo pit membranes. *Am. J. Bot.* 91, 386–400. doi: 10.3732/ajb.91.3.386

Hacke, U. G., Sperry, J. S., Pockman, W. T., Davis, S. D., and McCulloh, K. A. (2001). Trends in wood density and structure are linked to prevention of xylem implosion by negative pressure. *Oecologia* 126, 457–461. doi: 10.1007/s004420100628

Hargrave, K. R., Kolb, K. J., Ewers, F. W., and Davis, S. D. (1994). Conduit diameter and drought-induced embolism in *Salvia mellifera* Greene (Labiatae). *New Phytol.* 126, 695–705. doi: 10.1111/j.1469-8137.1994.tb02964.x

Harrell, F. E. Jr., and Dupont, C. (2020). Hmisc: *Harrell Miscellaneous. R package version 4.4-1*. Available Online at: https://CRAN.R-project.org/package=Hmisc (accessed December 02, 2021).

Held, M. (2019). *Xylem Plasticity: Tracheid and Pit Architecture of "Pinus sylvestris" Growing on a Dry and a Mesic Site*. Ph.D. thesis. Innsbruck: University of Innsbruck.

Holmes, R. (1986). "Quality control of crossdating and measuring. A user's manual for program COFECHA," in *Tree-ring chronologies of Western North America: California, Eastern Oregon and Northern Great Basin with procedures used in the chronology Development Work Including User's Manuals for Computer Programs COFECHA and ARSTAN*, eds R. Holmes, R. Adams, and H. Fritts (Tucson: Laboratory of Tree-Ring Research, University of Arizona), 41–49.

Jacobsen, A. L., Pratt, R. B., Venturas, M. D., and Hacke, U. G. (2019). Large volume vessels are vulnerable to water-stress-induced embolism in stems of poplar. *IAWA J.* 40, 4–22. doi: 10.1163/22941932-40190233

Jansen, S., Lamy, J.-B., Burlett, R., Cochard, H., Gasson, P., and Delzon, S. (2012). Plasmodesmatal pores in the torus of bordered pit membranes affect cavitation resistance of conifer xylem. *Plant Cell Environ.* 35, 1109–1120. doi: 10.1111/j.1365-3040.2011.02476.x

Kiorapostolou, N., Camarero, J. J., Carrer, M., Sterck, F., Brigita, B., Sangüesa-Barreda, G., et al. (2020). Scots pine trees react to drought by increasing xylem and phloem conductivities. *Tree Physiol.* 40, 774–781. doi: 10.1093/treephys/tpaa033

Kiorapostolou, N., Galiano-Pérez, L., von Arx, G., Gessler, A., and Petit, G. (2018). Structural and anatomical responses of *Pinus sylvestris* and *Tilia platyphyllos* seedlings exposed to water shortage. *Trees* 32, 1211–1218. doi: 10.1007/s00468-018-1703-2

Kramer, J. K., and Kozlowski, T. T. (1960). *Physiology of Trees*. New York: McGraw-Hill Book Company, Inc.

Land Tirol (2021). *tirisMaps*. Available Online at: https://maps.tirol.gv.at/synserver?user=guest&project=tmap_master (accessed November 7, 2021).

Lazzarin, M., Crivellaro, A., Williams, C. B., Dawson, T. E., Mozzi, G., and Anfodillo, T. (2016). Tracheid and pit anatomy vary in tandem in a tall Sequoiadendron giganteum tree. *IAWA J.* 37, 172–185. doi: 10.1163/22941932-20160129

Lintunen, A., and Kalliokoski, T. (2010). The effect of tree architecture on conduit diameter and frequency from small distal roots to branch tips in *Betula pendula*, *Picea abies* and *Pinus sylvestris*. *Tree Physiol.* 30, 1433–1447. doi: 10.1093/treephys/tpq085

Losso, A., Anfodillo, T., Ganthaler, A., Kofler, W., Markl, Y., Nardini, A., et al. (2018). Robustness of xylem properties in conifers: analyses of tracheid and pit dimensions along elevational transects. *Tree Physiol.* 38, 212–222. doi: 10.1093/treephys/tpx168

McDowell, N., Pockman, W. T., Allen, C. D., Brehears, D. D., Cobb, N., Kolb, T., et al. (2008). Mechanisms of plant survival and mortality during drought: why do some plants survive while others succumb to drought? *New Phytol.* 178, 719–739. doi: 10.1111/j.1469-8137.2008.02436.x

Oberhuber, W., Gruber, A., Kofler, W., and Swidrak, I. (2014). Radial stem growth in response to microclimate and soil moisture in a drought-prone mixed coniferous forest at an inner Alpine site. *Eur. J. Forest Res.* 133, 467–479. doi: 10.1007/s10342-013-0777-z

Olson, M. E., Anfodillo, T., Gleason, S. M., and McCulloh, K. A. (2021). Tip-to-base xylem conduit widening as an adaptation: causes, consequences, and empirical priorities. *New Phytol.* 229, 1877–1893. doi: 10.1111/nph.16961

Olson, M. E., Soriano, D., Rosell, J. A., Anfodillo, T., Donoghue, M. J., Edwards, E. J., et al. (2018). Plant height and hydraulic vulnerability to drought and cold. *Proc. Natl. Acad. Sci. U. S. A.* 115, 7551–7556. doi: 10.1073/pnas.1721728115

Patzelt, G., and Poscher, G. (1993). "Der Tschirgant-Bergsturz, in Geologie des Oberinntaler Raumes," in *Arbeitstagung der Geologischen Bundesanstalt in Mieming, Tirol - Schwerpunkt Blatt 144 Landeck*, eds C. Hauser, and A. Nowotny (Vienna: Geologische Bundesanstalt), 205–219.

R Core Team (2020). *R: A Language and Environment for Statistical Computing*. Vienna: R Foundation for Statistical Computing.

Roskilly, B., Keeling, E., Hood, S., Giuggiola, A., and Sala, A. (2019). Conflicting functional effects of xylem pit structure relate to the growth-longevity trade-off in a conifer species. *Proc. Natl. Acad. Sci. U. S. A.* 116, 15282–15287. doi: 10.1073/pnas.1900734116

Rosner, S., Svìtlík, J., Andreassen, K., Børja, I., Dalsgaard, L., Evans, R., et al. (2016). Novel hydraulic vulnerability proxies for a boreal conifer species reveal that opportunists may have lower survival prospects under extreme climatic events. *Front. Plant Sci.* 7:831. doi: 10.3389/fpls.2016.00831

RStudio Team (2020). *RStudio: Integrated Development Environment for R*. Boston: RStudio.

Ryan, M. G., and Yoder, B. J. (1997). Hydraulic limits to tree height and tree growth. *BioScience* 47, 235–242.

Schulte, P. J., and Hacke, U. G. (2021). Solid mechanics of the torus–margo in conifer intertracheid bordered pits. *New Phytol.* 229, 1431–1439. doi: 10.1111/nph.16949

Schulte, P. J., Hacke, U. G., and Schoonmaker, A. L. (2015). Pit membrane structure is highly variable and accounts for a major resistance to water flow through tracheid pits in stems and roots of two boreal conifer species. *New Phytol.* 208, 102–113. doi: 10.1111/nph.13437

Schweingruber, F. H. (1993). *Trees and Wood in Dendrochronology. Morphological, Anatomical and Tree-Ring Analytical Characteristics of Trees Frequently Used in Dendrochronology*. Berlin: Springer-Verlag.

Sperry, J. S., and Hacke, U. G. (2004). Analysis of circular bordered pit function I. Angiosperm vessels with homogenous pit membranes. *Am. J. Bot.* 91, 369–385. doi: 10.3732/ajb.91.3.369

Sperry, J. S., Nichols, K. L., Sullivan, J. E. M., and Eastlack, S. E. (1994). Xylem embolism in ring-porous, diffuse-porous, and coniferous trees of northern Utah and interior Alaska. *Ecology* 75, 1736–1752. doi: 10.2307/1939633

Sperry, J. S., and Tyree, M. T. (1990). Water-stress-induced xylem embolism in three species of conifers. *Plant Cell Environ.* 13, 427–436. doi: 10.1111/j.1365-3040.1990.tb01319.x

Sviderskaya, I. V., Vaganov, E. A., Fonti, M. V., and Fonti, P. (2021). Isometric scaling to model water transport in conifer tree rings across time and environments. *J. Exp. Bot.* 72, 2672–2685. doi: 10.1093/jxb/eraa595

Tyree, M. T., Stephen, D. D., and Cochard, H. (1994). Biophysical perspectives of xylem evolution: is there a trade-off of hydraulic efficiency for vulnerability to dysfunction? *IAWA J.* 15, 335–360. doi: 10.1163/22941932-90001369

von Klebelsberg, R. (1935). *Geologie von Tirol*. Berlin: Borntraeger.

Wickham, H., Averick, M., Bryan, J., Chang, W., McGowan, L. D., François, R., et al. (2019). Welcome to the tidyverse. *J. Open Sour. Softw.* 4:1686. doi: 10.21105/joss.01686

ZAMG (2021). *Klima*. Available Online at: http://www.zamg.ac.at/fix/klima/oe71-00/klima2000/klimadaten_oesterreich_1971_frame1.htm (accessed November 4, 2021).

Zimmermann, M. H. (1983). *Xylem Structure and the Ascent of Sap*. Berlin: Springer-Verlag.

Conflict of Interest: The authors declare that the research was conducted in the absence of any commercial or financial relationships that could be construed as a potential conflict of interest.

Publisher's Note: All claims expressed in this article are solely those of the authors and do not necessarily represent those of their affiliated organizations, or those of the publisher, the editors and the reviewers. Any product that may be evaluated in this article, or claim that may be made by its manufacturer, is not guaranteed or endorsed by the publisher.

frontiers in Plant Science

ORIGINAL RESEARCH
published: 17 February 2022
doi: 10.3389/fpls.2022.787837

Coordination Between Phloem Loading and Structure Maintains Carbon Transport Under Drought

Ryan C. Stanfield and Megan K. Bartlett*

Department of Viticulture and Enology, University of California, Davis, Davis, CA, United States

Maintaining phloem transport under water stress is expected to be crucial to whole-plant drought tolerance, but the traits that benefit phloem function under drought are poorly understood. Nearly half of surveyed angiosperm species, including important crops, use sucrose transporter proteins to actively load sugar into the phloem. Plants can alter transporter abundance in response to stress, providing a potential mechanism for active-loading species to closely regulate phloem loading rates to avoid drought-induced reductions or failures in phloem transport. We developed an integrated xylem-phloem-stomatal model to test this hypothesis by quantifying the joint impacts of transporter kinetics, phloem anatomy, and plant water status on sucrose export to sinks. We parameterized the model with phloem hydraulic resistances and sucrose transporter kinetic parameters compiled from the literature, and simulated loading regulation by allowing loading rates to decline exponentially with phloem pressure to prevent excessive sucrose concentrations from inducing viscosity limitations. In the absence of loading regulation, where loading rates were independent of phloem pressure, most resistance values produced unrealistic phloem pressures owing to viscosity effects, even under well-watered conditions. Conversely, pressure-regulated loading helped to control viscosity buildup and improved export to sinks for both lower and higher resistant phloem pathways, while maintaining realistic phloem pressures. Regulation also allowed for rapid loading and export in wet conditions while maintaining export and viable phloem pressures during drought. Therefore, we expect feedbacks between phloem pressure and loading to be critical to carbon transport in active-loading species, especially under drought, and for transporter kinetics to be strongly coordinated with phloem architecture and plant water status. This work provides an important and underexplored physiological framework to understand the ecophysiology of phloem transport under drought and to enhance the genetic engineering of crop plants.

Keywords: carbon transport, drought, phloem resistance, phloem loading (apoplasmic, symplasmic), viscosity limit, phloem anatomy, molecular regulation

OPEN ACCESS

Edited by:
Daniel Johnson,
University of Georgia, United States

Reviewed by:
Gerhard Buck-Sorlin,
Agrocampus Ouest, France
Rozenn Le Hir,
INRA UMR 1318 Institut Jean Pierre Bourgin, France

****Correspondence:***
Ryan C. Stanfield
rcstanfield@ucdavis.edu

Specialty section:
This article was submitted to Plant Physiology, a section of the journal Frontiers in Plant Science

Received: *01 October 2021*
Accepted: *27 January 2022*
Published: *17 February 2022*

Citation:
Stanfield RC and Bartlett MK (2022) Coordination Between Phloem Loading and Structure Maintains Carbon Transport Under Drought. Front. Plant Sci. 13:787837. doi: 10.3389/fpls.2022.787837

INTRODUCTION

The phloem is the "enigmatic central banker" that appropriates and transports carbon from the photosynthesizing sources to the carbon-consuming sinks (Ryan and Asao, 2014). For the plant to "cash-out" the carbon-rich phloem sap for growth, respiration, or storage, the phloem must maintain a sufficient pressure gradient from source to sink to drive bulk flow (Münch, 1930; van Bel, 2003). The phloem builds pressure at the source by drawing in water from the xylem,

making plant water status important to carbon transport. A wide range of xylem and stomatal traits have been linked to maintaining hydraulic function under water stress and adapting plants to dry environments (Meinzer et al., 2009; Bartlett et al., 2016). However, the traits that confer phloem drought tolerance by maintaining pressure gradients for carbon transport under water stress are not well understood, due to the technical difficulty of measuring phloem transport *in vivo* (Jensen et al., 2016; Savage et al., 2016).

Experimental constraints have made modeling approaches crucial to assess the impacts of phloem traits and plant hydraulics on phloem transport (e.g., Thompson and Holbrook, 2003a,b; Hölttä et al., 2006, 2009; Jensen et al., 2012). Many models have demonstrated an important role for the coupling of phloem sucrose loading rate with photosynthesis to maintain phloem transport in response to drought stress (Daudet et al., 2002; Hölttä et al., 2009; Nikinmaa et al., 2013; Huang et al., 2018). However, for active loading species, photosynthetic regulation of phloem transport may not be necessary, as phloem loading rates may be modulated in response to environmental conditions through molecular regulation of sucrose transporters (e.g., Xu et al., 2018, 2020; Bush, 2020). This added regulatory pathway is important to study, because up to 42% of species surveyed utilize an active sugar loading mechanism (Rennie and Turgeon, 2009), including economically important crops such as celery, tobacco, spinach, tomato, cotton, sunflower, wheat, and grapevine (Kuo et al., 1974; Davies et al., 1999; Rennie and Turgeon, 2009; Muller et al., 2014). Active-loading species use specialized transport proteins to load sugar into the phloem. Transgenic studies have tested upregulating these transporters as a strategy to improve crop performance, but with mixed success; these manipulations improved vegetative growth and grain yield in some species and not others (Leggewie et al., 2003; Dasgupta et al., 2014; Wang et al., 2015; Lu et al., 2020). A greater understanding of the impact of active transport mechanisms on phloem function is needed to inform crop improvement efforts (Lawlor, 2013; Braun et al., 2014) and to better understand the ecological and evolutionary significance of this loading strategy (Savage et al., 2016). Thus, we conducted the first study to our knowledge evaluating the impacts of sucrose transporter kinetics and loading regulatory mechanisms, and the interactive effects of phloem anatomy, on sugar translocation under drought.

Sucrose loading into phloem (Lemoine et al., 2013) as well as transport long distance from source to sink (Hölttä et al., 2006, 2009; Zhou et al., 2020) is closely linked to drought. Drought stress impacts phloem transport by making it more difficult for water to enter the phloem. As water potential becomes more negative (i.e., drier) in the leaf xylem, the phloem is hypothesized to compensate by increasing the sugar concentration in the loading zone (Turgeon, 2010). This mechanism reduces the osmotic potential and strengthens the water potential gradient drawing in water from the neighboring xylem. This influx of water generates the high turgor pressure in the loading zone that powers source-to-sink carbon transport. However, this presents a conundrum, since greater sucrose loading and the resulting higher concentrations increase the viscosity of the phloem sap and, thus, the hydraulic resistance of the phloem (Nikinmaa et al., 2013; Sevanto, 2014, 2018; Salmon et al., 2019). In well-watered conditions, the sugar concentrations measured in many species are consistent with those modeled to be optimal for efficient flow (Jensen et al., 2013). However, a higher viscosity pathway (i.e., higher phloem pathway resistance) means that even more loading is needed to generate the pressure differentials required for transport. This can create feedback between loading and resistance that becomes untenable, causing transport to slow or even stop as the sap becomes too viscous to push down to the sinks, (i.e., "viscosity limitation") (Hölttä et al., 2009; Nikinmaa et al., 2013; Sevanto et al., 2014).

In active loaders, membrane transporter proteins lining the phloem conduit (sieve element/companion cell complexes) membranes load in sugars from the surrounding extracellular space (apoplasm) (Rennie and Turgeon, 2009). Unlike passive (symplasmic) loaders, this mechanism decouples loading rates from the concentration gradient between the mesophyll and phloem loading complex (Lalonde et al., 2004; De Schepper et al., 2013; Schulz, 2015; Milne et al., 2018; Rockwell et al., 2018). This mechanism could reduce constraints on phloem transport by allowing loading to be regulated independently from photosynthesis (Nikinmaa et al., 2013; Huang et al., 2018; Xu et al., 2018), and is hypothesized to produce the higher phloem concentrations and pressure potentials observed in active loaders (Turgeon, 2010). These higher pressures could be advantageous in discouraging phloem-feeding pests or supporting faster growth rates (Savage et al., 2016), but potentially increase the risk of viscosity limitation during drought. However, active loading could also prove beneficial to translocation under drought, by tightly regulating sucrose transporter activity to increase phloem osmotic strength, while preventing viscosity limitations.

Sucrose loading transporters (SUTs or SUCs) are under dynamic regulation, especially in response to environmental stress (Ainsworth and Bush, 2011; Bush, 2020). This is evidenced by their rapid degradation in the loading complex membrane, with a half-life as short as 4 h (Liesche et al., 2011a). Under water stress, SUT transcript abundance can be upregulated (Ibraheem et al., 2011; Xu et al., 2018) or the transporters can be stabilized to prevent their breakdown from the plasma membrane (Ma et al., 2019), which would increase loading and strengthen the gradient for water uptake from the xylem. Alternatively, other experiments have shown high leaf sucrose concentrations to downregulate phloem loading rates (Chiou and Bush, 1998), pointing to a potential mechanism for active loaders to avoid viscosity limitations. The signal driving this dynamic regulation is unknown, but could be phloem turgor pressure, as loading rate has been demonstrated to respond to sieve tube pressure (Smith and Milburn, 1980). Moreover, phloem turgor has been hypothesized to trigger a hormonal signaling cascade that alters transporter expression or post-translational modification of sucrose transporters (Patrick et al., 2001). Thus, it is plausible that a mechanistic relationship regulates sucrose loading in a turgor-dependent manner, but the consequences for phloem function have yet to be explored. V_{max} (the maximum transport rate in Michaelis-Menten formalism) has only been measured for phloem loading proteins in less than six species (Cataldo, 1974; Kuo et al., 1974; Sovonick et al., 1974; Fondy and Geiger, 1977;

Wimmers and Turgeon, 1991; Weise et al., 2000; Borstlap and Schuurmans, 2004; Thompson and Wolniack, 2008), while the functional impacts of variation in V_{max} and its regulation in the context of viscosity limitation and drought are unknown. It is also unknown whether an active loading mechanism may aid in preventing detrimental viscosity build-up through the dynamic down-regulation of sucrose loading proteins.

Since viscosity limitation is caused by excessive resistance along the transport pathway, the structural resistance of the sieve tube is expected to impact the risk of transport failure. Both the sap viscosity and the dimensions of the sieve tube contribute to the vulnerability to viscosity limitation (Sevanto, 2014). More specifically, phloem anatomical properties such sieve tube diameter and end wall (sieve plate) porosity strongly impact phloem resistance (Hölttä et al., 2009; Mullendore et al., 2010; Jensen et al., 2012; Stanfield et al., 2019). Further, pathway resistance can suddenly increase due to callose accumulation (Esau et al., 1962) from insect or mechanical damage (Pickard and Minchin, 1992; Hao et al., 2008). In other words, conduits with higher resistance due to structure are more prone to viscosity limitation, especially in the presence of callose. However, phloem structural resistance (estimated from sieve tube anatomy) was not correlated with habitat water availability (Liesche et al., 2017); while many of those species were likely passive loaders, data we compiled also shows no relationship between loading mechanism, pathway resistance, and maximum drought stress (**Figure 1**). Viscosity limitation could potentially limit the maximum loading rate in a species with high structural resistance, selecting for coordination between phloem anatomy and transporter kinetics. Further, it can be hypothesized that active-loading species from environments with frequent drought could critically depend on downregulation of loading to control viscosity limitation, especially species with high structural phloem resistance.

Overall, our goal was to investigate the interactive effects of loading transporter kinetics and phloem anatomy on sugar transport across a range of water stresses. We predicted that the constraints of viscosity limitation to strongly coordinate phloem loading rates with phloem structural resistance and plant water stress. Specifically, this study addressed the questions: (1) what are the interactive effects of phloem anatomy and drought intensity (i.e., soil water potential) on sugar export by active-loading species? and (2) in scenarios where phloem resistance and drought induce viscosity limitation, how does changing loading transporter kinetics, including introducing pressure-coupled downregulation, impact sucrose export to sinks? We addressed these questions by integrating a stomatal-hydraulic model (modified from Bartlett et al., 2019) that calculated leaf water potentials and gas exchange rates from environmental and hydraulic trait inputs. We then combined this with a simple phloem transport model (De Schepper and Steppe, 2010) that calculated phloem pressure gradients and flow rates within a single sieve tube from leaf sucrose concentrations and water potentials, using the Michaelis-Menten enzyme formalism to represent active loading and unloading (**Figure 2**).

MATERIALS AND METHODS

Model Overview

Conceptually, the model was divided into three components: plant water status, gas exchange and phloem transport (**Figure 2**). The plant water status component calculated the leaf mesophyll and xylem water potentials (Ψ_m and Ψ_x) from an input soil water potential (Ψ_s), gas exchange and hydraulics. The gas exchange component calculated photosynthesis from the stomatal aperture, which was determined from the mesophyll water status (Ψ_m). The phloem transport component calculated a source – sink phloem sucrose concentration and pressure gradient generated from the Michaelis-Menten kinetics of loading/unloading sucrose and the water stress experienced by the phloem (Ψ_x or Ψ_s).

Model Assumptions

To simplify the model, we made the following assumptions:

(1) The simulated plant used active phloem loading and unloading, which captures the mechanisms driving crop production in many economically important species [e.g., grapevine (Zhang et al., 2006), tomato (Hackel et al., 2006), and kiwi (Gould et al., 2013)]. The unloading rates depended on the sucrose concentration in the phloem unloading zone, not the concentration gradient between the unloading zone and sink tissue. This also captures passive unloading dynamics for species that enzymatically convert unloaded sucrose to starch (Goeschl and Han, 2020), or use active uptake processes to remove sucrose immediately surrounding the phloem unloading zone into storage vacuoles (Saftner et al., 1983).

(2) Unloading did not constrain sucrose export, and all sucrose that reached the unloading zone was exported in the same timestep (i.e., the maximum unloading rate $V_{maxU} >> V_{maxL}$). This assumption has some empirical support, as unloading fluxes from the roots of pea plants (*Pisum sativum*) are 95.8% higher than in active loading rates from this species (Wimmers and Turgeon, 1991; Liesche, 2017). Further, we expected unloading limitations to simply exacerbate viscosity limitations by pressurizing the unloading zone and reducing the turgor gradient for phloem transport. Thus, in this study, we prevented unloading from having a confounding effect on viscosity limitation by assuming V_{maxU} was 20% greater than V_{maxL} (see **Supplementary Figure 1** on the consequence of loading limitation on phloem pressure).

(3) All sucrose produced by photosynthesis was available for loading into the transporting sieve elements (i.e., we do not model intermediary transport through the mesophyll or companion cells).

(4) Sucrose only entered/exited from the phloem loading/unloading zones, and the sucrose exported from the unloading zone arrives in sink tissue outside the sieve tube. Leakage of sucrose back out of the loading area by diffusion did not meaningfully impact sucrose export to sinks (**Supplementary Figure 2**).

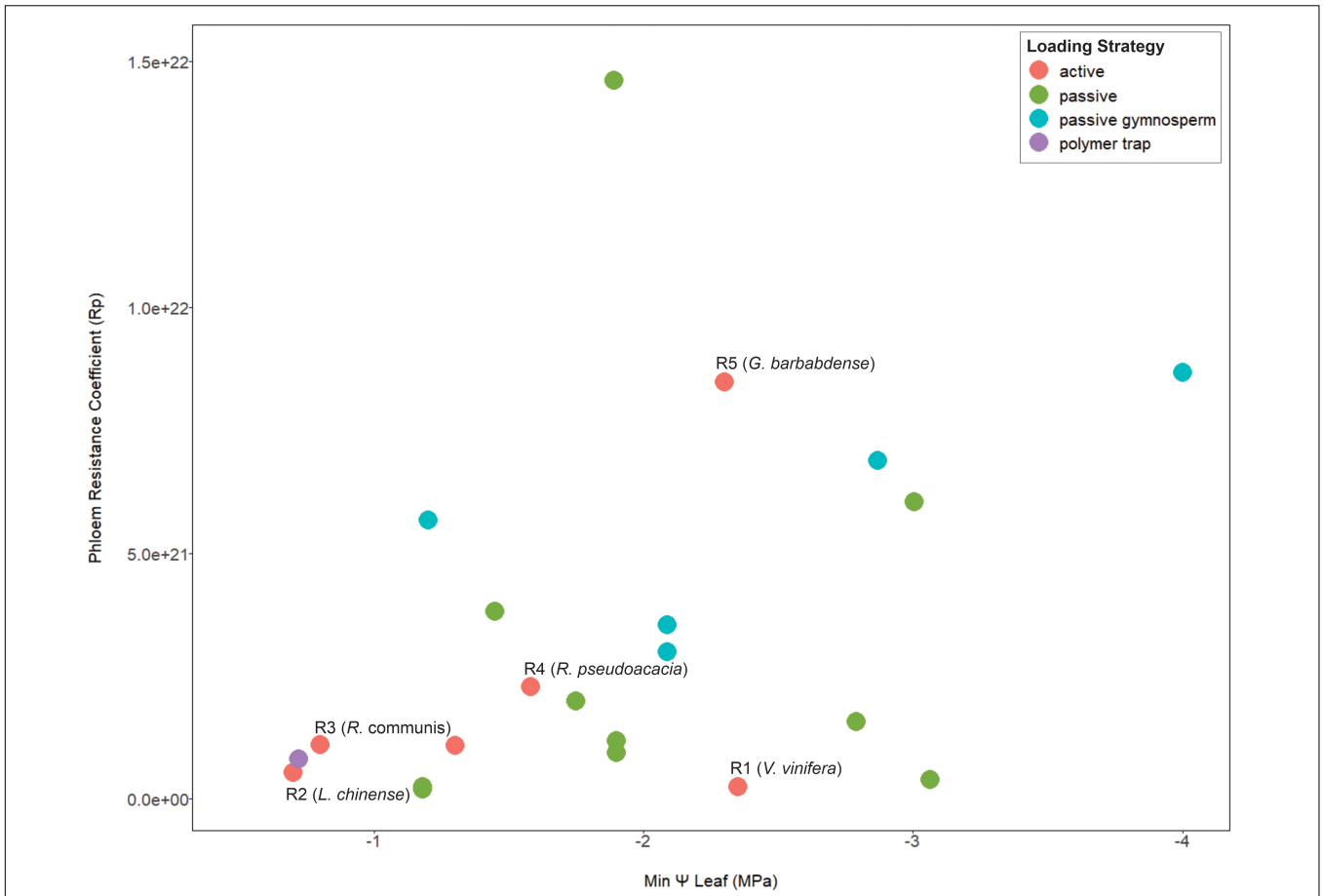

FIGURE 1 | A meta-analysis scatterplot for phloem resistance coefficients and minimum mid-day leaf Ψ that show no association between these two parameters in terms of loading type. Points are color coded by species phloem loading strategy. The species used in the model simulations are indicated from R1–R5 in order of increasing pathway resistance. Anatomical data is from Liesche et al. (2017) and scaled equally to obtain a phloem pressure of >0.6 MPa for all resistance values. Minimum mid-day leaf Ψ was obtained from Choat et al. (2012) and Bartlett et al. (2016). See Supporting Information **Table 1** for data and references used for loading types. Here we assume Gymnosperms are passive loaders, although a systematic study of this taxa for loading mechanism is still warranted (Liesche et al., 2011b; Liesche, 2017).

(5) Phloem water potentials equilibrate with the source xylem, but we did not explicitly model water flow or volume.
(6) Total phloem resistance ($R_{conduit}$) was calculated from sieve element structural resistance (R_p) and phloem sap viscosity (v), which increased with sucrose concentration ($R_{conduit} = Rp \times v$).
(7) Structural resistance was calculated from sieve element dimensions compiled from the literature for stem tissue in active loaders (Liesche et al., 2017; Jensen, 2019). These species were not measured for several factors that impact scaling from sieve element to whole-plant resistance, including total path length or anatomical variation along the path length (i.e., allometric scaling). Thus, these values should be considered plausible first-order estimates, rather than precise species-specific parameters.
Instead, we scaled resistance from individual sieve elements (*Rse*; representing the lumen and sieve plates) to a whole-plant phloem pathway by multiplying with a scalar value (2.5e23) and normalizing by the length of each sieve element (*Rsel*):

$$Rp = \frac{Rse \times 2.5e23}{Rsel} \quad (1)$$

Since phloem anatomical data to obtain a whole plant phloem resistance is only sparsely available, we selected a scalar value that produced reasonable phloem pressures for our baseline/default parameter values (**Table 1**) (i.e., a minimum phloem pressure in the loading zone (P_l) $\geq$ 0.6 MPa) (see **Supplementary Table 1** for *Rse* and *Rsel* values).
(8) Viable phloem pressures in the loading zone ranged from 0.6 to 2.4 MPa, which captures the range of pressures reported in the literature from empirical pressure probe measurements of source-adjacent phloem tissue (reviewed in Turgeon, 2010). Simulations which produced pressures outside this range were considered biologically unrealistic.
(9) Light was constant and non-limiting for photosynthesis.

TABLE 1 | Description of mathematical symbols used in the model.

Symbol	Definition	Value (or units)	References
af	Apoplastic fraction inside the leaf	0.3	Bartlett et al., 2019
ags	Shape parameter relating gsΨ_{50} and Ψ_m	2.0	Bartlett et al., 2019
A_{net}	Carbon assimilation through photosynthesis	(μmol CO_2 m^{-2} s^{-1})	
c_a	Atmospheric CO_2 concentration	400 Parts Per Million	Bartlett et al., 2019
C_m	Concentration of sucrose in mesophyll	(M)	
$C_{pL,U}$	Concentration of sucrose in phloem loading (L) or unloading (U) area	(mM)	
E_s	Rate of sucrose leaving phloem loading area	(m s^{-1})	
Fp	Volumetric flow rate of phloem	(m^3 s^{-1})	
g_{max}	Maximum stomatal conductance	400 mmol m^{-2} s^{-1} (default)	
g_s	Stomatal conductance	(mmol m^{-2} s^{-1})	
g_s Ψ_{50}	Water potential of mesophyll at 50% stomatal closure	−1.5 MPa	Bartlett et al., 2016
$K_{m,x}$	Hydraulic conductance of mesophyll (m) or xylem (x)	(mmol m^{-2} s^{-1})	
K_{max}	Maximum hydraulic conductance of the leaf	20 mmol m^{-2} s^{-1} MPa^{-1}	
M_S	The affinity of the sucrose molecule to the SUT protein	3.3 mM	Borstlap and Schuurmans, 2004
LA	Leaf area	47.4 cm^2	
$L_{sucL,U}$	Loading rate of sucrose per unit tissue area for the loading (l) or unloading (u) area	(mol m^{-2} s^{-1})	
mm	Molar mass of sucrose	342.3 g mol^{-1}	
$P_{l,u}$	Phloem pressure in loading (l) or unloading zone (u)	(MPa)	
r	Radius of phloem conduit	5.5e^{-6} m (tobacco)	Thompson and Wolniack, 2008
Rc	Gas constant	8.3 m^3 pa K^{-1} mol^{-1}	
$R_{conduit}$	Total resistance of the phloem conduit	(MPa s m^{-3})	
R_L	Leaf respiration rate, assumes 12 C atoms in 1 sucrose	0.25 μmol C m^{-2} s^{-1}	Bartlett et al., 2019
RF	Dimensionless value which determines if phloem is in water potential equilibrium with xylem	Dimensionless	Thompson and Holbrook, 2003b
Rp	Structural resistance coefficient of the phloem	See **Table 2**	Liesche et al., 2017
RWC_m	Relative water content of the mesophyll	(%)	
Sl	Leak rate of sucrose in the phloem conduit	7.3e^{-16} m s^{-1}	Edelman et al., 1971
S_m	Moles of sucrose in apoplasmic space	(mols)	
$S_{p,b}$	Mass of sucrose inside loading phloem (p) or unloading phloem (b)	(g)	
t	Run time of model	12 h	
T	Temperature	293 K	
v	Viscosity of phloem conduit sap	(MPa s)	
V_{maxL}	Maximum rate of sucrose uptake (phloem loading)	1.58e^{-7} mol m^{-2} s^{-1} (default)	Borstlap and Schuurmans (2004) (tobacco)
V_{maxU}	Maximum rate of sucrose export (phloem unloading)	V_{maxL} × 1.2 mol m^{-2} s^{-1} (default)	
VPD	Vapor pressure deficit of leaf	9.9e^{-3} (dimensionless)	
W_p	Water volume inside phloem	3.57e^{-11} m^3 (R1 and R2; default) 1.04e^{-8} m^3 (R3) 1.37e^{-8} m^3 (R4 and R5)	
α	Shape parameter for determining mesophyll conductance	2	Bartlett et al., 2019
ρ	Density of phloem sap	(g m^{-3})	
$\pi_{l,u}$	Osmotic potential of phloem @ loading (l) or unloading (u) zones	(MPa)	
$\Psi_{50,m}$	Mesophyll water potential at which 50% of the mesophyll conductance is lost.	−2.0 MPa	Bartlett et al., 2016
Ψ_m	Water potential- mesophyll	(MPa)	
Ψ_s	Water potential- soil	−0.001 MPa (default); See **Table 2** for drought	
Ψ_x	Water potential - xylem	(MPa)	Vs Description: Phloem velocity in loading area, unit: (ms^{-1})

If values are outputs of the model, then only units of the parameter are shown.

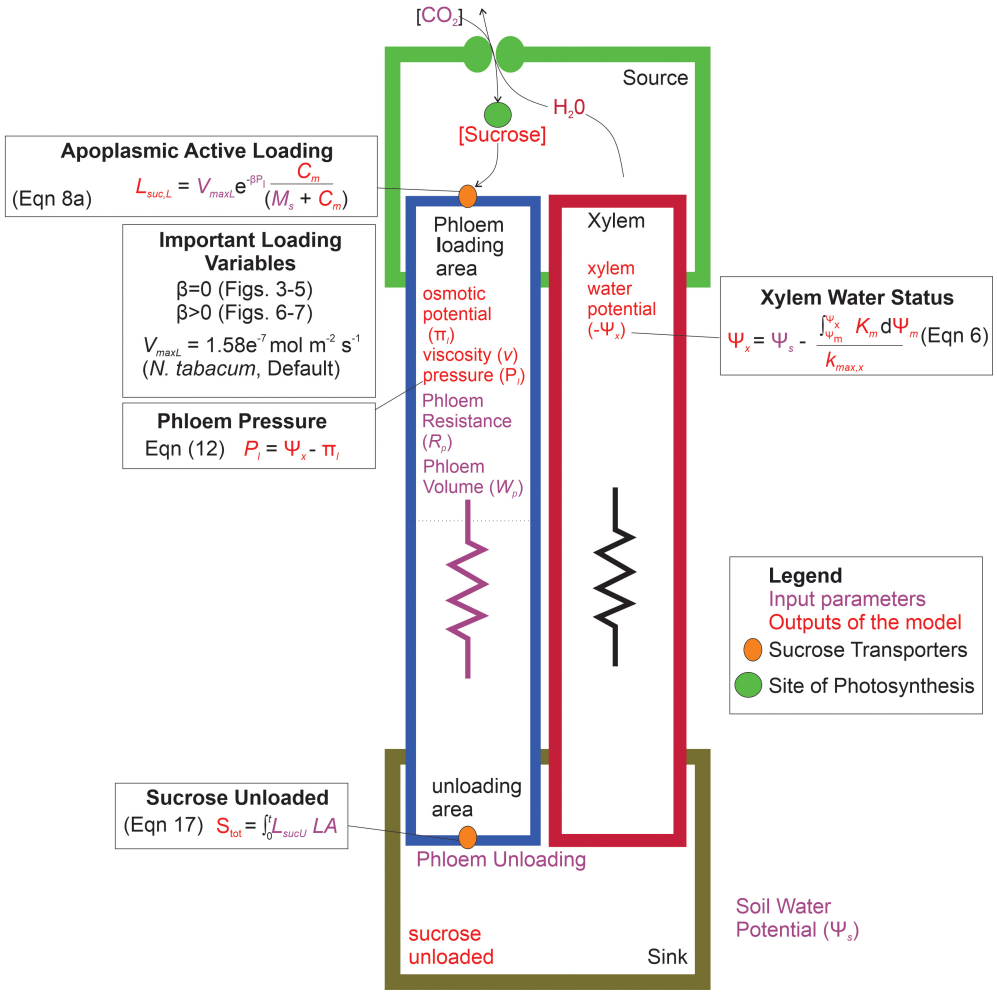

FIGURE 2 | Parameterization and conceptual schematic of the water and sugar transport model. The model inputs are shown in purple, while the outputs of the model are in red. The model first produced a xylem water potential based on the input soil water potential. Sucrose concentrations are built in the leaf compartment (source), and actively loaded into the phloem through protein transporters. Loading variables that were altered in the different simulations are shown, which impact the resulting phloem specific outputs such as: phloem osmotic potential, viscosity, pressure, and the eventual sucrose exported to the sink area. Symbols: L_{sucL} = loading rate per unit leaf area, V_{maxL} = maximum rate of sucrose uptake, β = shape parameter for loading downregulation, *Pl* = phloem pressure in loading area, *C* = concentration of sucrose in source area, M_S = Michaelis-Menten constant for sucrose affinity, S_{tot} = total sucrose exported over the entire simulation, L_{sucU} = total unloading rate, *LA* = leaf area, Ψ_m = water potential of source area, k_m = hydraulic conductivity of mesophyll, $k_{max,x}$ = maximum hydraulic conductivity of xylem.

(10) The water volume in the mesophyll changed over time, while the xylem was at steady state.
(11) Sucrose concentration in the mesophyll did not impact the water potential of the mesophyll.

Plant Water Status and Gas Exchange

We separated the plant into two hydraulic elements, the mesophyll of a single leaf and the root-to-leaf xylem network, to capture the protective effect of vulnerability segmentation (Tyree and Ewers, 1991). The leaf accounts for at least 30% of whole-plant hydraulic resistance, with the mesophyll tissue accounting for about half of this resistance (Sack and Holbrook, 2006; Scoffoni et al., 2011). This generates a strong water potential gradient across the mesophyll that buffers the xylem and phloem against water stress. We adapted the water balance equations from Sperry et al. (1998) to calculate the mesophyll and xylem water volume at each timestep:

$$\frac{dW_m}{dt} = \int_{\Psi_m}^{\Psi_x} K_m d\Psi - g_s VPD\, LA \tag{2a}$$

$$\frac{dW_x}{dt} = K_x(\Psi_s - \Psi_x) - \int_{\Psi_m}^{\Psi_x} K_m d\Psi = 0 \tag{2b}$$

where *W* is the water volume, Ψ is the water potential, and *K* is the hydraulic conductance of the mesophyll (subscript *m*) and xylem (subscript *x*). The *VPD* and Ψ_s are the environmental parameters, the vapor pressure deficit and soil water potential,

TABLE 2 | Parameters which varied during the simulations.

Symbol	Definition	Value
R_p	Estimated structural resistance coefficient of the phloem such that R1 obtains > 0.6 MPa loading pressures under wet soil conditions (i.e., $\Psi = -0.001$ MPa)	$2.4e^{20}$ m^{-3} (R1:; *Vitis vinifera*) $5.4e^{20}$ (R2:; *Liriodendron chinense*) $1.1e^{21}$ (R3:; *Ricinus communis*) $2.3e^{21}$ (R4:; *Robinia pseudoacacia*) $8.5e^{21}$ (R5:; *Gossypium barbadense*)
V_{maxL}	Maximum rate of sucrose uptake (phloem loading)	$1.58e^{-7}$ (Default, *N. tabacum*; Borstlap and Schuurmans, 2004) – see **Table 3** for range of values used in **Figure 7**
V_{maxU}	Maximum rate of sucrose export (phloem unloading)	$=V_{maxL} \times 1.2$
Ψ_s	Water potential of soil	$-0.001 - (-)1$ MPa

For R_p, sieve element resistances from stem tissue were based upon stem anatomical data from Liesche et al. (2017; see Eq. 1 for formulation).

TABLE 3 | Data on available apoplasmic active loader maximum loading rate (V_{max}) and phloem anatomical characters to calculate R_p.

Species	Maximum loading rate (mol m^{-2} s^{-1}) (V_{max})	Rp (for one sieve element)	References
Nicotiana tabacum	$1.6e^{-7}$ (1), $3.3e^{-7}$ (2)	9.86E+17 (3) (petiole)	Borstlap and Schuurmans, 2004 (1); Cataldo, 1974 (2); Thompson and Wolniack, 2008 (3)
Beta vulgaris	$1.6e^{-7}$ (1), $8.2e^{-7}$ (2)	–	Fondy and Geiger, 1977 (1); Sovonick et al., 1974 (2)
Vicia faba	$1.60e^{-7}$	–	Delrot and Bonnemain, 1980
Trticum aestivum	$2.30e^{-6}$	–	Kuo et al., 1974
Arabidopsis thaliana	$1.30e^{-8}$ (1)	2.03E+19 (2) (stem)	Weise et al., 2000 (1); Thompson and Wolniack, 2008 (2)
Solanum tuberosum	$1.10e^{-8}$	–	Weise et al., 2000
Pisum sativum	$2.90e^{-6}$		Wimmers and Turgeon, 1991

respectively; g_s is the stomatal conductance, and LA is the area of a single leaf (see **Table 1** for constant parameter values and **Table 2** for the parameters varied across simulations).

The mesophyll water volume is converted to a relative water content by dividing by the maximum water volume $\left(RWC_m = \frac{W_m}{V_{sat,m}}\right)$, and then to a water potential through the pressure-volume relationships:

$$\Psi_m = \begin{cases} \dfrac{\pi_0\left(1-a_f\right)}{RWC_m - a_f} - \pi_o - \varepsilon\left(1 - \dfrac{1-a_f}{RWC_m - a_f}\right) & \Psi_m > \pi_{tlp} \\ \dfrac{\pi_m}{RWC_m} & \Psi_m \leq \pi_{tlp} \end{cases} \quad (3)$$

where π_o, π_{tlp}, a_f, and ε are the leaf pressure-volume curve parameters of osmotic potential at full hydration turgor loss point, apoplasmic fraction, and cell wall modulus of elasticity, respectively (Bartlett et al., 2012). We considered the effects of mesophyll sugar content on water relations to be outside the scope of this study, and, thus, we assumed here that π_o was constant.

Water flow through the mesophyll was determined by integrating the mesophyll vulnerability curve:

$$K_m = \int_0^t \frac{K_{max,m}}{1 + e^{-\alpha\left(\Psi_m - \Psi_{50,m}\right)}} \quad (4)$$

where $K_{max,m}$ is the maximum hydraulic conductance of the mesophyll, normalized by leaf area, α is a shape parameter, and $\Psi_{50,m}$ is the mesophyll water potential at which 50% of conductance is lost. To simplify these calculations, we used a sufficiently negative xylem Ψ_{50} value (-2 MPa) to assume K_x was constant and equal to the maximum xylem conductance ($K_{max,x}$) over the range of xylem water potentials in these simulations.

We calculated g_s from the assumption that mesophyll water stress induced stomatal closure:

$$g_s = \frac{g_{max}}{1 + e^{-ags\left(\Psi_m - g_s\Psi_{50}\right)}} \quad (5)$$

where g_{max} is the maximum stomatal conductance, ags is the shape parameter for this relationship, and $g_{s\ 50}$ is the mesophyll water potential inducing 50% stomatal closure. Photosynthesis (A_{net}) was then calculated from g_s based upon an extrapolation of the original Farquhar equations (Farquhar et al., 1980; Bartlett et al., 2019).

At the beginning of each timestep, Ψ_m was calculated from the change in mesophyll volume over the previous timestep (Eqs 2a, 3). Mesophyll water flow was then calculated by integrating the mesophyll vulnerability curve over water potential, bounded by the new Ψ_m and the Ψ_x from the previous timestep (Eqs 2, 3). Stomatal conductance (g_s) was then calculated from the new Ψ_m (Eq. 5), and Ψ_x was updated from the new mesophyll water flow:

$$\Psi_{x,t} = \Psi_s - \frac{\int_{\Psi_{m,t}}^{\Psi_{x,t-1}} K_{m,t} d\Psi}{K_{max,x}} \quad (6)$$

where t indicates the current timestep and was used to determine the new xylem flow $K_{max,x}\left(\Psi_s - \Psi_x\right)$ (Eq. 2b). The new mesophyll flow and g_s values were then supplied to Eq. 2a to update the mesophyll volume for the next timestep. We ran

the model at a 1s timestep over 12 h simulations to achieve steady-state solutions, which were reported as the model results.

Phloem Transport

The mass of sucrose in the mesophyll (S_m) was increased by photosynthesis and reduced by loading into the phloem companion cells via sucrose transporters:

$$\frac{dS_m}{dt} = A_{net}LA - L_{sucL}LA \tag{7}$$

where L_{sucL} is the loading rate per unit leaf area. To simplify the model, we assumed all the sugar produced by photosynthesis is exported into the apoplasmic space surrounding the sieve element/companion cell complexes of the loading zone, and thus available for phloem loading. For loading (subscript $i = L$) or unloading (subscript $i = U$), $L_{suc,i}$ was calculated from the Michalis-Menten formalism for enzyme kinetics:

$$L_{suc,i} = V_{max,i}\frac{C}{M_S + C} \tag{8a}$$

$$C_m = \frac{S_m}{W_m} \tag{8b}$$

where $V_{max,i}$ is the maximum loading or unloading rate of the sucrose transporters, normalized by leaf area, and M_S is a shape parameter capturing transporter affinity for sucrose. C is either C_m, the sucrose concentration in the mesophyll outside the loading zone, or C_{pU}, the sucrose concentration in the unloading phloem zone. W_m is the mesophyll water volume (Eq. 2a), which changes the concentration of sucrose available for loading in Eq. 8b.

Loading increased the mass of sucrose in the phloem loading zone ($S_{p,L}$), which was transported to the unloading zone:

$$\frac{dS_{p,L}}{dt} = L_{SUCL}LA - E_s \tag{9}$$

where E_s is the mass flow rate of sucrose transport (g s^{-1}). E_s was calculated from the volumetric flow rate of the phloem sap (F_p; m^3 s^{-1}) and sucrose concentration in the loading zone ($C_{p,L}$; mol m^{-3}):

$$E_s = F_pC_{p,L}mm \tag{10a}$$

$$C_{p,L} = \frac{S_{p,L}}{W_p} \tag{10b}$$

where mm is the molar mass of sucrose and W_p is the maximum water volume in the loading zone. Thompson and Holbrook (2003a) found that accounting for *diurnal changes* in phloem volume did not substantially impact the flux of sucrose through the transport pipeline. Thus, we made the simplifying assumption that W_p was constant at the maximum loading zone phloem volume, so that C_{pL} only varied with the mass of sucrose.

The sucrose concentration determined the osmotic potential (π_i) in the loading (L) or unloading zone (U):

$$\pi_i = -RcTC_{p,i} \tag{11}$$

where Rc is the gas constant and T is the temperature within the phloem loading area. Following Thompson and Holbrook (2003b), we made the simplifying assumption that the water potential of the phloem loading zone equilibrates with the xylem water potential (Ψ_x) when the phloem is at steady state. Further, we estimate that the anatomical dimensions, osmotic strength, and enhanced permeability due to aquaporins (Muries et al., 2013; Stanfield et al., 2017) of our loading zone has an RF (axial to radial resistivity) value >> 1 (see Thompson and Holbrook, 2003b), which equates to phloem in water potential equilibrium with the xylem. The turgor pressure in the loading or unloading zone (P_i) was then determined from the water and osmotic potentials:

$$P_i = \Psi_x - \pi_i \tag{12}$$

Noting that for determining the phloem pressure in the unloading zone, Ψ_s is used. The volumetric phloem flow rate F_p (m^3 s^{-1}) was calculated from the pressure difference between the loading (P_L) and unloading (P_U) zones and the hydraulic resistance of the phloem ($R_{conduit}$):

$$F_p = \frac{P_L - P_U}{R_{conduit}} \tag{13}$$

which increased with the phloem sucrose concentration due to viscosity (v) effects (see **Appendix A**), and integrated into a resistance formula:

$$R_{conduit} = Rp \times v \tag{14}$$

where Rp is the resistance coefficient of the single phloem conduit, or sieve tube (see **Table 2**).

The velocity of sap flow (V_s) was calculated by normalizing volumetric flow by conduit area:

$$V_s = \frac{Fp}{\pi r^2} \tag{15}$$

where r is the radius of the conduit.

The same processes then take place when the sucrose reaches the unloading zone, where unloading is determined from:

$$\frac{dS_U}{dt} = E_s - L_{SUCU}LA \tag{16}$$

We made the simplifying assumptions that the source and sink area (LA) and the phloem volume in the loading and unloading zones (W_p) are equal.

Finally, we quantified sugar export (S_{tot}) as the cumulative mass of sucrose unloaded over the simulation, as:

$$S_{tot} = LA\int_0^t L_{SUCU}(t)\,dt \tag{17}$$

The model was implemented using MATLAB R2020a (9.8.0) (Mathworks, Inc., Natick, MA, United States). Access to the code may be obtained through DOI: 10.5281/zenodo.5907490.

Model Parameterizations to Test Hypotheses

We tested the impacts of water stress and phloem anatomy and transporter kinetics on phloem function by varying

the (1) soil water potential (Ψ_s), (2) phloem structural resistance (*Rp*), (3) phloem volume (*Wp*), (4) maximum sucrose loading rate (V_{maxL}), and (5) the shape parameter for the relationship between loading rate (L_{sucL}) and turgor (β) across simulations (see **Table 2** for parameter values). We parameterized a range in soil water stress by varying Ψ_s from well-watered to droughted values (−0.001 to −1 MPa). We used the published sieve element dimensions for stems from 5 active loading species to produce reasonable estimates of *Rp* (**Figure 1**; see model assumption #7). Data for source phloem volume is scarce, so we initially estimated *Wp* by multiplying the mean sieve element area for *Populus tremula x alba* leaf (Carvalho et al., 2017) by the total vein length in a grapevine leaf, as a representative active loader (Pagano et al., 2016). However, this estimation only accounted for 0.002% of total volume in our hypothetical leaf, while the phloem has been estimated to account for up to 0.4% of leaf volume (Sjolund, 1997). Thus, we parameterized the model with phloem volumes ranging from 0.002 to 0.8% of leaf volume to capture a wide range of potential parameter space. We compared the cumulative sucrose export (S_{tot}), phloem loading zone concentration (C_l), pressure (P_l), phloem viscosity (v) and velocity (V_s) across simulations.

Phloem resistance and volume had strong interactive effects on sugar export, with small volumes exacerbating viscosity limitations for high resistances (see "Results," **Figure 3**). Thus, we were concerned that incorrect assumptions about these parameter combinations could overestimate viscosity limitations under drought. We used our first simulations to identify the phloem volumes that (1) maximized sugar export with (2) viable phloem pressures under drought ($\Psi_s = -1$ MPa) for each *Rp* value. We used these values to parameterize the rest of the simulations, to evaluate the impacts of transporter kinetics on viscosity limitation under the most favorable anatomical parameterizations.

Next, we parameterized variation in maximum loading rate (V_{maxL}) by compiling published values for low (*Arabidopsis*), intermediate (tobacco), and high (wheat) rates (Weise et al., 2000; Borstlap and Schuurmans, 2004; Liesche and Schulz, 2013). We used the intermediate value from tobacco as our default unless otherwise noted (**Table 3**). We also tested whether regulating loading rates in response to pressure would protect the phloem from viscosity limitations, by reducing loading before reaching excessive concentrations and pressures. We used an exponential decay function to reduce the loading rate as a function of loading zone pressure:

$$L_{suc,L} = V_{max,L} e^{-\beta Pl} \frac{C}{M_S + C} \quad (18)$$

and increased the shape parameter (β) from 0 to 10 to test the impacts of loading downregulation. We first varied β and V_{maxL} independently, and then together, to identify the combinations that (1) maximized sucrose export and (2) obtained viable loading zone pressures (see model assumptions #8) for different resistances (R2 and R4) and soil moisture scenarios ($\Psi_s = -0.001$ and −1 MPa).

RESULTS

Coordination Between Phloem Anatomy Traits Strongly Influenced Phloem Vulnerability to Viscosity Limitation

The importance of viscosity limitations on sugar transport depended strongly on phloem anatomy (**Figure 4**). Simulations either reached stable, equilibrium sucrose concentrations over the course of the 12-h model runs (i.e., steady-state), or failed to converge on a stable concentration due to excessive viscosity (i.e., non-steady-state) under high water stress and/or sieve tube structural resistances and small phloem volumes. For example, a simulation with moderate structural resistance (R2) reached steady-state and achieved a stable loading zone concentration, pressure, total resistance, and flow rate under dry conditions ($\psi_s = -0.001$ and −1 MPa) (**Figure 4**, yellow lines). By contrast, a simulation with ∼25% greater structural resistance still reached steady-state in wet soil (**Figure 4**, blue lines), but failed to equilibrate under water stress and phloem concentration and pressure increased without limit (**Figures 4A,B**, red lines). In these non-steady-state simulations, phloem viscosity and total resistance remained too high for the loading zone pressure to overcome (**Figure 4C**, red line), even as concentrations increased, preventing phloem flow (**Figure 4D**, red line). In these scenarios, sugar export only proceeded for a small fraction of the 12-h simulation.

Coordinating phloem volume with pathway resistance alleviated runaway viscosity and avoided non-steady-state transport failure. There is little data available to parameterize phloem volume and resistance in leaves for active loading species, so we simply varied these parameters widely (i.e., by three orders of magnitude for phloem volume; see Methods) to evaluate the impacts on sucrose export (**Figures 3A,B**), phloem pressure (P_l; **Figures 3C,D**) and viscosity (v; **Figures 3E,F**). In the lower resistance pathways (R1 and R2), all phloem volumes allowed sucrose export to proceed without runaway viscosity, while the smallest volumes produced the greatest sucrose output, under both wet and dry conditions ($\Psi_s = -0.001$ and −1 MPa). However, for the intermediate (R3) and high (R4 and R5) phloem resistances, phloem pressure and viscosity reached intractable values at lower volumes; this effect was exacerbated under drier soils. Overall, larger phloem volumes were optimal for sucrose export in more resistive pathways and drier conditions. We also used the volumes that optimized export under drought (white asterisks) to parameterize volume for each resistance in the subsequent simulations, to avoid overestimating the importance of viscosity limitations by making incorrect assumptions about phloem anatomy (i.e., $W_p = 3.57e^{-11}$ m^3 for R1 and R2, $1.04e^{-8}$ m^3 for R3, and $1.37e^{-8}$ m^3 for R4 and R5; see "Materials and Methods" and **Table 2**).

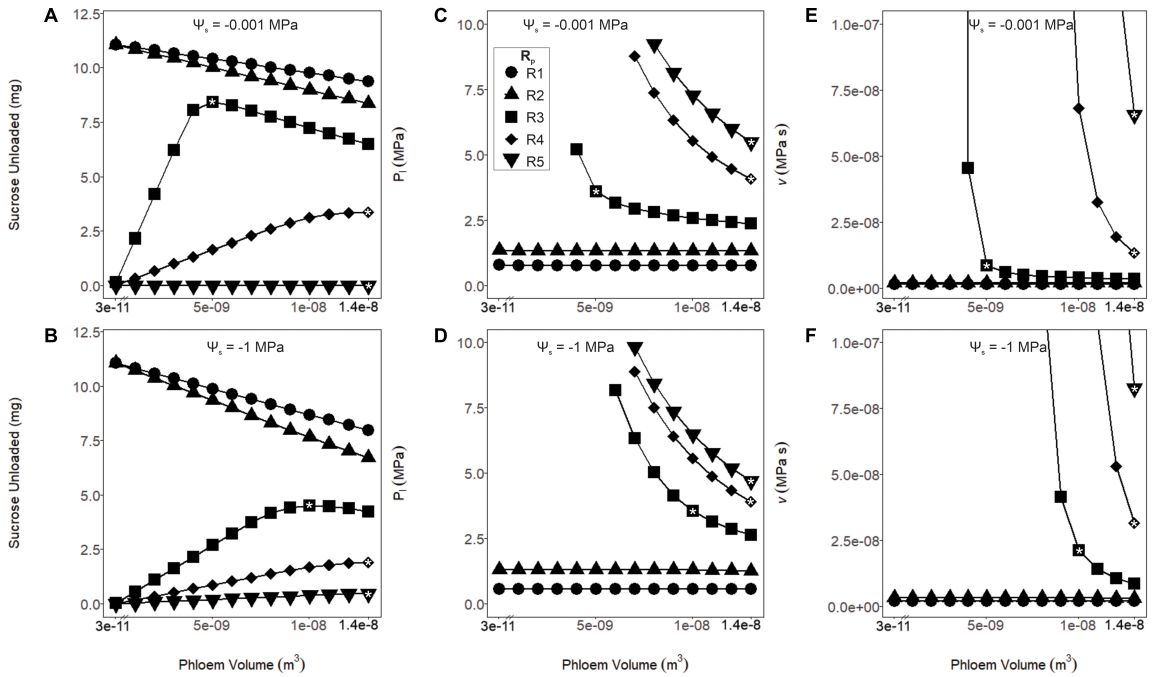

FIGURE 3 | Sucrose unloaded, phloem pressure (P_l) and viscosity (v) as a function of phloem volume and pathway resistance (R1–R5). These simulations were run under wet ($\Psi_S = -0.001$ MPa: **A,C,E**) or dry ($\Psi_S = -1$ MPa: **B,D,F**) soil conditions. **(A,B)** As phloem volume declined, sucrose export increased for the lower resistance pathways (R1 and R2). Export peaked at intermediate volumes and resistances (R3) and continued to increase at higher volumes and resistances (R4 and R5). This effect was intensified for the drier simulation. **(C,D)** Phloem pressure remained stable over all tested volumes for the lower resistance pathways (R1 and R2), while increased with lower volumes for the higher resistance pathways (R3–R5). For the higher resistance pathways and lower volumes, resulting pressures are not shown due to excessive values. **(E,F)** The phloem viscosity remained stable for lower resistance pathways (R1 and R2) over the range of volumes tested, while runaway viscosity began to occur at the lower phloem volumes for the higher resistance pathways (R3–R5). A drought scenario would induce the runaway viscosity effect at lower phloem volumes for these resistances. In subsequent analysis, volumes were chosen (white asterisks) for each resistance that maximized sucrose export while preventing the runaway viscosity effect over the range of Ψ_S tested: R1 and R2; 3.57 e^{-11} m^3, R3; 1.04e^{-8} m^3, and R4 and R5; 1.37e^{-8} m^3.

Sucrose Export Was Independent of Phloem Resistance and Xylem Water Status Until These Variables Reached Thresholds for Viscosity Limitation

Sugar export was constant over the soil water potentials tested for structural resistances below thresholds for viscosity limitation (**Figure 5A**, R1 and R2), and declined above these thresholds (**Figure 5A**, R3–R5). Below these thresholds, loading zone concentration and turgor increased until flow reached a steady-state equilibrium (see **Figure 4**), where the mass of sucrose imported into the phloem equaled the mass exported. Here, we assumed transport was not constrained by unloading and that all sucrose that entered the unloading area was immediately exported to sinks (i.e., $V_{maxU} >> V_{maxL}$; see "Materials and Methods": assumption #2). Thus, sucrose export in these lower resistance simulations (R1 and R2) were independent of water stress and phloem pressure. Drier conditions increased sap viscosity and reduced phloem velocity by changing the total resistance and source to sink pressure gradient (**Figures 5B,C**). For the least resistant phloem (**Figure 5D**, R1), phloem pressure slightly decreased with soil water potential, because the xylem water potential was decreasing at a greater rate than phloem osmotic potential (e.g., **Supplementary Figure 3**, green line).

In contrast, the simulations with the most resistant sieve tubes (R3–R5) not only declined in their overall sucrose output but varied in their response to the soil dry-down (**Figure 5A**). The decline in sucrose output was attributed to a viscosity limitation, as the higher resistance scenarios had both higher overall viscosity, and increased viscosity under higher drought stress (**Figure 5B**). As with the lower resistance pathways, velocity declined with soil water potential, but did so more rapidly (**Figure 5C**). Finally, phloem pressures in the higher resistance pathways were well above empirically measured values of 0.6–2.4 MPa (**Figure 5D**, red dashed lines). Of note was the intermediate resistance (R3) which showed increased phloem pressure with declining soil water, as a result of phloem osmotic potential increasing faster than xylem water potential (**Supplementary Figure 3**, red line).

Maximizing Export While Maintaining Viable Phloem Pressure Using Pressure Regulated Loading

Although increasing phloem volume helped alleviate runaway viscosity, higher resistance pathways where still under the effects of viscosity limitation, which caused phloem pressures to be unrealistic. Thus, we hypothesized maximum loading rates to be

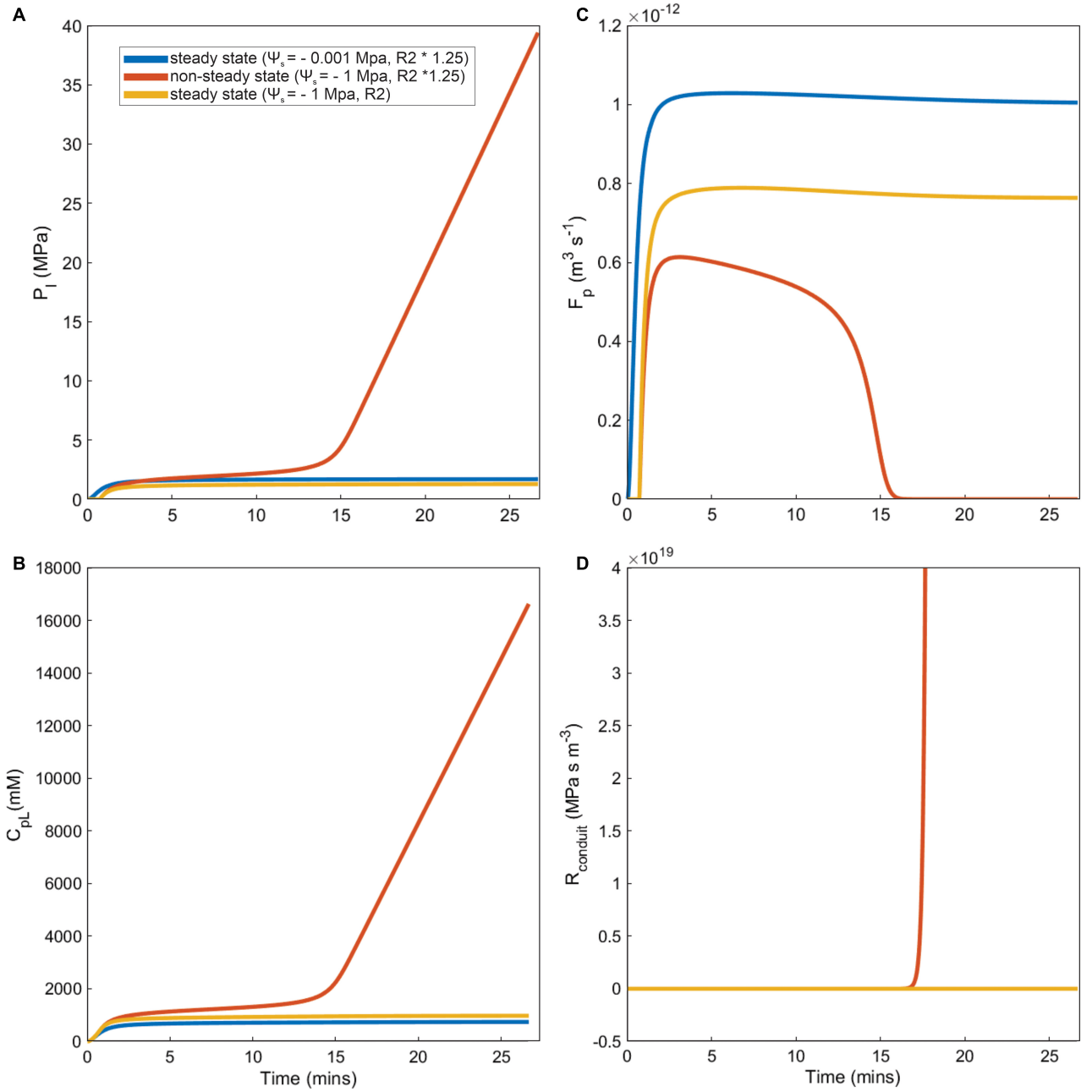

FIGURE 4 | Examples of steady state, and non-steady state simulations (caused by runaway viscosity) for different model outputs, over a subset of total simulation run time. Three scenarios represented by each line color are presented for differing soil water conditions (Ψ_S) and phloem structural resistance (R2): First, a steady state wet and higher phloem pathway resistance simulation ($\Psi_S = -0.001$, R2 × 1.25, blue lines). Second, a non-steady dry and higher resistance phloem pathway simulation ($\Psi_S = -1$, R2 × 1.25, red lines). Finally, a steady state dry and lower resistance pathway simulation ($\Psi_S = -1$, R2, yellow lines). Each panel represents **(A)** Phloem pressure in the loading area (P_l), **(B)** concentration of sucrose in phloem loading area (C_{pL}), **(C)** phloem sap flow (F_p), and **(D)** total resistance of the phloem sieve tube conduit in the loading area, which considers fluid viscosity and phloem structural resistance ($R_{conduit}$).

modulated according to these anatomical constraints, by either downregulating V_{maxL} constitutively (**Figures 6A,C**) or inducibly as a function of pressure (**Figures 6C,D**). Reducing the maximum loading rate by half (V_{maxL}) reduced sucrose output to sinks (**Figure 6A**) in comparison to the non-regulated loading, but lowered phloem pressures to reasonable bounds (**Figure 6C**, red dashed lines). However, using Eq. 18 to downregulate phloem loading as a function of pressure improved overall sucrose output over simply reducing V_{maxL} while maintaining viable phloem pressures over most soil water conditions (**Figures 6B,D**). Comparing wet soils ($\Psi_s = -0.001$MPa) between unregulated loading (**Figure 5A**) to pressure regulated loading (**Figure 6B**),

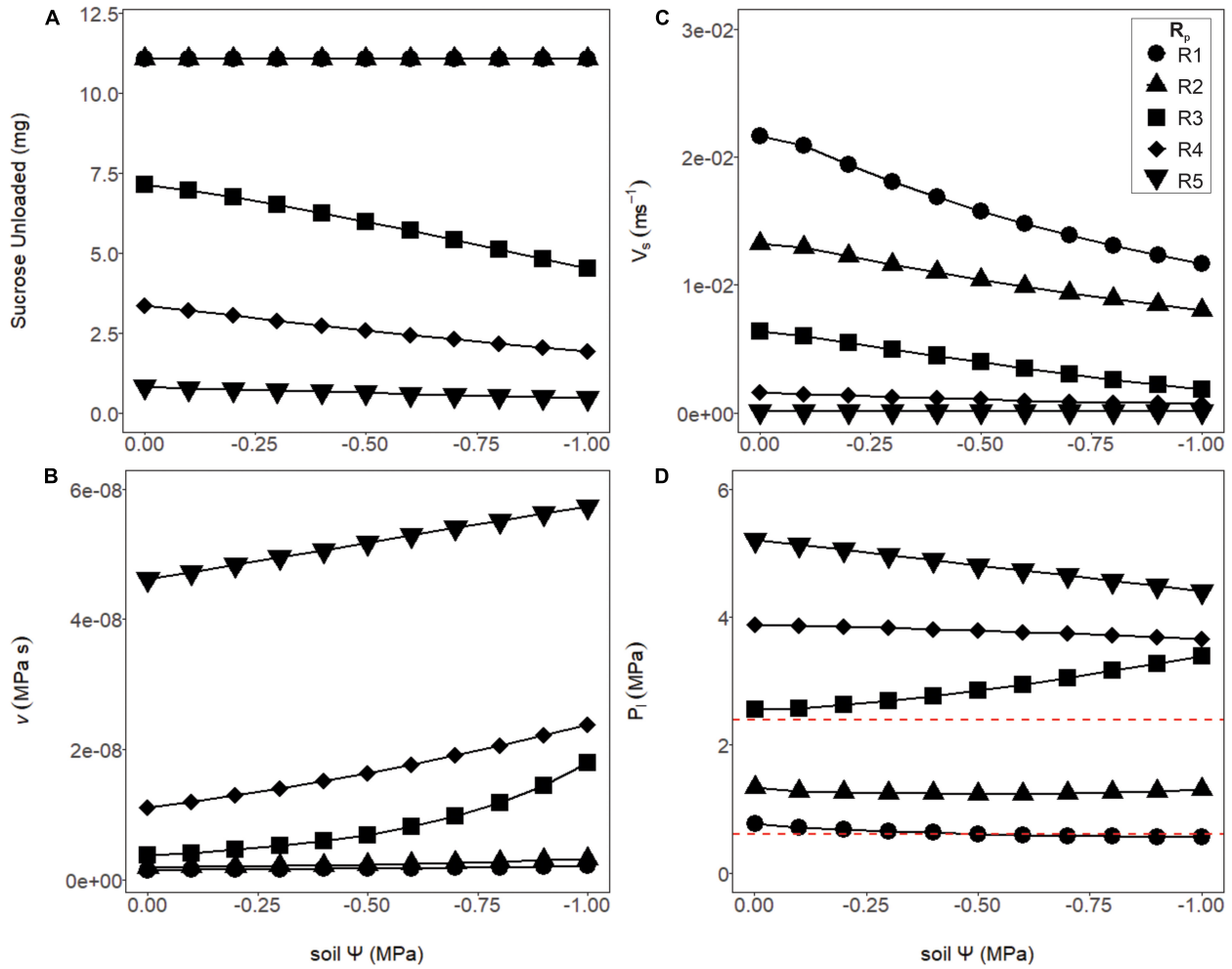

FIGURE 5 | Phloem output parameters modeled over varying soil water potentials and phloem resistance coefficients. **(A)** The amount of sucrose unloaded was consistent across soil water potentials for the first two structural resistance (R_p) values (R1 and R2), while R3–R5 exported a substantially lower amount. **(B)** The viscosity of the phloem sap increased as R_p increased, and the soil became drier. Note the intermediate resistance began to increase exponentially, as a sign that this resistance was approaching viscosity limitation. **(C)** The velocity of phloem transport declined with drier soil, as well as increasing (R_p). **(D)** Phloem pressures declined slightly under drier soils for the lower or higher resistance phloem (R1, R2 and R4, R5) but began increasing with drier soil at the intermediate resistance (R3) due to this resistance approaching viscosity limitation. Red dashed lines signify phloem pressure potentials measured empirically in past studies (0.6–2.4 MPa).

sucrose output dropped by 30.6, 27.8, and 2.36% for R1, R3, and R5 resistances, respectively ($\beta = 0.6$). However, under dry soils ($\Psi_s = -0.001$ MPa), sucrose output dropped by 22.9 and 8.5% for R1 and R3, respectively, but for the highest resistance (R5), improved by 3.2%. This led to the hypothesis that pressure regulated loading may be optimized according to both sieve tube anatomical traits (e.g., *Rp*), environmental conditions (e.g., Ψ_s) or maximum loading rates (e.g., V_{maxL}).

Maximizing Sucrose Export to Sinks Varies With Pressure-Regulated Maximum Loading Rate and Sieve Tube Resistance

We next sought to determine how the transporter kinetics that maximize sucrose export while maintaining viable phloem pressures depend on pathway resistance and soil moisture. We first identified the range of viable β values for each resistance and soil moisture scenario (i.e., $\Psi_s = -0.001$ and -1 MPa), assuming a constant V_{maxL} (i.e., for *N. tabacum*) (**Supplementary Figure 4**). We then varied V_{maxL} from $1.30e^{-8}$ (i.e., *Arabidopsis*) to $2.30e^{-6}$ mol m^{-2} s^{-1} (i.e., wheat) to identify the combinations of V_{maxL} and β that maximized export for each scenario (**Figure 7**).

Coordination between loading downregulation and the maximum loading rate strongly benefitted sucrose export (**Figure 7**). This simulation showed sugar export for the β and V_{maxL} combinations that produced viable phloem pressures (i.e., 0.6–2.4 MPa). For low-resistance phloem (R2) under wet conditions, sucrose export was maximized at 19.07 mg by $V_{maxL} = 1.79e^{-6}$ mol m^{-2} s^{-1} and $\beta = 0.79$ (**Figure 7A**). Drought reduced the maximum output at this

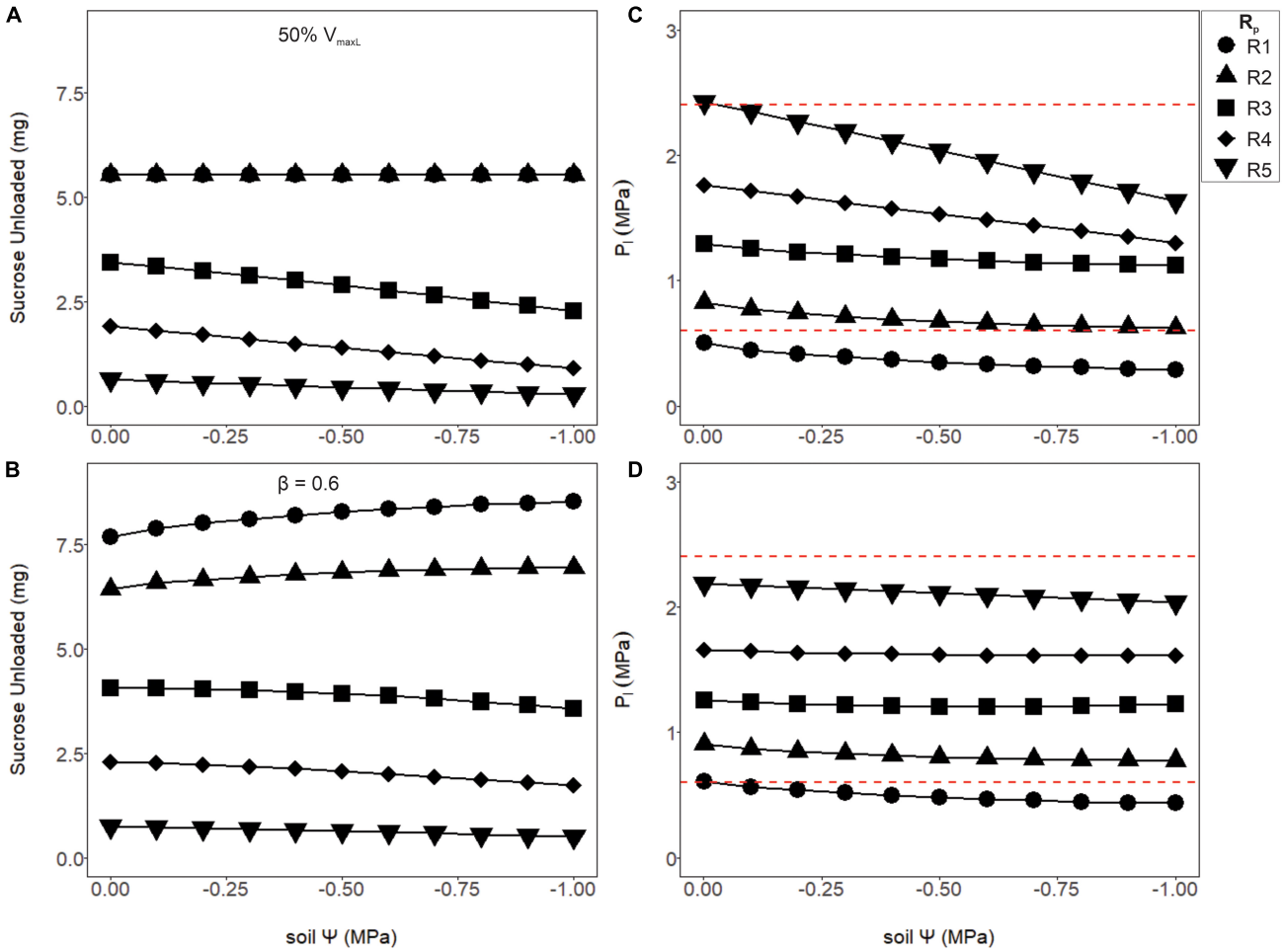

FIGURE 6 | The amount of sucrose unloaded or phloem pressure in the loading zone (P_1) as a function of soil water potential (Ψ_s) for two differing loading rate scenarios: a 50% reduction in V_{maxL} **(A,C)** or a pressure regulated reduction in the default VmaxL, with a downregulation strength of $\beta = 0.6$ (**B,D**; see Eq. 18). The first scenario **(A,C)** shows the amount of sucrose unloaded and P_1 for a 50% reduction in V_{maxL}. Output remained stable over the drought for R1 and R2 and began to decline with soil water for R3–R5. Meanwhile, phloem pressure began to fall with drier soils, with most R_p values falling within the empirical pressure window, except for the lowest pathway resistance which was under-pressured. **(B,D)** Using pressure downregulated loading, sucrose output slightly improved as the soil dried for lower R_p values (R1 and R2) but started to decline with higher values (R3–R5). Downregulation of loading allowed most of the tested resistances (R2–R5) to have phloem pressures within empirical bounds. Red dashed lines signify phloem pressure potentials recorded previously empirically (0.6–2.4 MPa).

Rp to 13.6 mg (i.e., a 29% reduction) (**Figure 7C**), which occurred at a higher V_{maxL} ($2.22e^{-6}$ mol m^{-2} s^{-1}) with stronger pressure-coupled downregulation ($\beta = 1.14$); in comparison to default V_{maxL}, the expanded V_{maxL} improved export by 50 and 28% for the wet and dry conditions, respectively, at this resistance.

Increasing resistance (R4) in wet conditions substantially reduced maximum output to only 4.18 mg (**Figure 7B**); this corresponded to a lower V_{maxL} and stronger downregulation than for R2 ($V_{maxL} = 1.68e^{-6}$ mol m^{-2} s^{-1} and a $\beta = 1.33$). Water stress reduced maximum output to 2.98 mg (a 29% reduction) (**Figure 7D**) and this corresponded to the strongest downregulation across scenarios ($V_{maxL} = 1.72e^{-6}$ mol m^{-2} s^{-1} and $\beta = 1.61$); this improved sucrose output by 27 and 33% over default V_{maxL} values for wet and dry conditions, respectively. Overall, when comparing the impacts of pressure regulated loading (**Figure 7**) vs. non-regulated loading (**Figure 5**), we found that non-water stressed, low resistant pathways and water stressed, high resistant pathways benefit the most from a pressure regulated loading mechanism (**Table 4**).

DISCUSSION

This study is the first to show that pressure-regulated loading is a potential strategy to circumvent viscosity limitations and improve the efficiency of sugar translocation, especially under drought and for highly resistive phloem pathways. Our findings also suggest sucrose loading proteins and phloem architecture (e.g., sieve tube anatomy) are highly coordinated. We discuss the potential molecular mechanisms

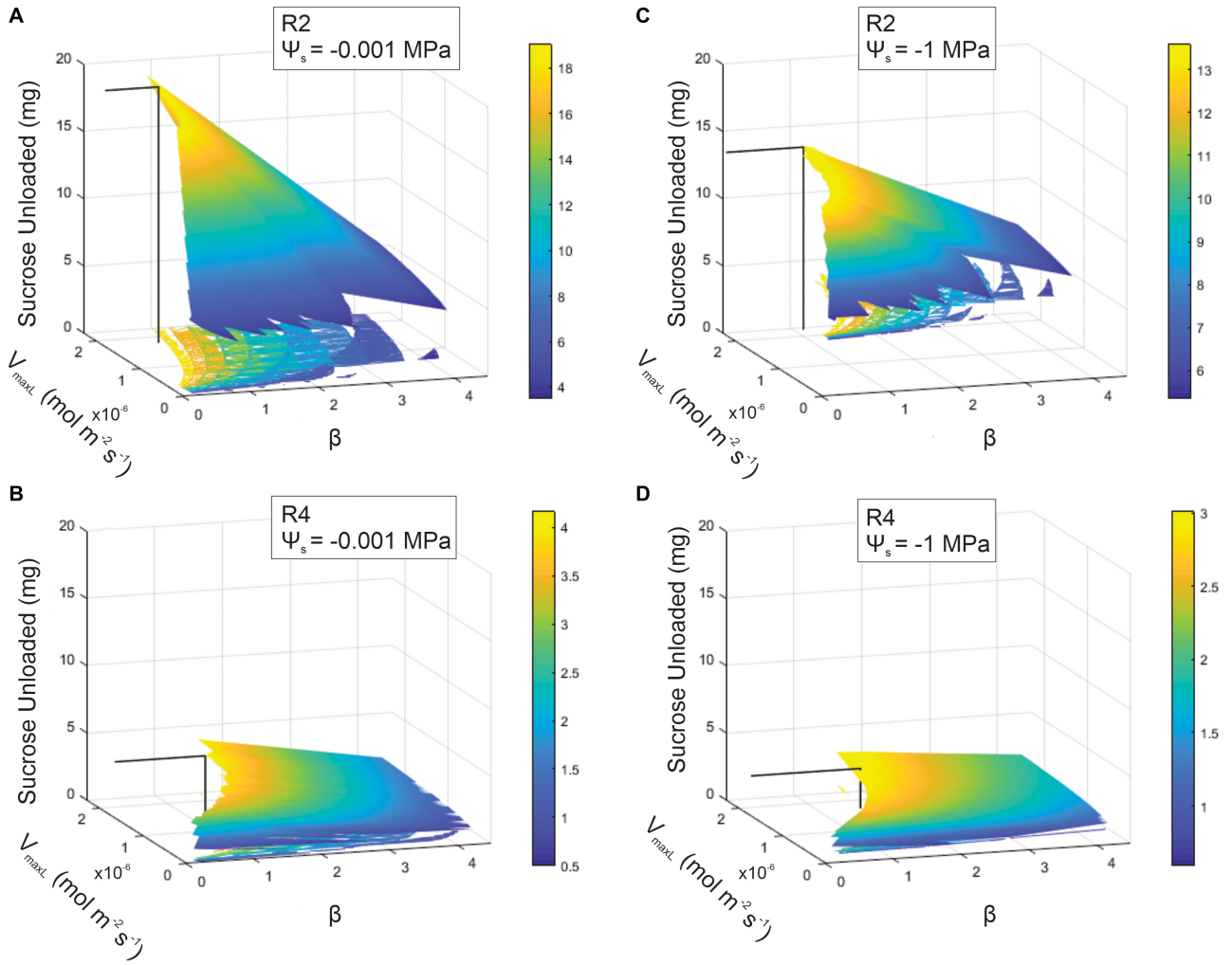

FIGURE 7 | Sucrose output as a function of loading downregulation (β) and the maximum rate of sucrose loading (V_{maxL}) over differing soil water potentials (Ψ_S = –0.001 or –1 MPa) or phloem structural resistances (*Rp*: R2 or R4). A range of V_{maxL} values were selected from *Arabidopsis* ($1.30e^{-8}$ mol m^{-2} s^{-1}) to wheat ($2.3e^{-6}$ mol m^{-2} s^{-1}). Sucrose output for: **(A)** R2 and wet soils (maximum sucrose output = 19.07 mg), **(B)** R4 and wet soils (maximum sucrose output = 4.18 mg), **(C)** R2 and dry soils (maximum sucrose output = 13.6 mg), and **(D)** R4 and dry soils (maximum sucrose output = 2.98 mg). The solid black line within each 3D space specifies the maximum sucrose output at a particular V_{maxL} and β.

driving pressure-adjusted loading during drought, the interacting effects between anatomy and viscosity limitations, and the potential for this model to inform future genetic transformation studies to increase crop yields.

Plants Benefit From Loading Regulation: A Molecular Regulation Perspective

Our study provides theoretical support for our hypothesis that loading regulation is adaptive for phloem function. Pressure-regulated loading prevented the excessive buildup of sugars that causes viscosity limitations, reducing the impacts of water stress on sugar transport for highly resistive phloem (**Figures 6**, **7**). Regulated loading also benefitted less resistive pathways by allowing for a higher V_{maxL} and, thus, greater sugar export, than in the absence of regulation (**Table 4**). These model findings are bolstered by empirical evidence supporting pressure-regulated behavior and the discovery of molecular mechanisms that could dynamically adjust sucrose loading during drought.

Previous experiments have shown that loading rates may be adjusted as a function of turgor and/or sucrose concentration during osmotic stress. For example, exposing tissues to membrane-impermeable sugars (i.e., sorbitol or mannitol) reduces the apoplasmic water potential outside the phloem, drawing out water and reducing phloem turgor (Smith and Milburn, 1980; Patrick, 1994; Bell and Leigh, 1996). These treatments showed that a decline in phloem pressure upregulated sucrose loading in castor bean leaf discs (Smith and Milburn, 1980) and sucrose unloading in bean seed coats (Patrick, 1994). Conversely, reducing external mannitol concentrations increased phloem turgor and decreased unloading rates in

TABLE 4 | Comparing the maximum sucrose output of the unregulated phloem loading scenario (**Figure 5**), to the pressure regulated loading scenario (data found in **Figure 7**).

Phloem resistance (R_p)	No regulation sucrose output (mg)	Pressure regulation sucrose output (mg)	% Change
$\Psi_s = -0.001$ MPa			
R1	11.06	41.02	271
R2	11.05	19.07	73
R3	7.13	9.22	29
R4	3.35	4.18	25
R5	0.81	1.06	30
$\Psi_s = -1$ MPa			
R1	11.05	27.75	151
R2	11.05	13.6	23
R3	4.5	6.18	37
R4	1.91	2.98	56
R5	0.48	0.81	70

beet root disks (Bell and Leigh, 1996). Supporting loading downregulation, isolated vesicles from beet leaf disks exposed to increasing sucrose concentrations showed declines in loading rate in a concentration-dependent manner (Chiou and Bush, 1998). This downregulation also corresponded to a reduction in sucrose symporter transcript abundance with increasing sucrose concentrations, causing maximum loading rate (V_{max}) to decline by up to 74% compared to controls which were not subjected to increased sucrose concentrations.

The empirical and modeling results suggest that plants would benefit from the ability to exhibit a range of loading rates, while the directionality of loading responses would depend on internal phloem conditions (e.g., anatomy or viscosity). For example, the model predicted that more resistive phloem would require stronger downregulation to optimize sugar transport under drought than less resistive pathways (**Figures 7B,D**; R4 vs. **Figures 7A,C**; R2). Weaker downregulation would allow excessive sucrose concentrations to build in the phloem, causing pressure and viscosity to rise and flow rates and export to decline (**Figure 6B**; R3–R5). Thus, upregulation could be beneficial during drought if resistance is below thresholds for viscosity limitation, allowing greater osmotic strength to compensate for the lowered xylem water potentials.

Changes in the regulation of sucrose transporter activity may be the primary cause of loading up- or downregulation and several mechanisms could allow these changes to occur in response to drought. Alteration in phloem turgor have been hypothesized to trigger a hormonal signaling cascade that alters transporter expression or post-translational modification (Patrick et al., 2001). This has been evidenced by water stress upregulating most (but not all) sucrose transporter subfamilies involved in phloem loading in some species (Medici et al., 2014; Xu et al., 2018). For example, *Arabidopsis*, soybean, barley, rice, wheat, and maize saw an overall upregulation of phloem loading SUT expression, but potato and tomato did not. However, phloem exudates from these studies indicate that sucrose concentrations decreased under water stress for all species, which contradicts the hypothesis that SUT transcript abundance alone drives differential loading rates but is consistent with our model results for differential control of V_{maxL} and pressure down-regulation of loading (**Figure 7**). Alternatively, post-translational modification of transporter proteins may regulate the rate of sugar movement past the phloem membrane (reviewed by Liesche et al., 2011a). For instance, ubiquitination of these proteins increases their degradation rate in the plasma membrane, while phosphorylation increases their affinity for sucrose in plants exposed to differing light (Xu et al., 2020) or drought (Ma et al., 2019). Interestingly, in high light conditions, photosynthesis and SUC2 phosphorylation were significantly increased, while SUC2 transcript remained stable (Xu et al., 2020). This implies that SUC/SUT transporter regulation is complex and under multiple controls. Future experiments may incorporate a variety of progressively intensified abiotic challenges (e.g., high light intensity, drought) and track both expression levels and post-translational modifications of SUTs/SUCs; this would help determine if thresholds of sucrose transporter upregulation exist, beyond which downregulation occurs to prevent viscosity limitation.

Loading Regulation to Prevent Viscosity Limitation May Extend to the Pre-phloem Pathway

The current work focuses on the role of regulating loading proteins at the companion cell/sieve element interface. However, there is emerging evidence that phloem loading may be controlled in the pre-phloem pathway (Liesche, 2017), which would expand the applicability of studying viscosity limitations past strict apoplasmic loaders; for example, passive loaders or species with alternating loading types (i.e., English Oak; Liesche, 2017). Understanding how loading regulation varies between species may also help to elucidate carbon allocation patterns in response to stress (Savage et al., 2016).

For example, poplar (*Populus trichocarpa*) shows regulation of sucrose in the pre-phloem pathway through differential expression of tonoplast sucrose transporters in mesophyll cells (Payyavula et al., 2011). Under drought stress, these transporters were downregulated, stem growth reduced, and leaf sugar accumulation increased (Frost et al., 2012), signaling that phloem export from the leaf was diminished (Liesche, 2017). It could be hypothesized that if the *Populus* phloem was on the verge of viscosity limitation, sucrose needed to be withheld from entering the phloem loading pathway by being sequestered in vacuoles to prevent viscosity build-ups. Alternatively, other species such as beech (*Fagus sylvatica*) did not show reduced carbon export from the leaf during drought, but instead saw a reduction in photosynthesis (Hommel et al., 2016; Liesche, 2017). Beech has been identified as a passive symplasmic loader (Rennie and Turgeon, 2009), which may make it more reliant on adjustments of photosynthesis to control proper sucrose gradients in the phloem. Future work will need to identify sucrose transporter proteins in

both the pre-phloem and phloem pathways to understand what role loading regulation plays in supporting efficient phloem transport across multiple plant taxa with differing loading strategies.

Linking Anatomical Traits With Phloem Export to Sinks

Pressure-based loading improved sucrose export to sinks over non-regulated scenarios by up to 3.7x, while the lowest resistance pathway (R1) improved loading over the highest (R5) by 38.7x (**Table 4**). This might imply that plants with higher growth rates correlate to a lower resistance phloem pathway. However, a recent meta-analysis on phloem anatomical traits did not find a significant trend between growth rates and sieve tube resistance (Liesche et al., 2017) but did find increased variability in taxonomic groups that actively load. Potentially, loading regulation allows for higher pathway resistances to achieve similar levels of export to sinks in comparison to non-regulated pathways, which would make anatomical characters less constrained.

Another interesting interaction in phloem anatomy that was highlighted here was the relationship between phloem volume and resistance. In our simulations, export was maximized at phloem volumes that were small enough for rapid loading, but large enough to avoid viscosity limitations (**Figure 3**). Further, optimal volumes were larger for more resistant pathways. The relationship between phloem volume and resistance would depend on the underlying traits; for example, doubling conduit radius would increase phloem volume four-fold and reduce resistance 16-fold, while doubling the number of parallel conduits per unit area would decrease resistance and increase volume linearly (Hölttä et al., 2009; Jensen, 2019). This flexibility suggests it is highly plausible for natural or artificial selection to achieve optimal coordination between resistance and volume, though more work is needed to determine whether the inverse relationships between volume and resistance would prevent highly resistive pathways from achieving optimal volumes.

Using Loading Regulation Mechanisms to Improve Genetic Engineering Outcomes

Previous studies have used genetic engineering to upregulate the expression of phloem loading sucrose transporters in pea (*Pisum sativum*; Lu et al., 2020), *Arabidopsis* (Dasgupta et al., 2014), potato (*Solanum tuberosum*, Leggewie et al., 2003), and rice (*Oryza sativa;* Wang et al., 2015). Although these transformations increased loading rates (Lu et al., 2020), the impacts on growth and viability varied by species. One successful example from pea plants saw the upregulation of *Ps*Sut1 which increased sucrose concentrations in the phloem exudate and significantly increased biomass and yield (Lu et al., 2020). The authors hypothesized that upregulating SUT1 enhanced both loading and unloading in the developing seeds, which was key to making this transformation successful (Lu et al., 2020). Similarly, we found that reducing sink limitations would minimize the buildup of sucrose that would encourage viscosity limitation (**Supplementary Figure 1**). Our study also suggests that lowering phloem pathway resistance in coordination with increasing maximum loading rate would lower pressure induced downregulation and increase sucrose output substantially (**Figure 7**). This could be achieved by screening potential lines of SUT transformation for sieve tube anatomical characteristics that lower resistance, such as sieve element length, diameter, and sieve plate porosity (Stanfield et al., 2019). While sieve tube anatomy may be a difficult genetic target, reducing plant height (dwarfing) could be a simple method to reduce pathlength resistance (e.g., Qiao and Zhao, 2011) to determine the interacting effects of SUT upregulation, lowered pathway resistance and yield. Further, elucidating the mechanisms that generate turgor-dependent signaling cascades that modify sucrose transporter expression (as suggested by Patrick et al., 2001) could allow genetic engineering approaches to optimally target maximum loading rates.

CONCLUSION

We present a model that highlights the interactive effects of regulated phloem loading, phloem architecture, and drought on the total export to sink tissue. We find that phloem pathway resistance and maximum sucrose loading rate (V_{max}) are coordinated and that higher resistance phloem pathways may experience viscosity limitations which result in diminished sucrose export to sinks. After coordinating phloem structural resistance with phloem volume, we hypothesized that the loading rate requires pressure-induced regulation to ease viscosity limits and maximize phloem export. Using pressure regulated loading, we found that phloem transport could be made more efficient across all phloem pathway resistances, and that this mechanism buffered against the effects of moderate drought stress. We suggest future studies that use genetic engineering tools to upregulate the abundance of phloem loading SUTs/SUCs integrate phloem architecture and regulatory pathways that control transporter expression in response to phloem water status. Studying the interactive effects of these traits has the potential to provide pathways to increase crop yield, and to elucidate the drivers of plant growth and mortality responses to climate change.

DATA AVAILABILITY STATEMENT

The datasets presented in this study can be found in online repositories. The names of the repository/repositories and accession number(s) can be found below: doi: 10.5281/zenodo.5907490.

AUTHOR CONTRIBUTIONS

RS constructed the figures and performed the literature review. RS and MB constructed the model, analyzed the results, wrote

the manuscript, contributed to the article, and approved the submitted version.

FUNDING

MB was supported by the University of California, Davis College of Agricultural and Environmental Sciences and Department of Viticulture and Enology, and generous donations from the Rossi family to the department.

ACKNOWLEDGMENTS

RS thank the Rossi Postdoctoral and Katherine Esau Postdoctoral fellowships for funding.

SUPPLEMENTARY MATERIAL

The Supplementary Material for this article can be found online at: https://www.frontiersin.org/articles/10.3389/fpls.2022.787837/full#supplementary-material

REFERENCES

Ainsworth, E. A., and Bush, D. R. (2011). Carbohydrate export from the leaf: a highly regulated process and target to enhance photosynthesis and productivity. *Plant Physiol.* 155, 64–69. doi: 10.1104/pp.110.167684

Bartlett, M. K., Detto, M., and Pacala, S. W. (2019). Predicting shifts in the functional composition of tropical forests under increased drought and CO 2 from trade-offs among plant hydraulic traits. *Ecol. Lett.* 22, 67–77. doi: 10.1111/ele.13168

Bartlett, M. K., Klein, T., Jansen, S., Choat, B., and Sack, L. (2016). The correlations and sequence of plant stomatal, hydraulic, and wilting responses to drought. *Proc. Natl. Acad. Sci.* 113, 13098–13103. doi: 10.1073/pnas.1604088113

Bartlett, M. K., Scoffoni, C., and Sack, L. (2012). The determinants of leaf turgor loss point and prediction of drought tolerance of species and biomes: a global meta-analysis. *Ecol. Lett.* 15, 393–405. doi: 10.1111/j.1461-0248.2012.01751.x

Bell, C. I., and Leigh, R. A. (1996). Differential effects of turgor on sucrose and potassium transport at the tonoplast and plasma membrane of sugar beet storage root tissue. *Plant Cell Environ.* 19, 191–200. doi: 10.1111/j.1365-3040.1996.tb00240.x

Borstlap, A. C., and Schuurmans, J. A. M. (2004). Sucrose transport into plasma membrane vesicles from tobacco leaves by H+ symport or counter exchange does not display a linear component. *J. Membrane Biol.* 198, 31–42. doi: 10.1007/s00232-004-0657-z

Braun, D. M., Wang, L., and Ruan, Y. L. (2014). Understanding and manipulating sucrose phloem loading, unloading, metabolism, and signalling to enhance crop yield and food security. *J. Exp. Bot.* 65, 1713–1735. doi: 10.1093/jxb/ert416

Bush, D. R. (2020). Identifying the pathways that control resource allocation in higher plants. *Proc. Natl. Acad. Sci.* 117, 8669–8671. doi: 10.1073/pnas.2002581117

Carvalho, M. R., Turgeon, R., Owens, T., and Niklas, K. J. (2017). The scaling of the hydraulic architecture in poplar leaves. *New Phytol.* 214, 145–157. doi: 10.1111/nph.14385

Cataldo, D. A. (1974). Vein loading: the role of the symplast in intercellular transport of carbohydrate between the mesophyll and minor veins of tobacco leaves. *Plant Physiol.* 53, 912–917. doi: 10.1104/pp.53.6.912

Chiou, T. J., and Bush, D. R. (1998). Sucrose is a signal molecule in assimilate partitioning. *Proc. Natl. Acad. Sci. U.S.A.* 95, 4784–4788. doi: 10.1073/pnas.95.8.4784

Choat, B., Jansen, S., Brodribb, T. J., Cochard, H., Delzon, S., Bhaskar, R., et al. (2012). Global convergence in the vulnerability of forests to drought. *Nature* 491, 752–755. doi: 10.1038/nature11688

Dasgupta, K., Khadilkar, A. S., Sulpice, R., Pant, B., Scheible, W. R., Fisahn, J., et al. (2014). Expression of sucrose transporter cDNAs specifically in companion cells enhances phloem loading and long-distance transport of sucrose but leads to an inhibition of growth and the perception of a phosphate limitation. *Plant Physiol.* 165, 715–731. doi: 10.1104/pp.114.238410

Daudet, F. A., Lacointe, A., Gaudillere, J. P., and Cruiziat, P. (2002). Generalized münch coupling between sugar and water fluxes for modelling carbon allocation as affected by water status. *J. Theor. Biol.* 214, 481–498. doi: 10.1006/jtbi.2001.2473

Davies, C., Wolf, T., and Robinson, S. P. (1999). Three putative sucrose transporters are differentially expressed in grapevine tissues. *Plant Sci.* 147, 93–100.

De Schepper, V., De Swaef, T., Bauweraerts, I., and Steppe, K. (2013). Phloem transport: a review of mechanisms and controls. *J. Exp. Bot.* 64, 4839–4850. doi: 10.1093/jxb/ert302

De Schepper, V., and Steppe, K. (2010). Development and verification of a water and sugar transport model using measured stem diameter variations. *J. Exp. Bot.* 61, 2083–2099. doi: 10.1093/jxb/erq018

Delrot, S., and Bonnemain, J. L. (1980). Involvement of protons as a substrate for the sucrose carrier during phloem loading in vicia faba leaves. *Plant Physiol.* 67, 560–564. doi: 10.1104/pp.67.3.560

Edelman, J., Schoolar, A. I., and Bonnor, W. B. (1971). Permeability of sugar-cane chloroplasts to sucrose. *J. Exp. Bot.* 22, 534–545.

Esau, K., Cheadle, V. I., and Risley, E. B. (1962). Development of sieve-plate pores. *Bot. Gazette* 123, 233–243.

Farquhar, G. D., von Caemmerer, S. V., and Berry, J. A. (1980). A biochemical model of photosynthetic CO 2 assimilation in leaves of C 3 species. *Planta* 149, 78–90. doi: 10.1007/BF00386231

Fondy, B. R., and Geiger, D. R. (1977). Sugar selectivity and other characteristics of phloem loading in beta vulgaris L. *Plant Physiol.* 59, 953–960. doi: 10.1104/pp.59.5.953

Frost, C. J., Nyamdari, B., Tsai, C. J., and Harding, S. A. (2012). The tonoplast-localized sucrose transporter in populus (PtaSUT4) regulates whole-plant water relations, responses to water stress, and photosynthesis. *PLoS One* 7:8. doi: 10.1371/journal.pone.0044467

Fu, Q., Cheng, L., Guo, Y., and Turgeon, R. (2011). Phloem loading strategies and water relations in trees and herbaceous plants. *Plant Physiol.* 157, 1518–1527. doi: 10.1104/pp.111.184820

Gamalei, Y. (1989). Structure and function of leaf minor veins in trees and herbs. *Trees* 3, 96–110.

Goeschl, J. D., and Han, L. (2020). A proposed drought response equation added to the münch-horwitz theory of phloem transport. *Front. Plant Sci.* 11:505153. doi: 10.3389/fpls.2020.505153

Gould, N., Morrison, D. R., Clearwater, M. J., Ong, S., Boldingh, H. L., and Minchin, P. E. (2013). Elucidating the sugar import pathway into developing kiwifruit berries (*Actinidia deliciosa*). *New Zealand J. Crop Hortic. Sci.* 41, 189–206.

Hackel, A., Schauer, N., Carrari, F., Fernie, A. R., Grimm, B., and Kühn, C. (2006). Sucrose transporter LeSUT1 and LeSUT2 inhibition affects tomato fruit development in different ways. *Plant J.* 45, 180–192. doi: 10.1111/j.1365-313X.2005.02572.x

Hao, P., Liu, C., Wang, Y., Chen, R., Tang, M., Du, B., et al. (2008). Herbivore-induced callose deposition on the sieve plates of rice: an important mechanism for host resistance. *Plant Physiol.* 146, 1810–1820. doi: 10.1104/pp.107.111484

Hölttä, T., Mencuccini, M., and Nikinmaa, E. (2009). Linking phloem function to structure: analysis with a coupled xylem–phloem transport model. *J. Theor. Biol.* 259, 325–337. doi: 10.1016/j.jtbi.2009.03.039

Hölttä, T., Vesala, T., Sevanto, S., Perämäki, M., and Nikinmaa, E. (2006). Modeling xylem and phloem water flows in trees according to cohesion theory and münch hypothesis. *Trees* 20, 67–78.

Hommel, R., Siegwolf, R., Zavadlav, S., Arend, M., Schaub, M., Galiano, L., et al. (2016). Impact of interspecific competition and drought on the allocation of new assimilates in trees. *Plant Biol.* 18, 785–796. doi: 10.1111/plb.12461

Huang, C. W., Domec, J. C., Palmroth, S., Pockman, W. T., Litvak, M. E., and Katul, G. G. (2018). Transport in a coordinated soil-root-xylem-phloem leaf system. *Adv. Water Res.* 119, 1–16. doi: 10.1016/j.advwatres.2018.06.002

Ibraheem, O., Dealtry, G., Roux, S., and Bradley, G. (2011). The effect of drought and salinity on the expressional levels of sucrose transporters in rice ('oryza sativa'nipponbare) cultivar plants. *Plant Omics* 4, 68–74.

Jensen, K. H. (2019). *Modeling the Hydraulic Conductivity of Phloem Sieve Elements*. New York, NY: Humana, 339–344.

Jensen, K. H., Berg-Sørensen, K., Bruus, H., Holbrook, N. M., Liesche, J., Schulz, A., et al. (2016). Sap flow and sugar transport in plants. *Rev. Mod. Phys.* 88:035007.

Jensen, K. H., Mullendore, D. L., Holbrook, N. M., Bohr, T., Knoblauch, M., and Bruus, H. (2012). Modeling the hydrodynamics of phloem sieve plates. *Front. Plant Sci.* 3:151. doi: 10.3389/fpls.2012.00151

Jensen, K. H., Savage, J. A., and Holbrook, N. M. (2013). Optimal concentration for sugar transport in plants. *J. R. Soc. Interface* 10:20130055. doi: 10.1098/rsif.2013.0055

Kuo, J., O'brien, T. P., and Canny, M. J. (1974). Pit-field distribution, plasmodesmatal frequency, and assimilate flux in the mestome sheath cells of wheat leaves. *Planta* 121, 97–118. doi: 10.1007/BF00388750

Lalonde, S., Wipf, D., and Frommer, W. B. (2004). Transport mechanisms for organic forms of carbon and nitrogen between source and sink. *Annu. Rev. Plant Biol.* 55, 341–372. doi: 10.1146/annurev.arplant.55.031903.141758

Lawlor, D. W. (2013). Genetic engineering to improve plant performance under drought: physiological evaluation of achievements, limitations, and possibilities. *J. Exp. Bot.* 64, 83–108. doi: 10.1093/jxb/ers326

Leggewie, G., Kolbe, A., Lemoine, R., Roessner, U., Lytovchenko, A., Zuther, E., et al. (2003). Overexpression of the sucrose transporter So SUT1 in potato results in alterations in leaf carbon partitioning and in tuber metabolism but has little impact on tuber morphology. *Planta* 217, 158–167. doi: 10.1007/s00425-003-0975-x

Lemoine, R., La Camera, S., Atanassova, R., Dédaldéchamp, F., Allario, T., Pourtau, N., et al. (2013). Source-to-sink transport of sugar and regulation by environmental factors. *Front. Plant Sci.* 4:272. doi: 10.3389/fpls.2013.00272

Liesche, J. (2017). Sucrose transporters and plasmodesmal regulation in passive phloem loading. *J. Integrat. Plant Biol.* 59, 311–321. doi: 10.1111/jipb.12548

Liesche, J., Krügel, U., He, H., Chincinska, I., Hackel, A., and Kühn, C. (2011a). Sucrose transporter regulation at the transcriptional, post-transcriptional and post-translational level. *J. Plant Physiol.* 168, 1426–1433. doi: 10.1016/j.jplph.2011.02.005

Liesche, J., Martens, H. J., and Schulz, A. (2011b). Symplasmic transport and phloem loading in gymnosperm leaves. *Protoplasma* 248, 181–190. doi: 10.1007/s00709-010-0239-0

Liesche, J., Pace, M. R., Xu, Q., Li, Y., and Chen, S. (2017). Height-related scaling of phloem anatomy and the evolution of sieve element end wall types in woody plants. *New Phytol.* 214, 245–256. doi: 10.1111/nph.14360

Liesche, J., and Schulz, A. (2013). Modeling the parameters for plasmodesmal sugar filtering in active symplasmic phloem loaders. *Front. Plant Sci.* 4:207. doi: 10.3389/fpls.2013.00207

Lu, M. Z., Snyder, R., Grant, J., and Tegeder, M. (2020). Manipulation of sucrose phloem and embryo loading affects pea leaf metabolism, carbon and nitrogen partitioning to sinks as well as seed storage pools. *Plant J.* 101, 217–236. doi: 10.1111/tpj.14533

Ma, Q. J., Sun, M. H., Lu, J., Kang, H., You, C. X., and Hao, Y. J. (2019). An apple sucrose transporter MdSUT2. 2 is a phosphorylation target for protein kinase MdCIPK22 in response to drought. *Plant Biotechnol. J.* 17, 625–637. doi: 10.1111/pbi.13003

Medici, A., Laloi, M., and Atanassova, R. (2014). Profiling of sugar transporter genes in grapevine coping with water deficit. *FEBS Lett.* 588, 3989–3997. doi: 10.1016/j.febslet.2014.09.016

Meinzer, F. C., Johnson, D. M., Lachenbruch, B., McCulloh, K. A., and Woodruff, D. R. (2009). Xylem hydraulic safety margins in woody plants: coordination of stomatal control of xylem tension with hydraulic capacitance. *Funct. Ecol.* 23, 922–930. doi: 10.1111/j.1365-2435.2009.01577.x

Milne, R. J., Grof, C. P., and Patrick, J. W. (2018). Mechanisms of phloem unloading: shaped by cellular pathways, their conductances and sink function. *Curr. Opin. Plant Biol.* 43, 8–15. doi: 10.1016/j.pbi.2017.11.003

Mullendore, D. L., Windt, C. W., Van As, H., and Knoblauch, M. (2010). Sieve tube geometry in relation to phloem flow. *Plant Cell* 22, 579–593. doi: 10.1105/tpc.109.070094

Muller, O., Cohu, C. M., Stewart, J. J., Protheroe, J. A., Demmig-Adams, B., and Adams, W. W. III (2014). Association between photosynthesis and contrasting features of minor veins in leaves of summer annuals loading phloem via symplastic versus apoplastic routes. *Physiol. Plant.* 152, 174–183. doi: 10.1111/ppl.12155

Münch, E. (1930). Stoffbewegungen in der Pflanze. Die Stoffbewegung in der Pflanze. *JENA Gustav Fischer* 234, 55–56. doi: 10.1074/jbc.M501785200

Muries, B., Carvajal, M., and del Carmen Martínez-Ballesta, M. (2013). Response of three broccoli cultivars to salt stress, in relation to water status and expression of two leaf aquaporins. *Planta* 237, 1297–1310. doi: 10.1007/s00425-013-1849-5

Nikinmaa, E., Hölttä, T., Hari, P., Kolari, P., Mäkelä, A., Sevanto, S., et al. (2013). Assimilate transport in phloem sets conditions for leaf gas exchange. *Plant Cell Environ.* 36, 655–669. doi: 10.1111/pce.12004

Pagano, M., Corona, P., and Storchi, P. (2016). Image analysis of the leaf vascular network: physiological considerations. *Photosynthetica* 54, 567–571.

Patrick, J. W. (1994). Turgor-dependent unloading of assimilates from coats of developing legume seed. assessment of the significance of the phenomenon in the whole plant. *Physiol. Plant.* 90, 645–654. doi: 10.1034/j.1399-3054.1994.900404.x

Patrick, J. W., Zhang, W., Tyerman, S. D., Offler, C. E., and Walker, N. A. (2001). Role of membrane transport in phloem translocation of assimilates and water. *Funct. Plant Biol.* 28, 697–709.

Payyavula, R. S., Tay, K. H., Tsai, C.-J., and Harding, S. A. (2011). The sucrose transporter family in *Populus*: the importance of a tonoplast PtaSUT4 to biomass and carbon partitioning. *Plant J.* 65, 757–770. doi: 10.1111/j.1365-313X.2010.04463.x

Pickard, W. F., and Minchin, P. E. (1992). The nature of the short-term inhibition of stem translocation produced by abrupt stimuli. *Funct. Plant Biol.* 19, 471–480. doi: 10.1071/pp9920471

Qiao, F., and Zhao, K. J. (2011). The influence of RNAi targeting of OsGA20ox2 gene on plant height in rice. *Plant Mol. Biol. Rep.* 29:952. doi: 10.1007/s11105-011-0309-2

Rennie, E. A., and Turgeon, R. (2009). A comprehensive picture of phloem loading strategies. *Proc. Natl. Acad. Sci. U.S.A.* 106, 14162–14167. doi: 10.1073/pnas.0902279106

Rockwell, F. E., Gersony, J. T., and Holbrook, N. M. (2018). Where does münch flow begin? Sucrose transport in the pre-phloem path. *Curr. Opin. Plant Biol.* 43, 101–107. doi: 10.1016/j.pbi.2018.04.007

Ryan, M. G., and Asao, S. (2014). Phloem transport in trees. *Tree Physiol.* 34, 1–4. doi: 10.1093/treephys/tpt123

Sack, L., and Holbrook, N. M. (2006). Leaf hydraulics. *Annu. Rev. Plant Biol.* 57, 361–381.

Saftner, R. A., Daie, J., and Wyse, R. E. (1983). Sucrose uptake and compartmentation in sugar beet taproot tissue. *Plant Physiol.* 72, 1–6. doi: 10.1104/pp.72.1.1

Salmon, Y., Dietrich, L., Sevanto, S., Hölttä, T., Dannoura, M., and Epron, D. (2019). Drought impacts on tree phloem: from cell-level responses to ecological significance. *Tree Physiol.* 39, 173–191. doi: 10.1093/treephys/tpy153

Savage, J. A., Clearwater, M. J., Haines, D. F., Klein, T., Mencuccini, M., Sevanto, S., et al. (2016). Allocation, stress tolerance and carbon transport in plants: how does phloem physiology affect plant ecology? *Plant Cell Environ.* 39, 709–725. doi: 10.1111/pce.12602

Schulz, A. (2015). Diffusion or bulk flow: how plasmodesmata facilitate pre-phloem transport of assimilates. *J. Plant Res.* 128, 49–61. doi: 10.1007/s10265-014-0676-5

Scoffoni, C., Rawls, M., McKown, A., Cochard, H., and Sack, L. (2011). Decline of leaf hydraulic conductance with dehydration: relationship to leaf size and venation architecture. *Plant Physiol.* 156, 832–843. doi: 10.1104/pp.111.173856

Sevanto, S. (2014). Phloem transport and drought. *J. Exp. Bot.* 65, 1751–1759. doi: 10.1093/jxb/ert467

Sevanto, S. (2018). Drought impacts on phloem transport. *Curr. Opin. Plant Biol.* 43, 76–81. doi: 10.1016/j.pbi.2018.01.002

Sevanto, S., Mcdowell, N. G., Dickman, L. T., Pangle, R., and Pockman, W. T. (2014). How do trees die? A test of the hydraulic failure and carbon starvation hypotheses. *Plant Cell Environ.* 37, 153–161. doi: 10.1111/pce.12141

Sjolund, R. D. (1997). The phloem sieve element: a river runs through it. *Plant Cell.* 9:1137. doi: 10.1105/tpc.9.7.1137

Smith, J. A. C., and Milburn, J. A. (1980). Phloem turgor and the regulation of sucrose loading in *Ricinus communis* L. *Planta* 148, 42–48. doi: 10.1007/BF00385440

Sovonick, S. A., Geiger, D. R., and Fellows, R. J. (1974). Evidence for active phloem loading in the minor veins of sugar beet. *Plant Physiol.* 54, 886–891. doi: 10.1104/pp.54.6.886

Sperry, J. S., Adler, F. R., Campbell, G. S., and Comstock, J. P. (1998). Limitation of plant water use by rhizosphere and xylem conductance: results from a model. *Plant Cell Environ.* 21, 347–359.

Stanfield, R. C., Hacke, U. G., and Laur, J. (2017). Are phloem sieve tubes leaky conduits supported by numerous aquaporins? *Am. J. Bot.* 104, 719–732. doi: 10.3732/ajb.1600422

Stanfield, R. C., Schulte, P. J., Randolph, K. E., and Hacke, U. G. (2019). Computational models evaluating the impact of sieve plates and radial water exchange on phloem pressure gradients. *Plant Cell Environ.* 42, 466–479. doi: 10.1111/pce.13414

Tamas, I. A., and Davies, P. J. (2016). Dynamics and control of phloem loading of indole-3-acetic acid in seedling cotyledons of *Ricinus communis*. *J. Exp. Bot.* 67, 4755–4765. doi: 10.1093/jxb/erw255

Thompson, M. V., and Holbrook, N. M. (2003a). Application of a single-solute non-steady-state phloem model to the study of long-distance assimilate transport. *J. Theor. Biol.* 220, 419–455. doi: 10.1006/jtbi.2003.3115

Thompson, M. V., and Holbrook, N. M. (2003b). Scaling phloem transport: water potential equilibrium and osmoregulatory flow. *Plant Cell Environ.* 26, 1561–1577.

Thompson, M. V., and Wolniack, S. M. (2008). A plasma membrane-anchored fluorescent protein fusion illuminates sieve element plasma membranes in arabidopsis and tobacco. *Plant Physiol.* 146, 1599–1610. doi: 10.1104/pp.107.113274

Turgeon, R. (2010). The puzzle of phloem pressure. *Plant Physiol.* 154, 578–581. doi: 10.1104/pp.110.161679

Tyree, M. T., and Ewers, F. W. (1991). The hydraulic architecture of trees and other woody plants. *New Phytol.* 119, 345–360. doi: 10.1111/j.1469-8137.1991.tb00035.x

van Bel, A. J. (2003). The phloem, a miracle of ingenuity. *Plant Cell Environ.* 26, 125–149. doi: 10.1046/j.1365-3040.2003.00963.x

Wang, L., Lu, Q., Wen, X., and Lu, C. (2015). Enhanced sucrose loading improves rice yield by increasing grain size. *Plant Physiol.* 169, 2848–2862. doi: 10.1104/pp.15.01170

Weise, A., Barker, L., Kühn, C., Lalonde, S., Buschmann, H., Frommer, W. B., et al. (2000). A new subfamily of sucrose transporters, SUT4, with low affinity/high capacity localized in enucleate sieve elements of plants. *Plant Cell* 12, 1345–1355. doi: 10.1105/tpc.12.8.1345

Wimmers, L. E., and Turgeon, R. (1991). Transfer cells and solute uptake in minor veins of *Pisum sativum* leaves. *Planta* 186, 2–12. doi: 10.1007/BF00201491

Xu, Q., Chen, S., Yunjuan, R., Chen, S., and Liesche, J. (2018). Regulation of sucrose transporters and phloem loading in response to environmental cues. *Plant Physiol.* 176, 930–945. doi: 10.1104/pp.17.01088

Xu, Q., Yin, S., Ma, Y., Song, M., Song, Y., Mu, S., et al. (2020). Carbon export from leaves is controlled via ubiquitination and phosphorylation of sucrose transporter SUC2. *Proc. Natl. Acad. Sci. U.S.A.* 117, 6223–6230. doi: 10.1073/pnas.1912754117

Zhang, X. Y., Wang, X. L., Wang, X. F., Xia, G. H., Pan, Q. H., Fan, R. C., et al. (2006). A shift of phloem unloading from symplasmic to apoplasmic pathway is involved in developmental onset of ripening in grape berry. *Plant Physiol.* 142, 220–232. doi: 10.1104/pp.106.081430

Zhou, X. R., Schnepf, A., Vanderborght, J., Leitner, D., Lacointe, A., Vereecken, H., et al. (2020). CPlantBox, a whole-plant modelling framework for the simulation of water-and carbon-related processes. *In Silico Plants* 2:diaa001.

Conflict of Interest: The authors declare that the research was conducted in the absence of any commercial or financial relationships that could be construed as a potential conflict of interest.

Publisher's Note: All claims expressed in this article are solely those of the authors and do not necessarily represent those of their affiliated organizations, or those of the publisher, the editors and the reviewers. Any product that may be evaluated in this article, or claim that may be made by its manufacturer, is not guaranteed or endorsed by the publisher.

APPENDIX A

The fluid viscosity of phloem sap was calculated using:

$$v = v_w e^{(0.032Sf-(0.012Sf)^2+(0.023Sf)^3)} \tag{1A}$$

$$Sf = \frac{CpL \times mm}{\rho} \tag{2A}$$

$$\rho = \frac{CpL}{1000}0.1256 + 1.0019 \tag{3A}$$

where ρ and v are the density and viscosity of the phloem sap, respectively. These equations follow Jensen et al. (2013), where v is calculated from v_w, the viscosity of pure water at 20°C, and Sf, the mass fraction of sucrose in the phloem (w/w), and ρ is calculated as a linear function of phloem sucrose concentration.

frontiers | Frontiers in Plant Science

REVIEW
published: 04 April 2022
doi: 10.3389/fpls.2022.835921

Unlocking Drought-Induced Tree Mortality: Physiological Mechanisms to Modeling

Ximeng Li[1,2], Benye Xi[3], Xiuchen Wu[4], Brendan Choat[2], Jinchao Feng[1], Mingkai Jiang[2,5] and David Tissue[2,6]**

[1]College of Life and Environmental Science, Minzu University of China, Beijing, China, [2]Hawkesbury Institute for the Environment, Western Sydney University, Richmond, NSW, Australia, [3]Ministry of Education Key Laboratory of Silviculture and Conservation, Beijing Forestry University, Beijing, China, [4]State Key Laboratory of Earth Surface Processes and Resource Ecology, Beijing Normal University, Beijing, China, [5]College of Life Sciences, Zhejiang University, Hangzhou, China, [6]Global Centre for Land-based Innovation, Western Sydney University, Richmond, NSW, Australia

Drought-related tree mortality has become a major concern worldwide due to its pronounced negative impacts on the functioning and sustainability of forest ecosystems. However, our ability to identify the species that are most vulnerable to drought, and to pinpoint the spatial and temporal patterns of mortality events, is still limited. Model is useful tools to capture the dynamics of vegetation at spatiotemporal scales, yet contemporary land surface models (LSMs) are often incapable of predicting the response of vegetation to environmental perturbations with sufficient accuracy, especially under stressful conditions such as drought. Significant progress has been made regarding the physiological mechanisms underpinning plant drought response in the past decade, and plant hydraulic dysfunction has emerged as a key determinant for tree death due to water shortage. The identification of pivotal physiological events and relevant plant traits may facilitate forecasting tree mortality through a mechanistic approach, with improved precision. In this review, we (1) summarize current understanding of physiological mechanisms leading to tree death, (2) describe the functionality of key hydraulic traits that are involved in the process of hydraulic dysfunction, and (3) outline their roles in improving the representation of hydraulic function in LSMs. We urge potential future research on detailed hydraulic processes under drought, pinpointing corresponding functional traits, as well as understanding traits variation across and within species, for a better representation of drought-induced tree mortality in models.

Keywords: drought, tree mortality, hydraulic failure, carbohydrates, functional traits, plant hydraulics, land surface models

OPEN ACCESS

Edited by:
Amanda A. Cardoso, Federal University of Alfenas, Brazil

Reviewed by:
Christoforos Pappas, Université TÉLUQ, Canada
Laurent J. Lamarque, Université du Québec à Trois-Rivières, Canada

***Correspondence:**
Ximeng Li
liximeng2009@hotmail.com
David Tissue
d.tissue@westernsydney.edu.au

Specialty section:
This article was submitted to Plant Physiology, a section of the journal Frontiers in Plant Science

Received: *15 December 2021*
Accepted: *04 March 2022*
Published: *04 April 2022*

Citation:
Li X, Xi B, Wu X, Choat B, Feng J, Jiang M and Tissue D (2022) Unlocking Drought-Induced Tree Mortality: Physiological Mechanisms to Modeling. Front. Plant Sci. 13:835921. doi: 10.3389/fpls.2022.835921

INTRODUCTION

The survival of forests around the globe is increasingly threatened by climatic extremes (Brodribb et al., 2020; Bennett et al., 2021; Gora and Esquivel-Muelbert, 2021). Massive forest dieback induced by climate change type drought has been recorded on every vegetated land within the past few decades (Adams et al., 2009; Allen et al., 2010, 2015). These events will become

more common given that climate projections indicate that future drought episodes will be typified by increased frequency, severity, and duration (Adams et al., 2009; Carnicer et al., 2011; Dai, 2013). Forests cover approximately 30% of the land surface area and provide numerous crucial ecological, economic and social benefits. Globally, forests store *ca.* 45% of the carbon in terrestrial ecosystems and sequester approximately 25% of annual anthropogenic carbon emissions each year (Bonan, 2008; Pan et al., 2011). In addition, forests can regulate the terrestrial energy budget and hydrological cycle by modifying surface albedo and evapotranspiration, which exert strong control over global carbon cycle. Forest mortality can therefore significantly influence ecosystem structure and function, resulting in cascading negative effects on biochemical and biophysical cycles, consequently generating a positive feedback to the climate (Adams et al., 2010; Anderegg et al., 2013).

Elucidating the spatial-temporal pattern of imminent mortality events is essential for ameliorating the detrimental consequences of tree death triggered by drought. Land surface models (LSMs) with mechanistic representations of vegetation and soil processes are an efficacious tool for predicting future plant dynamics (Geary et al., 2020). These models are capable of simulating growth, mortality, and reproduction of vegetation and are often coupled with climate models to predict the dynamics of biosphere-atmosphere interactions at large scales (Fisher et al., 2014). Early LSMs often poorly performed when simulating tree mortality events caused by drought, as evidenced by the existence of offsets between model outcomes and field observations (McDowell et al., 2013; Bugmann et al., 2019; Thrippleton et al., 2021). While subsequent progress in physiology research has led to updated model structure and components, thereby enabling better predictions of ecosystem fluxes as well as vegetation dynamics under drought with improved accuracy (De Kauwe et al., 2020; Sabot et al., 2020; Wang et al., 2021), predicting drought-related tree mortality remains a significant shortcoming of current LSMs (Trugman, 2021).

More accurate simulation of drought-induced tree mortality events requires detailed knowledge of the mechanisms through which drought affects plant physiology and the cascading effects on plant carbon and water status. Empirical models exist, but they often lack theoretical underpinnings; thus their predictive power for novel conditions or subjects is limited. Process-based models can overcome these weaknesses by representing biological processes in detail. Current experimental evidence points to the crucial role of plant hydraulic traits in explaining the pattern of drought-induced tree mortality (Anderegg et al., 2016; Zhu et al., 2018; Chen et al., 2019, 2021a; Powers et al., 2020; Nolan et al., 2021), which subsequently motivated the development and integration of plant hydraulic modules into LSMs (De Kauwe et al., 2020; Eller et al., 2020; Sabot et al., 2020; López et al., 2021). Nonetheless, physiological processes driving hydraulic dysfunction are incompletely integrated into these models, mainly because of knowledge gaps surrounding the physiological mechanisms of drought response, as well as inadequate empirical datasets enabling adequate model parameterization (Meir et al., 2015; Hartmann et al., 2018). Hence, modelers must employ largely unvalidated assumptions such as leaf phenology when drought strikes, lethal threshold during drought or post-drought recovery of hydraulic function, which consequently produce unrealistic outcomes (McDowell et al., 2013; Xu et al., 2016; De Kauwe et al., 2020), e.g., model suggests that trees in South-East Australia forests did not approach lethal water potential (De Kauwe et al., 2020), despite large-scale forest mortality was substantiated by field observation (Nolan et al., 2021).

In light of the modeling need, this review attempts to provide a brief overview of the current understanding of mechanisms leading to tree mortality under drought stress, with particular emphasis on carbon and hydraulic functions. Next, the development of hydraulic failure under drought stress, together with current understanding about key traits modulating this process, is outlined and discussed. We suggest that incorporating these hydraulic traits would improve the predictability in terms of mortality events during drought of process-based models. Finally, coordination among traits is discussed in the context of facilitating model parameterization. Here, we emphasize that this review does not attempt to provide a comprehensive summary of the gaps between data and models; such a summary must be interdisciplinary and requires iterative collaborations between modelers and experimentalists. Rather, our aim is to facilitate such an advancement by providing a physiological interpretation of the merit of functional traits, especially hydraulic traits involved in drought tolerance, to improve the predictive power of vegetation models under climate change. Finally, the matter of scale is a crucial but challenging consideration when incorporating plant hydraulic traits to predict drought-induced mortality in LSMs. While tree death at the individual level can be quantitatively determined *via* better representation of plant physiology, mortality events at the larger scales (e.g., population and landscape) are much more complex, involving interactions among individuals within and across species, heterogeneous plant-environment feedback across the landscape, and stochasticity to account for other co-variates that are difficult to capture in a typical LSM (e.g., insect and disease effects). Given that our overall objective is to frame a pathway linking plant hydraulic trait with improved predictive power in the models, the current review will focus exclusively on attributes at organ or canopy scale, while characteristics at other spatial scales are beyond the scope of discussion.

THE HISTORY OF TREE MORTALITY RESEARCH: PHYSIOLOGICAL MECHANISMS

Four decades ago, Manion (1981) proposed a slow decline hypothesis to explain the progress of tree mortality. In this theory, tree death begins with a moderate long-term stress that predisposes trees to mortality risk, which is intensified by a short-term severe stress, and death eventually occurs due to a contributing factor. Early modeling often builds on this original framework, with particular emphasis being placed on the role of carbon balance in tree mortality (McDowell et al., 2011; Sevanto and Xu, 2016). Based on the many physiological

processes documented in trees approaching death under drought stress, McDowell et al. (2008) put forward two physiological hypotheses that explain and generalize mechanisms underlying this phenomenon. The *carbon starvation* (*CS*) hypothesis suggests that downregulated stomatal conductance during chronic, moderate drought stress will lead to reduced carbon assimilation. As plants still require photosynthate to fuel metabolic processes such as respiration and osmoregulation, limited carbon supply, and the continued demand for it will eventually deplete plant carbon storage (e.g., non-structural carbohydrates, NSCs), which in turn causing tree death due to carbon starvation. Alternatively, the *hydraulic failure* (*HF*) hypothesis suggests that water transport failure-induced desiccation is the primary cause of tree mortality under drought stress. According to the air-seeding hypothesis (Zimmermann, 1983), when xylem water transport is operating under greater tension during acute drought due to high evaporative demand and/or decreased soil water availability, air will be aspirated from air-filled vessels into adjacent water-filled, functional vessels through inter-conduit pits, forming air bubbles, and consequently creating emboli that break the continuity of water transport in xylem. Embolized conduits are unable to transport water to distal organs and are unlikely to recover over short periods (Brodribb et al., 2010; Choat et al., 2015; Li et al., 2018b; Choat et al., 2019), eventually leading to desiccation and death at multiple organizational levels (i.e., cell, tissue, organ, and whole plant). It is worth noting that hydraulic failure does not exclusively occur in the vascular system of plants, but can also arise at the plant-soil interface as the hydraulic pathway connecting roots and soil is interrupted by air (Sperry et al., 1998). However, mortality under drought is still finalized by hydraulic failure of vascular system in this scenario.

Given the intimate link between carbon and water metabolism, the binary theory of tree mortality mechanisms during drought stress is apparently oversimplified. In recognition of the interdependency between *CS* and *HF*, an integrated mechanism was further proposed (McDowell et al., 2011). In this updated theory, *CS* and *HF* are synergistic and interrelated through a "carbon-hydraulic feedback loop." During drought stress, rates of carbon assimilation progressively decrease due to stomatal closure, consequently reducing the tissue non-structural carbohydrates content, which act as osmolytes facilitating water absorption by maintaining the water potential gradient between plant and soil. Inadequate water supply will result in increased xylem tension and degree of embolism, which diminishes hydraulic conductivity and leads to intensified physiological water deficit. This will ultimately feedback to leaves, causing enhanced stomatal closure or leaf shedding, which in turn exacerbates the NSCs deficiency. This integrated framework is generally supported, as both shifted tissue NSCs and xylem conductivity are often observed concomitantly in plants killed by drought (Adams et al., 2017). Therefore, pure CS or HF may not exist. Rather, *CS* and *HF* are likely the two endpoints of the "mortality mechanism spectrum". However, it is still necessary to identify the primary contributing factors for drought-induced tree mortality given that models require quantitative information on the tipping point where recovery is impossible, so as to accurately predict the dynamics of tree mortality under different environmental conditions. Incorporating both mechanisms will likely add extra complexity to computation without much improvement of predictive power.

NON-STRUCTURAL CARBOHYDRATES FACILITATE THE INTEGRITY OF XYLEM WATER TRANSPORT

Carbohydrate may be involved in the process of drought-related tree mortality through its effects on plant hydraulics, particularly by lowering the risk of xylem embolism. In support of this theoretical expectation, a strong relationship between the percentage loss of xylem conductivity (PLC) and the extent of NSC depletion has been observed (Trifilò et al., 2017; Tomasella et al., 2019). It has long been acknowledged that NSCs contribute to osmotic regulation, which may lower the risk of hydraulic failure by increasing plant water uptake (De Roo et al., 2020). For example, by manipulating tissue NSCs, O'Brien et al. (2014) showed that trees fed by exogenous NSCs exhibited higher survival rate during drought stress. Trees with enriched NSCs typically exhibited less negative water potential, which in turn reduced PLC, assuming xylem vulnerability to embolism was not shifted by the treatment. Alternatively, NSCs may lower the risk of xylem embolism by restraining the movement of air bubbles within the vascular system under negative pressure (De Baerdemaeker et al., 2017). It has been suggested that several carbon-based organic compounds, such as choline, amphiphilic lipids, or proteins, may act as surfactants that increase the stability of nanobubbles against increased tensile force, thereby lowering xylem vulnerability to embolism (Schenk et al., 2017). In addition, NSCs have been suggested to facilitate the repair of embolism by generating osmotic force that helps draw water from the reservoir to air-filled conduits (Liu et al., 2019) or change the embolism resistance by mediating the structure of vessels during the ontogenesis of xylem. Note that both NSC-mediated xylem refilling, and structural change requires sufficient time to occur and thus may not alter the fate for trees exposed to short-term pules of lethal drought.

HYDRAULIC DYSFUNCTION DETERMINES TREE DEATH DURING DROUGHT

The interplay between *CS* and *HF* is intricate, hence validating these mechanisms can be complex. In many studies, partial or complete loss of hydraulic conductivity in dead trees has been observed with little or no change in tissue carbohydrate concentration. A multi-species synthesis shows trees that died from drought typically exhibit more than 60% embolism with various degrees of carbon depletion, indicating hydraulic failure is a universal phenomenon for trees exposed to lethal drought stress (Adams et al., 2017). The role of plant hydraulics in tree death under drought is further supported by studies showing

correlative relationships between hydraulic traits related to embolism resistance and mortality patterns at both regional and global scales (Anderegg et al., 2016; Li et al., 2018a; Nolan et al., 2021; Chen et al., 2021a). In comparison, experimental evidence supporting carbon starvation as the main mechanism of mortality is relatively scarce. In Sevanto et al. (2014), tissue carbohydrate content decreased by nearly 70% in dead *Pinus edulis* treated with light exclusion, while both water potential and xylem conductivity were comparable to non-stressed controls. These results indicate that protracted carbon deficiency can generate tree death independent of hydraulic impairment. However, in the same study, trees killed by drought stress showed identical loss of xylem conductivity but different degrees of carbon depletion depending on the duration of drought exposure; hence, hydraulic failure remained the decisive factor generating tree mortality during drought stress.

DECIPHERING THE PROCESS OF DROUGHT-INDUCED HYDRAULIC FAILURE

Incorporating hydraulic failure into models requires its process to be elaborated. According to Choat et al. (2018), the development and progression of hydraulic failure under drought can be divided into two major phases (**Figure 1A**). During the initial phase (Phase I), drought stress develops as soil water availability declines due to decreased precipitation or depth to groundwater and can be exacerbated by an increase in the soil-atmosphere moisture gradient (i.e., vapor pressure deficit). Xylem tension becomes greater, as indicated by the continuously decreasing (i.e., more negative) maximum water potential (Ψ) of plants (e.g., predawn Ψ). Plants minimize water loss by reducing stomatal conductance until complete stomatal closure, either driven by the loss of turgor in guard cells and/or accumulation of cellular hormones (Buckley, 2019). It has been shown in many studies that the occurrence of complete stomatal closure precedes the inception of xylem embolism (Hochberg et al., 2017; Martin-StPaul et al., 2017; Creek et al., 2020). Therefore, the xylem water transport system remains largely intact during this stage, with no significant change in the hydraulic conductivity.

As drought stress persists, plant water potential slowly decreases. Roots can no longer extract water from soil due to xylem cavitation or disconnection between roots and soil, leading to decoupled water potentials between soil and plants. Once stomata are fully closed, water leaves the plant mainly through the leaf cuticle, leaky stomata, or other tissues, although with markedly reduced rates (Phase II; Duursma et al., 2019). Water will be extracted from intercellular spaces, apoplast, or living tissues (i.e., hydraulic capacitance), to meet the evaporation demand and maintain cellular water status. In some species, water loss during this stage can be further prevented by leaf shedding (Pivovaroff et al., 2014; Levionnois et al., 2020). If drought remains unalleviated, xylem water potential will ultimately exceed the threshold of embolism. Air bubbles rapidly propagate and spread within the vascular system until all vessels are embolized, with the spatial pattern of propagation depending on the vessel arrangement and connectivity (Johnson et al., 2020; Wason et al., 2021). Complete loss of water transport capacity results in desiccation of living tissue and cellular death, including meristematic cells that govern post-drought resilience, finally resulting in whole tree mortality (Li et al., 2016; Mantova et al., 2021).

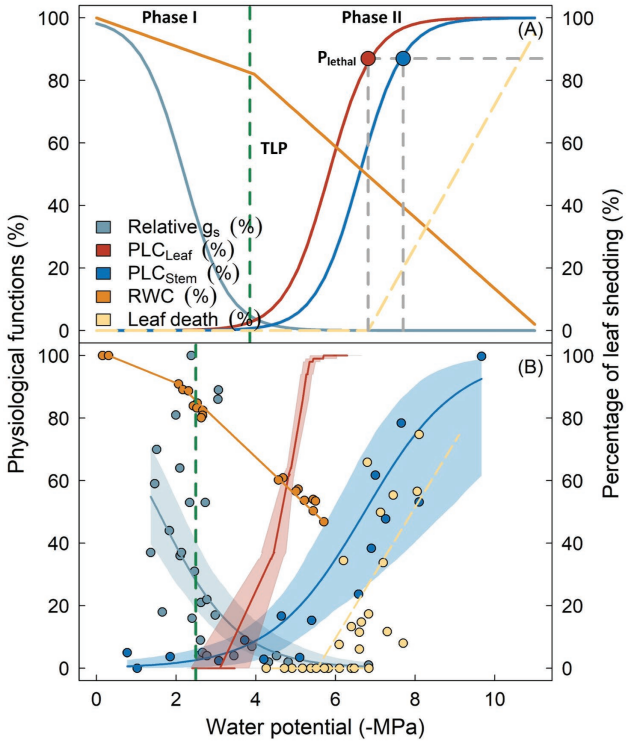

FIGURE 1 | Key physiological processes following reductions in plant water potential as outlined by the biphasic framework of drought-related tree mortality (panel **A**). Physiological functions including stomatal conductance (g_s, cyan), percentage loss of hydraulic conductivity in leaves (PLC_{Leaf}, red) and stems (PLC_{Stem}, blue), as well as branch relative water content (RWC, orange) are shown as percentage of maximum. Vertical dashed line indicates the leaf turgor loss point (TLP). Lethal water potential thresholds (P_{Lethal}) for leaves and stems are indicated by red and blue circles. Transition from Phase I to Phase II occurs when stomata are fully closed, which theoretically coincides with the turgor loss (broken dashed line). Panel **(B)** shows the observed variation of these physiological processes from *Eucalyptus sideroxylon* during a dry-down experiment conducted in a common garden (Blackman et al., 2019), with shaded regions surrounding the lines denoting the 95% confidence interval of fitted curves. Similarity in the two panels indicate that the biphasic framework is generally supported by the experimental evidence. Note that TLP in panel **(B)** occurred prior to complete stomatal closure, and leaf shedding was initiated when leaf xylem was completely embolized, indicating these traits may not be robust for predicting the timing of these physiological adjustments (see text for detail).

PARAMETERIZING DROUGHT-INDUCED HYDRAULIC FAILURE: WHAT TRAITS MATTER?

The timing of inception and progression of hydraulic failure can be complicated given it may be driven by impacts associated

with plant morphology, biochemistry, and physiology. Nonetheless, the biphasic hydraulic failure framework offers a simplified yet mechanistic approach for locating key traits involved in this process given that this framework is generally supported by empirical evidence (**Figure 1B**). Below, we list a few key aspects and corresponding traits with a brief discussion about their significance regarding plant drought response as well as current understanding and uncertainties. Of note, one implicit assumption for the development of xylem embolism during this phase is that plants and soil have become hydraulically disconnected prior to the occurrence of embolism in leaves and stems. This assumption is supported by some early studies showing that roots are often more vulnerable to embolism than stems or leaves (Johnson et al., 2016; Wason et al., 2018). However, some recent findings suggest that roots are comparably or even more tolerant to drought-induced embolism compared with other organs in some species (Rodriguez-Dominguez et al., 2018; Peters et al., 2020; Lübbe et al., 2021). Clearly, more studies are required to confirm the spatial pattern of vulnerability to embolism within plants, particularly within the root system and rhizosphere.

Rooting Depth

Rooting depth delimits the root zone extension of plants in the vertical direction and largely determines plant water acquisition capacity and the availability of water resources to plants. Therefore, rooting depth can significantly affect the response and resilience of plants to drought stress (Canadell et al., 1996), and has long been explicitly considered in most vegetation models, albeit using relatively simplistic mathematical representations (Zeng, 2001). Intuitively, species with deeper rooting systems have a greater chance to capitalize on relatively stable water resources such as deep soil water or groundwater, so there will be less risk of experiencing negative water potential during protracted drought stress. This suggests that the rooting depth trait can be informative in predicting species-specific mortality vulnerability, especially for co-occurring species or individuals showing contrasting drought response (Johnson et al., 2018b; Li et al., 2018b; Jiang et al., 2020). Interestingly, in a study conducted by Wu et al. (2018), the authors noted that the legacy effects of drought, as represented by the offsets between observed growth and predicted growth, persisted longer in deep-rooted trees compared with shallow-rooted functional types such as grasses or shrubs, indicating that deeper roots may compromise drought resilience, therefore questioning the role of deeper roots in facilitating overall fitness. Very few studies have related rooting depth to observed whole plant drought response, mainly due to lack of relevant information regarding this trait. It is well known that plant rooting depth is controlled by many climatic, edaphic, hydrological, and biological factors (Canadell et al., 1996; Fan et al., 2017). However, due to the great difficulty in studying roots, especially roots in the deep soil layer, and the high dynamics of root growth, information regarding rooting depth and its environmental drivers is still very scarce for many species, limiting our ability to better constrain the models. In a synthesis of 2,200 root observations for more than 1,000 species around the globe, Fan et al. (2017) established a hydrologic framework to interpret the spatial variation of plant rooting depth and demonstrated that soil hydrology is a globally common force driving rooting depth patterns from the landscape to global scale. This provides a useful approach to predict plant rooting depth based on the long-term characteristic of soil water profile, which is determined by both precipitation and groundwater level. Yet, the relationship between rooting depth and plant water absorption could become decoupled as the deep soil layer desiccates or the groundwater level declines beyond the capture extent of roots (Xi et al., 2018). Therefore, identifying the environmental and biological drivers for the variation of rooting depth warrants further study.

Stomatal Regulation

Strictly speaking, stomatal regulation during drought stress is not a trait, although it can be defined by quantitative metrics, which are the dynamics of stomatal conductance (g_s) in response to organ water status (i.e., leaf Ψ; **Figure 1**, cyan line). However, several key traits can be derived from this response curve and can encompass important implications to model drought-induced tree mortality (Klein, 2014; Blackman et al., 2019; Chen et al., 2019; De Kauwe et al., 2020). Current studies commonly measure g_s as a function of leaf Ψ, with the sensitivity of g_s to drought being quantified by the Ψ at the inception of complete stomatal closure (P_{gs}). Theoretically, stomatal closure at less negative water potentials during drought stress would significantly prevent water loss, which in turn reduces the risk of xylem embolism. However, given that stomatal closure also prevents the entry of CO_2 for carbon assimilation, closing stomata at the expense of carbon gain in the absence of embolism risk will negatively impact the plant and increase the probability of carbon starvation (McDowell et al., 2008). Therefore, water potential at stomatal closure *per se* would be less informative about overall species drought tolerance (Garcia-Forner et al., 2016; Martínez-Vilalta and Garcia-Forner, 2017). In a meta-analysis conducted by Martin-StPaul et al. (2017), the water potential triggering stomatal closure ranges between −1 MPa and approximately −4 MPa across a wide range of species; however, hydraulic safety is largely conferred by more negative water potential thresholds of xylem cavitation, especially for species in arid regions. Therefore, combining stomatal regulation with other traits can often yield metrics that are more informative to plant drought response. For example, by combining water potential thresholds at stomatal closure and xylem cavitation, Skelton et al. (2015) found that the risk of hydraulic failure can be well predicted by the safety margin defined by these two traits. Likewise, in the study of Chen et al. (2019), the percentage of tree survival was correlated with the safety margin based on the P_{gs}. Other typical examples include the index of desiccation time proposed by Blackman et al. (2016), which integrates stomatal regulation with many other traits potentially affecting plant drought response and shows great promise in estimating the duration from stomatal closure and mortality. Clearly, quantifiable information on hydraulic safety margin,

together with stomatal regulation, is useful to develop better models, yet traits delineating stomatal regulation (e.g., P_{gs}) are available for only a few species. Given the difficulties in measuring the response of stomata to drought, extrapolating these values from proper proxies will be instrumental for model parameterization (see below).

Minimum Conductance

Leaf minimum conductance (g_{min}) presumably becomes the main route for water leaving the plants, after complete stomatal closure during drought, and hence directly relates to the drought response strategy and survival of the plant (Duursma et al., 2019; Carignato et al., 2020; Lanning et al., 2020). Note that g_{min} characterizes the overall water loss rate after stomatal closure under field conditions; therefore, it can be higher than the conductance specifically measured for the adaxial side of leaves (i.e., cuticular conductance, g_{cut}) and is lower than the conductance value measured from leaves that are dark-adapted or with minimal photosynthetic rate (Duursma et al., 2019). Lower g_{min} should confer longer times for dehydration, but studies testing the functional significance of g_{min} in the process of drought-related tree mortality are scare. In an experiment designed to test the model described above, Blackman et al. (2019) found no correlation between observed g_{min} and observed time to desiccation. However, this does not mean that g_{min} plays no role in controlling water loss during dehydration. Instead, water loss during Phase II might be controlled by the conductance of other tissues such as bark. In support, Gleason et al. (2014) showed that desiccation time was significantly correlated with lower rates of transpiration in detached branches, which was the sum of water loss from both leaves and bark. It is also possible that the lack of a relationship was masked by the plasticity of g_{min}. It has been shown that g_{min} is highly responsive to various environmental stimuli, including temperature and water availability (Schuster et al., 2017). In Blackman et al. (2019), g_{min} may have acclimated to the environment in the common garden, showing only 2-fold variation despite the distinctly different times to mortality across species. More generalizable information regarding the variation in g_{min} is required to facilitate model advancement.

Relative Water Content

Relative water content (RWC) is the classic metric describing the water status of plants. The amount of water in cells governs cell turgor, the maintenance of which is essential for many cell functions. With respect to drought stress, water content in plants directly determines the duration of drought stress that plants can sustain, especially in Phase II when exogenous water supply is no longer available (Blackman et al., 2019). Furthermore, RWC is more than a simple indicator of cell hydration state. Under drought stress, plants need to retain a minimum amount of water to prevent complete cell desiccation. At this stage, the water balance of plants is co-regulated by the capacity of water supply *via* the vascular system, as well as the capacity to retain water in the cell by osmotic regulation; the former depends on xylem embolism resistance, while the latter primarily relies on NSCs (Martinez-Vilalta et al., 2019). The variation is therefore thought to reflect the integration of CS and HF. This concept is highly intriguing as it provides a tool for identifying mortality risk and also allows monitoring tree health at large scales given that RWC can be detected through remote sensing, thus enabling large-scale model evaluation (Konings et al., 2019). However, few studies have tested this concept to date. In Sapes et al. (2019), plant water content scaled linearly with PLC at both the organ and whole plant level in *Pinus ponderosa*, and water content could reflect NSCs content at a given soil water availability. Importantly, a threshold-like function was observed between population mortality risk and plant water content, suggesting the usefulness of this metric in ascertaining the probability of tree death under drought stress.

Hydraulic Capacitance

Plant hydraulic capacitance (C_p) refers to the water that can be extracted per unit change in water potential. The significance of water storage to whole plant water balance varies among species, and it has been suggested that C_p could contribute up to 50% of daily water loss from evapotranspiration (Pfautsch et al., 2015). During short-term drought, water stored in the apoplastic, intracellular capillary space or in living cells can be discharged, radially transported to xylem through ray parenchyma, thereby buffering the increasing tension of xylem sap to limit the development of embolism (Richards et al., 2014). In line with this suggestion, a negative correlation between C_p and the steepness of the xylem vulnerability curve, as represented by the slope of the rapidly increasing PLC phase, has been observed across species (Meinzer et al., 2009). During later phases of drought stress, when C_p becomes the only water source once water can no longer be taken up from the soil, a larger C_p should therefore allow plants to live longer. However, experimental evidence supporting this hypothesis is rare and equivocal (Gleason et al., 2014; Blackman et al., 2019). The inconsistent observations among different studies might be attributed to the scale (branch vs. whole plant) or plasticity of the response. For example, there are reports that the C_p of roots contains a comparable amount of extractable water as stems in some species, and C_p is also reportedly responsive to environmental moisture (Salomón et al., 2020). In addition, it is also possible that the water provided by C_p is not utilized to prevent xylem embolism but to sustain the vitality of other tissues such as the cambium (Knipfer et al., 2017, 2019). Nevertheless, C_p is a measurable trait that can potentially buffer the impact of drought on plant hydraulic status and therefore warrants further studies.

Leaf Shedding

Plant water loss primarily occurs through leaves; therefore, adjustments in canopy leaf area have significant influence on water balance of plants. Drought deciduous plants undergo annual cycles of leaf shedding and flushing in response to

regular seasonal drought; this phenological strategy allows deciduous trees to avoid water stress associated with the dry season. However, even in evergreen species prolonged drought stress can trigger leaf shedding (**Figure 1**, dashed yellow line). This phenomenon, commonly termed as hydraulic segmentation, is hypothesized to reduce the risk of xylem embolism given that water loss can be significantly minimized once leaves have been hydraulically isolated from the plant. Studies of hydraulic segmentation commonly focus on revealing its underlying mechanisms by identifying differences in vulnerability to embolism or hydraulic resistance across organs (Pivovaroff et al., 2014; Levionnois et al., 2020). It has been shown that embolism resistance or hydraulic resistance varies across organs in some species, but not in others, indicating that leaf shedding is not a universal strategy (Zhu et al., 2018). On the other hand, the effects of leaf shedding on plant water status are less well understood. Incorporating a leaf shedding function into models significantly increased the time to mortality and reduced the offset between predicted and observed values, suggesting that leaf area adjustment does facilitate water retention during drought stress (Blackman et al., 2019). However, the functional significance of this strategy may be debatable for some species exhibiting leaf shedding during drought stress. For instance, Wolfe et al. (2016) reported that the occurrence of leaf shedding coincided with a 50% loss of maximum xylem conductivity. Of note, one of the studied species, *Genipa americana*, showed continuously decreasing water potential after leaf shedding, indicating that leaf area adjustments may not always stabilize plant water status, if water loss with continuous drying is dominated by other organs. Similarly, in the study of Blackman et al. (2019), leaf shedding was initiated at water potentials triggering 50% loss of hydraulic conductivity in stems (P_{50}), suggesting that reducing canopy leaf area may have limited capacity to prevent the occurrence of xylem embolism (**Figure 2**).

Lethal Threshold

Given that hydraulic failure occurs due to massive xylem cavitation, it is intuitive that there is a lethal threshold in xylem vulnerability that generates a fatal degree of embolism. By subjecting plants to drought and then a re-watering treatment, Brodribb and Cochard (2009) showed that once the xylem of several gymnosperms lost 50% of the maximum hydraulic conductivity, recovery did not occur upon re-watering. Based on this finding, they suggested that the P_{50} of stems can be used as the lethal water potential threshold (P_{lethal}) for this functional group. Using the same approach, Urli et al. (2013) found that the P_{lethal} in angiosperms corresponds to the water potential threshold triggering 88–100% loss of xylem hydraulic conductivity (P_{88}). These thresholds are generally valid for whole plants and organs such as leaves (Blackman et al., 2009; **Figure 1**, P_{lethal}). However, uncertainty remains regarding the commonality of these water potential thresholds. Common approaches for determining P_{lethal} are often time-consuming; therefore, these threshold water potentials are derived from limited species. By compiling existing P_{lethal} data, Liang et al. (2021) recently showed that stem P_{50} and P_{88} explained 75 and 43% of the variation in P_{lethal} across gymnosperm and angiosperm species, respectively. In particular, lethal water potentials of some angiosperm species are much lower than P_{88}, as have been observed by Li et al. (2016). Tree death occurs under drought because living cells are dehydrated and therefore, trees are unable to regain metabolic function by reconstructing damaged tissues even after drought stress has been alleviated. Given the observed discrepancy between embolism threshold and P_{lethal}, it is likely that drought tolerance of some species can be organization level-specific, such that cell vitality can persist longer than the integrity of vascular water transport under drought stress. Therefore, assigning P_{lethal} based on cellular hydraulic failure represents a more mechanistic and robust approach, yet the vulnerability of cell vitality to dehydration remains unclear.

TOWARD A BETTER REPRESENTATION OF TREE DROUGHT MORTALITY IN MODELS WITH A MECHANISTIC APPROACH

Providing a mechanistic underpinning to better simulate drought mortality in trees is not an easy endeavor, as described above, but data-driven evidence is emerging and has led to an increasing momentum toward incorporating plant hydraulic traits in LSMs. Previously, predictive models often relied on empirical relationships to introduce soil moisture stress on plants and to induce the subsequent tree death (De Kauwe et al., 2015; Medlyn et al., 2015, 2016; Christoffersen et al., 2016; Trugman et al., 2018). Clearly this approach is not very applicable for novel conditions, which often change rapidly over space and time with global climate change. The abovementioned hydraulic traits and the associated ecophysiological processes offer a framework through which a more mechanistic simulation of drought mortality can be realized.

Indeed, many LSMs have incorporated some of these hydraulic traits and processes into their modeling framework. These models are often conceptually similar, i.e., plant hydraulics exert control on growth through leaf gas exchange, and tree mortality occurs once P_{lethal} is approached (**Figure 2**) but can differ in model structure and parameter. McDowell et al. (2013) evaluated six models of different scales using a data-model inter-comparison and highlighted that the capacity to simulate internal hydraulic and carbohydrate dynamics is crucial to capture observed tree mortality in the models. More recent modeling exercises showed a similar role for plant hydraulics. For example, De Kauwe et al. (2015) replaced the empirical scalar parameter (i.e., beta) for drought stress with a new expression for drought sensitivity of gas exchange that depends on leaf water potentials (i.e., Zhou et al., 2013, 2014) in the CABLE model. This new model feature led to improved simulation of gross primary production during the drought period, especially at the more xeric sites along a rainfall gradient

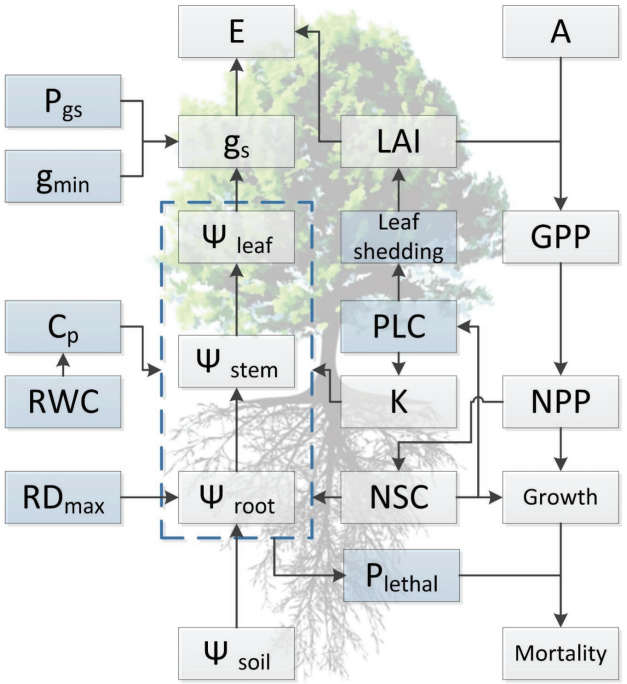

FIGURE 2 | Conceptual diagram summarizing current understanding regarding the relationship among functional traits and illustrating the general approach for simulating of tree dynamics in response to water availability with hydraulic traits in process-based models. Light blue boxes indicate traits that are directly involved in the occurrence of hydraulic failure during drought stress but are not well represented in current TBMs, either due to lack of trait values or insufficient knowledge regarding the variation at spatial or temporal scales. Traits presented in the diagram are maximum rooting depth (RD_{max}), water potential of soil, root, stem, and leaf (Ψ_{soil}, Ψ_{root}, Ψ_{stem}, and Ψ_{leaf}, respectively), relative water content (RWC), hydraulic capacitance (C_p), minimum conductance (g_{min}), water potential threshold of stomata respond to drought (P_{gs}), hydraulic conductivity (K), percentage loss of hydraulic conductivity (PLC), stomatal conductance (g_s), evaporation (E), leaf area index (LAI), leaf photosynthesis (A), non-structural carbohydrates (NSCs), lethal threshold (P_{lethal}), gross (GPP), and net primary productivity (NPP).

(De Kauwe et al., 2015). Similarly, Xu et al. (2016) introduced a trait-driven plant hydraulic module into the ED2 model, which led to more realistic predictions of plant hydraulic dynamics, such as leaf water potential and stem sap-flow and better spatial predictions of leaf area index. Kennedy et al. (2019) implemented a plant hydraulic stress configuration to the Community Land Model (CLM5) that better connects stomatal conductance to water stress *via* the influence of vegetation water potential, allowing hydraulic redistribution and compensatory root water uptake to buffer shortfalls in rainfall (Kennedy et al., 2019). All these abovementioned model developments regarding plant hydraulics could have significant implications for the simulated land-climate feedback, thereby providing crucial benefits to better anticipate cascading climate change consequences. Nonetheless, few LSMs have explicitly integrated current state-of-art knowledge regarding the development of hydraulic dysfunction into modeling due to existing data uncertainties for many traits mentioned above. We suggest that advancing our mechanistic understanding and building sufficient datasets, that allow traits variation at spatial or temporal scales to be predicted, will help to reduce these uncertainties (**Table 1**). Overall, this will facilitate data-model integration and improve the representation of drought-induced tree mortality in LSMs.

EXPANDING THE TRAIT DATABASE USING EASILY MEASURED PROXIES

A critical pre-requisite of process-based modeling is the information regarding traits values and the pattern of variation. Global databases of functional traits are becoming increasingly available but are often constrained to limited trait types and species (Kattge et al., 2020). This poses a major obstacle to its application, especially when predicting drought-induced tree mortality, the occurrence of which is likely ubiquitous across diverse tree species and is often a function of various traits (Blackman et al., 2016; Choat et al., 2018; Blackman et al., 2019; Chen et al., 2021a). With regard to plant hydraulics, many of the fundamental traits engaged in the process of hydraulic failure are only available for a few hundred species (Bartlett et al., 2012; Choat et al., 2012; Klein, 2014; Bartlett et al., 2016), which accounts for a trivial portion of the vast plant taxa. One important reason for the lack of sufficient data is that traits representing plant hydraulics are usually difficult to measure. Assessments of key functional traits (e.g., thresholds for stomatal closure, xylem embolism, or tree death) are often time- and labor-consuming, and can often be hard to realize under field conditions. Although new techniques are emerging to address these issues (Gauthey et al., 2020; Chen et al., 2021b), building substantial datasets still requires considerable time.

In plants, many functional traits are mathematically correlated across species. Positive correlation can arise because of shared ancestry, functional convergence, or subjected to co-selection, while negative correlative relationships can result from functional or structural trade-offs (Wright et al., 2007; Reich, 2014; Bartlett et al., 2016). Such correlative relationships not only provide insights into many key ecological questions, such as principles governing community assembly or species coexistence, but also offer the opportunity to rapidly gain information regarding traits variation across diverse species. Using easily measured traits (i.e., soft traits), as proxies of traits that are difficult to measure (i.e., hard traits), has become a common approach in traits-based ecology, especially when TBMs are parameterized (Rogers et al., 2017). Importantly, these relationships often reflect mechanistic implications rather than demonstrated causality (Reich et al., 1998).

With respect to plant water relations, coordination and trade-offs have been found among various hydraulic or structural traits. Among others, woody density (WD), which is thought to integrate a suite of plant functions, has been shown to be a strong predictor of xylem vulnerability to embolism

TABLE 1 | Key summary of plant hydraulic traits and/or variables and their model integration recommendations.

Measurable trait/variable	Definition	Drought-related functionality	Data-model integration recommendations	Data uncertainty to support model integration
RWC	Relative water content in plant tissue	Affects plant hydraulic capacitance and plant drought tolerance	Need to generalize the functional relationship to guide model development, possibly *via* a variable RWC (within bound) in response to environmental perturbation	High
RD_{max}	The maximum rooting depth	Affects plant water uptake from the soil and plant drought tolerance	Refine PFT-specific parameter in the model to better reflect plant and landscape heterogeneity	Low
ψ	Water potential of major plant tissue	Affects plant hydraulic conductivity and water loss *via* stomatal conductance, also affects plant carbon uptake and transport	Incorporate the functional relationship into models, in particular those plant hydraulic vulnerability and carbon status, and collect model evaluation datasets	Moderate
C_p	Plant hydraulic capacitance: the amount of water that can be extracted per unit change in ψ	Affects plant xylem vulnerability and plant hydraulic conductivity	Incorporate this parameter to better reflect its functional effect in the model	Moderate
K	Whole plant hydraulic conductance	Determines the capacity for plant to transport water during drought	Develop datasets to generalize its functional effect	High
g_{min}	Leaf minimum stomatal conductance	Characterizes plant water loss *via* leaf after stomatal closure during drought	Incorporate this parameter in the model and allow decoupling between carbon assimilation and stomatal conductance during drought	Moderate
P_{gs}	Leaf water potential at the inception of complete stomatal closure	Affects plant hydraulic conductivity, stomatal water loss and plant desiccation time during drought	Collect this parameter together with g_{min} and integrate into the functional relationship of plant hydraulics in the model	Moderate
P_{50}	50% loss of xylem conductivity	Affects plant hydraulic conductivity and desiccation time	Develop a dataset and integrate into the functional relationship of plant hydraulics in the model	Moderate
P_{88}	88% loss of xylem conductivity	Affects plant hydraulic conductivity and desiccation time	Develop a dataset and integrate into the functional relationship of plant hydraulics in the model	Moderate
P_{lethel}	Lethal threshold of loss of xylem conductivity	Indicates plant mortality	Develop a dataset and integrate into the functional relationship of plant hydraulics in the model	Moderate

Note that the data uncertainty to support model integration is a qualitative assessment based on available literature and thus should be considered in caution. PFT denotes plant-functional group.

(Markesteijn et al., 2011; Li et al., 2018a; Liang et al., 2021). Furthermore, wood density is correlated with sapwood hydraulic capacitance, which may facilitate both drought resistance and resilience (Li et al., 2018a; Santiago et al., 2018). It has been observed that species with high wood density are more resistant to drought-induced xylem embolism. Mechanisms underpinning this observation may be due to reinforced vessel walls, which can resist xylem implosion and therefore cavitation (Hacke et al., 2001), although collapse of xylem vessels is seldomly reported in stems. The correlation between WD and xylem embolism resistance has been adopted by some models. For instance, in the work of Xu et al. (2016), WD was used to predict the water potential threshold of xylem embolism, and the latter was then used to parameterize the hydraulic module of ED2. However, caution should be taken when extrapolating this correlation to assess mortality risk for field-grown trees given that the two traits are not always related (**Figure 3A**). For example, some species characterized by high WD tend to exhibit a higher mortality ratio during drought stress (Hoffmann et al., 2011). One possible reason is that WD is not consistently correlated with embolism resistance. Indeed, high WD can be supported by features that are unrelated to plant hydraulics, such as fiber traits (Russo et al., 2010). Additionally, the occurrence of hydraulic failure, as discussed above, is a function of multiple traits. A species characterized by embolism-resistant xylem can still die rapidly during drought stress due to a profligate water regulation strategy or water acquisition ability (Hoffmann et al., 2011; Fu et al., 2019).

Another valuable trait is leaf water potential at turgor loss point (TLP), which has been used to assess drought tolerance in plant physiology for decades (Bartlett et al., 2012). TLP is often correlated with water potential thresholds triggering stomatal closure and xylem embolism (**Figure 3B**), either because of mechanistic linkages given that stomatal closure is structurally driven by the turgor loss of guard cells, or functional linkages as less resistance xylem typically requires early stomatal closure to minimize water loss (Buckley, 2019). Recent findings also suggest that TLP integrates a wide range of hydraulic traits and thereby describes the overall water use strategy of plants (Meinzer et al., 2016; Fu et al., 2019; Li et al., 2019). Furthermore,

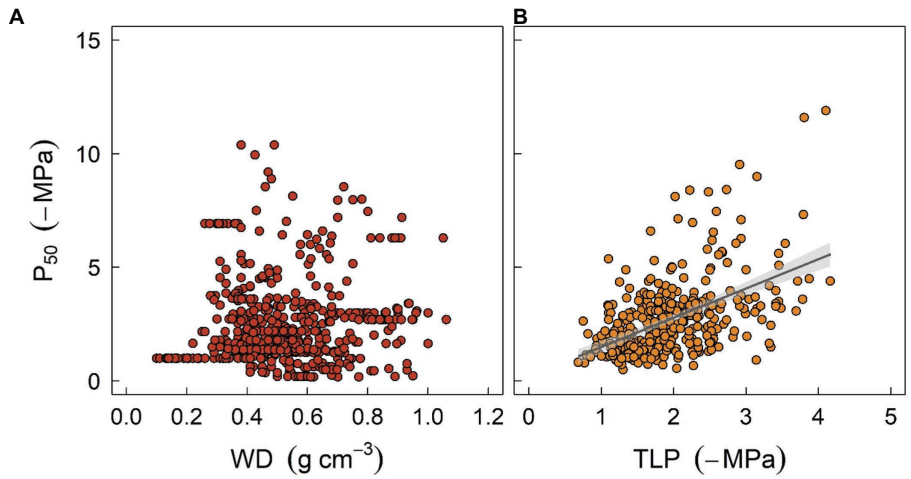

FIGURE 3 | The relationships between stem water potential at 50% loss of xylem hydraulic conductivity (P_{50}) and two easily measured traits, sapwood density (WD, panel **A**), and leaf turgor loss point (TLP, panel **B**), at global scale. P_{50} data were obtained from Choat et al. (2012). Data for WD were sourced from Zanne et al. (2009), and TLP data were compiled from Bartlett et al. (2012) and Zhu et al. (2018). Regression formula for panel **(B)** $y = 1.34x + 0.25$ ($R^2 = 0.22$, $p < 0.001$).

it has been shown that TLP can also be correlated with economic traits such as specific leaf area, photosynthetic rate, or leaf longevity, although the correlations can be much weaker (Zhu et al., 2018), suggesting that diverse aspects of plant strategy can probably converge to a simple trait (Reich, 2014). Indeed, several meta-analysis studies have shown that TLP varies systematically with site water availability within and across biomes, indicating that TLP does provide some adaptive advantages (Bartlett et al., 2012; Zhu et al., 2018). However, the correlation between TLP and traits such as xylem embolism threshold is still surprising as TLP is known to be highly plastic (Farrell et al., 2017; Johnson et al., 2018a), while embolism threshold is more conservative within and across species (Lamy et al., 2014; Li et al., 2018a). Again, one should be cautious when using TLP as a surrogate given that it can easily become decoupled from other hydraulic traits due to growth conditions. Overall, soft traits like WD or TLP provide a rapid tool for generating other traits essential for model parameterization, as well as assessing plant strategy for a considerable number of species. Nonetheless, "true" values of hard traits are warranted to increase the precision of model outcomes.

PATHWAY FORWARD

The elusive nature of physiological mechanisms underpinning drought-induced tree mortality suggest that detailed biological processes and their interactions from the beginning of drought response to complete desiccation can be difficult to model. Nonetheless, the identification of hydraulic dysfunction as a major driver of tree death during drought stress, together with the biphasic framework depicting the development of xylem embolism, allows us to locate key functional traits involved in this complicated phenomenon and to predict its occurrence using a mechanistic approach. To better represent hydraulic failure in process-based models, we suggest that the following areas require future attention.

Firstly, physiological mechanisms for plant water regulation strategy during drought stress need to be better elucidated. Drought-induced tree death occurs when plant water potential approaches a critical threshold where xylem water transport is largely blocked by embolism. To prevent water potential from reaching this tipping point, plants would adopt diverse regulation strategies to maintain a reasonable water status. However, many of these strategies are not well represented in current models. For example, hydraulic segmentation has long been thought to mitigate the decline of water potential. Yet, the physiological basis of this phenomenon remains unclear. Hypotheses explaining leaf shedding during drought stress include differences in vulnerability to embolism or hydraulic resistance across organs, both of which are supported by experimental evidence, but can generate distinct ecological consequences. A similar example is xylem refilling, which still represents a research frontier in the field of plant hydraulics. Whether an embolized vessel can hydraulically recover after drought is still controversial. Several mechanisms have been proposed, but it remains unknown whether it is common in species, the nature of the circumstances leading to xylem refilling, and potential impacts on water transport. Identification of these physiological mechanisms is crucial because it determines how this strategy will be represented and parameterized in models.

Secondly, functional traits influencing water transport of plants need to be fully examined, especially for traits governing belowground hydraulic processes. Although data of key hydraulic traits such as vulnerability to embolism are rapidly accumulating, information regarding other functional traits affecting plant hydraulics is limited. With respect to aboveground water relations, traits, such as cuticular conductance, hydraulic capacitance, or water potential threshold for stomatal closure, are only available for a relatively small number of species compared with embolism

thresholds. In addition, trait variation with the environment is also largely unknown. Likewise, belowground traits affecting water uptake and conductance are limited. Root functional traits that can be measured with relatively simple approaches should be the focus, such as maximum rooting depth, vertical root distribution, proportions of fine (absorption) and coarse (transport) roots, and water uptake vulnerability to soil desiccation. In addition, the variability of root traits with tree age should be determined to facilitate assessment of impacts in a dynamic way.

Patterns and sources of intraspecific trait variation at spatial and temporal scales require further investigation. The interspecific variation of traits related to water regulation has been extensively studied and many of these traits vary systematically along an aridity gradient. However, the pattern of intraspecific trait variation is less clear, with the environmental drivers somewhat inconclusive. In some species, the variation of hydraulic traits among populations shares a similar pattern as variation across species, i.e., traits generally shift toward an increased drought tolerance as habitat water availability becomes limited. However, in other species, hydraulic traits can be highly conservative despite variation in environmental dryness. In addition, traits may also vary over time for a given population, but studies focusing on this aspect are infrequent. It has been shown that some hydraulic traits, including vulnerability to embolism or hydraulic capacitance, can shift seasonally or interannually (Guo et al., 2020; Sorek et al., 2021; Wu et al., 2021), leading to temporally altered overall water regulation strategy. This type of variation can be due to differences in ontogeny or shifts in environmental conditions over time. A useful framework for understanding observed differences in traits within species is to separate the observed difference into genotype variation and phenotypic plasticity and to unravel the source of variation using common garden experiments. If trait expression is governed by genetics, then we would expect small differences in targeted traits across populations, and we could apply a single trait value in models, regardless of the population-specific growth conditions. However, if phenotypic plasticity is dominant, then controlled environment experiments or transect studies in the field will be needed to uncover the environmental driver and then calculate the trait value as a function of environmental variables in models.

CONCLUSION

In conclusion, drought-related tree mortality is a ramification of complex interactions, consisting of multiple physiological processes associated with carbon and hydraulic dynamics. Recent advancements in plant physiology indicate the crucial role of hydraulic failure in determining tree mortality under drought, which offers a pathway for LSMs to represent mortality events with a simplified, but efficacious approach. In particular, the biphasic framework describing the development of hydraulic failure is generally supported by current experimental evidence and is therefore instrumental in locating key traits. The incorporation of these key traits will have the potential to boost the predictability of tree mortality under drought, without introducing much complexity to the algorithms and burdening the computational capacity. Nonetheless, many hydraulic processes within this framework are not mechanistically understood or remain controversial, which represents the priority of future research in the field of plant hydraulics. In addition, traits coordination and variation at different levels (e.g., intra- and inter-specific) and scales (i.e., spatial and temporal) also warrant further study, which would facilitate model parameterization by providing and constraining trait values.

AUTHOR CONTRIBUTIONS

XL drafted the early version of this manuscript, with inputs from BX on root hydraulics and MJ on ecosystem models. DT provided critical edits. All authors contributed to the article and approved the submitted version.

FUNDING

XL is financially supported by research initializing funding from Minzu University of China (nos. 0210040217 and 2020CXTD). BX is supported by the National Natural Science Foundation of China (no. 32171763). JF receives funds from the interdisciplinary research program of Minzu University of China (nos. 2020MDJC09 and 2021XSTD02). MJ acknowledges funding from the Australia Research Council (DE210101654).

ACKNOWLEDGMENTS

The authors appreciate the advice from Belinda Medlyn on the modeling section of this manuscript. This manuscript is adapted from the first chapter of XL's PhD thesis at Western Sydney University. XL therefore thanks Peter Franks from University of Sydney and Patrick Meir from Australian National University, who were examiners of XL's PhD thesis, for their valuable comments on the prototype of this paper.

REFERENCES

Adams, H. D., Guardiola-Claramonte, M., Barron-Gafford, G. A., Villegas, J. C., Breshears, D. D., Zou, C. B., et al. (2009). Temperature sensitivity of drought-induced tree mortality portends increased regional die-off under global-change-type drought. *Proc. Natl. Acad. Sci. U. S. A.* 106, 7063–7066. doi: 10.1073/pnas.0901438106

Adams, H. D., Macalady, A. K., Breshears, D. D., Allen, C. D., Stephenson, N. L., Saleska, S. R., et al. (2010). Climate-induced tree mortality: earth system consequences. *EOS Trans. Am. Geophys. Union* 91, 153–154. doi: 10.1029/2010EO170003

Adams, H. D., Zeppel, M. J., Anderegg, W. R., Hartmann, H., Landhäusser, S. M., Tissue, D. T., et al. (2017). A multi-species synthesis of physiological mechanisms in drought-induced tree mortality. *Nat. Ecol. Evol.* 1, 1285–1291. doi: 10.1038/s41559-017-0248-x

Allen, C. D., Breshears, D. D., and Mcdowell, N. G. (2015). On underestimation of global vulnerability to tree mortality and forest die-off from hotter drought in the Anthropocene. *Ecosphere* 6, art129–art155. doi: 10.1890/ES15-00203.1

Allen, C. D., Macalady, A. K., Chenchouni, H., Bachelet, D., Mcdowell, N., Vennetier, M., et al. (2010). A global overview of drought and heat-induced tree mortality reveals emerging climate change risks for forests. *For. Ecol. Manag.* 259, 660–684. doi: 10.1016/j.foreco.2009.09.001

Anderegg, W. R., Kane, J. M., and Anderegg, L. D. (2013). Consequences of widespread tree mortality triggered by drought and temperature stress. *Nat. Clim. Chang.* 3, 30–36. doi: 10.1038/nclimate1635

Anderegg, W. R., Klein, T., Bartlett, M., Sack, L., Pellegrini, A. F., Choat, B., et al. (2016). Meta-analysis reveals that hydraulic traits explain cross-species patterns of drought-induced tree mortality across the globe. *Proc. Natl. Acad. Sci. U. S. A.* 113, 5024–5029. doi: 10.1073/pnas.1525678113

Bartlett, M. K., Klein, T., Jansen, S., Choat, B., and Sack, L. (2016). The correlations and sequence of plant stomatal, hydraulic, and wilting responses to drought. *Proc. Natl. Acad. Sci. U. S. A.* 113, 13098–13103. doi: 10.1073/pnas.1604088113

Bartlett, M. K., Scoffoni, C., and Sack, L. (2012). The determinants of leaf turgor loss point and prediction of drought tolerance of species and biomes: a global meta-analysis. *Ecol. Lett.* 15, 393–405. doi: 10.1111/j.1461-0248.2012.01751.x

Bennett, A. C., Dargie, G. C., Cuni-Sanchez, A., Mukendi, J. T., Hubau, W., Mukinzi, J. M., et al. (2021). Resistance of African tropical forests to an extreme climate anomaly. *Proc. Natl. Acad. Sci. U. S. A.* 118:e2003169118. doi: 10.1073/pnas.2003169118

Blackman, C. J., Brodribb, T. J., and Jordan, G. J. (2009). Leaf hydraulics and drought stress: response, recovery and survivorship in four woody temperate plant species. *Plant Cell Environ.* 32, 1584–1595. doi: 10.1111/j.1365-3040.2009.02023.x

Blackman, C. J., Li, X., Choat, B., Rymer, P. D., De Kauwe, M. G., Duursma, R. A., et al. (2019). Desiccation time during drought is highly predictable across species of *Eucalyptus* from contrasting climates. *New Phytol.* 224, 632–643. doi: 10.1111/nph.16042

Blackman, C. J., Pfautsch, S., Choat, B., Delzon, S., Gleason, S. M., and Duursma, R. A. (2016). Toward an index of desiccation time to tree mortality under drought. *Plant Cell Environ.* 39, 2342–2345. doi: 10.1111/pce.12758

Bonan, G. B. (2008). Forests and climate change: forcings, feedbacks, and the climate benefits of forests. *Science* 320, 1444–1449. doi: 10.1126/science.1155121

Brodribb, T. J., Bowman, D. J., Nichols, S., Delzon, S., and Burlett, R. (2010). Xylem function and growth rate interact to determine recovery rates after exposure to extreme water deficit. *New Phytol.* 188, 533–542. doi: 10.1111/j.1469-8137.2010.03393.x

Brodribb, T. J., and Cochard, H. (2009). Hydraulic failure defines the recovery and point of death in water-stressed conifers. *Plant Physiol.* 149, 575–584. doi: 10.1104/pp.108.129783

Brodribb, T. J., Powers, J., Cochard, H., and Choat, B. (2020). Hanging by a thread? Forests and drought. *Science* 368, 261–266. doi: 10.1126/science.aat7631

Buckley, T. N. (2019). How do stomata respond to water status? *New Phytol.* 224, 21–36. doi: 10.1111/nph.15899

Bugmann, H., Seidl, R., Hartig, F., Bohn, F., Brůna, J., Cailleret, M., et al. (2019). Tree mortality submodels drive simulated long-term forest dynamics: assessing 15 models from the stand to global scale. *Ecosphere* 10:e02616. doi: 10.1002/ecs2.2616

Canadell, J., Jackson, R., Ehleringer, J., Mooney, H., Sala, O., and Schulze, E. D. (1996). Maximum rooting depth of vegetation types at the global scale. *Oecologia* 108, 583–595. doi: 10.1007/BF00329030

Carignato, A., Vázquez-Piqué, J., Tapias, R., Ruiz, F., and Fernández, M. (2020). Variability and plasticity in cuticular transpiration and leaf permeability allow differentiation of *Eucalyptus* clones at an early age. *Forests* 11:9. doi: 10.3390/f11010009

Carnicer, J., Coll, M., Ninyerola, M., Pons, X., Sanchez, G., and Penuelas, J. (2011). Widespread crown condition decline, food web disruption, and amplified tree mortality with increased climate change-type drought. *Proc. Natl. Acad. Sci. U. S. A.* 108, 1474–1478. doi: 10.1073/pnas.1010070108

Chen, Y. J., Choat, B., Sterck, F., Maenpuen, P., Katabuchi, M., Zhang, S. B., et al. (2021a). Hydraulic prediction of drought-induced plant dieback and top-kill depends on leaf habit and growth form. *Ecol. Lett.* 24, 2350–2363. doi: 10.1111/ele.13856

Chen, Z., Li, S., Luan, J., Zhang, Y., Zhu, S., Wan, X., et al. (2019). Prediction of temperate broadleaf tree species mortality in arid limestone habitats with stomatal safety margins. *Tree Physiol.* 39, 1428–1437. doi: 10.1093/treephys/tpz045

Chen, Y. J., Maenpuen, P., Zhang, Y. J., Barai, K., Katabuchi, M., Gao, H., et al. (2021b). Quantifying vulnerability to embolism in tropical trees and lianas using five methods: can discrepancies be explained by xylem structural traits? *New Phytol.* 229, 805–819. doi: 10.1111/nph.16927

Choat, B., Brodersen, C. R., and McElrone, A. J. (2015). Synchrotron X-ray microtomography of xylem embolism in *Sequoia sempervirens* saplings during cycles of drought and recovery. *New Phytol.* 205, 1095–1105. doi: 10.1111/nph.13110

Choat, B., Brodribb, T. J., Brodersen, C. R., Duursma, R. A., López, R., and Medlyn, B. E. (2018). Triggers of tree mortality under drought. *Nature* 558, 531–539. doi: 10.1038/s41586-018-0240-x

Choat, B., Jansen, S., Brodribb, T. J., Cochard, H., Delzon, S., Bhaskar, R., et al. (2012). Global convergence in the vulnerability of forests to drought. *Nature* 491, 752–755. doi: 10.1038/nature11688

Choat, B., Nolf, M., Lopez, R., Peters, J. M., Carins-Murphy, M. R., Creek, D., et al. (2019). Non-invasive imaging shows no evidence of embolism repair after drought in tree species of two genera. *Tree Physiol.* 39, 113–121. doi: 10.1093/treephys/tpy093

Christoffersen, B. O., Gloor, M., Fauset, S., Fyllas, N. M., Galbraith, D. R., Baker, T. R., et al. (2016). Linking hydraulic traits to tropical forest function in a size-structured and trait-driven model (TFS v. 1-Hydro). *Geosci. Model Dev.* 9, 4227–4255. doi: 10.5194/gmd-9-4227-2016

Creek, D., Lamarque, L. J., Torres-Ruiz, J. M., Parise, C., Burlett, R., Tissue, D. T., et al. (2020). Xylem embolism in leaves does not occur with open stomata: evidence from direct observations using the optical visualization technique. *J. Exp. Bot.* 71, 1151–1159. doi: 10.1093/jxb/erz474

Dai, A. (2013). Increasing drought under global warming in observations and models. *Nat. Clim. Chang.* 3, 52–58. doi: 10.1038/nclimate1633

De Baerdemaeker, N. J., Salomón, R. L., De Roo, L., and Steppe, K. (2017). Sugars from woody tissue photosynthesis reduce xylem vulnerability to cavitation. *New Phytol.* 216, 720–727. doi: 10.1111/nph.14787

De Kauwe, M. G., Medlyn, B. E., Ukkola, A. M., Mu, M., Sabot, M. E., Pitman, A. J., et al. (2020). Identifying areas at risk of drought-induced tree mortality across South-Eastern Australia. *Glob. Chang. Biol.* 26, 5716–5733. doi: 10.1111/gcb.15215

De Kauwe, M. G., Zhou, S. X., Medlyn, B. E., Pitman, A. J., Wang, Y. P., Duursma, R. A., et al. (2015). Do land surface models need to include differential plant species responses to drought? Examining model predictions across a mesic-xeric gradient in Europe. *Biogeosciences* 12, 7503–7518. doi: 10.5194/bg-12-7503-2015

De Roo, L., Salomón, R. L., Oleksyn, J., and Steppe, K. (2020). Woody tissue photosynthesis delays drought stress in *Populus tremula* trees and maintains starch reserves in branch xylem tissues. *New Phytol.* 228, 70–81. doi: 10.1111/nph.16662

Duursma, R. A., Blackman, C. J., Lopéz, R., Martin-Stpaul, N. K., Cochard, H., and Medlyn, B. E. (2019). On the minimum leaf conductance: its role in models of plant water use, and ecological and environmental controls. *New Phytol.* 221, 693–705. doi: 10.1111/nph.15395

Eller, C. B., Rowland, L., Mencuccini, M., Rosas, T., Williams, K., Harper, A., et al. (2020). Stomatal optimization based on xylem hydraulics (SOX) improves land surface model simulation of vegetation responses to climate. *New Phytol.* 226, 1622–1637. doi: 10.1111/nph.16419

Fan, Y., Miguez-Macho, G., Jobbágy, E. G., Jackson, R. B., and Otero-Casal, C. (2017). Hydrologic regulation of plant rooting depth. *Proc. Natl. Acad. Sci. U. S. A.* 114, 10572–10577. doi: 10.1073/pnas.1712381114

Farrell, C., Szota, C., and Arndt, S. K. (2017). Does the turgor loss point characterize drought response in dryland plants? *Plant Cell Environ.* 40, 1500–1511. doi: 10.1111/pce.12948

Fisher, J. B., Huntzinger, D. N., Schwalm, C. R., and Sitch, S. (2014). Modeling the terrestrial biosphere. *Annu. Rev. Environ. Resour.* 39, 91–123. doi: 10.1146/annurev-environ-012913-093456

Fu, X., Meinzer, F. C., Woodruff, D. R., Liu, Y. Y., Smith, D. D., Mcculloh, K. A., et al. (2019). Coordination and trade-offs between leaf and stem hydraulic traits and stomatal regulation along a spectrum of isohydry to anisohydry. *Plant Cell Environ.* 42, 2245–2258. doi: 10.1111/pce.13543

Garcia-Forner, N., Adams, H. D., Sevanto, S., Collins, A. D., Dickman, L. T., Hudson, P. J., et al. (2016). Responses of two semiarid conifer tree species to reduced precipitation and warming reveal new perspectives for stomatal regulation. *Plant Cell Environ.* 39, 38–49. doi: 10.1111/pce.12588

Gauthey, A., Peters, J., Carins-Murphy, M., Rodriguez-Dominguez, C., Li, X., Delzon, S., et al. (2020). Evaluating methods used to measure cavitation resistance in seven woody species with differing xylem anatomy: a comparison of visual and hydraulic techniques. *New Phytol.* 228, 884–897. doi: 10.1111/nph.16746

Geary, W. L., Bode, M., Doherty, T. S., Fulton, E. A., Nimmo, D. G., Tulloch, A. I., et al. (2020). A guide to ecosystem models and their environmental applications. *Nat. Ecol. Evol.* 4, 1459–1471. doi: 10.1038/s41559-020-01298-8

Gleason, S. M., Blackman, C. J., Cook, A. M., Laws, C. A., and Westoby, M. (2014). Whole-plant capacitance, embolism resistance and slow transpiration rates all contribute to longer desiccation times in woody angiosperms from arid and wet habitats. *Tree Physiol.* 34, 275–284. doi: 10.1093/treephys/tpu001

Gora, E. M., and Esquivel-Muelbert, A. (2021). Implications of size-dependent tree mortality for tropical forest carbon dynamics. *Nat. Plants* 7, 384–391. doi: 10.1038/s41477-021-00879-0

Guo, J. S., Hultine, K. R., Koch, G. W., Kropp, H., and Ogle, K. (2020). Temporal shifts in iso/anisohydry revealed from daily observations of plant water potential in a dominant desert shrub. *New Phytol.* 225, 713–726. doi: 10.1111/nph.16196

Hacke, U. G., Stiller, V., Sperry, J. S., Pittermann, J., and Mcculloh, K. A. (2001). Cavitation fatigue. Embolism and refilling cycles can weaken the cavitation resistance of xylem. *Plant Physiol.* 125, 779–786. doi: 10.1104/pp.125.2.779

Hartmann, H., Moura, C. F., Anderegg, W. R., Ruehr, N. K., Salmon, Y., Allen, C. D., et al. (2018). Research frontiers for improving our understanding of drought-induced tree and forest mortality. *New Phytol.* 218, 15–28. doi: 10.1111/nph.15048

Hochberg, U., Windt, C. W., Ponomarenko, A., Zhang, Y. J., Gersony, J., Rockwell, F. E., et al. (2017). Stomatal closure, basal leaf embolism, and shedding protect the hydraulic integrity of grape stems. *Plant Physiol.* 174, 764–775. doi: 10.1104/pp.16.01816

Hoffmann, W. A., Marchin, R. M., Abit, P., and Lau, O. L. (2011). Hydraulic failure and tree dieback are associated with high wood density in a temperate forest under extreme drought. *Glob. Chang. Biol.* 17, 2731–2742. doi: 10.1111/j.1365-2486.2011.02401.x

Jiang, P., Meinzer, F. C., Wang, H., Kou, L., Dai, X., and Fu, X. (2020). Belowground determinants and ecological implications of shrub species' degree of isohydry in subtropical pine plantations. *New Phytol.* 226, 1656–1666. doi: 10.1111/nph.16502

Johnson, D. M., Berry, Z. C., Baker, K. V., Smith, D. D., Mcculloh, K. A., and Domec, J. C. (2018a). Leaf hydraulic parameters are more plastic in species that experience a wider range of leaf water potentials. *Funct. Ecol.* 32, 894–903. doi: 10.1111/1365-2435.13049

Johnson, K. M., Brodersen, C., Carins-Murphy, M. R., Choat, B., and Brodribb, T. J. (2020). Xylem embolism spreads by single-conduit events in three dry forest angiosperm stems. *Plant Physiol.* 184, 212–222. doi: 10.1104/pp.20.00464

Johnson, D. M., Domec, J. C., Carter Berry, Z., Schwantes, A. M., Mcculloh, K. A., Woodruff, D. R., et al. (2018b). Co-occurring woody species have diverse hydraulic strategies and mortality rates during an extreme drought. *Plant Cell Environ.* 41, 576–588. doi: 10.1111/pce.13121

Johnson, D. M., Wortemann, R., Mcculloh, K. A., Jordan-Meille, L., Ward, E., Warren, J. M., et al. (2016). A test of the hydraulic vulnerability segmentation hypothesis in angiosperm and conifer tree species. *Tree Physiol.* 36, 983–993. doi: 10.1093/treephys/tpw031

Kattge, J., Bönisch, G., Díaz, S., Lavorel, S., Prentice, I. C., Leadley, P., et al. (2020). TRY plant trait database-enhanced coverage and open access. *Glob. Chang. Biol.* 26, 119–188. doi: 10.1111/gcb.14904

Kennedy, D., Swenson, S., Oleson, K. W., Lawrence, D. M., Fisher, R., Lola da Costa, A. C., et al. (2019). Implementing plant hydraulics in the community land model, version 5. *J. Adv. Model. Earth Syst.* 11, 485–513. doi: 10.1029/2018MS001500

Klein, T. (2014). The variability of stomatal sensitivity to leaf water potential across tree species indicates a continuum between isohydric and anisohydric behaviours. *Funct. Ecol.* 28, 1313–1320. doi: 10.1111/1365-2435.12289

Knipfer, T., Cuneo, I. F., Earles, J. M., Reyes, C., Brodersen, C. R., and Mcelrone, A. J. (2017). Storage compartments for capillary water rarely refill in an intact woody plant. *Plant Physiol.* 175, 1649–1660. doi: 10.1104/pp.17.01133

Knipfer, T., Reyes, C., Earles, J. M., Berry, Z. C., Johnson, D. M., Brodersen, C. R., et al. (2019). Spatiotemporal coupling of vessel cavitation and discharge of stored xylem water in a tree sapling. *Plant Physiol.* 179, 1658–1668. doi: 10.1104/pp.18.01303

Konings, A. G., Rao, K., and Steele-Dunne, S. C. (2019). Macro to micro: microwave remote sensing of plant water content for physiology and ecology. *New Phytol.* 223, 1166–1172. doi: 10.1111/nph.15808

Lamy, J. B., Delzon, S., Bouche, P. S., Alia, R., Vendramin, G. G., Cochard, H., et al. (2014). Limited genetic variability and phenotypic plasticity detected for cavitation resistance in a Mediterranean pine. *New Phytol.* 201, 874–886. doi: 10.1111/nph.12556

Lanning, M., Wang, L., and Novick, K. A. (2020). The importance of cuticular permeance in assessing plant water-use strategies. *Tree Physiol.* 40, 425–432. doi: 10.1093/treephys/tpaa020

Levionnois, S., Ziegler, C., Jansen, S., Calvet, E., Coste, S., Stahl, C., et al. (2020). Vulnerability and hydraulic segmentations at the stem-leaf transition: coordination across Neotropical trees. *New Phytol.* 228, 512–524. doi: 10.1111/nph.16723

Li, X., Blackman, C. J., Choat, B., Duursma, R. A., Rymer, P. D., Medlyn, B. E., et al. (2018a). Tree hydraulic traits are coordinated and strongly linked to climate-of-origin across a rainfall gradient. *Plant Cell Environ.* 41, 646–660. doi: 10.1111/pce.13129

Li, X., Blackman, C. J., Peters, J. M., Choat, B., Rymer, P. D., Medlyn, B. E., et al. (2019). More than iso/anisohydry: hydroscapes integrate plant water use and drought tolerance traits in 10 eucalypt species from contrasting climates. *Funct. Ecol.* 33, 1035–1049. doi: 10.1111/1365-2435.13320

Li, X., Blackman, C. J., Rymer, P. D., Quintans, D., Duursma, R. A., Choat, B., et al. (2018b). Xylem embolism measured retrospectively is linked to canopy dieback in natural populations of *Eucalyptus piperita* following drought. *Tree Physiol.* 38, 1193–1199. doi: 10.1093/treephys/tpy052

Li, S., Feifel, M., Karimi, Z., Schuldt, B., Choat, B., and Jansen, S. (2016). Leaf gas exchange performance and the lethal water potential of five European species during drought. *Tree Physiol.* 36, tpv117–tpv192. doi: 10.1093/treephys/tpv117

Liang, X., Ye, Q., Liu, H., and Brodribb, T. J. (2021). Wood density predicts mortality threshold for diverse trees. *New Phytol.* 229, 3053–3057. doi: 10.1111/nph.17117

Liu, J., Gu, L., Yu, Y., Huang, P., Wu, Z., Zhang, Q., et al. (2019). Corticular photosynthesis drives bark water uptake to refill embolized vessels in dehydrated branches of *Salix matsudana*. *Plant Cell Environ.* 42, 2584–2596. doi: 10.1111/pce.13578

Liu, Y. Y., Wang, A. Y., An, Y. N., Lian, P. Y., Wu, D. D., Zhu, J. J., et al. (2018). Hydraulics play an important role in causing low growth rate and dieback of aging *Pinus sylvestris* var. *mongolica* trees in plantations of Northeast China. *Plant Cell Environ.* 41, 1500–1511. doi: 10.1111/pce.13160

López, R., Cano, F. J., Martin-Stpaul, N. K., Cochard, H., and Choat, B. (2021). Coordination of stem and leaf traits define different strategies to regulate water loss and tolerance ranges to aridity. *New Phytol.* 230, 497–509. doi: 10.1111/nph.17185

Lübbe, T., Lamarque, L. J., Delzon, S., Torres Ruiz, J. M., Burlett, R., Leuschner, C., et al. (2021). High variation in hydraulic efficiency but not xylem safety between roots and branches in four temperate broad-leaved tree species. *Funct. Ecol.* 36, 699–712. doi: 10.1111/1365-2435.13975

Manion, P. D. (1981). *Tree Disease Concepts*. Upper Saddle River, NJ, USA: Prentice Hall.

Mantova, M., Herbette, S., Cochard, H., and Torres-Ruiz, J. M. (2021). Hydraulic failure and tree mortality: from correlation to causation. *Trends Plant Sci* 27, 335–345. doi: 10.1016/j.tplants.2021.10.003

Markesteijn, L., Poorter, L., Paz, H., Sack, L., and Bongers, F. (2011). Ecological differentiation in xylem cavitation resistance is associated with stem and leaf structural traits. *Plant Cell Environ.* 34, 137–148. doi: 10.1111/j.1365-3040.2010.02231.x

Martinez-Vilalta, J., Anderegg, W. R., Sapes, G., and Sala, A. (2019). Greater focus on water pools may improve our ability to understand and anticipate

drought-induced mortality in plants. *New Phytol.* 223, 22–32. doi: 10.1111/nph.15644

Martínez-Vilalta, J., and Garcia-Forner, N. (2017). Water potential regulation, stomatal behaviour and hydraulic transport under drought: deconstructing the iso/anisohydric concept. *Plant Cell Environ.* 40, 962–976. doi: 10.1111/pce.12846

Martin-Stpaul, N., Delzon, S., and Cochard, H. (2017). Plant resistance to drought depends on timely stomatal closure. *Ecol. Lett.* 20, 1437–1447. doi: 10.1111/ele.12851

McDowell, N. G., Beerling, D. J., Breshears, D. D., Fisher, R. A., Raffa, K. F., and Stitt, M. (2011). The interdependence of mechanisms underlying climate-driven vegetation mortality. *Trends Ecol. Evol.* 26, 523–532. doi: 10.1016/j.tree.2011.06.003

McDowell, N. G., Fisher, R. A., Xu, C., Domec, J. C., Hölttä, T., Mackay, D. S., et al. (2013). Evaluating theories of drought-induced vegetation mortality using a multimodel-experiment framework. *New Phytol.* 200, 304–321. doi: 10.1111/nph.12465

McDowell, N., Pockman, W. T., Allen, C. D., Breshears, D. D., Cobb, N., Kolb, T., et al. (2008). Mechanisms of plant survival and mortality during drought: why do some plants survive while others succumb to drought? *New Phytol.* 178, 719–739. doi: 10.1111/j.1469-8137.2008.02436.x

Medlyn, B. E., De Kauwe, M. G., and Duursma, R. A. (2016). New developments in the effort to model ecosystems under water stress. *New Phytol.* 212, 5–7. doi: 10.1111/nph.14082

Medlyn, B. E., Zaehle, S., De Kauwe, M. G., Walker, A. P., Dietze, M. C., Hanson, P. J., et al. (2015). Using ecosystem experiments to improve vegetation models. *Nat. Clim. Chang.* 5, 528–534. doi: 10.1038/nclimate2621

Meinzer, F. C., Johnson, D. M., Lachenbruch, B., Mcculloh, K. A., and Woodruff, D. R. (2009). Xylem hydraulic safety margins in woody plants: coordination of stomatal control of xylem tension with hydraulic capacitance. *Funct. Ecol.* 23, 922–930. doi: 10.1111/j.1365-2435.2009.01577.x

Meinzer, F. C., Woodruff, D. R., Marias, D. E., Smith, D. D., McCulloh, K. A., Howard, A. R., et al. (2016). Mapping 'hydroscapes' along the iso-to anisohydric continuum of stomatal regulation of plant water status. *Ecol. Lett.* 19, 1343–1352. doi: 10.1111/ele.12670

Meir, P., Mencuccini, M., and Dewar, R. C. (2015). Drought-related tree mortality: addressing the gaps in understanding and prediction. *New Phytol.* 207, 28–33. doi: 10.1111/nph.13382

Nolan, R. H., Gauthey, A., Losso, A., Medlyn, B. E., Smith, R., Chhajed, S. S., et al. (2021). Hydraulic failure and tree size linked with canopy die-back in eucalypt forest during extreme drought. *New Phytol.* 230, 1354–1365. doi: 10.1111/nph.17298

O'Brien, M. J., Leuzinger, S., Philipson, C. D., Tay, J., and Hector, A. (2014). Drought survival of tropical tree seedlings enhanced by non-structural carbohydrate levels. *Nat. Clim. Chang.* 4, 710–714. doi: 10.1038/nclimate2281

Pan, Y., Birdsey, R. A., Fang, J., Houghton, R., Kauppi, P. E., Kurz, W. A., et al. (2011). A large and persistent carbon sink in the world's forests. *Science* 333, 988–993. doi: 10.1126/science.1201609

Peters, J. M., Gauthey, A., Lopez, R., Carins-Murphy, M. R., Brodribb, T. J., and Choat, B. (2020). Non-invasive imaging reveals convergence in root and stem vulnerability to cavitation across five tree species. *J. Exp. Bot.* 71, 6623–6637. doi: 10.1093/jxb/eraa381

Pfautsch, S., Renard, J., Tjoelker, M. G., and Salih, A. (2015). Phloem as capacitor: radial transfer of water into xylem of tree stems occurs via symplastic transport in ray parenchyma. *Plant Physiol.* 167, 963–971. doi: 10.1104/pp.114.254581

Pivovaroff, A. L., Sack, L., and Santiago, L. S. (2014). Coordination of stem and leaf hydraulic conductance in southern California shrubs: a test of the hydraulic segmentation hypothesis. *New Phytol.* 203, 842–850. doi: 10.1111/nph.12850

Powers, J. S., Vargas, G. G., Brodribb, T. J., Schwartz, N. B., Pérez-Aviles, D., Smith-Martin, C. M., et al. (2020). A catastrophic tropical drought kills hydraulically vulnerable tree species. *Glob. Chang. Biol.* 26, 3122–3133. doi: 10.1111/gcb.15037

Reich, P. B. (2014). The world-wide 'fast-slow' plant economics spectrum: a traits manifesto. *J. Ecol.* 102, 275–301. doi: 10.1111/1365-2745.12211

Reich, P., Ellsworth, D., and Walters, M. (1998). Leaf structure (specific leaf area) modulates photosynthesis-nitrogen relations: evidence from within and across species and functional groups. *Funct. Ecol.* 12, 948–958. doi: 10.1046/j.1365-2435.1998.00274.x

Richards, A. E., Wright, I. J., Lenz, T. I., and Zanne, A. E. (2014). Sapwood capacitance is greater in evergreen sclerophyll species growing in high compared to low-rainfall environments. *Funct. Ecol.* 28, 734–744. doi: 10.1111/1365-2435.12193

Rodriguez-Dominguez, C. M., Carins Murphy, M. R., Lucani, C., and Brodribb, T. J. (2018). Mapping xylem failure in disparate organs of whole plants reveals extreme resistance in olive roots. *New Phytol.* 218, 1025–1035. doi: 10.1111/nph.15079

Rogers, A., Medlyn, B. E., Dukes, J. S., Bonan, G., Von Caemmerer, S., Dietze, M. C., et al. (2017). A roadmap for improving the representation of photosynthesis in earth system models. *New Phytol.* 213, 22–42. doi: 10.1111/nph.14283

Russo, S. E., Jenkins, K. L., Wiser, S. K., Uriarte, M., Duncan, R. P., and Coomes, D. A. (2010). Interspecific relationships among growth, mortality and xylem traits of woody species from New Zealand. *Funct. Ecol.* 24, 253–262. doi: 10.1111/j.1365-2435.2009.01670.x

Sabot, M. E., De Kauwe, M. G., Pitman, A. J., Medlyn, B. E., Verhoef, A., Ukkola, A. M., et al. (2020). Plant profit maximization improves predictions of European forest responses to drought. *New Phytol.* 226, 1638–1655. doi: 10.1111/nph.16376

Salomón, R. L., Steppe, K., Ourcival, J. M., Villers, S., Rodríguez-Calcerrada, J., Schapman, R., et al. (2020). Hydraulic acclimation in a Mediterranean oak subjected to permanent throughfall exclusion results in increased stem hydraulic capacitance. *Plant Cell Environ.* 43, 1528–1544. doi: 10.1111/pce.13751

Santiago, L. S., De Guzman, M. E., Baraloto, C., Vogenberg, J. E., Brodie, M., Hérault, B., et al. (2018). Coordination and trade-offs among hydraulic safety, efficiency and drought avoidance traits in Amazonian rainforest canopy tree species. *New Phytol.* 218, 1015–1024. doi: 10.1111/nph.15058

Sapes, G., Roskilly, B., Dobrowski, S., Maneta, M., Anderegg, W. R., Martinez-Vilalta, J., et al. (2019). Plant water content integrates hydraulics and carbon depletion to predict drought-induced seedling mortality. *Tree Physiol.* 39, 1300–1312. doi: 10.1093/treephys/tpz062

Schenk, H. J., Espino, S., Romo, D. M., Nima, N., Do, A. Y., Michaud, J. M., et al. (2017). Xylem surfactants introduce a new element to the cohesion-tension theory. *Plant Physiol.* 173, 1177–1196. doi: 10.1104/pp.16.01039

Schuster, A. C., Burghardt, M., and Riederer, M. (2017). The ecophysiology of leaf cuticular transpiration: are cuticular water permeabilities adapted to ecological conditions? *J. Exp. Bot.* 68, 5271–5279. doi: 10.1093/jxb/erx321

Sevanto, S., Mcdowell, N. G., Dickman, L. T., Pangle, R., and Pockman, W. T. (2014). How do trees die? A test of the hydraulic failure and carbon starvation hypotheses. *Plant Cell Environ.* 37, 153–161. doi: 10.1111/pce.12141

Sevanto, S., and Xu, C. (2016). Towards more accurate vegetation mortality predictions. *Tree Physiol.* 36, 1191–1195. doi: 10.1093/treephys/tpw082

Skelton, R. P., West, A. G., and Dawson, T. E. (2015). Predicting plant vulnerability to drought in biodiverse regions using functional traits. *Proc. Natl. Acad. Sci. U. S. A.* 112, 5744–5749. doi: 10.1073/pnas.1503376112

Sorek, Y., Greenstein, S., Netzer, Y., Shtein, I., Jansen, S., and Hochberg, U. (2021). An increase in xylem embolism resistance of grapevine leaves during the growing season is coordinated with stomatal regulation, turgor loss point and intervessel pit membranes. *New Phytol.* 229, 1955–1969. doi: 10.1111/nph.17025

Sperry, J. S., Adler, F., Campbell, G., and Comstock, J. (1998). Limitation of plant water use by rhizosphere and xylem conductance: results from a model. *Plant Cell Environ.* 21, 347–359. doi: 10.1046/j.1365-3040.1998.00287.x

Thrippleton, T., Hülsmann, L., Cailleret, M., and Bugmann, H. (2021). An evaluation of multi-species empirical tree mortality algorithms for dynamic vegetation modelling. *Sci. Rep.* 11:19845. doi: 10.1038/s41598-021-98880-2

Tomasella, M., Casolo, V., Aichner, N., Petruzzellis, F., Savi, T., Trifilò, P., et al. (2019). Non-structural carbohydrate and hydraulic dynamics during drought and recovery in Fraxinus ornus and Ostrya carpinifolia saplings. *Plant Physiol. Biochem.* 145, 1–9. doi: 10.1016/j.plaphy.2019.10.024

Trifilò, P., Casolo, V., Raimondo, F., Petrussa, E., Boscutti, F., Gullo, M. A. L., et al. (2017). Effects of prolonged drought on stem non-structural carbohydrates content and post-drought hydraulic recovery in *Laurus nobilis* L.: the possible link between carbon starvation and hydraulic failure. *Plant Physiol. Biochem.* 120, 232–241. doi: 10.1016/j.plaphy.2017.10.003

Trugman, A. T. (2021). Integrating plant physiology and community ecology across scales through trait-based models to predict drought mortality. *New Phytol.* 234, 21–27. doi: 10.1111/nph.17821

Trugman, A. T., Detto, M., Bartlett, M. K., Medvigy, D., Anderegg, W. R. L., Schwalm, C., et al. (2018). Tree carbon allocation explains forest drought-kill and recovery patterns. *Ecol. Lett.* 21, 1552–1560. doi: 10.1111/ele.13136

Urli, M., Porté, A. J., Cochard, H., Guengant, Y., Burlett, R., and Delzon, S. (2013). Xylem embolism threshold for catastrophic hydraulic failure in angiosperm trees. *Tree Physiol.* 33, 672–683. doi: 10.1093/treephys/tpt030

Wang, Y., Köhler, P., He, L., Doughty, R., Braghiere, R. K., Wood, J. D., et al. (2021). Testing stomatal models at the stand level in deciduous angiosperm and evergreen gymnosperm forests using CliMA land (v0.1). *Geosci. Model Dev.* 14, 6741–6763. doi: 10.5194/gmd-14-6741-2021

Wason, J. W., Anstreicher, K. S., Stephansky, N., Huggett, B. A., and Brodersen, C. R. (2018). Hydraulic safety margins and air-seeding thresholds in roots, trunks, branches and petioles of four northern hardwood trees. *New Phytol.* 219, 77–88. doi: 10.1111/nph.15135

Wason, J., Bouda, M., Lee, E. F., Mcelrone, A. J., Phillips, R. J., Shackel, K. A., et al. (2021). Xylem network connectivity and embolism spread in grapevine (*Vitis vinifera* L.). *Plant Physiol.* 186, 373–387. doi: 10.1093/plphys/kiab045

Wolfe, B. T., Sperry, J. S., and Kursar, T. A. (2016). Does leaf shedding protect stems from cavitation during seasonal droughts? A test of the hydraulic fuse hypothesis. *New Phytol.* 212, 1007–1018. doi: 10.1111/nph.14087

Wright, I. J., Ackerly, D. D., Bongers, F., Harms, K. E., Ibarra-Manriquez, G., Martinez-Ramos, M., et al. (2007). Relationships among ecologically important dimensions of plant trait variation in seven Neotropical forests. *Ann. Bot.* 99, 1003–1015. doi: 10.1093/aob/mcl066

Wu, G., Guan, K., Li, Y., Novick, K. A., Feng, X., Mcdowell, N. G., et al. (2021). Interannual variability of ecosystem iso/anisohydry is regulated by environmental dryness. *New Phytol.* 229, 2562–2575. doi: 10.1111/nph.17040

Wu, X., Liu, H., Li, X., Ciais, P., Babst, F., Guo, W., et al. (2018). Differentiating drought legacy effects on vegetation growth over the temperate northern hemisphere. *Glob. Chang. Biol.* 24, 504–516. doi: 10.1111/gcb.13920

Xi, B., Di, N., Liu, J., Zhang, R., and Cao, Z. (2018). Hydrologic regulation of plant rooting depth: pay attention to the widespread scenario with intense seasonal groundwater table fluctuation. *Proc. Natl. Acad. Sci. U. S. A.* 115, E3863–E3864. doi: 10.1073/pnas.1803987115

Xu, X., Medvigy, D., Powers, J. S., Becknell, J. M., and Guan, K. (2016). Diversity in plant hydraulic traits explains seasonal and inter-annual variations of vegetation dynamics in seasonally dry tropical forests. *New Phytol.* 212, 80–95. doi: 10.1111/nph.14009

Zeng, X. (2001). Global vegetation root distribution for land modeling. *J. Hydrometeorol.* 2, 525–530. doi: 10.1175/1525-7541(2001)002<0525:GVRDFL>2.0.CO;2

Zhou, S., Duursma, R. A., Medlyn, B. E., Kelly, J. W., and Prentice, I. C. (2013). How should we model plant responses to drought? An analysis of stomatal and non-stomatal responses to water stress. *Agric. For. Meteorol.* 182–183, 204–214. doi: 10.1016/j.agrformet.2013.05.009

Zhou, S., Medlyn, B., Sabaté, S., Sperlich, D., and Prentice, I. C. (2014). Short-term water stress impacts on stomatal, mesophyll and biochemical limitations to photosynthesis differ consistently among tree species from contrasting climates. *Tree Physiol.* 34, 1035–1046. doi: 10.1093/treephys/tpu072

Zhu, S. D., He, P. C., Li, R. H., Fu, S. L., Lin, Y. B., Zhou, L. X., et al. (2018). Drought tolerance traits predict survival ratio of native tree species planted in a subtropical degraded hilly area in South China. *For. Ecol. Manag.* 418, 41–46. doi: 10.1016/j.foreco.2017.09.016

Zanne, A. E., Lopez-Gonzalez, G., Coomes, D. A., Ilic, J., Jansen, S., Lewis, S. L., et al. (2009). Data from: Towards a worldwide wood economics spectrum. *Dryad, Dataset.* doi: 10.5061/dryad.234

Zimmermann, M. H. (1983). *Xylem Structure and the Ascent of Sap*. Berlin, Germany: Springer Science & Business Media.

Conflict of Interest: The authors declare that the research was conducted in the absence of any commercial or financial relationships that could be construed as a potential conflict of interest.

Publisher's Note: All claims expressed in this article are solely those of the authors and do not necessarily represent those of their affiliated organizations, or those of the publisher, the editors and the reviewers. Any product that may be evaluated in this article, or claim that may be made by its manufacturer, is not guaranteed or endorsed by the publisher.

frontiers | Frontiers in Plant Science

REVIEW
published: 29 April 2022
doi: 10.3389/fpls.2022.824720

Optimizing Crop Water Use for Drought and Climate Change Adaptation Requires a Multi-Scale Approach

James D. Burridge[1], Alexandre Grondin[1,2,3] and Vincent Vadez[1,2,3,4]**

[1]*DIADE Group, Cereal Root Systems, Institute de Recherche pour le Développement/Université de Montpellier, Montpellier, France,* [2]*Adaptation des Plantes et Microorganismes Associés aux Stress Environnementaux, Laboratoire Mixte International, Dakar, Senegal,* [3]*Centre d'Étude Régional pour l'Amélioration de l'Adaptation à la Sécheresse, Thiès, Senegal,* [4]*International Crops Research Institute for Semi-Arid Tropics (ICRISAT), Patancheru, India*

OPEN ACCESS

Edited by:
Dongliang Xiong, Huazhong Agricultural University, China

Reviewed by:
Eric Ober, National Institute of Agricultural Botany (NIAB), United Kingdom
Haibing He, Anhui Agricultural University, China

***Correspondence:**
James D. Burridge
jimmy.burridge@ird.fr
Vincent Vadez
vincent.vadez@ird.fr

Specialty section:
This article was submitted to Plant Physiology, a section of the journal Frontiers in Plant Science

Received: *29 November 2021*
Accepted: *11 April 2022*
Published: *29 April 2022*

Citation:
Burridge JD, Grondin A and Vadez V (2022) Optimizing Crop Water Use for Drought and Climate Change Adaptation Requires a Multi-Scale Approach. Front. Plant Sci. 13:824720. doi: 10.3389/fpls.2022.824720

Selection criteria that co-optimize water use efficiency and yield are needed to promote plant productivity in increasingly challenging and variable drought scenarios, particularly dryland cereals in the semi-arid tropics. Optimizing water use efficiency and yield fundamentally involves transpiration dynamics, where restriction of maximum transpiration rate helps to avoid early crop failure, while maximizing grain filling. Transpiration restriction can be regulated by multiple mechanisms and involves cross-organ coordination. This coordination involves complex feedbacks and feedforwards over time scales ranging from minutes to weeks, and from spatial scales ranging from cell membrane to crop canopy. Aquaporins have direct effect but various compensation and coordination pathways involve phenology, relative root and shoot growth, shoot architecture, root length distribution profile, as well as other architectural and anatomical aspects of plant form and function. We propose gravimetric phenotyping as an integrative, cross-scale solution to understand the dynamic, interwoven, and context-dependent coordination of transpiration regulation. The most fruitful breeding strategy is likely to be that which maintains focus on the phene of interest, namely, daily and season level transpiration dynamics. This direct selection approach is more precise than yield-based selection but sufficiently integrative to capture attenuating and complementary factors.

Keywords: drought, cross-scale coordination, water acquisition and use, selection criteria, transpiration restriction, vapor pressure deficit

INTRODUCTION

Increasing temperature, aridity, and unpredictability of rainfall events motivates the development of dryland cereal crops that produce grain in severe and variable drought scenarios, but still have high yield potential in less stressful scenarios. In these agroecological zones, high temperature, and low relative humidity can combine to make extremely taxing vapor pressure deficit (VPD) conditions, meaning more water transpired per carbon gained. High VPD conditions are predicted to become more common and more severe (Grossiord et al., 2020).

Root system architectural and anatomical traits or phenes (phene is to phenome as gene is to genome, thus phenotype is composed of phenes) that optimize water acquisition per unit carbon invested (Lynch, 2007, 2019) and "right-size" plant water usage (Borrell et al., 2014a; Lynch, 2018) are a positive step. Identifying and selecting for root trait plasticity may also be a useful step (Topp, 2016; Schneider and Lynch, 2020). Similarly, the ratio of shoot to root area is of fundamental importance for plant water balance (Hsiao and Acevedo, 1974). However, optimized root to shoot growth can have limited utility when there is simply a limited amount of soil water available.

In these scenarios, a strategy based upon parsimonious water usage co-optimizes transpiration, carbon fixation, and yield by conserving soil water for the grain filling stage (Richards et al., 2002; Zaman-Allah et al., 2011; Vadez et al., 2013a; Borrell et al., 2014b; Vadez, 2014; Hammer et al., 2020). Conserving soil water for grain filling can be achieved by limiting leaf area, limiting transpiration rate, or accelerating senescence of older leaves (Borrell et al., 2014a; George-Jaeggli et al., 2017; Sinclair et al., 2017). However, these adaptations may entail reduced yield potential under less stressful conditions (Gao et al., 2020a). Constraining daily transpiration rates from climbing above a certain threshold, when VPD is high (i.e., when the trade-offs between carbon fixation and water loss becomes too costly), is promising means to conserve water for the grain filling period, without reducing total leaf (Sinclair et al., 2017).

Inducible limitation of maximum transpiration increases transpiration efficiency saves water over the course of a day and over the course of the season (Sinclair et al., 2005, 2017). Modeling studies have shown the great benefit with little trade-off of high VPD induced transpiration restriction in soybean (Sinclair et al., 2010), maize (Messina et al., 2015), and sorghum (Sinclair and Muchow, 2001; Kholová et al., 2014). However, there may be trade-offs between leaf cooling and transpiration restriction under very high temperatures. Field studies indicate that transpiration restriction is related to greater yield for maize, sorghum, pearl millet, and wheat under severe terminal drought conditions (Sinclair et al., 2017; Tharanya et al., 2018a; Medina et al., 2019). Selection for transpiration restriction phenotypes has been implemented in peanut, maize, and soybean breeding programs and cultivars have been generated exhibiting soil water conservation strategies (Shekoofa and Sinclair, 2018). Similar transpiration restriction strategies may conserve soil water and increase dryland production of other annual crops (Belko et al., 2012; Polania et al., 2016). Understanding species and genotype level variation in transpiration restriction may help accelerate crop genetic improvement.

PART 1: REGULATION OF TRANSPIRATION RESTRICTION BY PLANT HYDRAULICS

Plants connect the pedosphere, with relatively high water potential, to the atmosphere, with relatively low water potential. Water movement along this soil–plant–air continuum is driven by a water potential gradient, as described by Ohm's law and the cohesion–tension theory (Tyree, 1997; Carminati and Javaux, 2020). Plants use a network of specialized architectural, anatomical, morphological, and functional mechanisms to regulate the axial and radial flow of water (Steudle, 2000). Root radial water transport involves passage through the epidermis, cortex, endodermis, and xylem parenchyma *via* the symplastic (cell to cell) or apoplasticaly (through cell walls and intercellular spaces; McCully and Canny, 1988; Bramley et al., 2007). Water ascends axially by tension and cohesion through root, stem, petiole, and leaf vein xylem vessels. Tension draws water from the leaf veins, across multiple sets of cell membranes, including the bundle sheath, mesophyll, or epidermal cells. Water vapor then diffuses through the cuticle, or in a highly controlled fashion through the stomatal cavity. The actors and processes involved in hydraulic regulation are presented using a non-structured, conceptual arrangement in **Figure 1**, which serves to guide the literature review. Supporting information is supplied in **Table 1**; **Supplementary Table 1**. Functionally structured perspectives of plant hydraulic regulation are provided in **Figure 2**; **Supplementary Figure 1**.

Root Conductance

Root-based regulation of transpiration can be divided into radial and axial conductance. Root axial water conductance is typically not considered the most rate limiting step, but genotypic differences do exist in xylem number and diameter, which determine axial conductance capacity, and can relate to transpiration dynamics and adaptation to drought stress (Prince et al., 2017; Nogueira et al., 2020; Strock et al., 2020). Reduced seminal root xylem conductance capacity was the basis of developing wheat cultivars

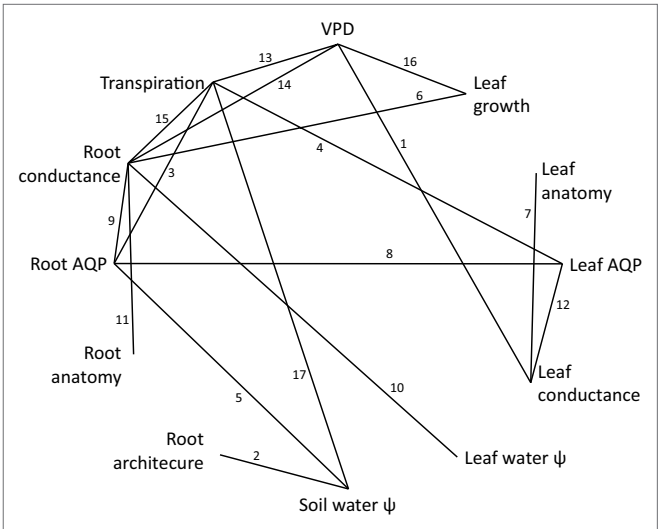

FIGURE 1 | Non-hierarchical arrangement of actors and processes involved in plant water acquisition, water transport, and transpiration regulation across all levels of plant organization. Numbered lines between circled actors correspond to publications demonstrating indicated connection, listed in **Table 1**. The network is not intended to be exhaustively populated, but rather representative, and indicates a high degree of interconnectivity, yet with substantial lacunae among actors and processes that are logically related. It suggests that as we accumulate more data, we find more interactions and more complexity.

adapted to the water-limited Australian context (Richards and Passioura, 1989). The utility of reduced root axial conductance capacity for late season soil water conservation in wheat has been further supported in recent work (Hendel et al., 2021). There may also be the possibility for longitudinal adjustments of xylem conduits (Meunier et al., 2017), regulation at the root to shoot junction (Meunier et al., 2018), as well as among the various attributes of protoxylem and metaxylem vessels, their pits (Xu et al., 2020) or perforation plates (Gao et al., 2020b). These may be part of a suite of embolism response traits and do not preclude the possibility that embolism is itself a means of restricting transpiration (McCully, 1999), in which aquaporins play a key recovery role (Secchi et al., 2017).

TABLE 1 | List of publications demonstrating links between nodes.

Edge	Node 1	Node 2	Reference numbers
1	VPD	Leaf conductance	1, 18
2	Soil water potential	RSA	2, 3, 40
3	Root AQP	Transpiration	4, 5, 6, 20, 22, 25, 26, 31, 32
4	Leaf AQP	Transpiration	7, 18, 19, 21, 27, 28, 33
5	Soil water potential	Root AQP	8, 9
6	Leaf growth	Root conductance	10, 11, 22, 25, 31, 32
7	Leaf anatomy	Leaf conductance	7, 13, 14, 30, 37, 41, 42
8	Root AQP	Leaf AQP	8
9	Root AQP	Root conductance	15, 16, 17, 23, 24, 25, 31, 32, 34, 38, 39
10	Root conductance	Leaf water potential	22
11	Root anatomy	Root conductance	12, 16, 23, 24
12	Leaf conductance	Leaf AQP	29, 33, 35, 36, 38
13	VPD	Transpiration	43, 44, 45, 46, 47, 49, 50, 51, 52
14	VPD	Root conductance	44, 48
15	Root conductance	Transpiration	44, 48
16	VPD	Leaf growth	49, 53
17	Soil water potential	Transpiration	52, 54, 55, 56

Edge numbers correspond to links between nodes in ***Figure 1****. References and reference numbers presented in* ***Supplementary Table 1****.*

Root anatomical phenes related to radial water transport include distance between root tip and suberized zone, as well as completeness of suberization (Barberon et al., 2016; Doblas et al., 2017) and lignification (Foster and Miklavcic, 2017). Construction of Casparian bands, suberin lamellae, and lignification may respond dynamically to abiotic stress factors and be deployed differentially on roots of different diameters and class (Tylová et al., 2017). Variation in cortex cell file number, or cortex cell size may lead to a different proportion of cell-to-intercellular spaces, which are hypothesized to affect root hydraulics (Vadez, 2014), with some evidence in pearl millet (Kholová et al., 2016). Genotypic variation in radial conductance pathways has been observed in chickpea (Sivasakthi et al., 2017, 2020). Similar effects of anatomical differences in the root radial water transport pathway were observed in wheat and lupin, showing predominance of apoplast water transport in lupin, whereas wheat dependent mostly on Hg-sensitive aquaporin in the endodermis (Bramley et al., 2007).

Root radial conductance is influenced by AQP at various membranes including; epidermis, outer cortex

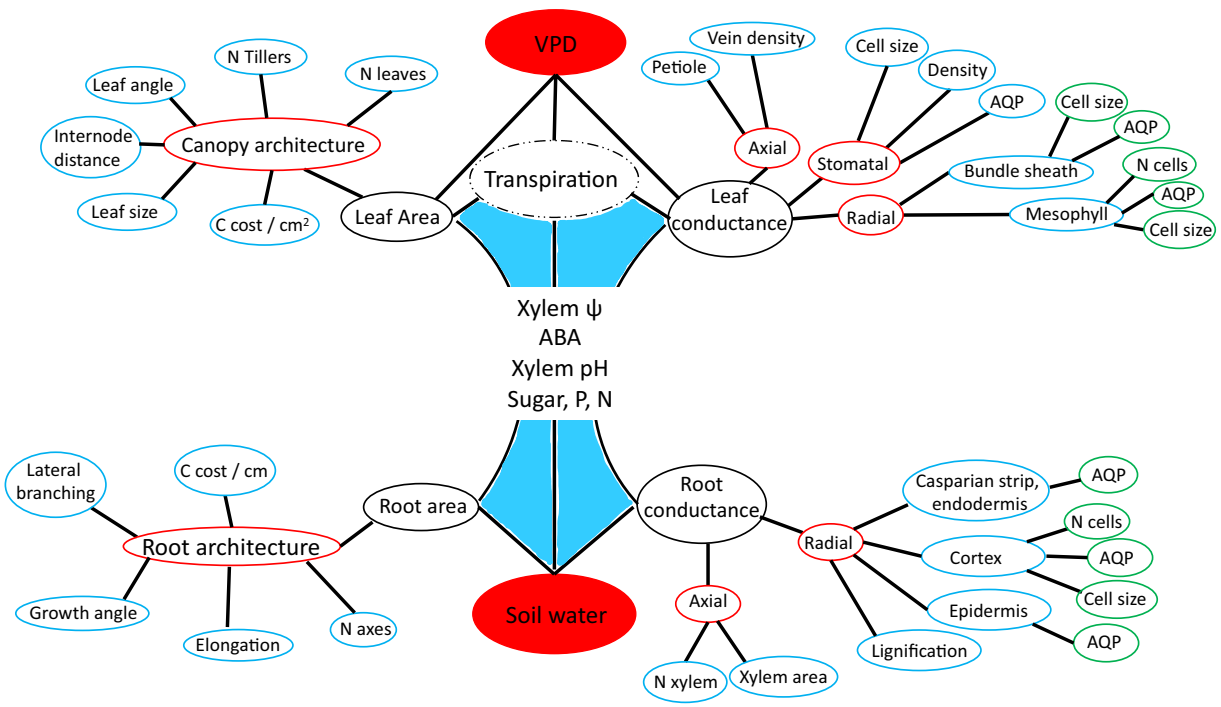

FIGURE 2 | Hierarchically structured network diagram of phenes influencing plant water acquisition and transport, including the same actors and processes as in **Figure 1**. This projection of plant hydraulic regulation highlights the distal position of aquaporins in relation to tissue level conductance, the complementary role of relative shoot and root growth, and the nested structure of plant form and function. C is an abbreviation for carbon and *N* for number.

(Ranathunge et al., 2004), endodermis, and Casparian strip (Grondin et al., 2016). AQP expression in rice shoots and roots suggests AQP mediated root conductance was most limiting to mid-day transpiration (Nada and Abogadallah, 2014). A pearl millet aquaporin gene transferred to tobacco conferred greater drought, heat, and higher water use efficiency (Reddy et al., 2022). Knockout and overexpression mutants showed a specific AQP isoform in maize roots was an important regulator of root hydraulic conductance, with effects on plant growth (Ding et al., 2020). The same study suggested non-uniform patterns of radial conductance, implying aquaporin function must integrate with root anatomy.

Leaf Conductance

Leaf conductance is an aggregate phene, *sensu* (York et al., 2013), integrating leaf vein anatomy, stomatal density size, and aperture, as well as xylem parenchyma, bundle sheath, and mesophyll cell number, size, and density, in addition to AQP function (Sack and Holbrook, 2006). This presents a variety of regulatory opportunities operating at different scales, involving different actors and signaling pathways. Outside xylem conductance, meaning conductance on the path between xylem and sites of evaporation (Scoffoni et al., 2017; Corso et al., 2020) contributes to transpiration restriction (Sinclair et al., 2008). Guard cell conductance is involved in transpiration regulation in response to VPD (Sinclair et al., 2008). Regulation of conductance by bundle sheath cells, likely attributable to AQP, was demonstrated using applied ABA and mercury (Shatil-Cohen et al., 2011). Subsequent work used microRNA AQP silencing to demonstrate a role of AQP at the bundle sheath to mesophyll transition (Sade et al., 2014, 2015). Knockout mutants were used to demonstrate that light-dependent activity of a single AQP isoform in leaf veins is a major regulator of leaf conductance (Prado et al., 2013).

Anatomy, and its interaction with membrane level conductance, may play a role in regulating transpiration dynamics. Within the leaf, two-thirds of outside xylem hydraulic conductance was attributed to vapor transport, which is strongly influenced by distance between veins, distance between vein terminus and stomata, as well as spongy mesophyll anatomy (Sack and Frole, 2006; Sack and Holbrook, 2006; Brodribb et al., 2007; Sack and Scoffoni, 2013; Buckley et al., 2015). One study noted various leaf anatomic factors involved in transpiration efficiency and observed distinct association of anatomy and aquaporin function at different drought intensities (Henry et al., 2019). Transpiration restriction phenotypes were associated with modified epidermal cell size and stomatal density in response to VPD in cotton (Devi and Reddy, 2018). Leaf petiole conductance, and by implication, all of xylem axial conductance could be involved in hydraulic regulation (Postaire et al., 2010). The integration of these water transport factors into a complex series has potential regulatory ability in addition to the regulation of individual components (Zwieniecki et al., 2007). Indeed, canopy development, leaf anatomy, root growth, and water uptake have been related to the stay-green phenotype (Borrell et al., 2014a), which has transpiration restriction as an underlying phenotype. We conclude that focus is needed on the interactions among steps of the water transport pathway, as well as interactions with anatomy, irradiance, leaf water status, and growth to fully understand the regulation of leaf hydraulics (Prado and Maurel, 2013).

Cross-Organ Environmental Responses

Highly dynamic root and leaf expression of multiple AQP was related to maintenance of water use efficiency over the course of a day in sorghum but not in maize (Hasan et al., 2017). Maize, sorghum, and pearl millet may deploy transpiration restriction strategies along a spectrum of reduced leaf area expansion rate or restricted transpiration rate (Sinclair et al., 2017; Choudhary et al., 2020). These species may also vary in their transpiration restriction across different soils (Vadez et al., 2021). At high VPD maize restricted maximum transpiration rate, and transpiration rate became more sensitive to soil drying, while pearl millet and sorghum relied mainly on reduced leaf expansion as a means to reduce transpiration (Choudhary et al., 2020). Genotypic variation also exists for the ability to restrict transpiration rate in response to environmental cues, such as high VPD or highly negative soil matric potential (Choudhary and Sinclair, 2014; Sinclair et al., 2017; Medina et al., 2019). Measurements of leaf and whole plant hydraulic conductance in 12 maize genotypes suggest coordination between root and shoot conductance effectively regulated transpiration in response to high VPD (Sunita et al., 2014). However, work using 20 sorghum genotypes found genotypic variation in both leaf and root conductance and suggested a shoot-based causal mechanism of limited maximum transpiration rate (Choudhary and Sinclair, 2014). Growth chamber, glass house, and field experiments on sorghum linked genetic variation for response of maximum, transpiration rate under increasing VDP to water saving, but observed significantly different results between experiments (Karthika et al., 2019). In sum, the data suggest there are different transpiration restriction strategies and mechanisms with substantial species and genotypic level variation, some of which is environmentally dependent.

PART 2: TRANSPIRATION RESTRICTION CAN INVOLVE MULTIPLE SIGNALS, HYSTERESIS, AND PHENOTYPIC INTEGRATION

Transpiration is a dynamic process, involving coordination of structural and functional aspects across organizational scales in both roots and shoots. Therefore, identifying transpiration restriction mechanisms can be very complex (**Figure 2**; **Supplementary Figure 1**). Outcomes of studies on transpiration restriction are influenced by plant size (Sadok and Sinclair, 2010), time interval studied (Tardieu and Parent, 2017), timing of water stress (Shekoofa and Sinclair, 2018), stage of water stress (Pou et al., 2013), severity of stress (Lovisolo et al., 2010), temperature (Yang et al., 2012), and breeding history (Vadez et al., 2011). Transpiration restriction can also be influenced by employing an isohydric or anisohydric strategy

(Vandeleur et al., 2009), and generally if plants are "water savers" or "water spenders."

A water spender, or profligate water use strategy, is associated with large leaf area and/or unrestricted transpiration in response to high VPD. A water saver, or conservative water use strategy, would reduce leaf area and/or restrict transpiration at high VPD. Isohydric behavior entails sensitive stomatal control that maintains relatively constant leaf water potential, even when soil water is limited or VPD is high. An anisohyric strategy would tolerate a drop in leaf water potential (Grossiord et al., 2020). Genotypes with a water saver strategy may rely more on the apoplastic pathway, whereas water spenders may rely more on the symplastic pathway, but pathway utilization can also depend on growth rate (Grondin et al., 2020; Sivasakthi et al., 2020).

Practices, such as deficit irrigation (Chaves et al., 2010) and cropping system (Sadras et al., 1989), can influence if a plant employs an isohydric or anisohydric strategy. However, these are just two points on a spectrum and strategy can vary by genotype and over time within a single plant (Knipfer et al., 2020). This flexibility along the iso- to anisohydric continuum has been characterized using the hydroscape concept, defined as the area between predawn and mid-day plant water potential regression lines, which captures processes across the soil–plant–atmosphere pathway (Meinzer et al., 2016; Javaux and Carminati, 2021). We conclude that a more robust, yet accurate, selection for transpiration restriction involves the cross-scale dynamic coordination of a spatially and temporally complex set of interacting phenes and processes.

Multiple Types of Signals Can Influence Membrane Conductance

Coordination of root and shoot AQP expression, localization, and function makes use of multiple signals, such as ABA, xylem pH (Davies et al., 2002), and xylem pressure potential itself (Chaumont and Tyerman, 2014; Vandeleur et al., 2014) and may require the integration of multiple signals (Comstock, 2002). Multiple lines of research suggest the importance of a hydraulic signal but differ as to if that signal originates from root or shoot (Fuchs and Livingston, 1996; Yao et al., 2001; Vandeleur et al., 2014). Soil hydraulic conductivity, referring to the hydraulic connection between roots and the soil, has recently been identified as an important signal and regulator of plant hydraulics, transpiration, and stomatal response to drought (Carminati and Javaux, 2020; Hayat et al., 2020; Cai et al., 2021). The rapidity of transpiration response to VPD suggests hydraulic rather than biochemical signals are the immediate mechanisms (Kholová et al., 2010b). However, there is evidence that hydraulic and biochemical signals interact, perhaps over longer time scales (Christmann et al., 2013).

Similarly, partial root drying studies suggest root originating signals that do not involve AQP transcription (Li et al., 2008). For example, ABA and xylem pH can influence transpiration (Davies et al., 2002). The role of ABA as both a local and long-distance signal of soil water limitation has been identified in several species (Dodd, 2005; Wang et al., 2019), although a role for cytokinin has also been suggested (Kudoyarova et al., 2007). Other work suggests ABA signaling operates in conjunction with hydraulic signals, which in turn affects hydraulic conductance of bundle sheath cells (Sade et al., 2014) and may promote root growth, all while being sensitive to stress severity (Miao et al., 2021). Other research suggesting both root and shoot need to be in communication (Castro et al., 2019) are consistent with the multiple signal hypotheses. ABA accumulation in the root has been linked to increased root hydraulic conductivity (Sharipova et al., 2016). However, enhanced root ABA production was linked to reduced leaf conductance under non-limiting conditions, and greater transpiration restriction under high VPD (Thompson et al., 2007).

In summary, particular signaling mechanisms have demonstratable involvement in communicating and responding to particular environmental conditions in particular experimental systems. Studies on membrane or organ level conductance usually involve transgenic, pharmacological, stem girdling, or de-topping approaches that have distinct limitations. These types of studies may fail to account for compensatory mechanisms at other organs and scales, like the opposite effects of ABA on leaf and root conductance described above (Thompson et al., 2007; Sharipova et al., 2016). Furthermore, there appears to be little consistency in signals identified as mechanisms of transpiration regulation across experimental systems. This suggests a high degree of environmental dependency and implies that the actors, forces, and signals identified may not be commensurate with an unperturbed system. For these reasons reductionist experimental systems are ill-suited to deciphering the complexity of the whole system (Tardieu and Parent, 2017) and a broader perspective is warranted.

Hysteresis Influences Plant Responses

Hysteresis, in the context of a water acquisition and use, involves how the plant's environment and history affects signal and response mechanisms. Hysteresis can thus describe a type of cross-scale legacy effect, involving previous architectural, anatomical, and cellular responses. Hysteresis also implies functional factors, such as stomatal aperture, water use strategy, and isohydricity, and if water is being absorbed into the root *via* symplastic or apoplastic pathways, which can make use of different AQP (Javot et al., 2003). Shifting between isohydric vs. anisohydric strategies (Sade et al., 2012) may depend upon a combination of soil moisture, VPD, and hormonal cues (Rogiers et al., 2012) interacting in a tissue-specific and dose-dependent manner (Rosales et al., 2019). The shift in strategies likely involves modified AQP expression (Sade et al., 2009), different root radial transport pathways (Tharanya et al., 2018b), as well as different signaling pathways in different scenarios (Aroca et al., 2012; Moshelion et al., 2015; Rosales et al., 2019). For example, Pou et al. (2013) found that the apoplastic pathway was more important during water stress. Furthermore, dynamic transpiration regulation, and its regulation by aquaporins, can depend upon N availability (Cramer et al., 2009; Di Pietro et al., 2013; Ding et al., 2018) and its degree and duration of deprivation (Dodd et al., 2003).

The existence of multiple overlapping regulation pathways is further shown with research in grapevine, suggesting not only that there is variation in water use strategy by cultivar, which has impact on WUE, and is dependent on type and severity of stress (Lovisolo et al., 2010), but also that the same cultivar can employ different strategies based on legacy effects (Chaves et al., 2010). Transpiration response to VPD may involve different mechanisms under different environmental scenarios (Pou et al., 2013; Sunita et al., 2014; Henry et al., 2019). A study comparing maize, sorghum, and pearl millet growth under contrasting VPD conditions, and then exposed to high VPD, showed species level variation in transpiration dynamics and leaf area, contingent upon growing conditions (Choudhary et al., 2020). Work in pearl millet found diurnal variation and VPD treatment dependency on AQP expression patterns among VPD sensitive and insensitive genotypes (Reddy et al., 2017). The impact of AQP overexpression in two rice cultivars on growth, transpiration patterns, and ultimately water use efficiency, was contingent upon root to shoot ratio and the expression of other aquaporins (Nada and Abogadallah, 2020). AQP downregulation can be balanced by increases in root size, bundle sheath cell osmotic permeability, and other mechanism (Kaldenhoff et al., 1998; Martre et al., 2002; Siefritz et al., 2002; Vandeleur et al., 2014). These examples demonstrate the existence of dynamic cross-scale compensation and a high degree of interconnectivity in transpiration regulation.

In terms of environmental interactions, temperature influences transient transpiration response to VPD (Seversike et al., 2013) and soil drying influences root morphology and transpiration response in soybean (Seversike et al., 2014). Genetic differences in root architecture and variation in root growth response to environmental factors may interact with transpiration regulation and have different impacts on transpiration, canopy temperature, and yield in different environments (Henry et al., 2011). Fully describing a signal—response pathway may require multiple theories, similar to how explanations of nutrient regulation of plant growth differ in accord with the limiting nutrient (Rubio et al., 2003). Indeed, it has been proposed that ABA signals originating from either root or shoot overlap with and mediate hydraulic signals to influence stomatal conductance and leaf hydraulic conductance (Pantin et al., 2013). The high level of interactivity among signals and environmental dependence suggests multiple signals operate in an integrated fashion to influence the emergent transpiration response phenotype. In summary, the legacy of previous physiological responses dictates available responses to the next set of conditions and needs to be taken into account when examining transient responses.

Phenotypes Integrate Across Scales

The integration of water acquisition, transport, and daily and season level water use dynamics, along with phenology, influence the effectiveness of the plant water use strategy in a given environment. Temporal dynamics in water availability and use introduces the need for cross-scale coordination of processes, such as plastic root growth (Topp, 2016; Schneider and Lynch, 2020), involving both architectural (Schneider et al., 2020b) and anatomical (Schneider et al., 2020a) adjustments. Spatio-temporal variation in hydraulic conductance among different root classes and ages highlights an additional layer of variation (Schneider et al., 2020c). Root architecture, xylem characteristics, and stomatal conductance integrate as a coordinated network in maize to enhance performance (Gleason et al., 2019). Integrated root architectural, xylem conductance capacity and maturity group phenotypes have been related to performance and water use strategies in *Phaseolus* (Strock et al., 2020) and in *Zea mays* (York and Lynch, 2015; Klein et al., 2020). Integrated phenotypes involving root architecture, root hydraulic conductance capacity, and phenology have been hypothesized to exist in grain legumes (Burridge et al., 2020) and observed at the gene pool and race level in common bean (Jochua et al., 2020).

There are likely multiple mechanisms for transpiration optimization that are composed of distinct integrated phenotypes involving architectural, anatomical, cellular, and even soil and canopy elements integrating with growth, phenology, and transpiration patterns. For instance, decades of research on the slow wilting phenomenon in soybean have uncovered multiple mechanisms (Kunert and Vorster, 2020) including reduced stomatal conductance (Tanaka et al., 2010), contrasting leaf morphology (Hudak and Patterson, 1995), a larger, more fibrous root system (Pantalone et al., 1996) and by unknown mechanism(s) (Bagherzadi et al., 2017). A recent paper (Ye et al., 2020) used different soybean germplasm than a previous study and identified transpiration restriction mechanisms distinct from the previously identified silver sensitive mechanism (Sadok and Sinclair, 2010). These findings support early work suggesting multiple water conservation mechanisms in soybean (Charlson et al., 2009) and again suggest phenotypes integrate to coordinate transpiration, growth, and soil water use.

Integrated transpiration regulation phenotypes involving conductance, transpiration, canopy size, and phenology have also been observed in sorghum, wheat, chickpea, and pearl millet. A study of four stay-green QTL in sorghum found the four QTL regulated canopy size but also affected leaf anatomy, root growth, and water uptake (Borrell et al., 2014a). Contrasting integrated phenotypes, involving root axial and transmembrane conductance, could be involved in wheat drought tolerance strategies (Schoppach and Sadok, 2012; Schoppach et al., 2014). In chickpea, early vigor, as gauged by canopy size, was related to transpiration restriction and preferential use of the root apoplastic pathway (Sivasakthi et al., 2020). Similarly, greater propensity to restrict transpiration *via* root conductance was associated with larger canopy size in pearl millet (Kholová et al., 2010b; Tharanya et al., 2018b) and chickpea (Zaman-Allah et al., 2011) suggesting transpiration regulation mechanisms specific for large or small canopy size.

Root hairs provide another example for how phenotypic integration connects to the issue of coordination between root and leaf conductance. In addition to xylem embolisms, hydraulic disruptions between root and soil (Newman, 1969; Draye et al., 2010; Carminati and Javaux, 2020; Hayat et al., 2020) may be another type of hydraulic signal, which is theoretically impacted by heterogenous soil conductivity and particle size

(von Jeetze et al., 2020). Recent evidence demonstrates that roots signal this localized hydraulic resistance, which in turn triggers stomatal closure before leaf conductivity reduces (Rodriguez-Dominguez and Brodribb, 2020). Apart from potentially being involved in this signaling, root hairs may help maintain rhizosphere to bulk soil connectivity (Segal et al., 2008; Draye et al., 2010; Lobet et al., 2014; Carminati et al., 2017). Root hair length and density may thus integrate with root length distribution profile and daily transpiration dynamics to promote increased season level transpiration (Tardieu and Parent, 2017).

PART 3: TOWARD EFFECTIVE INTEGRATIVE PHENOTYPING

There seems to be consensus in the literature that the primary short-term mechanisms for fine-tuning transpiration to environment and plant needs involve aquaporins. Aquaporins regulate conductance at the membrane level in both root and leaf (Hachez et al., 2006a, 2008, 2012; Wang et al., 2019). For that reason, selection for particular AQP isoforms or AQP expression levels are tempting targets for engineering transpiration efficiency, even while intricacies of AQP function are acknowledged (Hachez et al., 2006b; Afzal et al., 2016; Zargar et al., 2017). One of the challenges is that there is no consensus on a correlation between AQP abundance and tissue level conductivity (Aroca et al., 2012). The challenges these intricacies pose for genetic improvement are further indicated by how different research programs, using different experimental designs and species, have contrastingly attributed hydraulic regulation almost exclusively to the root (Rodriguez-Dominguez and Brodribb, 2020) or the shoot (Sinclair et al., 2008; **Figure 1**; **Table 1**). Delving into the many studies on aquaporins makes clear only that there is extensive interaction, compensation, and redundancy among aquaporins within and across scales, across organs, as well as architectural and anatomical effects. We therefore conclude that AQP are currently ill-suited to be used as a selection criterion for the genetic improvement of transpiration responses to environmental conditions.

Identification of robust selection criteria, with good heritability, becomes complicated when phenotypes are complex, cross-scale, as well as legacy and environmentally dependent. Inducible transpiration restriction is one such multi-scale phenotype. It requires the coordination of plant water acquisition, transport, growth, and transpiration and is regulated by multiple actors and pathways. These actors and pathways can vary according to type, severity, and timing of stress, and in relation to plant size, phenology, and hysteresis. Viewing the dynamic coordination of plant transpiration and growth from this perspective highlights three potential approaches to accelerate crop genetic improvement. Firstly, multi-scale modeling and machine learning could be used to predict outcomes and limit the number of phenotypic combinations to test empirically. Secondly, there is a potentially indicative phene. Thirdly, we propose an integrative direct selection strategy.

Multi-Scale Models

Understanding how modifications of transpiration and growth feedback and feedforward with tissue hydraulic conductance, stomatal conductance, shoot, and root architecture, hormones, and aquaporins is critical for identifying selection criteria for inducible transpiration restriction phenotypes (Tardieu and Parent, 2017). Multiple recent calls for integrating multi-scale computation models with crops simulations emphasize the need to integrate across spatial and temporal scales (Chew et al., 2017; Marshall-Colon et al., 2017; Benes et al., 2020; Peng et al., 2020), across disciplines (Hammer, 2020) and even beyond the plant and into the rhizosphere and soil (Lobet et al., 2014).

Organizing soil, plant, and canopy simulation models in nested networks, linked in multiple ways mirrors the function of the inducible transpiration restriction phenotype. Developing and benchmarking multi-scale models offers the potential to apply machine learning to data generated by said models. While truly multi-scale models are only just emerging (Ajmera et al., 2022), and benchmarking has much progress to make (Schnepf et al., 2020), machine learning could conceivably help identify latent features and highlight selection targets. Models may help decipher how modifying a particular phene integrates with other phenes and effects the emergent phenotype of yield, in a given environment. A yield-risk approach (Hammer et al., 2020) could then be applied to evaluate the influence of the timing, sensitivity, and degree of changes in transpiration. Emergent phenotypes related to transpiration optimization could then be directly selected for using traditional breeding techniques.

Xylem Conductance Capacity May Indicate Transpiration Strategy

Elementary plant phenes may indicate broader strategies, similarly to how selection for genes that lie at the hubs of gene networks likely modulate more complex phenotypes than genes at the outer spokes of a network (Dietz et al., 2010). Root axial conductance capacity, as estimated by xylem vessel number and diameter using the Hagen–Poiseuille equation, is an example (Tyree et al., 1994). Xylem conductance capacity can be estimated using laser ablation tomography and has been linked to performance (Nogueira et al., 2020; Schneider et al., 2020a; Strock et al., 2020; Hendel et al., 2021). Potentially further facilitating selection, is the observation that xylem conductance phenotypes of young plants were related to mature plant phenotype (Falk et al., 2020). It should be noted here that the targeted phenotype, that is, xylem conductance, would be an estimate, which could overestimate the actual value. Root anatomical modifications, such as suberization and lignin deposition, are also identifiable using laser ablation tomography (Strock et al., 2019) and lignification may have added benefits related to soil resistivity as well as pathogen and root pest resistance (Schneider et al., 2021). AQP may integrate with xylem parenchyma traits to refill xylem embolisms (Secchi et al., 2017), which laser ablation tomography could help address by quantifying parenchyma number, size, and positioning.

Xylem conductance capacity could indicate water use strategy for two reasons. Firstly, under-utilizing a high conductance

capacity xylem phenotype would unnecessarily increase the risk of cavitation. Empirical and modeling evidence suggests that plants operate near the upper threshold of xylem imposed limits on hydraulic conductance (Sperry et al., 1998). Conceptually this makes sense, to avoid cavitation risk and to not waste the construction and maintenance costs of xylem and parenchyma. Secondly, elevated transpiration rates could not occur with a low xylem conductance phenotype, precluding the possibility for high transpiration, photosynthesis, and growth rates. Selection for reduced xylem conductance capacity estimated using root anatomical cross sections may thus be an easy way to select for reduced transpiration rate. Alternatively, a high conductance capacity phenotype may indicate a risk-taking approach involving highly dynamic transpiration regulation imposed at the cell membrane scale.

Direct Selection for Transpiration Restriction

Direct phenotypic selection of inducible transpiration restriction in the target environment using realistic systems, such as gravimetric phenotyping, overcomes the potentially confounding cross-scale interactions and compensatory mechanisms to which organ level or controlled environment studies are sensitive. This type of direct phenotypic selection targets the emergent, or integrated phenotype, rather than lower-level component phenes, and acknowledges that feedbacks and compensation among component processes can obscure plant level processes and the ultimate target, yield (Vadez et al., 2013a; Kholová et al., 2016).

Phenotyping transpiration dynamics in a field-based lysimeter system, with realistic VPD and progressive soil drying captures the aggregate phenotype of interest as well as component phenes (Vadez et al., 2015; Kar et al., 2020, 2021). While field-based lysimeters have significant construction and operating costs, they have demonstrated utility for both trait-based and QTL-based selection (Kholová et al., 2012; Karthika et al., 2019). Heritability values for metrics describing transpiration dynamics range from moderate to high (Aparna et al., 2015; Sivasakthi et al., 2018; Tharanya et al., 2018a). This type of system uses lysimeters of large enough depth and total volume that permits additional root exploration, but with density similar to farmer's conditions. It facilitates direct phenotypic selection of transpiration restriction, particular transpiration strategies and transpiration efficiency without eliminating dynamic and interacting environmental and plant factors (Kholová et al., 2012; Vadez et al., 2013b; Tharanya et al., 2018a,b). Weekly weighings are adequate to identify genotypes that employ early season water conservation and enable late season transpiration and grain filling (Vadez et al., 2013a; Tharanya et al., 2018a). However, weekly weights do not necessarily permit distinguishing if the mechanisms of water saving arises from leaf area dynamics, daily transpiration dynamics, or weekly transpiration dynamics.

Significant insight on daily dynamics, and in particular transpiration restriction in response to daily VPD (Ryan et al., 2016), can be gleaned from three (Kholová et al., 2012) or even one daily measurement (Choudhary et al., 2020). A similar system enables minute level resolution transpiration measurements and permits selection for amplitude of daily transpiration restriction (Vadez et al., 2015; Sivasakthi et al., 2018). Studying daily transpiration dynamics under variable VPD, as well as under progressive soil drying (Karthika et al., 2019), may reveal multiple useful transpiration patterns (Kholová et al., 2016). Non-destructive shoot imaging enables quantification of leaf area dynamics. Root systems of smaller plants can be washed and measured to reveal differences in root system size and root to shoot ratio. Combined utilization of these lysimeter systems capture hourly, daily, and season level interactions between soil water acquisition and use. These systems can quantify feedbacks among root investment, leaf area development, phenology, and density. By imposing realistic environmental conditions and enabling complex feedbacks to impact performance, gravimetric phenotyping offers the chance to identify superior integrated phenotypes and accelerate genetic improvement.

Next Challenges

Of primary importance for selecting for resilience to current and future climates is addressing the utility of favorable transpiration dynamics in progressive soil drying scenarios. Enhanced resilience to terminal drought likely involves multi-scale coordination of water acquisition and use. Feedbacks among environment and phenes including axial root and leaf growth dynamics, tiller initiation, and transpiration dynamics quickly become complex and result in many trait combinations. The question of tillering, which relates to canopy density, leads to another very interesting set of questions involving if increasing planting density may reduce soil evaporation and create a favorable in-canopy micro-climate that improves the water loss to carbon gain ratio. In short, the challenge is to develop the conceptual frameworks, phenotyping platforms, and models that integrate across scales and capture overarching meta-mechanisms, such as inducible transpiration restriction, in order to identify important and selectable phenes.

CONCLUSION

Our ultimate goal is the identification of robust selection criteria for water acquisition and use optimization, likely including inducible transpiration restriction. These selection criteria should optimize yield in increasingly variable high-temperature and drought-prone environments. A review of the literature suggests that transpiration restriction can lead to an optimized transpiration phenotype through multiple mechanisms and that multiple coordination pathways may be involved. Pharmacological or gene editing tools, when used in isolation, are poorly positioned to detect dynamic, hysteretic, multi-element, and multi-scale coordination associated with overlapping transpiration regulation pathways. Directly phenotyping for transpiration restriction in response to high VPD or limited soil water has demonstrated its utility for QTL and trait-based selection. Efforts to increase drought tolerance *via* the optimization of water acquisition and transpiration should focus on daily and season level transpiration dynamics at the whole plant level.

This direct selection approach is likely to identify key integrated phenotypes and coordination mechanisms that have immediate utility for a breeding pipeline.

AUTHOR CONTRIBUTIONS

JB, AG, and VV conceived the review. VV secured the funding. JB wrote the review with comments and edits from AG and VV. All authors contributed to the article and approved the submitted version.

FUNDING

The paper was written and supported under the Make Our Planet Great Again (MOPGA) ICARUS project (Improve Crops in Arid Regions and Future Climates) funded by the Agence Nationale de la Recherche (ANR, grant ANR-17-MPGA-0011).

SUPPLEMENTARY MATERIAL

The Supplementary Material for this article can be found online at: https://www.frontiersin.org/articles/10.3389/fpls.2022.824720/full#supplementary-material

Supplementary Figure 1 | Functional projection of plant hydraulic regulation foregrounding nested structural hierarchies associated with the four general mechanisms (root and shoot architecture and conductance) governing transpiration and growth. Solid arrows depict biochemical and hydraulic signaling mechanisms within and between structural hierarchies and include transmembrane pressure potential, xylem pressure potential, pH, hormones, as well as carbohydrate, and nutrient concentration. Dashed arrows indicate interactions with environmental factors. Dotted arrows indicate interactions with phenology and planting density.

REFERENCES

Afzal, Z., Howton, T. C., Sun, Y., and Mukhtar, M. S. (2016). The roles of aquaporins in plant stress responses. *J. Dev. Biol.* 4:9. doi: 10.3390/jdb4010009

Ajmera, I., Henry, A., Radanielson, A. M., Klein, S. P., Ianevski, A., Bennett, M. J., et al. (2022). Integrated root phenotypes for improved rice performance under low nitrogen availability. *Plant Cell Environ.* 45, 805–822. doi: 10.1111/pce.14284

Aparna, K., Nepolean, T., Srivastsava, R. K., Kholová, J., Rajaram, V., Kumar, S., et al. (2015). Quantitative trait loci associated with constitutive traits control water use in pearl millet [*Pennisetum glaucum* (L.) R. Br.]. *Plant Biol.* 17, 1073–1084. doi: 10.1111/plb.12343

Aroca, R., Porcel, R., and Ruiz-Lozano, J. M. (2012). Regulation of root water uptake under abiotic stress conditions. *J. Exp. Bot.* 63, 43–57. doi: 10.1093/jxb/err266

Bagherzadi, L., Sinclair, T. R., Zwieniecki, M., Secchi, F., Hoffmann, W., Carter, T. E., et al. (2017). Assessing water-related plant traits to explain slow-wilting in soybean PI 471938. *J. Crop Improv.* 31, 400–417. doi: 10.1080/15427528.2017.1309609

Bao, Y., Aggarwal, P., Robbins, N. E., Sturrock, C. J., Thompson, M. C., Tan, H. Q., et al. (2014). Plant roots use a patterning mechanism to position lateral root branches toward available water. *Proc. Natl. Acad. Sci. U. S. A.* 111, 9319–9324. doi: 10.1073/pnas.1400966111

Barberon, M., Vermeer, J. E. M., De Bellis, D., Wang, P., Naseer, S., Andersen, T. G., et al. (2016). Adaptation of root function by nutrient-induced plasticity of endodermal differentiation. *Cell* 164, 447–459. doi: 10.1016/j.cell.2015.12.021

Belko, N., Zaman-allah, M., Cisse, N., Ndack Diop, N., Zombre, G., Ehlers, J. D., et al. (2012). Lower soil moisture threshold for transpiration decline under water deficit correlates with lower canopy conductance and higher transpiration efficiency in drought-tolerant cowpea. *Funct. Plant Biol.* 39, 306–322. doi: 10.1071/FP11282

Benes, B., Guan, K., Lang, M., Long, S. P., Lynch, J. P., Marshall-Colón, A., et al. (2020). Multiscale computational models can guide experimentation and targeted measurements for crop improvement. *Plant J.* 103, 21–31. doi: 10.1111/tpj.14722

Borrell, A. K., Mullet, J. E., George-Jaeggli, B., Van Oosterom, E. J., Hammer, G. L., Klein, P. E., et al. (2014a). Drought adaptation of stay-green sorghum is associated with canopy development, leaf anatomy, root growth, and water uptake. *J. Exp. Bot.* 65, 6251–6263. doi: 10.1093/jxb/eru232

Borrell, A. K., van Oosterom, E. J., Mullet, J. E., George-Jaeggli, B., Jordan, D. R., Klein, P. E., et al. (2014b). Stay-green alleles individually enhance grain yield in sorghum under drought by modifying canopy development and water uptake patterns. *New Phytol.* 203, 817–830. doi: 10.1111/nph.12869

Bramley, H., Turner, N. C., Turner, D. W., and Tyerman, S. D. (2009). Roles of morphology, anatomy, and aquaporins in determining contrasting hydraulic behavior of roots. *Plant Physiol.* 150, 348–364. doi: 10.1104/pp.108.134098

Bramley, H., Turner, D. W., Tyerman, S. D., and Turner, N. C. (2007). Water flow in the roots of crop species: the influence of root structure, aquaporin activity, and waterlogging. *Adv. Agron.* 96, 133–196. doi: 10.1016/S0065-2113(07)96002-2

Brodribb, T. J., Feild, T. S., and Jordan, G. J. (2007). Leaf maximum photosynthetic rate and venation are linked by hydraulics. *Plant Physiol.* 144, 1890–1898. doi: 10.1104/pp.107.101352

Buckley, T. N., John, G. P., Scoffoni, C., and Sack, L. (2015). How does leaf anatomy influence water transport outside the xylem? *Plant Physiol.* 168, 1616–1635. doi: 10.1104/pp.15.00731

Burridge, J. D., Rangarajan, H., and Lynch, J. P. (2020). Comparative phenomics of annual grain legume root architecture. *Crop Sci.* 60, 2574–2593. doi: 10.1002/csc2.20241

Cai, G., Carminati, A., Abdalla, M., and Ahmed, M. A. (2021). Soil textures rather than root hairs dominate water uptake and soil-plant hydraulics under drought. *Plant Physiol.* 187, 858–872. doi: 10.1093/plphys/kiab271

Carminati, A., and Javaux, M. (2020). Soil rather than xylem vulnerability controls stomatal response to drought. *Trends Plant Sci.* 25, 868–880. doi: 10.1016/j.tplants.2020.04.003

Carminati, A., Passioura, J. B., Zarebanadkouki, M., Ahmed, M. A., Ryan, P. R., Watt, M., et al. (2017). Root hairs enable high transpiration rates in drying soils. *New Phytol.* 216, 771–781. doi: 10.1111/nph.14715

Castro, P., Puertolas, J., and Dodd, I. C. (2019). Stem girdling uncouples soybean stomatal conductance from leaf water potential by enhancing leaf xylem ABA concentration. *Environ. Exp. Bot.* 159, 149–156. doi: 10.1016/j.envexpbot.2018.12.020

Charlson, D. V., Bhatnagar, S., King, C. A., Ray, J. D., Sneller, C. H., Carter, T. E., et al. (2009). Polygenic inheritance of canopy wilting in soybean [*Glycine max* (L.) Merr.]. *Theor. Appl. Genet.* 119, 587–594. doi: 10.1007/s00122-009-1068-4

Chaumont, F., and Tyerman, S. D. (2014). Aquaporins: highly regulated channels controlling plant water relations. *Plant Physiol.* 164, 1600–1618. doi: 10.1104/pp.113.233791

Chaves, M. M., Zarrouk, O., Francisco, R., Costa, J. M., Santos, T., Regalado, A. P., et al. (2010). Grapevine under deficit irrigation: hints from physiological and molecular data. *Ann. Bot.* 105, 661–676. doi: 10.1093/aob/mcq030

Chew, Y. H., Seaton, D. D., and Millar, A. J. (2017). Multi-scale modelling to synergise plant systems biology and crop science. *Field Crop. Res.* 202, 77–83. doi: 10.1016/j.fcr.2016.02.012

Choudhary, S., Guha, A., Kholova, J., Pandravada, A., Messina, C. D., Cooper, M., et al. (2020). Maize, sorghum, and pearl millet have highly contrasting species strategies to adapt to water stress and climate change-like conditions. *Plant Sci.* 295:110297. doi: 10.1016/j.plantsci.2019.110297

Choudhary, S., Mutava, R. N., Shekoofa, A., Sinclair, T. R., and Prasad, P. V. V. (2013). Is the stay-green trait in sorghum a result of transpiration sensitivity

to either soil drying or vapor pressure deficit? *Crop Sci.* 53, 2129–2134. doi: 10.2135/cropsci2013.01.0043

Choudhary, S., and Sinclair, T. R. (2014). Hydraulic conductance differences among sorghum genotypes to explain variation in restricted transpiration rates. *Funct. Plant Biol.* 41, 270–275. doi: 10.1071/FP13246

Christmann, A., Grill, E., and Huang, J. (2013). Hydraulic signals in long-distance signaling. *Curr. Opin. Plant Biol.* 16, 293–300. doi: 10.1016/j.pbi.2013.02.011

Comstock, J. P. (2002). Hydraulic and chemical signalling in the control of stomatal conductance and transpiration. *J. Exp. Bot.* 53, 195–200. doi: 10.1093/jexbot/53.367.195

Corso, D., Delzon, S., Lamarque, L. J., Cochard, H., Torres-Ruiz, J. M., King, A., et al. (2020). Neither xylem collapse, cavitation, or changing leaf conductance drive stomatal closure in wheat. *Plant Cell Environ.* 43, 854–865. doi: 10.1111/pce.13722

Cramer, M. D., Hawkins, H. J., and Verboom, G. A. (2009). The importance of nutritional regulation of plant water flux. *Oecologia* 161, 15–24. doi: 10.1007/s00442-009-1364-3

Cui, X. H., Hao, F. S., Chen, H., Chen, J., and Wang, X. C. (2008). Expression of the Vicia faba VfPIP1 gene in *Arabidopsis thaliana* plants improves their drought resistance. *J. Plant Res.* 121, 207–214. doi: 10.1007/s10265-007-0130-z

Davies, W. J., Wilkinson, S., and Loveys, B. (2002). Stomatal control by chemical signalling and the exploitation of this mechanism to increase water use efficiency in agriculture. *New Phytol.* 153, 449–460. doi: 10.1046/j.0028-646X.2001.00345.x

Devi, M. J., and Reddy, V. R. (2018). Transpiration response of cotton to vapor pressure deficit and its relationship with stomatal traits. *Front. Plant Sci.* 871:1572. doi: 10.3389/fpls.2018.01572

Di Pietro, M., Vialaret, J., Hem, S., Prado, K., Rossignol, M., Maurel, C., et al. (2013). Coordinated post-translational responses of aquaporins to abiotic and nutritional stimuli in arabidopsis roots. *Mol. Cell. Proteomics* 12, 3886–3897. doi: 10.1074/mcp.M113.028241

DIetrich, D., Pang, L., Kobayashi, A., Fozard, J. A., Boudolf, V., Bhosale, R., et al. (2017). Root hydrotropism is controlled via a cortex-specific growth mechanism. *Nat. Plants* 3:17057. doi: 10.1038/s41477-017-0064-y

Dietz, K. J., Jacquot, J. P., and Harris, G. (2010). Hubs and bottlenecks in plant molecular signalling networks. *New Phytol.* 188, 919–938. doi: 10.1111/j.1469-8137.2010.03502.x

Ding, L., Li, Y., Gao, L., Lu, Z., Wang, M., Ling, N., et al. (2018). Aquaporin expression and water transport pathways inside leaves are affected by nitrogen supply through transpiration in rice plants. *Int. J. Mol. Sci.* 19:256. doi: 10.3390/ijms19010256

Ding, L., Milhiet, T., Couvreur, V., Nelissen, H., Meziane, A., Parent, B., et al. (2020). Modification of the expression of the aquaporin ZmPIP2;5 affects water relations and plant growth. *Plant Physiol.* 182, 2154–2165. doi: 10.1104/pp.19.01183

Ding, L., Uehlein, N., Kaldenhoff, R., Guo, S., Zhu, Y., and Kai, L. (2019). Aquaporin PIP2;1 affects water transport and root growth in rice (*Oryza sativa* L.). *Plant Physiol. Biochem.* 139, 152–160. doi: 10.1016/j.plaphy.2019.03.017

Doblas, V. G., Geldner, N., and Barberon, M. (2017). The endodermis, a tightly controlled barrier for nutrients. *Curr. Opin. Plant Biol.* 39, 136–143. doi: 10.1016/j.pbi.2017.06.010

Dodd, I. C. (2005). Root-to-shoot signalling: assessing the roles of "up" in the up and down world of long-distance signalling in planta. *Plant Soil* 274, 251–270. doi: 10.1007/s11104-004-0966-0

Dodd, I. C., Tan, L. P., and He, J. (2003). Do increases in xylem sap pH and/or ABA concentration mediate stomatal closure following nitrate deprivation? *J. Exp. Bot.* 54, 1281–1288. doi: 10.1093/jxb/erg122

Draye, X., Kim, Y., Lobet, G., and Javaux, M. (2010). Model-assisted integration of physiological and environmental constraints affecting the dynamic and spatial patterns of root water uptake from soils. *J. Exp. Bot.* 61, 2145–2155. doi: 10.1093/jxb/erq077

Ehlert, C., Maurel, C., Tardieu, F., and Simonneau, T. (2009). Aquaporin-mediated reduction in maize root hydraulic conductivity impacts cell turgor and leaf elongation even without changing transpiration. *Plant Physiol.* 150, 1093–1104. doi: 10.1104/pp.108.131458

Falk, K. G., Jubery, T. Z., O'Rourke, J. A., Singh, A., Sarkar, S., Ganapathysubramanian, B., et al. (2020). Soybean root system architecture trait study through genotypic, phenotypic, and shape-based clusters. *Plant Phenomics* 2020, 1–23. doi: 10.34133/2020/1925495

Foster, K. J., and Miklavcic, S. J. (2017). A comprehensive biophysical model of ion and water transport in plant roots. I. Clarifying the roles of endodermal barriers in the salt stress response. *Front. Plant Sci.* 8:1326. doi: 10.3389/fpls.2017.01326

Fuchs, E. E., and Livingston, N. J. (1996). Hydraulic control of stomatal conductance in Douglas fir [*Pseudotsuga menziesii* (Mirb.) Franco] and alder [*Alnus rubra* (bong)] seedlings. *Plant Cell Environ.* 19, 1091–1098. doi: 10.1111/j.1365-3040.1996.tb00216.x

Gao, X. B., Guo, C., Li, F. M., Li, M., and He, J. (2020a). High soybean yield and drought adaptation being associated with canopy architecture, water uptake, and root traits. *Agronomy* 10:608. doi: 10.3390/AGRONOMY10040608

Gao, Y., Yang, Z., Wang, G., Sun, J., and Zhang, X. (2020b). Discerning the difference between lumens and scalariform perforation plates in impeding water flow in single xylem vessels and vessel networks in cotton. *Front. Plant Sci.* 11:246. doi: 10.3389/fpls.2020.00246

George-Jaeggli, B., Mortlock, M. Y., and Borrell, A. K. (2017). Bigger is not always better: reducing leaf area helps stay-green sorghum use soil water more slowly. *Environ. Exp. Bot.* 138, 119–129. doi: 10.1016/j.envexpbot.2017.03.002

Gleason, S. M., Cooper, M., Wiggans, D. R., Bliss, C. A., Romay, M. C., Gore, M. A., et al. (2019). Stomatal conductance, xylem water transport, and root traits underpin improved performance under drought and well-watered conditions across a diverse panel of maize inbred lines. *Field Crop. Res.* 234, 119–128. doi: 10.1016/j.fcr.2019.02.001

Grondin, A., Affortit, P., Tranchant-Dubreuil, C., de la Fuente-Cantó, C., Mariac, C., Gantet, P., et al. (2020). Aquaporins are main contributors to root hydraulic conductivity in pearl millet [*Pennisetum glaucum* (L) R. Br.]. *PLoS One* 15:e0233481. doi: 10.1371/journal.pone.0233481

Grondin, A., Mauleon, R., Vadez, V., and Henry, A. (2016). Root aquaporins contribute to whole plant water fluxes under drought stress in rice (Oryza sativa L.). *Plant Cell Environ.* 39, 347–365. doi: 10.1111/pce.12616

Grossiord, C., Buckley, T. N., Cernusak, L. A., Novick, K. A., Poulter, B., Siegwolf, R. T. W., et al. (2020). Plant responses to rising vapor pressure deficit. *New Phytol.* 226, 1550–1566. doi: 10.1111/nph.16485

Hachez, C., Heinen, R. B., Draye, X., and Chaumont, F. (2008). The expression pattern of plasma membrane aquaporins in maize leaf highlights their role in hydraulic regulation. *Plant Mol. Biol.* 68, 337–353. doi: 10.1007/s11103-008-9373-x

Hachez, C., Moshelion, M., Zelazny, E., Cavez, D., and Chaumont, F. (2006a). Localization and quantification of plasma membrane aquaporin expression in maize primary root: a clue to understanding their role as cellular plumbers. *Plant Mol. Biol.* 62, 305–323. doi: 10.1007/s11103-006-9022-1

Hachez, C., Veselov, D., Ye, Q., Reinhardt, H., Knipfer, T., Fricke, W., et al. (2012). Short-term control of maize cell and root water permeability through plasma membrane aquaporin isoforms. *Plant Cell Environ.* 35, 185–198. doi: 10.1111/j.1365-3040.2011.02429.x

Hachez, C., Zelazny, E., and Chaumont, F. (2006b). Modulating the expression of aquaporin genes in planta: a key to understand their physiological functions? *Biochim. Biophys. Acta* 1758, 1142–1156. doi: 10.1016/j.bbamem.2006.02.017

Hammer, G. (2020). The roles of credibility and transdisciplinarity in modelling to support future crop improvement. *In silico Plants* 2, 1–3. doi: 10.1093/insilicoplants/diaa004

Hammer, G. L., McLean, G., van Oosterom, E., Chapman, S., Zheng, B., Wu, A., et al. (2020). Designing crops for adaptation to the drought and high-temperature risks anticipated in future climates. *Crop Sci.* 60, 605–621. doi: 10.1002/csc2.20110

Hasan, S. A., Rabei, S. H., Nada, R. M., and Abogadallah, G. M. (2017). Water use efficiency in the drought-stressed sorghum and maize in relation to expression of aquaporin genes. *Biol. Plant.* 61, 127–137. doi: 10.1007/s10535-016-0656-9

Hayat, F., Ahmed, M. A., Zarebanadkouki, M., Javaux, M., Cai, G., and Carminati, A. (2020). Transpiration reduction in maize (Zea mays L) in response to soil drying. *Front. Plant Sci.* 10:1695. doi: 10.3389/fpls.2019.01695

Hendel, E., Bacher, H., Oksenberg, A., Walia, H., Schwartz, N., and Peleg, Z. (2021). Deciphering the genetic basis of wheat seminal root anatomy uncovers

ancestral axial conductance alleles. *Plant Cell Environ.* 44, 1921–1934. doi: 10.1111/pce.14035

Henry, A., Cal, A. J., Batoto, T. C., Torres, R. O., and Serraj, R. (2012). Root attributes affecting water uptake of rice (*Orza sativa*) under drought. *J. Exp. Bot.* 63, 4751–4763. doi: 10.1093/jxb/ers150

Henry, A., Gowda, V. R. P., Torres, R. O., McNally, K. L., and Serraj, R. (2011). Variation in root system architecture and drought response in rice (*Oryza sativa*): phenotyping of the OryzaSNP panel in rainfed lowland fields. *Field Crop. Res.* 120, 205–214. doi: 10.1016/j.fcr.2010.10.003

Henry, A., Stuart-Williams, H., Dixit, S., Kumar, A., and Farquhar, G. (2019). Stomatal conductance responses to evaporative demand conferred by rice drought-yield quantitative trait locus qDTY12.1. *Funct. Plant Biol.* 46, 660–669. doi: 10.1071/FP18126

Hsiao, T. C., and Acevedo, E. (1974). Plant responses to water deficits, water-use efficiency, and drought resistance. *Agric. Meteorol.* 14, 59–84. doi: 10.1016/0002-1571(74)90011-9

Hudak, C. M., and Patterson, R. P. (1995). Vegetative growth analysis of a drought-resistant soybean plant introduction. *Crop Sci.* 35:464. doi: 10.2135/cropsci1995.0011183X003500020031x

Javaux, M., and Carminati, A. (2021). Soil hydraulics affect the degree of isohydricity. *Plant Physiol.* 186, 1378–1381. doi: 10.1093/plphys/kiab154

Javot, H., Lauvergeat, V., Santoni, V., Martin-Laurent, F., Güçlü, J., Vinh, J., et al. (2003). Role of a single aquaporin isoform in root water uptake. *Plant Cell* 15, 509–522. doi: 10.1105/tpc.008888

Jochua, C. N., Strock, C. F., and Lynch, J. P. (2020). Root phenotypic diversity in common bean (*Phaseolus vulgaris* L.) reveals contrasting strategies for soil resource acquisition among gene pools and races. *Crop Sci.* 60, 1–17. doi: 10.1002/csc2.20312

Kaldenhoff, R., Grote, K., Zhu, J. J., and Zimmermann, U. (1998). Significance of plasmalemma aquaporins for water-transport in *Arabidopsis thaliana*. *Plant J.* 14, 121–128. doi: 10.1046/j.1365-313X.1998.00111.x

Kar, S., Purbey, V. K., Suradhaniwar, S., Korbu, L. B., Kholová, J., Durbha, S. S., et al. (2021). An ensemble machine learning approach for determination of the optimum sampling time for evapotranspiration assessment from high-throughput phenotyping data. *Comput. Electron. Agric.* 182:105992. doi: 10.1016/j.compag.2021.105992

Kar, S., Tanaka, R., Korbu, L. B., Kholová, J., Iwata, H., Durbha, S. S., et al. (2020). Automated discretization of 'transpiration restriction to increasing VPD' features from outdoors high-throughput phenotyping data. *Plant Methods* 16, 1–20. doi: 10.1186/s13007-020-00680-8

Karthika, G., Kholova, J., Alimagham, S., Ganesan, M., Chadalavada, K., Kumari, R., et al. (2019). Measurement of transpiration restriction under high vapor pressure deficit for sorghum mapping population parents. *Plant Physiol. Rep.* 24, 74–85. doi: 10.1007/s40502-019-0432-x

Kelly, G., Sade, N., Attia, Z., Secchi, F., Zwieniecki, M., Holbrook, N. M., et al. (2014). Relationship between hexokinase and the aquaporin PIP1 in the regulation of photosynthesis and plant growth. *PLoS One* 9:e87888. doi: 10.1371/journal.pone.0087888

Kholová, J., Hash, C. T., Kakkera, A., Koová, M., and Vadez, V. (2010a). Constitutive water-conserving mechanisms are correlated with the terminal drought tolerance of pearl millet [*Pennisetum glaucum* (L.) R. Br.]. *J. Exp. Bot.* 61, 369–377. doi: 10.1093/jxb/erp314

Kholová, J., Hash, C. T., Kumar, P. L., Yadav, R. S., Koová, M., and Vadez, V. (2010b). Terminal drought-tolerant pearl millet [*Pennisetum glaucum* (L.) R. Br.] have high leaf ABA and limit transpiration at high vapour pressure deficit. *J. Exp. Bot.* 61, 1431–1440. doi: 10.1093/jxb/erq013

Kholová, J., Murugesan, T., Kaliamoorthy, S., Malayee, S., Baddam, R., Hammer, G. L., et al. (2014). Modelling the effect of plant water use traits on yield and stay-green expression in sorghum. *Funct. Plant Biol.* 41, 1019–1034. doi: 10.1071/FP13355

Kholová, J., Nepolean, T., Tom Hash, C., Supriya, A., Rajaram, V., Senthilvel, S., et al. (2012). Water saving traits co-map with a major terminal drought tolerance quantitative trait locus in pearl millet [*Pennisetum glaucum* (L.) R. Br.]. *Mol. Breed.* 30, 1337–1353. doi: 10.1007/s11032-012-9720-0

Kholová, J., Zindy, P., Malayee, S., Baddam, R., Murugesan, T., Kaliamoorthy, S., et al. (2016). Component traits of plant water use are modulated by vapour pressure deficit in pearl millet (*Pennisetum glaucum* (L.) r.Br.). *Funct. Plant Biol.* 43, 423–437. doi: 10.1071/FP15115

Klein, S. P., Schneider, H. M., Perkins, A. C., Brown, K. M., and Lynch, J. P. (2020). Multiple integrated root phenotypes are associated with improved drought tolerance. *Plant Physiol.* 183, 1011–1025. doi: 10.1104/pp.20.00211

Knipfer, T., Bambach, N., Isabel Hernandez, M., Bartlett, M. K., Sinclair, G., Duong, F., et al. (2020). Predicting stomatal closure and turgor loss in woody plants using predawn and midday water potential. *Plant Physiol.* 184, 881–894. doi: 10.1104/pp.20.00500

Kudoyarova, G. R., Vysotskaya, L. B., Cherkozyanova, A., and Dodd, I. C. (2007). Effect of partial rootzone drying on the concentration of zeatin-type cytokinins in tomato (*Solanum lycopersicum* L.) xylem sap and leaves. *J. Exp. Bot.* 58, 161–168. doi: 10.1093/jxb/erl116

Kunert, K., and Vorster, B. J. (2020). In search for drought-tolerant soybean: is the slow-wilting phenotype more than just a curiosity? *J. Exp. Bot.* 71, 457–460. doi: 10.1093/jxb/erz235

Li, G. W., Peng, Y. H., Yu, X., Zhang, M. H., Cai, W. M., Sun, W. N., et al. (2008). Transport functions and expression analysis of vacuolar membrane aquaporins in response to various stresses in rice. *J. Plant Physiol.* 165, 1879–1888. doi: 10.1016/j.jplph.2008.05.002

Lobet, G., Couvreur, V., Meunier, F., Javaux, M., and Draye, X. (2014). Plant water uptake in drying soils. *Plant Physiol.* 164, 1619–1627. doi: 10.1104/pp.113.233486

Lovisolo, C., Perrone, I., Carra, A., Ferrandino, A., Flexas, J., Medrano, H., et al. (2010). Drought-induced changes in development and function of grapevine (Vitis spp.) organs and in their hydraulic and non-hydraulic interactions at the whole-plant level: a physiological and molecular update. *Funct. Plant Biol.* 37, 98–116. doi: 10.1071/FP09191

Lynch, J. P. (2007). Roots of the second green revolution. *Aust. J. Bot.* 55, 493–512. doi: 10.1071/BT06118

Lynch, J. P. (2018). Rightsizing root phenotypes for drought resistance. *J. Exp. Bot.* 69, 3279–3292. doi: 10.1093/jxb/ery048

Lynch, J. P. (2019). Root phenotypes for improved nutrient capture: an underexploited opportunity for global agriculture. *New Phytol.* 223, 548–564. doi: 10.1111/nph.15738

Marshall-Colon, A., Long, S. P., Allen, D. K., Allen, G., Beard, D. A., Benes, B., et al. (2017). Crops in silico: generating virtual crops using an integrative and multi-scale modeling platform. *Front. Plant Sci.* 8:786. doi: 10.3389/fpls.2017.00786

Martre, P., Morillon, R., Barrieu, F., North, G. B., Nobel, P. S., and Chrispeels, M. J. (2002). Plasma membrane aquaporins play a significant role during recovery from water deficit. *Plant Physiol.* 130, 2101–2110. doi: 10.1104/pp.009019

McCully, M. E. (1999). Root xylem embolisms and refilling. Relation to water potentials of soil, roots, and leaves, and osmotic potentials of root xylem sap. *Plant Physiol.* 119, 1001–1008. doi: 10.1104/pp.119.3.1001

McCully, M. E., and Canny, M. J. (1988). Pathways and processes of water and nutrient movement in roots. *Plant Soil* 111, 159–170. doi: 10.1007/BF02139932

Medina, S., Vicente, R., Nieto-Taladriz, M. T., Aparicio, N., Chairi, F., Vergara-Diaz, O., et al. (2019). The plant-transpiration response to vapor pressure deficit (VPD) in durum wheat is associated with differential yield performance and specific expression of genes involved in primary metabolism and water transport. *Front. Plant Sci.* 9:1994. doi: 10.3389/fpls.2018.01994

Meinzer, F. C., Woodruff, D. R., Marias, D. E., Smith, D. D., McCulloh, K. A., Howard, A. R., et al. (2016). Mapping 'hydroscapes' along the iso- to anisohydric continuum of stomatal regulation of plant water status. *Ecol. Lett.* 19, 1343–1352. doi: 10.1111/ele.12670

Meng, D., Walsh, M., and Fricke, W. (2016). Rapid changes in root hydraulic conductivity and aquaporin expression in rice (*Oryza sativa* l.) in response to shoot removal – xylem tension as a possible signal. *Ann. Bot.* 118, 809–819. doi: 10.1093/aob/mcw150

Messina, C. D., Sinclair, T. R., Hammer, G. L., Curan, D., Thompson, J., Oler, Z., et al. (2015). Limited-transpiration trait may increase maize drought tolerance in the US corn belt. *Agron. J.* 107, 1978–1986. doi: 10.2134/agronj15.0016

Meunier, F., Draye, X., Vanderborght, J., Javaux, M., and Couvreur, V. (2017). A hybrid analytical-numerical method for solving water flow equations in root hydraulic architectures. *Appl. Math. Model.* 52, 648–663. doi: 10.1016/j.apm.2017.08.011

Meunier, F., Zarebanadkouki, M., Ahmed, M. A., Carminati, A., Couvreur, V., and Javaux, M. (2018). Hydraulic conductivity of soil-grown lupine and

maize unbranched roots and maize root-shoot junctions. *J. Plant Physiol.* 227, 31–44. doi: 10.1016/j.jplph.2017.12.019

Miao, R., Yuan, W., Wang, Y., Garcia-Maquilon, I., Dang, X., Li, Y., et al. (2021). Low ABA concentration promotes root growth and hydrotropism through relief of ABA INSENSITIVE 1-mediated inhibition of plasma membrane H+-ATPase 2. *Sci. Adv.* 7, 4113–4130. doi: 10.1126/sciadv.abd4113

Moshelion, M., Halperin, O., Wallach, R., Oren, R., and Way, D. A. (2015). Role of aquaporins in determining transpiration and photosynthesis in water-stressed plants: crop water-use efficiency, growth and yield. *Plant Cell Environ.* 38, 1785–1793. doi: 10.1111/pce.12410

Nada, R. M., and Abogadallah, G. M. (2014). Aquaporins are major determinants of water use efficiency of rice plants in the field. *Plant Sci.* 227, 165–180. doi: 10.1016/j.plantsci.2014.08.006

Nada, R. M., and Abogadallah, G. M. (2020). Contrasting root traits and native regulation of aquaporin differentially determine the outcome of overexpressing a single aquaporin (OsPIP2;4) in two rice cultivars. *Protoplasma* 257, 583–595. doi: 10.1007/s00709-019-01468-x

Newman, E. I. (1969). Resistance to water flow in soil and plant. I. Soil resistance in relation to amounts of root: theoretical estimates. *J. Appl. Ecol.* 6, 1–12. doi: 10.2307/2401297

Nogueira, M., Livingston, D., Tuong, T., and Sinclair, T. R. (2020). Xylem vessel radii comparison between soybean genotypes differing in tolerance to drought. *J. Crop Improv.* 34, 404–413. doi: 10.1080/15427528.2020.1724225

Pantalone, V. R., Rebetzke, G. J., Burton, J. W., and Carter, T. E. (1996). Phenotypic evaluation of root traits in soybean and applicability to plant breeding. *Crop Sci.* 36, 456–459. doi: 10.2135/cropsci1996.0011183X003600020039x

Pantin, F., Monnet, F., Jannaud, D., Costa, J. M., Renaud, J., Muller, B., et al. (2013). The dual effect of abscisic acid on stomata. *New Phytol.* 197, 65–72. doi: 10.1111/nph.12013

Parent, B., Hachez, C., Redondo, E., Simonneau, T., Chaumont, F., and Tardieu, F. (2009). Drought and abscisic acid effects on aquaporin content translate into changes in hydraulic conductivity and leaf growth rate: a trans-scale approach1[w][OA]. *Plant Physiol.* 149, 2000–2012. doi: 10.1104/pp.108.130682

Peng, B., Guan, K., Tang, J., Ainsworth, E. A., Asseng, S., Bernacchi, C. J., et al. (2020). Towards a multiscale crop modelling framework for climate change adaptation assessment. *Nat. Plants* 6, 338–348. doi: 10.1038/s41477-020-0625-3

Polania, J. A., Poschenrieder, C., Beebe, S., and Rao, I. M. (2016). Effective use of water and increased dry matter partitioned to grain contribute to yield of common bean improved for drought resistance. *Front. Plant Sci.* 7:660. doi: 10.3389/fpls.2016.00660

Postaire, O., Tournaire-Roux, C., Grondin, A., Boursiac, Y., Morillon, R., Schäffner, A. R., et al. (2010). A PIP1 aquaporin contributes to hydrostatic pressure-induced water transport in both the root and rosette of Arabidopsis. *Plant Physiol.* 152, 1418–1430. doi: 10.1104/pp.109.145326

Pou, A., Medrano, H., Flexas, J., and Tyerman, S. D. (2013). A putative role for TIP and PIP aquaporins in dynamics of leaf hydraulic and stomatal conductances in grapevine under water stress and re-watering. *Plant Cell Environ.* 36, 828–843. doi: 10.1111/pce.12019

Prado, K., Boursiac, Y., Tournaire-Roux, C., Monneuse, J. M., Postaire, O., Da Ines, O., et al. (2013). Regulation of Arabidopsis leaf hydraulics involves light-dependent phosphorylation of aquaporins in veins. *Plant Cell* 25, 1029–1039. doi: 10.1105/tpc.112.108456

Prado, K., Cotelle, V., Li, G., Bellati, J., Tang, N., Tournaire-Roux, C., et al. (2019). Oscillating aquaporin phosphorylation and 14-3-3 proteins mediate the circadian regulation of leaf hydraulics. *Plant Cell* 31, 417–429. doi: 10.1105/tpc.18.00804

Prado, K., and Maurel, C. (2013). Regulation of leaf hydraulics: from molecular to whole plant levels. *Front. Plant Sci.* 4:255. doi: 10.3389/fpls.2013.00255

Prince, S. J., Murphy, M., Mutava, R. N., Durnell, L. A., Valliyodan, B., Grover Shannon, J., et al. (2017). Root xylem plasticity to improve water use and yield in water-stressed soybean. *J. Exp. Bot.* 68, 2027–2036. doi: 10.1093/jxb/erw472

Ranathunge, K., Kotula, L., Steudle, E., and Lafitte, R. (2004). Water permeability and reflection coefficient of the outer part of young rice roots are differently affected by closure of water channels (aquaporins) or blockage of apoplastic pores. *J. Exp. Bot.* 55, 433–447. doi: 10.1093/jxb/erh041

Reddy, P. S., Dhaware, M. G., Sivasakthi, K., Divya, K., Nagaraju, M., Sri Cindhuri, K., et al. (2022). Pearl millet aquaporin gene PgPIP2;6 improves abiotic stress tolerance in transgenic tobacco. *Front. Plant Sci.* 13:820996. doi: 10.3389/fpls.2022.820996

Reddy, P. S., Tharanya, M., Sivasakthi, K., Srikanth, M., Hash, C. T., Kholova, J., et al. (2017). Molecular cloning and expression analysis of aquaporin genes in pearl millet [*Pennisetum glaucum* (L) R. Br.] genotypes contrasting in their transpiration response to high vapour pressure deficits. *Plant Sci.* 265, 167–176. doi: 10.1016/j.plantsci.2017.10.005

Riar, M. K., Sinclair, T. R., and Prasad, P. V. V. (2015). Persistence of limited-transpiration-rate trait in sorghum at high temperature. *Environ. Exp. Bot.* 115, 58–62. doi: 10.1016/j.envexpbot.2015.02.007

Richards, R. A., and Passioura, J. B. (1989). A breeding program to reduce the diameter of the major xylem vessel in the seminal roots of wheat and its effect on grain yield in rain-fed environments. *Aust. J. Agric. Res.* 40, 943–950. doi: 10.1071/AR9890943

Richards, R. A., Rebetzke, G. J., Condon, A. G., and van Herwaarden, A. F. (2002). Breeding opportunities for increasing the efficiency of water use and crop yield. *Crop Sci.* 42, 111–121. doi: 10.2135/cropsci2002.1110

Robbins, N. E., and Dinneny, J. R. (2018). Growth is required for perception of water availability to pattern root branches in plants. *Proc. Natl. Acad. Sci. U. S. A.* 115, E822–E831. doi: 10.1073/pnas.1710709115

Rodriguez-Dominguez, C. M., and Brodribb, T. J. (2020). Declining root water transport drives stomatal closure in olive under moderate water stress. *New Phytol.* 225, 126–134. doi: 10.1111/nph.16177

Rogiers, S. Y., Greer, D. H., Hatfield, J. M., Hutton, R. J., Clarke, S. J., Hutchinson, P. A., et al. (2012). Stomatal response of an anisohydric grapevine cultivar to evaporative demand, available soil moisture and abscisic acid. *Tree Physiol.* 32, 249–261. doi: 10.1093/treephys/tpr131

Rosales, M. A., Maurel, C., and Nacry, P. (2019). Abscisic acid coordinates dose-dependent developmental and hydraulic responses of roots to water deficit. *Plant Physiol.* 180, 2198–2211. doi: 10.1104/pp.18.01546

Rubio, G., Zhu, J., and Lynch, J. P. (2003). A critical test of the two prevailing theories of plant response to nutrient availability. *Am. J. Bot.* 90, 143–152. doi: 10.3732/ajb.90.1.143

Ryan, A. C., Dodd, I. C., Rothwell, S. A., Jones, R., Tardieu, F., Draye, X., et al. (2016). Gravimetric phenotyping of whole plant transpiration responses to atmospheric vapour pressure deficit identifies genotypic variation in water use efficiency. *Plant Sci.* 251, 101–109. doi: 10.1016/j.plantsci.2016.05.018

Sack, L., and Frole, K. (2006). Leaf structural diversity is related to hydraulic capacity in tropical rain forest trees. *Ecology* 87, 483–491. doi: 10.1890/05-0710

Sack, L., and Holbrook, N. M. (2006). Leaf hydraulics. *Annu. Rev. Plant Biol.* 57, 361–381. doi: 10.1146/annurev.arplant.56.032604.144141

Sack, L., and Scoffoni, C. (2013). Leaf venation: structure, function, development, evolution, ecology and applications in the past, present and future. *New Phytol.* 198, 983–1000. doi: 10.1111/nph.12253

Sade, N., Gebremedhin, A., and Moshelion, M. (2012). Risk-taking plants: anisohydric behavior as a stress-resistance trait. *Plant Signal. Behav.* 7, 767–770. doi: 10.4161/psb.20505

Sade, N., Shatil-Cohen, A., Attia, Z., Maurel, C., Boursiac, Y., Kelly, G., et al. (2014). The role of plasma membrane aquaporins in regulating the bundle sheath-mesophyll continuum and leaf hydraulics. *Plant Physiol.* 166, 1609–1620. doi: 10.1104/pp.114.248633

Sade, N., Shatil-Cohen, A., and Moshelion, M. (2015). Bundle-sheath aquaporins play a role in controlling Arabidopsis leaf hydraulic conductivity. *Plant Signal. Behav.* 10:e1017177. doi: 10.1080/15592324.2015.1017177

Sade, N., Vinocur, B. J., Diber, A., Shatil, A., Ronen, G., Nissan, H., et al. (2009). Improving plant stress tolerance and yield production: is the tonoplast aquaporin SlTIP2;2 a key to isohydric to anisohydric conversion? *New Phytol.* 181, 651–661. doi: 10.1111/j.1469-8137.2008.02689.x

Sadok, W., and Sinclair, T. R. (2010). Transpiration response of "slow-wilting" and commercial soybean (*Glycine max* (L.) Merr.) genotypes to three aquaporin inhibitors. *J. Exp. Bot.* 61, 821–829. doi: 10.1093/jxb/erp350

Sadras, V. O., Hall, A. J., Trapani, N., and Vilella, F. (1989). Dynamics of rooting and root-length: leaf-area relationships as affected by plant population in sunflower crops. *Field Crop. Res.* 22, 45–57. doi: 10.1016/0378-4290(89)90088-9

Sakurai-Ishikawa, J., Murai-Hatano, M., Hayashi, H., Ahamed, A., Fukushi, K., Matsumoto, T., et al. (2011). Transpiration from shoots triggers diurnal

changes in root aquaporin expression. *Plant Cell Environ.* 34, 1150–1163. doi: 10.1111/j.1365-3040.2011.02313.x

Schneider, H. M., Klein, S. P., Hanlon, M. T., Kaeppler, S., Brown, K. M., and Lynch, J. P. (2020a). Genetic control of root anatomical plasticity in maize. *Plant Genome* 13:e20003. doi: 10.1002/tpg2.20003

Schneider, H. M., Klein, S. P., Hanlon, M. T., Nord, E. A., Kaeppler, S., Brown, K. M., et al. (2020b). Genetic control of root architectural plasticity in maize. *J. Exp. Bot.* 71, 3185–3197. doi: 10.1093/jxb/eraa084

Schneider, H. M., and Lynch, J. P. (2020). Should root plasticity be a crop breeding target? *Front. Plant Sci.* 11:546. doi: 10.3389/fpls.2020.00546

Schneider, H. M., Postma, J. A., Kochs, J., Pflugfelder, D., Lynch, J. P., and van Dusschoten, D. (2020c). Spatio-temporal variation in water uptake in seminal and nodal root systems of barley plants grown in soil. *Front. Plant Sci.* 11:1247. doi: 10.3389/fpls.2020.01247

Schneider, H. M., Strock, C. F., Hanlon, M. T., Vanhees, D. J., Perkins, A. C., Ajmera, I. B., et al. (2021). Multiseriate cortical sclerenchyma enhance root penetration in compacted soils. *Proc. Natl. Acad. Sci. U. S. A.* 118:e2012087118. doi: 10.1073/pnas.2012087118

Schnepf, A., Black, C. K., Couvreur, V., Delory, B. M., Doussan, C., Koch, A., et al. (2020). Call for participation: collaborative benchmarking of functional-structural root architecture models. The case of root water uptake. *Front. Plant Sci.* 11:316. doi: 10.3389/fpls.2020.00316

Schoppach, R., and Sadok, W. (2012). Differential sensitivities of transpiration to evaporative demand and soil water deficit among wheat elite cultivars indicate different strategies for drought tolerance. *Environ. Exp. Bot.* 84, 1–10. doi: 10.1016/j.envexpbot.2012.04.016

Schoppach, R., Wauthelet, D., Jeanguenin, L., and Sadok, W. (2014). Conservative water use under high evaporative demand associated with smaller root metaxylem and limited trans-membrane water transport in wheat. *Funct. Plant Biol.* 41, 257–269. doi: 10.1071/FP13211

Scoffoni, C., Albuquerque, C., Brodersen, C. R., Townes, S. V., John, G. P., Bartlett, M. K., et al. (2017). Outside-xylem vulnerability, not xylem embolism, controls leaf hydraulic decline during dehydration. *Plant Physiol.* 173, 1197–1210. doi: 10.1104/pp.16.01643

Secchi, F., Pagliarani, C., and Zwieniecki, M. A. (2017). The functional role of xylem parenchyma cells and aquaporins during recovery from severe water stress. *Plant Cell Environ.* 40, 858–871. doi: 10.1111/pce.12831

Segal, E., Kushnir, T., Mualem, Y., and Shani, U. (2008). Water uptake and hydraulics of the root hair rhizosphere. *Vadose Zone J.* 7:1027. doi: 10.2136/vzj2007.0122

Seversike, T. M., Sermons, S. M., Sinclair, T. R., Carter, T. E., and Rufty, T. W. (2013). Temperature interactions with transpiration response to vapor pressure deficit among cultivated and wild soybean genotypes. *Physiol. Plant.* 148, 62–73. doi: 10.1111/j.1399-3054.2012.01693.x

Seversike, T. M., Sermons, S. M., Sinclair, T. R., Carter, T. E., and Rufty, T. W. (2014). Physiological properties of a drought-resistant wild soybean genotype: transpiration control with soil drying and expression of root morphology. *Plant Soil* 374, 359–370. doi: 10.1007/s11104-013-1757-2

Sharipova, G., Veselov, D., Kudoyarova, G., Fricke, W., Dodd, I. C., Katsuhara, M., et al. (2016). Exogenous application of abscisic acid (ABA) increases root and cell hydraulic conductivity and abundance of some aquaporin isoforms in the ABA-deficient barley mutant Az34. *Ann. Bot.* 118, 777–785. doi: 10.1093/aob/mcw117

Shatil-Cohen, A., Attia, Z., and Moshelion, M. (2011). Bundle-sheath cell regulation of xylem-mesophyll water transport via aquaporins under drought stress: a target of xylem-borne ABA? *Plant J.* 67, 72–80. doi: 10.1111/j.1365-313X.2011.04576.x

Shekoofa, A., and Sinclair, T. (2018). Aquaporin activity to improve crop drought tolerance. *Cell* 7:123. doi: 10.3390/cells7090123

Shekoofa, A., Sinclair, T. R., Messina, C. D., and Cooper, M. (2016). Variation among maize hybrids in response to high vapor pressure deficit at high temperatures. *Crop Sci.* 56, 392–396. doi: 10.2135/cropsci2015.02.0134

Siefritz, F., Tyree, M. T., Lovisolo, C., Schubert, A., and Kaldenhoff, R. (2002). PIP1 plasma membrane aquaporins in tobacco: from cellular effects to function in plants. *Plant Cell* 14, 869–876. doi: 10.1105/tpc.000901

Sinclair, T. R., Devi, J., Shekoofa, A., Choudhary, S., Sadok, W., Vadez, V., et al. (2017). Limited-transpiration response to high vapor pressure deficit in crop species. *Plant Sci.* 260, 109–118. doi: 10.1016/j.plantsci.2017.04.007

Sinclair, T. R., Hammer, G. L., and Van Oosterom, E. J. (2005). Potential yield and water-use efficiency benefits in sorghum from limited maximum transpiration rate. *Funct. Plant Biol.* 32, 945–952. doi: 10.1071/FP05047

Sinclair, T. R., Messina, C. D., Beatty, A., and Samples, M. (2010). Assessment across the United States of the benefits of altered soybean drought traits. *Agron. J.* 102, 475–482. doi: 10.2134/agronj2009.0195

Sinclair, T. R., and Muchow, R. C. (2001). System analysis of plant traits to increase grain yield on limited water supplies. *Agron. J.* 93, 263–270. doi: 10.2134/agronj2001.932263x

Sinclair, T. R., Zwieniecki, M. A., and Holbrook, N. M. (2008). Low leaf hydraulic conductance associated with drought tolerance in soybean. *Physiol. Plant.* 132, 446–451. doi: 10.1111/j.1399-3054.2007.01028.x

Sivasakthi, K., Tharanya, M., Kholová, J., Muriuki, R. W., Thirunalasundari, T., and Vadez, V. (2017). Chickpea genotypes contrasting for vigor and canopy conductance also differ in their dependence on different water transport pathways. *Front. Plant Sci.* 8:1663. doi: 10.3389/fpls.2017.01663

Sivasakthi, K., Tharanya, M., Zaman-Allah, M., Kholová, J., Thirunalasundari, T., and Vadez, V. (2020). Transpiration difference under high evaporative demand in chickpea (*Cicer arietinum* L.) may be explained by differences in the water transport pathway in the root cylinder. *Plant Biol.* 22, 769–780. doi: 10.1111/plb.13147

Sivasakthi, K., Thudi, M., Tharanya, M., Kale, S. M., Kholová, J., Halime, M. H., et al. (2018). Plant vigour QTLs co-map with an earlier reported QTL hotspot for drought tolerance while water saving QTLs map in other regions of the chickpea genome. *BMC Plant Biol.* 18:29. doi: 10.1186/s12870-018-1245-1

Sperry, J. S., Adler, F. R., Campbell, G. S., and Comstock, J. P. (1998). Limitation of plant water use by rhizosphere and xylem conductance: results from a model. *Plant Cell Environ.* 21, 347–359. doi: 10.1046/j.1365-3040.1998.00287.x

Steudle, E. (2000). Water uptake by plant roots: an integration of views. *Plant Soil* 226, 45–56. doi: 10.1023/A:1026439226716

Strock, C. F., Burridge, J. D., Niemiec, M. D., Brown, K. M., and Lynch, J. P. (2020). Root metaxylem and architecture phenotypes integrate to regulate water use under drought stress. *Plant Cell Environ.* 44, 49–67. doi: 10.1111/pce.13875

Strock, C. F., Schneider, H. M., Galindo-Castañeda, T., Hall, B. T., Van Gansbeke, B., Mather, D. E., et al. (2019). Laser ablation tomography for visualization of root colonization by edaphic organisms. *J. Exp. Bot.* 70, 5327–5342. doi: 10.1093/jxb/erz271

Sunita, C., Sinclair, T. R., Messina, C. D., and Cooper, M. (2014). Hydraulic conductance of maize hybrids differing in transpiration response to vapor pressure deficit. *Crop Sci.* 54, 1147–1152. doi: 10.2135/cropsci2013.05.0303

Sutka, M., Li, G., Boudet, J., Boursiac, Y., Doumas, P., and Maurel, C. (2011). Natural variation of root hydraulics in Arabidopsis grown in normal and salt-stressed conditions. *Plant Physiol.* 155, 1264–1276. doi: 10.1104/pp.110.163113

Tanaka, Y., Fujii, K., and Shiraiwa, T. (2010). Variability of leaf morphology and stomatal conductance in soybean [*Glycine max* (L.) Merr.] cultivars. *Crop Sci.* 50, 2525–2532. doi: 10.2135/cropsci2010.02.0058

Tardieu, F., and Parent, B. (2017). Predictable 'meta-mechanisms' emerge from feedbacks between transpiration and plant growth and cannot be simply deduced from short-term mechanisms. *Plant Cell Environ.* 40, 846–857. doi: 10.1111/pce.12822

Tharanya, M., Kholova, J., Sivasakthi, K., Seghal, D., Hash, C. T., Raj, B., et al. (2018a). Quantitative trait loci (QTLs) for water use and crop production traits co-locate with major QTL for tolerance to water deficit in a fine-mapping population of pearl millet (*Pennisetum glaucum* L. r.Br.). *Theor. Appl. Genet.* 131, 1509–1529. doi: 10.1007/s00122-018-3094-6

Tharanya, M., Sivasakthi, K., Barzana, G., Kholová, J., Thirunalasundari, T., and Vadez, V. (2018b). Pearl millet (*Pennisetum glaucum*) contrasting for the transpiration response to vapour pressure deficit also differ in their dependence on the symplastic and apoplastic water transport pathways. *Funct. Plant Biol.* 45, 719–736. doi: 10.1071/FP17161

Thompson, A. J., Andrews, J., Mulholland, B. J., McKee, J. M. T., Hilton, H. W., Horridge, J. S., et al. (2007). Overproduction of abscisic acid in tomato increases transpiration efficiency and root hydraulic conductivity and influences leaf expansion. *Plant Physiol.* 143, 1905–1917. doi: 10.1104/pp.106.093559

Topp, C. N. (2016). Hope in change: the role of root plasticity in crop yield stability. *Plant Physiol.* 172, 5–6. doi: 10.1104/pp.16.01257

Tylová, E., Pecková, E., Blascheová, Z., and Soukup, A. (2017). Casparian bands and suberin lamellae in exodermis of lateral roots: an important trait of roots system response to abiotic stress factors. *Ann. Bot.* 120, 71–85. doi: 10.1093/aob/mcx047

Tyree, M. T. (1997). The cohesion-tension theory of sap ascent: current controversies. *J. Exp. Bot.* 48, 1753–1765. doi: 10.1093/jxb/48.10.1753

Tyree, M. T., Davis, S. D., and Cochard, H. (1994). Biophysical perspectives of xylem evolution: is there a tradeoff of hydraulic efficiency for vulnerability to dysfunction? *IAWA J.* 15, 335–360. doi: 10.1163/22941932-90001369

Vadez, V. (2014). Root hydraulics: the forgotten side of roots in drought adaptation. *Field Crop. Res.* 165, 15–24. doi: 10.1016/j.fcr.2014.03.017

Vadez, V., Choudhary, S., Kholová, J., Hash, C. T., Srivastava, R., Kumar, A. A., et al. (2021). Transpiration efficiency: insights from comparisons of C4 cereal species. *J. Exp. Bot.* 72, 5221–5234. doi: 10.1093/jxb/erab251

Vadez, V., Deshpande, S. P., Kholova, J., Hammer, G. L., Borrell, A. K., Talwar, H. S., et al. (2011). Stay-green quantitative trait loci's effects on water extraction, transpiration efficiency and seed yield depend on recipient parent background. *Funct. Plant Biol.* 38, 553–566. doi: 10.1071/FP11073

Vadez, V., Kholová, J., Hummel, G., Zhokhavets, U., Gupta, S. K., and Hash, C. T. (2015). LeasyScan: a novel concept combining 3D imaging and lysimetry for high-throughput phenotyping of traits controlling plant water budget. *J. Exp. Bot.* 66, 5581–5593. doi: 10.1093/jxb/erv251

Vadez, V., Kholová, J., Yadav, R. S., and Hash, C. T. (2013a). Small temporal differences in water uptake among varieties of pearl millet (*Pennisetum glaucum* (L.) R. Br.) are critical for grain yield under terminal drought. *Plant Soil* 371, 447–462. doi: 10.1007/s11104-013-1706-0

Vadez, V., Kholova, J., Zaman-Allah, M., and Belko, N. (2013b). Water: the most important "molecular" component of water stress tolerance research. *Funct. Plant Biol.* 40, 1310–1322. doi: 10.1071/FP13149

Vandeleur, R. K., Mayo, G., Shelden, M. C., Gilliham, M., Kaiser, B. N., and Tyerman, S. D. (2009). The role of plasma membrane intrinsic protein aquaporins in water transport through roots: diurnal and drought stress responses reveal different strategies between isohydric and anisohydric cultivars of grapevine. *Plant Physiol.* 149, 445–460. doi: 10.1104/pp.108.128645

Vandeleur, R. K., Sullivan, W., Athman, A., Jordans, C., Gilliham, M., Kaiser, B. N., et al. (2014). Rapid shoot-to-root signalling regulates root hydraulic conductance via aquaporins. *Plant Cell Environ.* 37, 520–538. doi: 10.1111/pce.12175

von Jeetze, P. J., Zarebanadkouki, M., and Carminati, A. (2020). Spatial heterogeneity enables higher root water uptake in dry soil but protracts water stress after transpiration decline: a numerical study. *Water Resour. Res.* 56:e2019WR025501. doi: 10.1029/2019WR025501

Wang, P., Calvo-Polanco, M., Reyt, G., Barberon, M., Champeyroux, C., Santoni, V., et al. (2019). Surveillance of cell wall diffusion barrier integrity modulates water and solute transport in plants. *Sci. Rep.* 9:4227. doi: 10.1038/s41598-019-40588-5

Xu, T., Zhang, L., and Li, Z. (2020). Computational fluid dynamics model and flow resistance characteristics of *Jatropha curcas* L xylem vessel. *Sci. Rep.* 10:14728. doi: 10.1038/s41598-020-71576-9

Yang, Z., Sinclair, T. R., Zhu, M., Messina, C. D., Cooper, M., and Hammer, G. L. (2012). Temperature effect on transpiration response of maize plants to vapour pressure deficit. *Environ. Exp. Bot.* 78, 157–162. doi: 10.1016/j.envexpbot.2011.12.034

Yao, C., Moreshet, S., and Aloni, B. (2001). Water relations and hydraulic control of stomatal behaviour in bell pepper plant in partial soil drying. *Plant Cell Environ.* 24, 227–235. doi: 10.1111/j.1365-3040.2001.00667.x

Ye, H., Song, L., Schapaugh, W. T., Ali, M. L., Sinclair, T. R., Riar, M. K., et al. (2020). The importance of slow canopy wilting in drought tolerance in soybean. *J. Exp. Bot.* 71, 642–652. doi: 10.1093/jxb/erz150

York, L. M., and Lynch, J. P. (2015). Intensive field phenotyping of maize (*Zea mays* L.) root crowns identifies phenes and phene integration associated with plant growth and nitrogen acquisition. *J. Exp. Bot.* 66, 5493–5505. doi: 10.1093/jxb/erv241

York, L. M., Nord, E. A., and Lynch, J. P. (2013). Integration of root phenes for soil resource acquisition. *Front. Plant Sci.* 4:355. doi: 10.3389/fpls.2013.00355

Zaman-Allah, M., Jenkinson, D. M., and Vadez, V. (2011). A conservative pattern of water use, rather than deep or profuse rooting, is critical for the terminal drought tolerance of chickpea. *J. Exp. Bot.* 62, 4239–4252. doi: 10.1093/jxb/err139

Zargar, S. M., Nagar, P., Deshmukh, R., Nazir, M., Wani, A. A., Masoodi, K. Z., et al. (2017). Aquaporins as potential drought tolerance inducing proteins: towards instigating stress tolerance. *J. Proteome* 169, 233–238. doi: 10.1016/j.jprot.2017.04.010

Zhou, S., Hu, W., Deng, X., Ma, Z., Chen, L., Huang, C., et al. (2012). Overexpression of the wheat aquaporin gene, TaAQP7, enhances drought tolerance in transgenic tobacco. *PLoS One* 7:e52439. doi: 10.1371/journal.pone.0052439

Zwieniecki, M. A., Brodribb, T. J., and Holbrook, N. M. (2007). Hydraulic design of leaves: insights from rehydration kinetics. *Plant Cell Environ.* 30, 910–921. doi: 10.1111/j.1365-3040.2007.001681.x

Conflict of Interest: The authors declare that the research was conducted in the absence of any commercial or financial relationships that could be construed as a potential conflict of interest.

Publisher's Note: All claims expressed in this article are solely those of the authors and do not necessarily represent those of their affiliated organizations, or those of the publisher, the editors and the reviewers. Any product that may be evaluated in this article, or claim that may be made by its manufacturer, is not guaranteed or endorsed by the publisher.

frontiers | Frontiers in Plant Science

ORIGINAL RESEARCH
published: 04 May 2022
doi: 10.3389/fpls.2022.868108

Seasonal Responses of Hydraulic Function and Carbon Dynamics in Spruce Seedlings to Continuous Drought

Yangang Han[1,2], *Jiaojiao Deng*[1], *Wangming Zhou*[1], *Qing-Wei Wang*[1]* and *Dapao Yu*[1]*

[1] CAS Key Laboratory of Forest Ecology and Management, Institute of Applied Ecology, Chinese Academy of Sciences, Shenyang, China, [2] University of Chinese Academy of Sciences, Beijing, China

OPEN ACCESS

Edited by:
Dongliang Xiong, Huazhong Agricultural University, China

Reviewed by:
Annie Desrochers, Université du Québec en Abitibi Témiscamingue, Canada
Dongmei Yang, Zhejiang Normal University, China

***Correspondence:**
Qing-Wei Wang
wangqingwei@iae.ac.cn
Dapao Yu
yudp2003@iae.ac.cn

Specialty section:
This article was submitted to Plant Physiology, a section of the journal Frontiers in Plant Science

Received: *08 February 2022*
Accepted: *18 March 2022*
Published: *04 May 2022*

Citation:
Han Y, Deng J, Zhou W, Wang Q-W and Yu D (2022) Seasonal Responses of Hydraulic Function and Carbon Dynamics in Spruce Seedlings to Continuous Drought. Front. Plant Sci. 13:868108. doi: 10.3389/fpls.2022.868108

Drought is expected to increase in the frequency and duration associated with climate change. Although hydraulic function and carbon (C) storage have been widely recognized as key components to plant survival under a single drought, the physiological responses to continuous drought remain largely unknown, particularly for high northern temperate and boreal forests which are sensitive to water stress. In this study, we quantified the survival, growth, gas exchange, water relations, and nonstructural carbohydrates (NSCs) in 3-year-old Jezo spruce (*Picea jezoensis*) seedlings responding to continuous drought stress. Seedlings were maintained in drought conditions for 392 days, covering two growing and one dormant winter season. Seedlings subjected to drought showed a significant decrease in net photosynthesis rate (A_{net}) and stomatal conductance (g_s) in both growing seasons, and biomass in the second growing season. The seedling mortality continuously increased to 35.6% at the experimental end. Notably, responses of C storage and leaf water potential to drought varied greatly depending on seasons. Living seedlings exposed to drought and control treatments had similar NSC concentrations in both growing seasons. However, seedlings with concentrations of both the soluble sugars and starch less than 1% in root died in the winter dormant season. In the second growing season, compared with the control treatment, droughted seedlings had significantly lower leaf water potential and stem wood-specific hydraulic conductivity (K_w). Meanwhile, the leaf predawn water potential did not recover overnight. These suggest that C starvation might be an important reason for seedlings that died in the winter dormant season, while in the growing season drought may limit seedling survival and growth through inducing hydraulic failure. Such seasonal dependence in hydraulic dysfunction and C depletion may lead to higher mortality in spruce forests facing extended drought duration expected in the future.

Keywords: northern temperate forests, drought, mortality, C starvation, dormant season, growing season, *Picea jezoensis*

INTRODUCTION

Climate change has been leading to frequent and continuous drought globally (Dai, 2013). Extreme drought events could increase the massive tree mortality, especially in the temperate and boreal regions, where forests are much sensitive to changes in water conditions (Allen et al., 2015). For instance, the 2011 unprecedented drought induced the mortality of more than 300 million trees in the USA (Yan et al., 2022). The severe drought and massive tree mortality would compromise forest ecosystems, the regional ecological security, and the terrestrial carbon (C) sink (McDowell et al., 2020). Thus, understanding the response and adaptation mechanism of trees to continuous drought is crucial to predicting how forest ecosystems and the C-cycle feedbacks respond to climate change (Choat et al., 2018).

Empirical evidence has shown that hydraulic failure is the primary reason for tree mortality induced by drought (Adams et al., 2017), which is resulted from the irreversible dysfunction in xylem water transportation (McDowell et al., 2008). However, tree mortality under continuous drought may be caused by both water and C relation which are interdependent inside trees (McDowell et al., 2008). Continuous drought could not only inhibit tree water transport, leading to severe xylem hydraulic dysfunction before death (López et al., 2021) but also hinder photosynthetic function by inducing embolism in the vascular conduits, consequently reducing nonstructural carbohydrates (NSCs) reserve (Ivanov et al., 2019). In turn, C depletion causes less support for the refilling of the embolisms which is essential for the repair of hydraulic function (Secchi and Zwieniecki, 2011; Tomasella et al., 2019, 2021). The complex relationship between water and C confuses understanding of mechanisms of drought-induced mortality (Gessler et al., 2018). Furthermore, previous studies also reported that these two mechanisms occurred in the same species accounting for tree death, e.g., *Pinus edulis* (Sevanto et al., 2014), while the occurrence timing may depend on the drought stage (Kono et al., 2019). These suggest that the causes of drought-induced mortality vary with drought duration (Mitchell et al., 2013; Kono et al., 2019).

In temperate forests, variation in the season and duration of drought differently affects hydraulic and C dynamics in trees (Gebauer et al., 2020; Charrier et al., 2021). In summer (growing seasons), trees require more water for transpiration and photosynthesis due to relatively high temperatures and active physiological activities (Morales et al., 2021). It leads trees to face a high risk of hydraulic failure (Nardini et al., 2013), accompanied by C depletion under drought conditions during the growing season (McDowell et al., 2008). In winter (dormant seasons), the C reserve is critical for tree survival rather than water transportation because C reserve plays a key role in cold and frost resistance (Charrier et al., 2021), while severe embolism (with percentage loss of conductance (PLC) closed to 100%) is not lethal due to the low transpiration and cessation of water absorption (Christensen-Dalsgaard and Tyree, 2014; Maruta et al., 2020; Mayr et al., 2020). These findings suggest that mechanisms of drought-induced tree mortality interact with seasonality in temperate forest ecosystems. In addition, C accumulation in trees only occurs in the growing season, which is critical for the survival and regrowth of trees in the following seasons (Tixier et al., 2019; D'Andrea et al., 2021). However, most of the studies generally focus on the response of hydraulic and C storage to drought conducted in growing seasons. Up to now, how hydraulic and C storage in trees respond to continuous drought stress across seasons still remains poorly understood (Galvez et al., 2013).

Spruce (*Picea spp.*) is widely distributed in northern temperate and boreal forests (Brenzel, 2001), and is more sensitive to water stress than other conifer species (Kharuk et al., 2015). Drought has been generally considered as a driver to spruce mortality occurring in the world (Schuldt et al., 2020; Obladen et al., 2021). In the last two decades, considerable mortality of Jezo spruce (*Picea jezoensis*) was also observed in Changbai Mountains Natural Reserve (CMNR) in northeast China, the largest primitive temperate forest reserve at the same latitude in the world. The tree-ring data showed that Jezo spruce might suffer from the warming-induced water deficit in the early and late growing season (Yu et al., 2021). To clarify the internal physiological mechanisms, we conducted a 392-day drought manipulation experiment on 3-year-old Jezo spruce seedlings and quantified seedling survival, growth, gas exchange, water relations, and C storage and dynamics responding to continuous drought over two growing and one winter dormant seasons. We explored the following questions: (1) How do the gas exchange, growth, and C and hydraulic of Jezo spruce seedlings respond to continuous drought? (2) Whether the cause of drought-induced mortality of Jezo spruce seedlings varies between seasons during continuous drought in temperate forests?

MATERIALS AND METHODS

Population Distribution Area

The spruce-fir forest, naturally distributing between 1,100 and 1,800 m a.s.l. (above sea level), is one of the main forest types in CMNR in the north temperate climate zone of eastern Eurasia (41°31′-42°28′ N and 127°09′-128°55′ E). The climate here is classified as the temperate continental monsoon climate with the characteristics of warm and rainy summer, and cold and dry winter. The monthly mean temperature ranges between −17.5°C in January and 20.1°C in July. The mean annual precipitation is 680 mm, with 80% of precipitation in the growing season (Yu et al., 2011, 2013).

Experimental Design

In April 2019, we established the experiment at the Changbai Mountain Forest Ecosystem Research Station, Chinese Academy of Sciences. The ambient climate data in the station were shown in **Supplementary Figure S1**.

Three-year-old Jezo spruce seedlings were collected from a local nursery garden and planted into 31 wooden rectangle containers (length × width × height: 120 × 25 × 25 cm) with 7 individuals per container on 30th April 2019. Wooden rectangle containers were placed under a transparent rain roof in a forest gap, avoiding rapid water loss due to strong sunlight exposure. The light condition was similar in different positions under the roof according to condition premeasurement. The soil used in the

TABLE 1 | The seedlings' size before the experiment. Values were mean ± SE. The difference in the size between control and drought was not significant ($p > 0.05$).

Treatment	Stem base diameter/mm	Height/cm
Control ($n = 84$)	3.95 ± 0.67	20.25 ± 3.2
Drought ($n = 132$)	3.98 ± 0.59	21.20 ± 2.81

experiment was obtained from local forests' topsoil without the large stone and roots. Since 5th July 2019, 132 healthy seedlings in 19 containers were not watered throughout the experiment as the drought treatment, while water was continually supplied to the amount of 84 homogeneous seedlings in 12 containers in the control treatment (see the initial seedling status in **Table 1**). The significant difference in the size (stem base diameter and height) between control and drought was not detected ($p > 0.05$).

The experiment period was from 5th July 2019 to 30th July 2020 (392 days in total), including the first growing season (GS2019: D1–D88, 5th July to 30th September), winter dormant season (DP2019: D89–D180, 1st October to 31st December; DP2020: D181–D301, 1st January to 30th April), and the second growing season (GS2020: D302–D392, 1st May to 31st July) referring to Yu et al. (2021). In the dormant season, irrigation was stopped as the stomatal closure and transpiration stopped, referring to previous studies (Fajstavr et al., 2019).

During the drought process, the soil water content was measured with the gravimetric method. The soil water content was determined as the ratio of water weight to the soil sample weight (Piper and Fajardo, 2016). The soil water content was not measured in the winter dormant season due to low evapotranspiration and soil frost in the study area (Yang et al., 2006).

According to the phenology, we harvested seedlings on the D49 (August 2019, the middle growing season), D127 (November 2019, the early dormant period), D270 (March 2020, the late dormant period), and D392 (July 2020, the middle growing season). For each harvest, one container of each treatment was randomly selected, and all living seedlings in that container were sampled and then transported to the laboratory in a cooling box. Collected seedlings were divided into leaves, branches (including stems and twigs), and roots. Samples were dried at 105°C for 30 min to stop the enzymatic activity, then oven-dried at 65°C for 48 h, and finally stored at −20°C for further NSC analyses (Huang et al., 2019).

Measurement of Seedling Mortality

To evaluate the effects of drought on seedlings' survival, we examined seedling mortality weekly during the growing season and biweekly during the dormant season. It is difficult to determine the exact death time of the evergreen species. In this study, dead seedlings were identified when all leaves turned yellow and fallen (referring to previous studies, e.g., Hartmann et al., 2013; Ivanov et al., 2019). The mortality rate of seedlings was counted during the experimental period. In this work, we calculated the mortality rate on the D49, D127, D350, D372, and D392 as:

$$\text{Cumulative mortality rate (\%)} = 100 \times \sum n_i / N \quad (1)$$

where i is the days after the treatment; n_i is the number of dead seedlings from D_1 to D_i; and N is the total number of seedlings of each treatment at the beginning of the experiment.

Measurement of Leaf Water Potential

Leaf predawn water potential (ψ_{pd}) between 3:00 and 4:00 and middy water potential (ψ_{md}) between 12:00 and 13:00 from 4 to 7 living seedlings were measured on sunny days (D17, D47, D349, D370, and D390) using a pressure chamber (PMS1000; Albany, OR, USA; maximum measurement: 8 MPa). One twig from each seedling was selected for the measurement. No repeated measurement was conducted on the same seedling throughout the experiment.

Measurement of Stem Hydraulic Conductivity

The hydraulic conductivity was measured on the same seedlings that were used for leaf water potential measurement at D350, D371, and D391, respectively. The seedlings were cut at the stem base in the next early morning (before sunrise) after leaf water potential measurement. Stems were cut immediately under water to avoid the formation of embolism during sampling, and were transported to the laboratory (<100 m). In the laboratory, the stem segment was recut repeatedly under water at two ends to release the tension. The segment with 7 cm length was used to measure native hydraulic conductivity (K_h, kg m s^{-1} MPa^{-1}). The K_h was measured using a pressure induced by the gravity of a hydraulic head of 50 cm with the 20 mM KCl solution. The K_h was calculated by: $K_h = J_v / (F / L)$, where J_v is the flow rate (kg s^{-1}), F is the gravity-induced driving pressure (MPa), and L is the length of the segment (m). The K_h was divided by the xylem wood area to calculate the stem wood-specific hydraulic conductivity (K_w, kg m^{-1} s^{-1} MPa^{-1}) (Fang et al., 2018).

Measurement of Net Photosynthesis Rate and Stomatal Conductance

Net photosynthesis rate (A_{net}) and stomatal conductance (g_s) were measured between 9:00 and 12:00 on sunny days (D17, D47, D349, D370, and D390). The measurements were done under the ambient light (*c.* 1,000 μmol m^{-2} s^{-1}) and CO_2 concentration (*c.* 400 μmol mol^{-1}). The relative difference in A_{net} and g_s between drought and control was calculated: Relative to control (%) =100 × (Value$_{drought}$ / Mean$_{control}$), where the Value$_{drought}$ is the value of drought seedling and Mean$_{control}$ is the mean value of control at the same time.

Nonstructural Carbohydrates (NSCs) Quantification

Nonstructural carbohydrate (NSC) concentrations (soluble sugars + starch) were quantified according to the standardized protocols by Landhausser et al. (2018). For soluble sugars

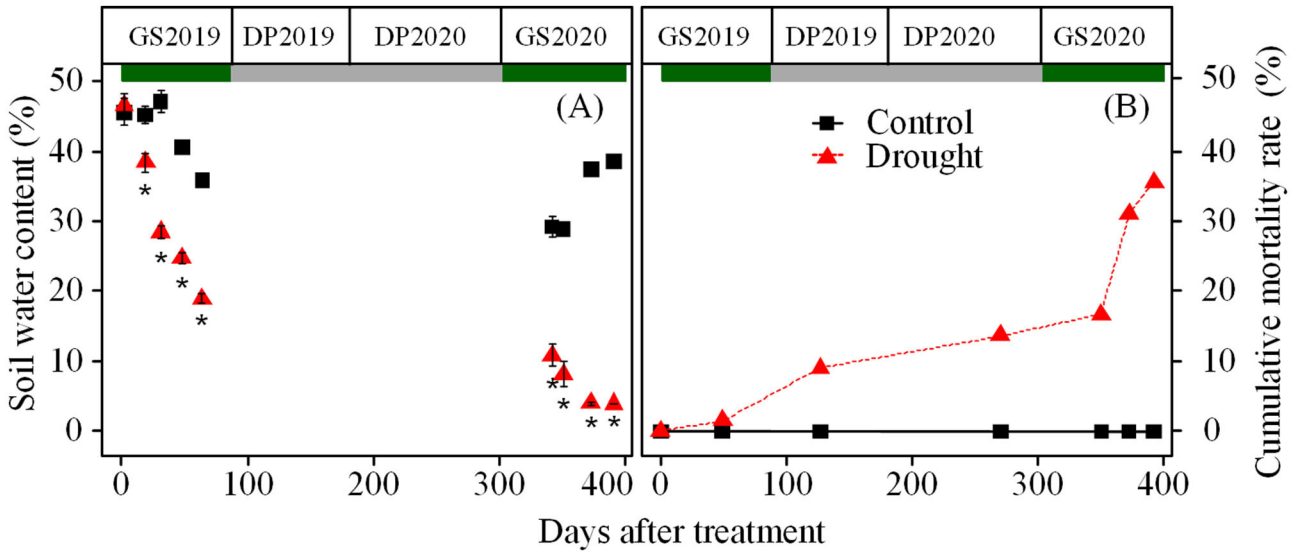

FIGURE 1 | Variation in soil water content **(A)**, and cumulative mortality rate **(B)** over the experimental period. Green and gray rectangles indicate growing and dormant seasons, respectively. GS2019, the first growing season (D1–D88); DP2019 and DP2020, the early and late winter dormant seasons (D89–D180 and D181–D301); and GS2020, the second growing season (D302–D392). Black square and red triangle represent control and drought treatments, respectively. Asterisk indicates a significant difference ($p < 0.05$) in soil water content between control and drought treatments, analyzed using Wilcoxon rank-sum test. Values are mean ± SE ($n = 4$–6) **(A)**.

extraction, approximately 30 mg sample was bathed at 90°C for 10 min after mixing with 1.5 ml 80% (v/v) ethanol. The mixture was centrifuged at 3,500 rpm for 10 min, and the supernatant was used for soluble sugars quantification. For soluble sugars quantification, the solution was colored with phenol-sulfuric and the absorbance was determined at 490 nm with a microplate reader [Multiskan Sky, Thermofisher Scientific (China) Co., Ltd.]. For starch digestion, the pellet after soluble sugars extraction was digested at 85°C for 1 h with the α-amylase from *Aspergillus oryzae* (600 U/ml, Macklin A861434). The supernatant obtained after centrifuging was further digested with amyloglucosidase from *Aspergillus niger* (100 U/ml, Macklin A800618). For starch quantification, the solution color was regulated by peroxidase-glucose oxidase, and the absorbance was determined at 525 nm. Concentrations of soluble sugars, starch, and NSC were expressed as a percentage of dry matter (% d.w.).

Statistical Analysis

Two-way ANOVA was used to analyze the effects of season, drought, and their interaction on concentrations of NSC, soluble sugars, and starch. The difference in variables among control, drought, and dead seedlings was assessed using least significant difference (LSD) with package "agricolae" (Mendiburu, 2021). The difference in soil water content, A_{net}, and g_s between control and drought seedlings was evaluated using Wilcoxon rank-sum test with the package "stats" (R Core Team, 2020). In addition, the difference between ψ_{pd} and ψ_{md} at the same date was evaluated by Wilcoxon rank-sum test. The starch concentration in the root and the K_w were logarithmic (ln) transformed to meet normality and homogeneity before the analysis. Statistical analysis for all data was conducted in R 4.0.0 (R Core Team, 2020).

RESULTS

Response of Seedling Mortality Rate to Continuous Drought

Soil water content in control ranged from 47.1 to 35.8% in the GS2019 and stabled at 38% in the GS2020, but in drought condition rapidly decreased from 47.1 to 19.0% in GS2019 and from 10.8 to 4.0% in the GS2020 (**Figure 1A**). Accordingly, from the DP2019, seedlings exposed to drought showed a considerable increase in cumulative mortality rate toward the experimental end (D392) from 9.1 to 35.6% (**Figure 1B**).

Response of Seedling Growth to Continuous Drought

Effects of continuous drought on seedling biomass varied significantly depending on season and organ. The whole-plant biomass was similar between control and drought treatments in the GS2019 and DP2019 (**Figures 2A,B**), but significantly different in the GS2020 (**Figure 2C**). Seedlings exposed to drought were categorized into living and dead individuals to clarify the detailed response in biomass. Branch biomass of dead but not living individuals was lower than that of seedlings in control in the DP2019 (**Figure 2B**). However, leaf and branch biomass of both living and dead seedlings was significantly lower than those in control in the GS2020 (**Figure 2C** and **Supplementary Table S1**). A similar trend was observed in leaf biomass in the GS2020. Root biomass had no significant variation between treatments and among organs across the experimental period.

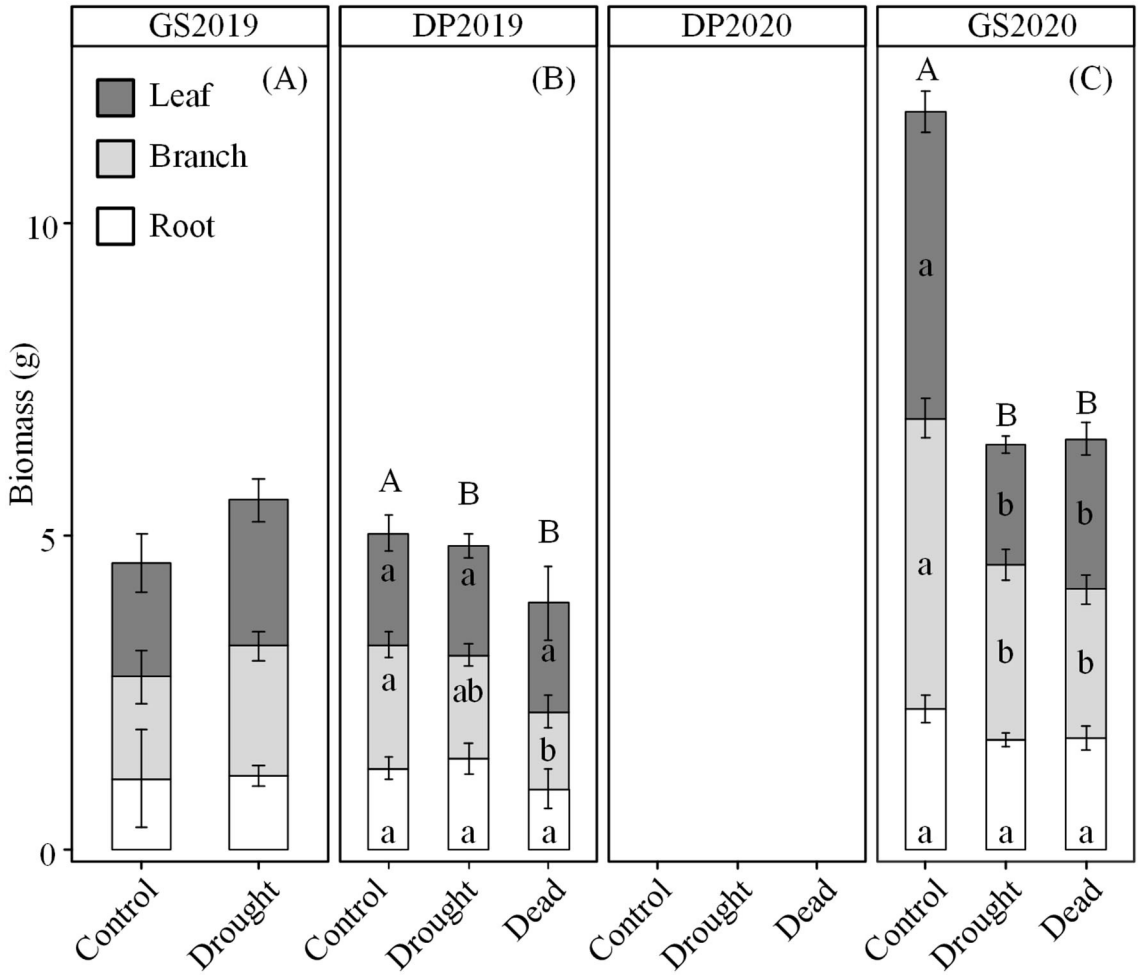

FIGURE 2 | Variation in seedling biomass over the experiment period. **(A)** GS2019, the first growing season (D1–D88); **(B)** DP2019 and DP2020, the early and late winter dormant seasons (D89–D180 and D181–D301); and **(C)** GS2020, the second growing season (D302–D392). In DP2020, the biomass was not measured. Different capital letters indicate significant differences in total biomass among control, drought living, and dead seedlings on the same sampling date. Different lowercase letters indicate significant differences ($p < 0.05$) in leaf (dark gray), branch (light gray), and root (blank) among control, drought living, and dead seedlings on the same sampling date. Values are mean ± SE ($n = 4$–7).

Response of Hydraulic Status to Continuous Drought

Leaf water potential was significantly affected by the interaction between treatment and season (**Figure 3**). Leaf ψ_{pd} and ψ_{md} showed no significant difference between control and drought treatments in the GS2019 (**Figures 3A,B**), while both variables in seedlings exposed to drought were much lower than those to control especially in the middle and late GS2020 (**Figures 3A,B**). Specifically, ψ_{pd} and ψ_{md} significantly decreased from −0.9 and −1.4 MPa on D349 to −4.3 and −4.0 MPa on D390, respectively. ψ_{pd} was significantly higher than ψ_{md} in both control and drought treatments in the GS2019, while ψ_{pd} and ψ_{md} existed no significant difference under drought condition since middle GS2020 (**Figures 3A,B**). In terms of stem hydraulic conductivity, K_w in seedlings exposed to drought was significantly lower than those of control in the middle and late GS2020 (**Figure 3C**). Specifically, K_w was 27.4 and 20.2% of the control on D371 and D391, respectively (**Figure 3C**).

Response of Seedling Gas Exchange to Continuous Drought

Seedlings exposed to drought showed an evident decrease in A_{net} and g_s from the GS2019 to GS2020 (**Figure 4**). A_{net} was significantly lower under drought than control since D17 and accounted for 55.1% of that in control, and reached below zero in the GS2020. g_s under drought had a similar trend with A_{net} since D47. The g_s under drought decreased to 10.6% of that in control at the end of GS2020.

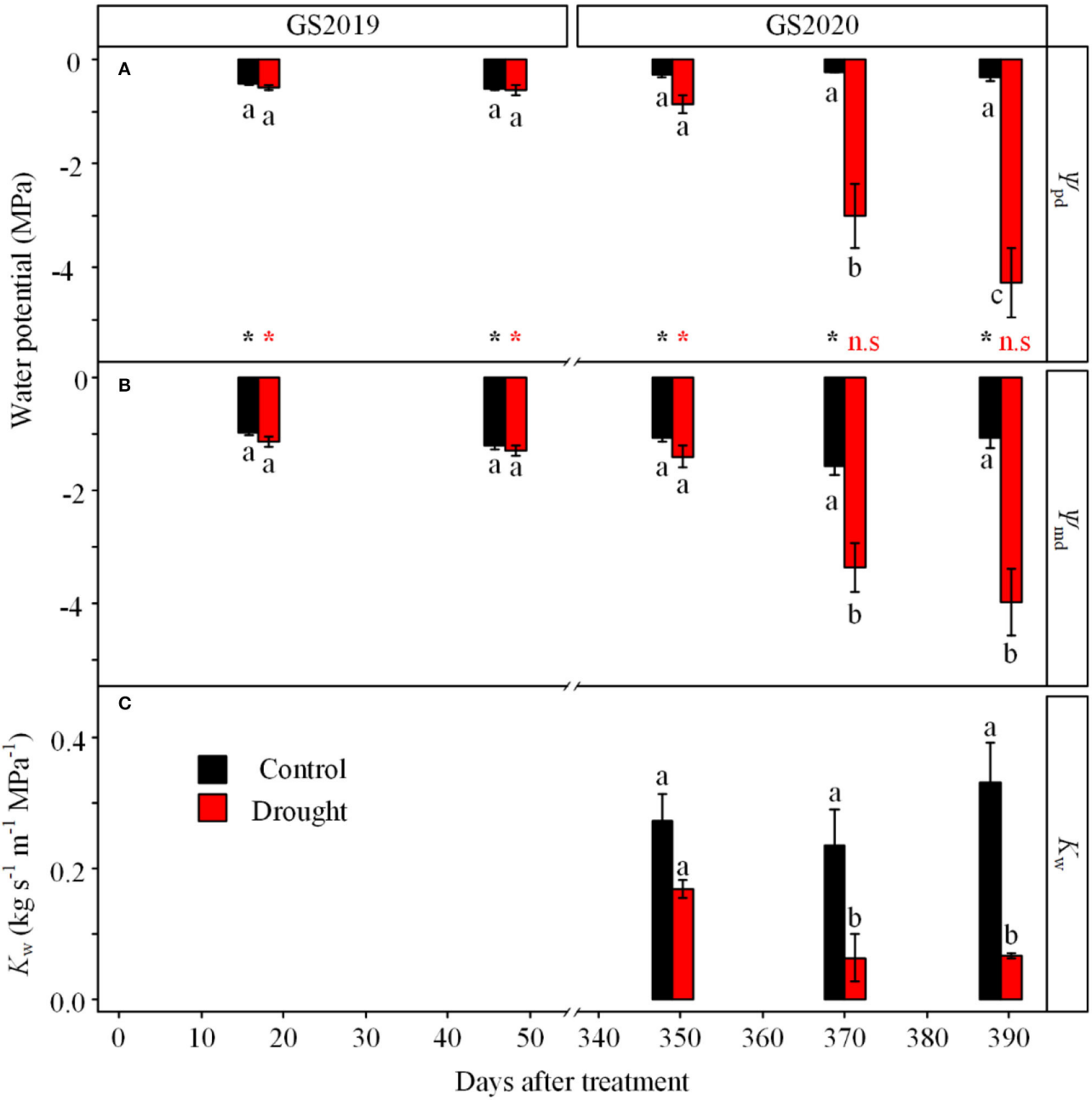

FIGURE 3 | Variation in leaf water potential and stem wood-specific hydraulic conductivity (K_w) in response to continuous drought. Leaf predawn water potential (ψ_{pd}, **A**) and leaf midday water potential (ψ_{md}, **B**) under control (black) and drought (red) treatments were measured in the GS2019 (D1–D88) and GS2020 (D302–D392). Stem wood hydraulic conductivity (K_w, **C**) was measured in the GS2020. Different letters indicate significant differences among all measurement dates and between the two treatments on each measurement date ($p < 0.05$) based on the LSD test. The statistical difference between ψ_{pd} and ψ_{md} on the same measurement date is labeled with (*$p < 0.05$) and n.s. (not significant) at the bottom in **(A)**. Values are mean ± SE ($n = 4$–7).

Response of Seedling C Dynamic to Continuous Drought

Drought treatment, season, and their interaction significantly affected concentrations of NSC and its components, but the effect magnitude depended on organs (**Table 2** and **Supplementary Tables S2–S4**). In two growing seasons, NSC concentrations were similar irrespective of drought treatment or organs (**Figure 5**). The exception was that dead individuals exposed to drought had higher NSC concentrations in leaves than control (**Figure 5J**). However, such response in concentrations of NSC and its components was opposite in woody organs across the winter dormant season (except for leaf in the DP2019).

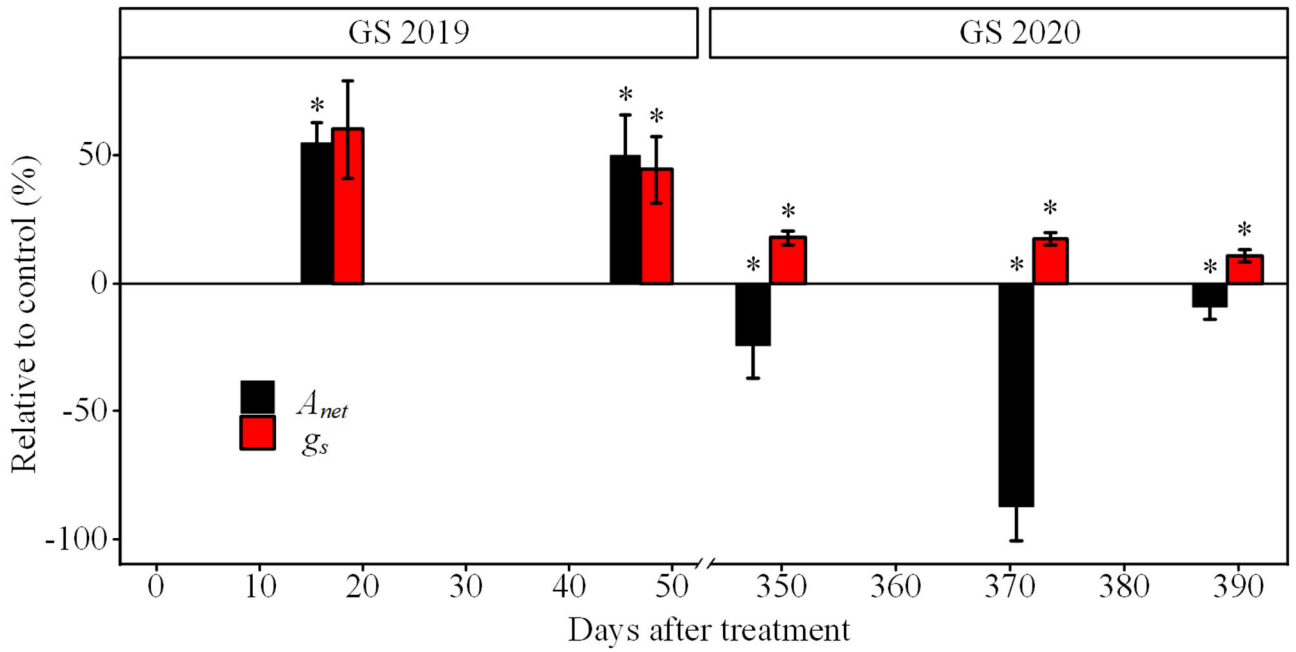

FIGURE 4 | The relative difference in net photosynthetic rate (*Anet*) and stomatal conductance (g_s) of seedlings exposed to drought and control. Asterisk indicates a significant difference between drought and corresponding control treatment on the same measurement date ($p < 0.05$) based on Wilcoxon rank-sum test. GS2019 and GS2020, the first and the second growing seasons (D1–D88 and D302–D392). Values are mean ± SE ($n = 4$–7).

Especially in roots, concentrations of soluble sugars, starch, and NSC for dead individuals from drought averagely reached 0.6, 0.4, and 1.0%, respectively. Meanwhile, the concentrations of soluble sugars, starch, and NSC were 9.8, 15.4, and 11.5% of the control (**Figures 5F,I**).

DISCUSSION

Dynamic of Hydraulic and C Under Continuous Drought

The stomatal closure, one of the earliest reactions to decrease in the soil water (**Figure 4**), reduced the canopy water loss and maintained high water potential in the GS2019 and the early GS2020 (**Figure 3**). This behavior suggests a protective mechanism against embolism (McDowell et al., 2008; Xiong and Nadal, 2020), which is consistent with the finding from another spruce species (*P. abies*) (Hajickova et al., 2021). However, the water loss did not stop due to passive water loss and incomplete stomatal closure (Duursma et al., 2019). Moreover, water loss could be exacerbated by the relatively high temperature in the growing season (Hartmann, 2015; Yan et al., 2020). The ongoing water loss could lead to massive embolism, which constrains xylem water transport (Gebauer et al., 2020). In this study, two results could support the xylem hydraulic dysfunction in the GS2020.

First, drought significantly decreased K_w in the middle and late GS2020 (**Figure 3**). In this study, the K_w in living seedlings exposed to drought reduced *c.* 80% compared to the control, and complete loss of hydraulic conductivity was detected in dead seedlings. This is consistent with the previous results that severe long-term drought led to great damage in stem hydraulic integrity and hydraulic conductivity (Chen et al., 2020; Li et al., 2020).

Second, ψ_{pd} was similar to ψ_{md} in droughted seedlings since D370 (**Figure 3**). ψ_{pd} and ψ_{md} correspond to the daily maximum and minimum leaf water potentials, respectively (Donovan et al., 2001). ψ_{pd} recovers overnight through xylem water transport under normal water conditions (Gleason et al., 2017). Similar values of ψ_{pd} and ψ_{md} in this study suggest that massive embolism impaired water transport. Therefore, the hydraulic dysfunction might be a primary reason for mortality in the GS2020, which has been proven in field trees and potted seedlings in many extreme drought events (Adams et al., 2017; Arend et al., 2021).

Unexpectedly, living seedlings exposed to drought had similar hydraulic conductivity with control at D351 (Jun, 2020). This might indicate that the hydraulic conductance is above the critical threshold (McDowell et al., 2019) since the xylem embolism formed in the winter dormant season might be repaired (Maruta et al., 2020). It is necessary to frequently measure hydraulic dynamics after winter drought in future work.

Under continuous drought, trees may adjust phenology to maintain the C dynamic (Jin et al., 2018). In the GS2020, seedlings exposed to drought showed higher NSC but lower growth than control (**Figures 2**, **5**). It is possible that seedlings sacrificed growth to maintain higher NSC for subsequent C

TABLE 2 | Results of two-way ANOVA for effects of season, drought, and their interaction on concentrations of soluble sugars, starch, and NSC among organs.

Tissue	Factor	*Df*	Sugars		Starch		NSC	
			F	*p*	*F*	*p*	*F*	*p*
Leaf	Season	3	**7.9**	**<0.001**	**30.7**	**<0.001**	**27.8**	**<0.001**
	Drought	2	**5.2**	**0.009**	0.4	0.839	3.1	0.054
	Season × Drought	5	**7.1**	**<0.001**	**13.4**	**0.020**	**16.1**	**<0.001**
Branch	Season	3	**3.5**	**0.023**	**21.8**	**<0.001**	1.4	0.267
	Drought	2	**15.8**	**<0.001**	1.0	0.390	**12.5**	**<0.001**
	Season × Drought	5	**3.8**	**0.006**	**8.6**	**<0.001**	**5.1**	**0.001**
Root	Season	3	7.3	0.063	**5.6**	**0.002**	6.5	0.090
	Drought	2	**7.5**	**0.024**	**27.9**	**<0.001**	**11.7**	**0.003**
	Season × Drought	5	**17.6**	**0.003**	**5.0**	**0.001**	**15.9**	**0.007**

Bold indicates statistical significance ($p < 0.05$).

use (e.g., osmoregulation) (Huang et al., 2021; Luo et al., 2021). In addition, as a drought-defoliation species, Jezo spruce fell off leaves to protect the hydraulic system, which may also stimulate C accumulation in branches and roots (Santos et al., 2022). However, C reserve may be unavailable under drought stress, and less change at the time of death (Sala et al., 2010; Jin et al., 2018; Wiley et al., 2019), which may lead to high-level NSC in drought and dead seedlings (**Figure 5**). Alternatively, seedlings that died in the GS2020 were collected earlier than the drought and control seedlings. The higher NSC in dead seedlings than living seedlings exposed to drought might result from an earlier occurrence of use constraint and (or) the shorter time duration of negative A_{net}.

Seedling Survival and C Reserve in the Winter Dormant Season

The mortality rate increased in the winter dormant season (**Figure 1**), suggesting that droughted seedlings might be more vulnerable in the winter dormant season. The temperature below −32°C is expected to induce frost damage to Jezo spruce (data from https://www.worldplants.ca). The minimum temperature reached −33.7°C during the experiment. Furthermore, the winter drought might aggravate the freezing damage of plants (Charrier et al., 2015; Fernández-Pérez et al., 2018).

Nonstructural carbohydrate (NSC) plays a critical role in drought and cold tolerance of temperate trees (Charrier et al., 2015). In contrast to the growing season, we detected NSC depletion in the roots of dead seedlings in the winter dormant season (**Figure 5**). This is consistent with the results of Galvez et al. (2013), which showed that insufficient NSC reserve in roots might be the primary reason for seedling mortality of two poplar species in the winter dormant season. However, the concentrations of soluble sugars and starch did not decrease to zero in dead seedlings, indicating that there may be a minimum threshold of NSC reserve for tree survival (McDowell, 2011). In this work, NSC concentration in dead seedlings is consistent with the life-threatening NSC level in previous drought studies (Schönbeck et al., 2020), defoliation (Barker Plotkin et al., 2021), and shade (Weber et al., 2018, 2019).

In this study, drought (living) seedlings had higher or similar soluble sugars than control (**Figure 5**). Similar results were also observed in previous studies, e.g., Chuste et al. (2020) and Schönbeck et al. (2020). These support the theory that NSC concentration initially increases and shifts to decrease with drought persisting (McDowell, 2011). It is possible that NSC reserve might increase or be stable during the early drought stage by limiting growth respiration and consuming with drought persisting (McDowell, 2011). In this work, different death times among seedlings under drought treatment might indicate the different exact physiological stress stages among seedlings (Zhang et al., 2021). However, the reason why seedlings exposed to the same drought showed different death times should be further investigated.

The insufficient NSC reserve and severe embolism may threaten tree survival in the winter (Galvez et al., 2013). Since the lack of hydraulic conductivity and PLC data in the winter dormant season, it is unable to assess the direct contribution of hydraulic dysfunction to seedling mortality during the dormant season. However, almost complete loss of hydraulic conductance may not be damaging due to stomatal closure and reduction in water uptake (Beikircher et al., 2016). As shown in previous studies (Ogasa et al., 2019; Mayr et al., 2020), trees that experienced near to 100% PLC in winter recovered growth in the following seasons, suggesting the whole tree and tissues were still alive in the winter dormant season. Thus, future studies are required to explore the appropriate methods for assessing the linkage between tree mortality and hydraulic dysfunction in the winter dormant season under drought stress.

CONCLUSION

This study demonstrated that seedlings subjected to continuous drought showed a significant decrease in net photosynthesis rate, stomatal conductance, and biomass in the second than the

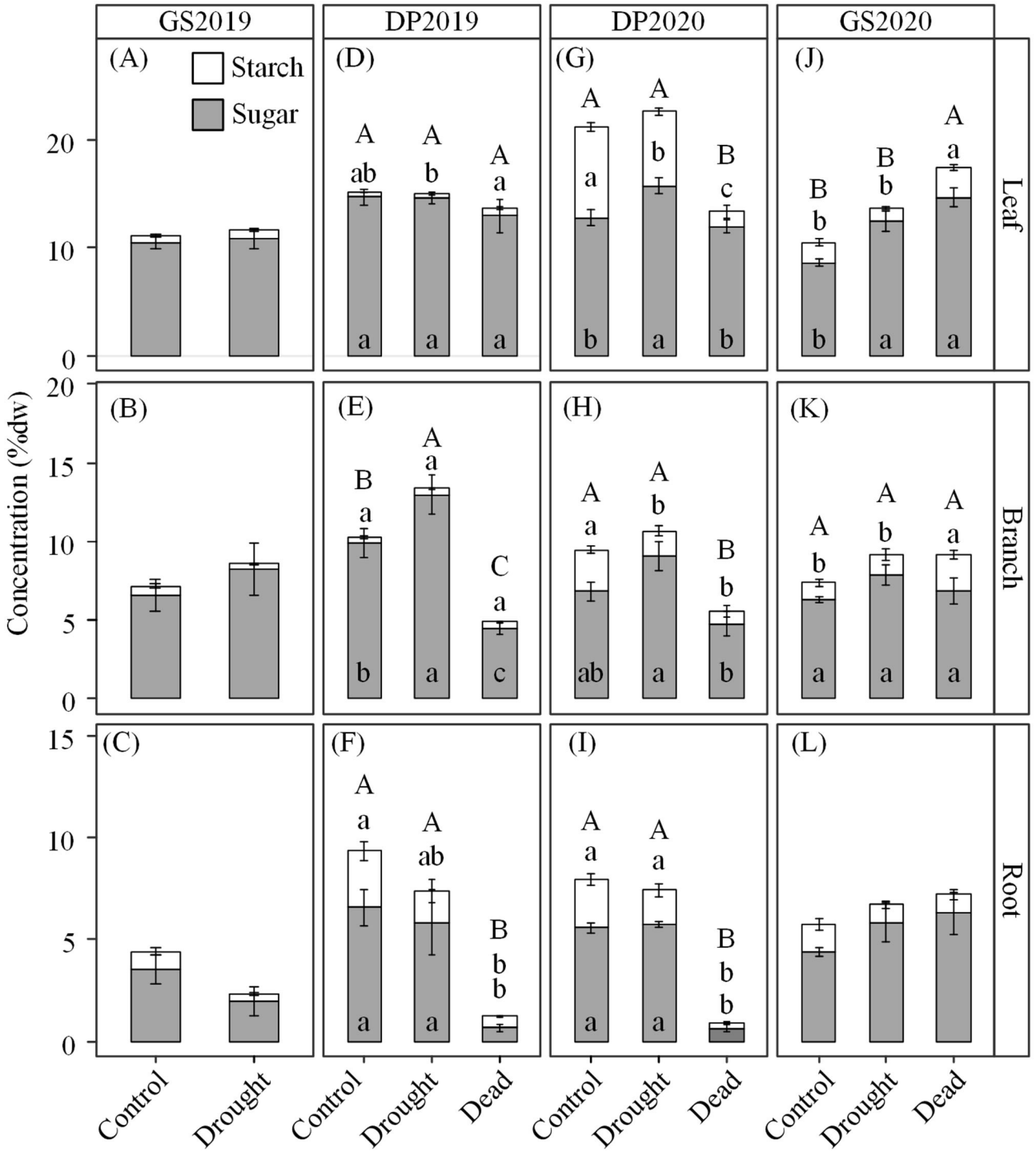

FIGURE 5 | (A–L) Variations in concentrations of nonstructural carbohydrates (NSCs) in each organ under drought treatment over the experimental periods. GS2019, the first growing season (D1–D88); DP2019 and DP2020, the early and late winter dormant seasons (D89–D180 and D181–D301); GS2020, the second growing season (D302–D392). Different capital letters indicate significant differences ($p < 0.05$) in NSC among control, drought living, and dead seedlings. Different lowercase letters indicate significant differences ($p < 0.05$) in soluble sugars (lower) and starch (upper) among control, drought living, and dead seedlings. Gray and blank bars represent the concentrations of soluble sugars and starch, respectively. Result without significant difference was not labeled. Values are mean ± SE ($n = 4–7$).

first growing season, while the seedling mortality continually increased toward the end of the second growing season. Under drought stress, seedlings with root concentrations of both soluble sugars and starch less than 1% died in the winter dormant season. Hydraulic conductivity was significantly lost in the growing season. These suggest that C starvation may partly explain seedling mortality in the winter dormant season, while hydraulic failure may determine seedling survival in following growing seasons with continuous drought. Two processes may interactively cause more tree death in northern temperate forests in the case that the drought duration is projected to extend associated with climate change in the future.

DATA AVAILABILITY STATEMENT

The original contributions presented in the study are included in the article/**Supplementary Material**, further inquiries can be directed to the corresponding authors.

AUTHOR CONTRIBUTIONS

DY and YH made the experimental design. YH conducted the experiment and drafted the manuscript. JD, Q-WW, and WZ improved the manuscript draft. DY and Q-WW revised and finalized the manuscript. All authors contributed to manuscript completion and revision.

FUNDING

This work was supported by the National Natural Science Foundation of China (41871105 and 41971148).

ACKNOWLEDGMENTS

The authors thank Mr. G. Dai for providing help in the preparation of experimental materials; Ms. Q. Ning for providing technical guidance in hydraulic conductivity measurements; Ms. Y. Ma, Y. Zhang, L. Chang, and Mr. D. Chen for providing help in measurement and sampling. The authors thank the editor and two reviewers for their constructive comments and suggestions. The authors also thank everyone who participated in the experiment.

SUPPLEMENTARY MATERIAL

The Supplementary Material for this article can be found online at: https://www.frontiersin.org/articles/10.3389/fpls.2022.868108/full#supplementary-material

REFERENCES

Adams, H. D., Zeppel, M. J. B., Anderegg, W. R. L., Hartmann, H., Landhausser, S. M., Tissue, D. T., et al. (2017). A multi-species synthesis of physiological mechanisms in drought-induced tree mortality. *Nat. Ecol. Evol.* 1, 1285–1291. doi: 10.1038/s41559-017-0248-x

Allen, C. D., Breshears, D. D., and McDowell, N. G. (2015). On underestimation of global vulnerability to tree mortality and forest die-off from hotter drought in the Anthropocene. *Ecosphere* 6, 129. doi: 10.1890/ES15-00203.1

Arend, M., Link, R. M., Patthey, R., Hoch, G., Schuldt, B., and Kahmen, A. (2021). Rapid hydraulic collapse as cause of drought-induced mortality in conifers. *Proc. Natl. Acad. Sci. U. S. A.* 118, e2025251118. doi: 10.1073/pnas.2025251118

Barker Plotkin, A., Blumstein, M., Laflower, D., Pasquarella, V. J., Chandler, J. L., Elkinton, J. S., et al. (2021). Defoliated trees die below a critical threshold of stored carbon. *Funct. Ecol.* 35, 2156–2167. doi: 10.1111/1365-2435.13891

Beikircher, B., Mittmann, C., and Mayr, S. (2016). Prolonged soil frost affects hydraulics and phenology of apple trees. *Front. Plant Sci.* 7, 867. doi: 10.3389/fpls.2016.00867

Brenzel, K. N. (2001). *Western Garden Book*. Menlo Park, CA: Sunset Publishing.

Charrier, G., Martin-StPaul, N., Damesin, C., Delpierre, N., Hanninen, H., Torres-Ruiz, J. M., et al. (2021). Interaction of drought and frost in tree ecophysiology: rethinking the timing of risks. *Ann. For. Sci.* 78, 40. doi: 10.1007/s13595-021-01052-5

Charrier, G., Ngao, J., Saudreau, M., and Ameglio, T. (2015). Effects of environmental factors and management practices on microclimate, winter physiology, and frost resistance in trees. *Front. Plant Sci.* 6, 259. doi: 10.3389/fpls.2015.00259

Chen, X., Zhao, P., Ouyang, L., Zhu, L., Ni, G., and Schäfer, K. V. R. (2020). Whole-plant water hydraulic integrity to predict drought-induced *Eucalyptus urophylla* mortality under drought stress. *For. Ecol. Manage.* 468, 118179. doi: 10.1016/j.foreco.2020.118179

Choat, B., Brodribb, T. J., Brodersen, C. R., Duursma, R. A., Lopez, R., and Medlyn, B. E. (2018). Triggers of tree mortality under drought. *Nature* 558, 531–539. doi: 10.1038/s41586-018-0240-x

Christensen-Dalsgaard, K. K., and Tyree, M. T. (2014). Frost fatigue and spring recovery of xylem vessels in three diffuse-porous trees *in situ*. *Plant Cell Environ.* 37, 1074–1085. doi: 10.1111/pce.12216

Chuste, P.-A., Maillard, P., Bréda, N., Levillain, J., Thirion, E., Wortemann, R., et al. (2020). Sacrificing growth and maintaining a dynamic carbohydrate storage are key processes for promoting beech survival under prolonged drought conditions. *Trees* 34, 381–394. doi: 10.1007/s00468-019-01923-5

Dai, A. (2013). Increasing drought under global warming in observations and models. *Nat. Clim. Chang.* 3, 52–58. doi: 10.1038/nclimate1633

D'Andrea, E., Scartazza, A., Battistelli, A., Collalti, A., Proietti, S., Rezaie, N., et al. (2021). Unraveling resilience mechanisms in forests: role of non-structural carbohydrates in responding to extreme weather events. *Tree Physiol.* 41, 1808–1818. doi: 10.1093/treephys/tpab044

Donovan, L., Linton, M., and Richards, J. (2001). Predawn plant water potential does not necessarily equilibrate with soil water potential under well-watered conditions. *Oecologia* 129, 328–335. doi: 10.1007/s004420100738

Duursma, R. A., Blackman, C. J., Lopez, R., Martin-StPaul, N. K., Cochard, H., and Medlyn, B. E. (2019). On the minimum leaf conductance: its role in models of plant water use, and ecological and environmental controls. *New Phytol.* 221, 693–705. doi: 10.1111/nph.15395

Fajstavr, M., Bednarova, E., Nezval, O., Giagli, K., Gryc, V., Vavrcik, H., et al. (2019). How needle phenology indicates the changes of xylem cell formation during drought stress in *Pinus sylvestris* L. *Dendrochronologia* 56,125600. doi: 10.1016/j.dendro.2019.05.004

Fang, L.-D., Zhao, Q., Liu, Y.-Y., and Hao, G.-Y. (2018). The influence of a five-year nitrogen fertilization treatment on hydraulic architecture of *Pinus sylvestris* var. mongolica in a water-limited plantation of NE China. *For. Ecol. Manag.* 418, 15–22. doi: 10.1016/j.foreco.2017.11.059

Fernández-Pérez, L., Villar-Salvador, P., Martínez-Vilalta, J., Toca, A., and Zavala, M. A. (2018). Distribution of pines in the Iberian Peninsula agrees with

species differences in foliage frost tolerance, not with vulnerability to freezing-induced xylem embolism. *Tree Physiol.* 38, 507–516. doi: 10.1093/treephys/tpx171

Galvez, D. A., Landhäusser, S. M., and Tyree, M. T. (2013). Low root reserve accumulation during drought may lead to winter mortality in poplar seedlings. *New Phytol.* 198, 139–148. doi: 10.1111/nph.12129

Gebauer, R., Plichta, R., Urban, J., Volarik, D., and Hajickova, M. (2020). The resistance and resilience of European beech seedlings to drought stress during the period of leaf development. *Tree Physiol.* 40, 1147–1164. doi: 10.1093/treephys/tpaa066

Gessler, A., Cailleret, M., Joseph, J., Schönbeck, L., Schaub, M., Lehmann, M., et al. (2018). Drought induced tree mortality–a tree-ring isotope based conceptual model to assess mechanisms and predispositions. *New Phytol.* 219, 485–490. doi: 10.1111/nph.15154

Gleason, S. M., Wiggans, D. R., Bliss, C. A., Young, J. S., Cooper, M., Willi, K. R., et al. (2017). Embolized stems recover overnight in *Zea mays*: the role of soil water, root pressure, and nighttime transpiration. *Front. Plant Sci.* 8, 662. doi: 10.3389/fpls.2017.00662

Hajickova, M., Plichta, R., Urban, J., Volarik, D., and Gebauer, R. (2021). Low resistance but high resilience to drought of flushing Norway spruce seedlings. *Tree Physiol.* 41, 1848–1860. doi: 10.1093/treephys/tpab043

Hartmann, H. (2015). Carbon starvation during drought-induced tree mortality–are we chasing a myth? *J. Plant Hydraul.* 2, e005. doi: 10.20870/jph.2015.e005

Hartmann, H., Ziegler, W., Trumbore, S., and Knapp, A. (2013). Lethal drought leads to reduction in nonstructural carbohydrates in Norway spruce tree roots but not in the canopy. *Funct. Ecol.* 27, 413–427. doi: 10.1111/1365-2435.12046

Huang, J., Hammerbacher, A., Gershenzon, J., van Dam, N. M., Sala, A., McDowell, N. G., et al. (2021). Storage of carbon reserves in spruce trees is prioritized over growth in the face of carbon limitation. *Proc. Natl. Acad. Sci. U.S.A.* 118, e2023297118. doi: 10.1073/pnas.2023297118

Huang, J., Hammerbacher, A., Weinhold, A., Reichelt, M., Gleixner, G., Behrendt, T., et al. (2019). Eyes on the future-evidence for trade-offs between growth, storage and defense in Norway spruce. *New Phytol.* 222, 144–158. doi: 10.1111/nph.15522

Ivanov, Y. V., Kartashov, A. V., Zlobin, I. E., Sarvin, B., Stavrianidi, A. N., and Kuznetsov, V. V. (2019). Water deficit-dependent changes in non-structural carbohydrate profiles, growth and mortality of pine and spruce seedlings in hydroculture. *Environ. Exp. Bot.* 157, 151–160. doi: 10.1016/j.envexpbot.2018.10.016

Jin, Y., Li, J., Liu, C., Liu, Y., Zhang, Y., Sha, L., et al. (2018). Carbohydrate dynamics of three dominant species in a Chinese savanna under precipitation exclusion. *Tree Physiol.* 38, 1371–1383. doi: 10.1093/treephys/tpy017

Kharuk, V. I., Im, S. T., Dvinskaya, M. L., Golukov, A. S., and Ranson, K. J. (2015). Climate-induced mortality of spruce stands in Belarus. *Environ. Res. Lett.* 10, 1–10. doi: 10.1088/1748-9326/10/12/125006

Kono, Y., Ishida, A., Saiki, S. T., Yoshimura, K., Dannoura, M., Yazaki, K., et al. (2019). Initial hydraulic failure followed by late-stage carbon starvation leads to drought-induced death in the tree *Trema orientalis*. *Commun. Biol.* 2, 1–9. doi: 10.1038/s42003-018-0256-7

Landhausser, S. M., Chow, P. S., Dickman, L. T., Furze, M. E., Kuhlman, I., Schmid, S., et al. (2018). Standardized protocols and procedures can precisely and accurately quantify non-structural carbohydrates. *Tree Physiol.* 38, 1764–1778. doi: 10.1093/treephys/tpy118

Li, Q., Zhao, M., Wang, N., Liu, S., Wang, J., Zhang, W., et al. (2020). Water use strategies and drought intensity define the relative contributions of hydraulic failure and carbohydrate depletion during seedling mortality. *Plant Physiol. Biochem.* 153, 106–118. doi: 10.1016/j.plaphy.2020.05.023

López, R., Cano, F. J., Rodríguez-Calcerrada, J., Sangüesa-Barreda, G., Gazol, A., Camarero, J. J., et al. (2021). Tree-ring density and carbon isotope composition are early-warning signals of drought-induced mortality in the drought tolerant Canary Island pine. *Agric. For. Meteorol.* 310, 108634. doi: 10.1016/j.agrformet.2021.108634

Luo, N., Villar-Salvador, P., Li, G., and Wang, J. (2021). The dark side of nursery photoperiod reduction on summer plantation performance of a temperate conifer: High winter mortality mediated by reduced seedling carbohydrate and nitrogen storage. *For. Ecol. Manage.* 491, 119171. doi: 10.1016/j.foreco.2021.119171

Maruta, E., Kubota, M., and Ikeda, T. (2020). Effects of xylem embolism on the winter survival of *Abies veitchii* shoots in an upper subalpine region of central Japan. *Sci. Rep.* 10, 6594. doi: 10.1038/s41598-020-62651-2

Mayr, S., Schmid, P., Beikircher, B., Feng, F., and Badel, E. (2020). Die hard: timberline conifers survive annual winter embolism. *New Phytol.* 226, 13–20. doi: 10.1111/nph.16304

McDowell, N., Pockman, W. T., Allen, C. D., Breshears, D. D., Cobb, N., Kolb, T., et al. (2008). Mechanisms of plant survival and mortality during drought: why do some plants survive while others succumb to drought? *New Phytol.* 178, 719–739. doi: 10.1111/j.1469-8137.2008.02436.x

McDowell, N. G. (2011). Mechanisms linking drought, hydraulics, carbon metabolism, and vegetation mortality. *Plant Physiol.* 155, 1051–1059. doi: 10.1104/pp.110.170704

McDowell, N. G., Allen, C. D., Anderson-Teixeira, K., Aukema, B. H., Bond-Lamberty, B., Chini, L., et al. (2020). Pervasive shifts in forest dynamics in a changing world. *Science* 368, 964. doi: 10.1126/science.aaz9463

McDowell, N. G., Brodribb, T. J., and Nardini, A. (2019). Hydraulics in the 21st century. *New Phytol.* 224, 537–542. doi: 10.1111/nph.16151

Mendiburu, F. d. (2021). *agricolae: Statistical Procedures for Agricultural Research*. R package version 1.3–5.

Mitchell, P. J., O'Grady, A. P., Tissue, D. T., White, D. A., Ottenschlaeger, M. L., and Pinkard, E. A. (2013). Drought response strategies define the relative contributions of hydraulic dysfunction and carbohydrate depletion during tree mortality. *New Phytol.* 197, 862–872. doi: 10.1111/nph.12064

Morales, A., López-Bernal, Á., Testi, L., and Villalobos, F. J. (2021). Transpiration and photosynthesis of holm oak trees in southern Spain. *Trees For. People* 5, 100115. doi: 10.1016/j.tfp.2021.100115

Nardini, A., Battistuzzo, M., and Savi, T. (2013). Shoot desiccation and hydraulic failure in temperate woody angiosperms during an extreme summer drought. *New Phytol.* 200, 322–329. doi: 10.1111/nph.12288

Obladen, N., Dechering, P., Skiadaresis, G., Tegel, W., Keßler, J., Höllerl, S., et al. (2021). Tree mortality of European beech and Norway spruce induced by 2018-2019 hot droughts in central Germany. *Agric. For. Meteorol.* 307, 108482. doi: 10.1016/j.agrformet.2021.108482

Ogasa, M. Y., Taneda, H., Ooeda, H., Ohtsuka, A., and Maruta, E. (2019). Repair of severe winter xylem embolism supports summer water transport and carbon gain in flagged crowns of the subalpine conifer *Abies veitchii*. *Tree Physiol.* 39, 1725–1735. doi: 10.1093/treephys/tpz066

Piper, F. I., and Fajardo, A. (2016). Carbon dynamics of Acer pseudoplatanus seedlings under drought and complete darkness. *Tree Physiol.* 36, 1400–1408. doi: 10.1093/treephys/tpw063

R Core Team (2020). *R: A language and Environment for Statistical Computing*. Vienna: R Foundation for Statistical Computing.

Sala, A., Piper, F., and Hoch, G. (2010). Physiological mechanisms of drought-induced tree mortality are far from being resolved. *New Phytol.* 186, 274–281. doi: 10.1111/j.1469-8137.2009.03167.x

Santos, M., Nicodemos, J., and Santos, M. G. (2022). Dynamics of non-structural carbohydrates in a deciduous woody species from tropical dry forests under recurrent water deficit. *Physiol Plant* 174, e13632. doi: 10.1111/ppl.13632

Schönbeck, L., Gessler, A., Schaub, M., Rigling, A., Hoch, G., Kahmen, A., et al. (2020). Soil nutrients and lowered source:sink ratio mitigate effects of mild but not of extreme drought in trees. *Environ. Exp. Bot.* 169, 103905. doi: 10.1016/j.envexpbot.2019.103905

Schuldt, B., Buras, A., Arend, M., Vitasse, Y., Beierkuhnlein, C., Damm, A., et al. (2020). A first assessment of the impact of the extreme 2018 summer drought on Central European forests. *Basic App. Ecol.* 45, 86–103. doi: 10.1016/j.baae.2020.04.003

Secchi, F., and Zwieniecki, M. A. (2011). Sensing embolism in xylem vessels: the role of sucrose as a trigger for refilling. *Plant Cell Environ.* 34, 514–524. doi: 10.1111/j.1365-3040.2010.02259.x

Sevanto, S., McDowell, N. G., Dickman, L. T., Pangle, R., and Pockman, W. T. (2014). How do trees die? A test of the hydraulic failure and carbon starvation hypotheses. *Plant Cell Environ.* 37, 153–161. doi: 10.1111/pce.12141

Tixier, A., Gambetta, G. A., Godfrey, J., Orozco, J., and Zwieniecki, M. A. (2019). Non-structural carbohydrates in dormant woody perennials; the

tale of winter survival and spring arrival. *Front. For. Glob. Chang.* 2, 18. doi: 10.3389/ffgc.2019.00018

Tomasella, M., Casolo, V., Natale, S., Petruzzellis, F., Kofler, W., Beikircher, B., et al. (2021). Shade-induced reduction of stem non-structural carbohydrates increases xylem vulnerability to embolism and impedes hydraulic recovery in *Populus nigra*. *New Phytol.* 231, 108–121. doi: 10.1111/nph.17384

Tomasella, M., Petrussa, E., Petruzzellis, F., Nardini, A., and Casolo, V. (2019). The possible role of non-structural carbohydrates in the regulation of tree hydraulics. *Int. J. Mol. Sci.* 21, 1–20. doi: 10.3390/ijms21010144

Weber, R., Gessler, A., and Hoch, G. (2019). High carbon storage in carbon-limited trees. *New Phytol.* 222, 171–182. doi: 10.1111/nph.15599

Weber, R., Schwendener, A., Schmid, S., Lambert, S., Wiley, E., Landhausser, S. M., et al. (2018). Living on next to nothing: tree seedlings can survive weeks with very low carbohydrate concentrations. *New Phytol.* 218, 107–118. doi: 10.1111/nph.14987

Wiley, E., King, C., and Landhausser, S. M. (2019). Identifying the relevant carbohydrate storage pools available for remobilization in aspen roots. *Tree Physiol.* 39, 1109–1120. doi: 10.1093/treephys/tpz051

Xiong, D., and Nadal, M. (2020). Linking water relations and hydraulics with photosynthesis. *Plant J.* 101, 800–815. doi: 10.1111/tpj.14595

Yan, M., Liu, Z., Subei, M. R., Liang, L., and Xi, W. (2022). The complex impacts of unprecedented drought on forest tree mortality: a case study of dead trees in east Texas, USA. *Acta Ecol. Sin.* 42, 1034–1046. doi: 10.5846/stxb202101150152

Yan, W., Zhong, Y., and Shangguan, Z. (2020). Elevated temperature exacerbates the effects of drought on the carbon and hydraulic characteristics of *Robinia pseudoacacia* seedlings. *Agric. For. Meteorol.* 280, 107794. doi: 10.1016/j.agrformet.2019.107794

Yang, H., Pei, T., Guan, D., Jin, C., and Wang, A. (2006). Soil moisture dynamics under broad-leaved Korean pine f orest in Changbai Mountains. *Chin. J. Appl. Ecol.* 17, 587–591. doi: 10.13287/j.1001-9332.2006.0119

Yu, D., Liu, J., Benard, J., L., Zhou, L., Zhou, W., et al. (2013). Spatial variation and temporal instability in the climate–growth relationship of Korean pine in the Changbai Mountain region of Northeast China. *For. Ecol. Manage.* 300, 96–105. doi: 10.1016/j.foreco.2012.06.032

Yu, D., Wang, Q., Wang, Y., Zhou, W., Ding, H., Fang, X., et al. (2011). Climatic effects on radial growth of major tree species on Changbai Mountain. *Ann. For. Sci.* 68, 921–933. doi: 10.1007/s13595-011-0098-7

Yu, J., Chen, J., Meng, S., Zhou, H., Zhou, G., Gao, L., et al. (2021). Response of radial growth of *Pinus sylvestriformis* and *Picea jezoensis* to climate warming in the ecotone of Changbai Mountain,Northeast China. *Chin. J. Appl. Ecol.* 32, 46–56. doi: 10.13287/j.1001-9332.202101.004

Zhang, P., McDowell, N. G., Zhou, X., Wang, W., Leff, R. T., Pivovaroff, A. L., et al. (2021). Declining carbohydrate content of Sitka-spruce trees dying from seawater exposure. *Plant Physiol.* 185, 1682–1696. doi: 10.1093/plphys/kiab002

Conflict of Interest: The authors declare that the research was conducted in the absence of any commercial or financial relationships that could be construed as a potential conflict of interest.

Publisher's Note: All claims expressed in this article are solely those of the authors and do not necessarily represent those of their affiliated organizations, or those of the publisher, the editors and the reviewers. Any product that may be evaluated in this article, or claim that may be made by its manufacturer, is not guaranteed or endorsed by the publisher.

frontiers | Frontiers in Plant Science

ORIGINAL RESEARCH
published: 06 May 2022
doi: 10.3389/fpls.2022.873036

Leaf Venation Architecture in Relation to Leaf Size Across Leaf Habits and Vein Types in Subtropical Woody Plants

*Guoquan Peng[1], Yingjie Xiong[1], Mengqi Yin[1], Xiaolin Wang[1], Wei Zhou[1], Zhenfeng Cheng[1], Yong-Jiang Zhang[2] and Dongmei Yang[1]**

[1] College of Chemistry and Life Sciences, Zhejiang Normal University, Jinhua, China, [2] School of Biology and Ecology, University of Maine, Orono, ME, United States

Leaves are enormously diverse in their size and venation architecture, both of which are core determinants of plant adaptation to environments. Leaf size is an important determinant of leaf function and ecological strategy, while leaf venation, the main structure for support and transport, determines the growth, development, and performance of a leaf. The scaling relationship between venation architecture and leaf size has been explored, but the relationship within a community and its potential variations among species with different vein types and leaf habits have not been investigated. Here, we measured vein traits and leaf size across 39 broad-leaved woody species within a subtropical forest community in China and analyzed the scaling relationship using ordinary least squares and standard major axis method. Then, we compared our results with the global dataset. The major vein density, and the ratio of major (1° and 2°) to minor (3° and higher) vein density both geometrically declined with leaf size across different vein types and leaf habits. Further, palmate-veined species have higher major vein density and a higher ratio of major to minor vein density at the given leaf size than pinnate-veined species, while evergreen and deciduous species showed no difference. These robust trends were confirmed by reanalyzing the global dataset using the same major vein classification as ours. We also found a tradeoff between the cell wall mass per vein length of the major vein and the major vein density. These vein scaling relationships have important implications on the optimization of leaf size, niche differentiation of coexisting species, plant drought tolerance, and species distribution.

Keywords: leaf habit, leaf size, leaf vein type, scaling relationship, subtropical forest, vein density, vein distribution

OPEN ACCESS

Edited by:
Dongliang Xiong, Huazhong Agricultural University, China

Reviewed by:
Yajun Chen, Xishuangbanna Tropical Botanical Garden (CAS), China
Jun Sun, Fujian Normal University, China

***Correspondence:**
Dongmei Yang
yangdm@zjnu.cn

Specialty section:
This article was submitted to Plant Physiology, a section of the journal Frontiers in Plant Science

Received: *10 February 2022*
Accepted: *21 March 2022*
Published: *06 May 2022*

Citation:
Peng G, Xiong Y, Yin M, Wang X, Zhou W, Cheng Z, Zhang Y-J and Yang D (2022) Leaf Venation Architecture in Relation to Leaf Size Across Leaf Habits and Vein Types in Subtropical Woody Plants. Front. Plant Sci. 13:873036. doi: 10.3389/fpls.2022.873036

INTRODUCTION

The leaf is the main organ of photosynthesis in higher plants and a critical component in the plant water transport system, which accounts for 30% or more of whole-plant hydraulic resistance (Sack and Holbrook, 2006). Leaf size is an important determinant of plant physiological function and ecological strategy. It reflects the efficiency of light interception and the ability of carbon capture

in plants (Parkhurst and Loucks, 1972; Givnish and Vermeij, 1976). Leaf size also shapes the tradeoff between carbon assimilation and water use efficiency, which is crucial for leaf temperature regulation under different climatic conditions (Michaletz et al., 2014; Fauset et al., 2018; Li et al., 2020). Leaf venation is the main structure for physical support and water/nutrient transport in the leaf, which has an important role in maintaining the growth and development of a leaf. It also transports photosynthate and signal molecules from the mesophyll to the rest of the plant. Thus, leaf venation is strongly related to the leaf hydraulic conductance, gas exchange rates, and plant performance (Niklas, 1999; Sack and Holbrook, 2006; Sack et al., 2012, 2013). The leaf hydraulic conductance (K_{leaf}) is determined by the conductance of a series of the xylem (K_x) and outside-xylem pathways (K_{ox}). The vein density is a determinant of both K_x and K_{ox} because higher densities provide more numerous xylem flow pathways that are parallel per leaf area and shorten pathways for water movement outside the xylem (Cochard et al., 2004; Sack and Frole, 2006; Brodribb et al., 2007; McKown et al., 2010). The higher vein densities and conductivities are expected to be adaptations to higher-resource conditions (Sack et al., 2005; McKown et al., 2010), and large leaves are predominant in moister and/or shaded habitats (Givnish, 1987; Fonseca et al., 2000). Smaller leaves and higher major vein densities are more frequent in dry habitats (Givnish, 1987; Ackerly, 2004; Scoffoni et al., 2011). In addition, the development of the algorithm for vein formation during leaf expansion also provides the basis correlation for vein trait and leaf size (Sack and Scoffoni, 2013). Hence, leaf venation has an important role in the optimization of leaf size. In addition, the variation of leaf size would be closely related to leaf venation architecture.

The scaling of vein traits with leaf size across species has been explored by several studies, but not systematically (except for Sack et al., 2012, 2013). Hence, the conclusions are not consistent. Previous studies with fewer species ($\leq$10) found a negative correlation between major vein density and leaf size, while no relationship between minor vein density and leaf size was found in most studies (Sack et al., 2008; Dunbar-Co et al., 2009; Scoffoni et al., 2011). However, Walls (2011) showed a weak relationship (R^2 = 0.11). Then, Price et al. (2012) showed that vein density was independent of leaf size by using an automated analysis of low-resolution images, but did not distinguish vein orders in 339 species collected from the National Cleared Leaf Collection at the Museum of Natural History, Smithsonian Institution. Another study analyzed 485 globally distributed species with new, high-resolution measurements of vein systems (Sack et al., 2012). They found that larger leaves had major veins with larger diameters, but lower major vein density. Meanwhile, minor vein traits were independent of leaf size, and total leaf vein density was not related to leaf size for both palmate-veined (multiple 1° veins) and pinnate-veined (with a single 1° veins) species. These inconsistent conclusions were not only because of the different image resolutions of leaf venation, but also the different classification standards of major veins and minor veins. In Sack et al. (2012), the major vein included 1°, 2°, and 3° veins, while the minor veins were defined as all more higher-order veins (Sack et al., 2012). In contrast, Price et al. (2012) did not distinguish vein orders. However, the major vein might also be defined based on different formation timing and the gene expression during development (Haritatos et al., 2000; Evert, 2006). Based on the newly developed synthetic model for the development of vein hierarchy, the formation of 1° and 2° veins coincides with the first slow phases, while most 3° and higher-order veins form during the rapid expansion phase (Sack et al., 2012). Hence, it could be reasonable to define the major vein as the sum of 1° and 2° veins, and the minor veins as the 3° and higher-order veins. This classification is the same as in Ellis et al. (2009) and Walls (2011), which will be used in this study. To the best of our knowledge, although the scaling relationship between leaf venation architecture and leaf size has been studied within the given genera and families and at the global level, it has not been investigated within a community sharing similar environmental conditions. It is not clear if this general scaling relationship is conserved across species that coexist in a community.

The major and minor veins differ in the timing of development and xylem and phloem formation (Sack et al., 2012; Sack and Scoffoni, 2013). The variation in the ratio of major to minor vein density could affect leaf hydraulic conductance and vulnerability to cavitation (Scoffoni et al., 2011). Hence, the ratio of major to minor vein density should be considered because even within species with the same total vein density and leaf size, leaf vein distribution could be different. Additionally, the major vein continually thickens with the increase of the leaf size, while the diameter of the minor vein quickly reaches the maximum and is kept constant with the further increase in leaf size (Sack et al., 2012). Thus, the construction cost of extending the major vein and minor vein should be different. Also, the cell wall mass of veins should be considered when studying the scaling relationship between vein architecture and leaf size. These will be helpful for us to understand the covariant relationship of leaf venation structure with leaf size.

In addition, species with different vein types (palmate- vs. pinnate-veined) have different numbers of midribs, resulting in different major vein densities and tolerance to vein damages (Sack et al., 2008; Scoffoni et al., 2011). Species with different leaf habits (*i.e.,* evergreen versus deciduous species) also present significant differences in leaf size, leaf mass per area (LMA), vessel size, photosynthesis, and stress tolerance (Cavender-Bares and Holbrook, 2001; Wright et al., 2004; Yang et al., 2008). Therefore, leaf habits and leaf vein types might also change the general scaling relationship.

Here, we measured leaf size, leaf vein length, and leaf vein cell wall dry mass across 39 broad-leaved woody species within a subtropical forest community in Tiantong National Forest Park of China. These species belong to 27 genera in 18 families, including different leaf habits and leaf vein types, with leaf sizes ranging from 7.68 to 196.00 cm^2. We aimed to (1) test whether the general scaling relationship of leaf vein density with leaf size holds across species within a community, (2) determine whether the ratio of major to minor vein density and vein cell wall mass per length are also related to leaf size, and (3) test whether the scaling exponents are consistent between different leaf habits and different leaf vein-type species.

Additionally, we compiled the global dataset from Sack et al. (2012), redefined the major vein and minor vein as we did in this study, and reanalyzed and compared the scaling relationship between our data and data from Sack et al. (2012). This comprehensive study on the scaling trends of leaf venation with leaf size would provide a fundamental understanding of the adaptive significance of leaf size and venation and their ecological strategies.

MATERIALS AND METHODS

Study Sites and Leaf Materials

Leaf materials were collected from 39 broad-leaved woody species (including 8 palmate-veined deciduous, 7 pinnate-veined deciduous, and 24 pinnate-veined evergreen species) in an evergreen broad-leaved forest of Tiantong National Forest Park, China (29°48′ N, 121°47′ E) on August 2019 when leaf expansion was completed. In all collected species, there were only a few that were not native species, but have been planted for many years in the park. The study site has a subtropical monsoon climate. The mean annual temperature and precipitation from 2012 to 2017 was approximately 16.6°C and 1824.4 mm, respectively. The meteorological data were from the Zhejiang Tiantong Forest Ecosystem National Observation and Research Station.

For each species, four to five healthy adult individuals within a similar environment were selected, and three to five random branches with tips at the outer edge of the middle layer of the plant crown were chosen. Healthy, undamaged, and fully developed current-year leaves located on the third or fourth leaf position were sampled for venation architecture and leaf traits measurements.

Vein Systems Analysis

One leaf per branch from three branches on each of five individuals was collected. Therefore, a total of 15 leaves per species were used for vein system measurements. The leaf vein orders were classified and divided into major (including 1° and 2° veins) and minor veins (3° veins and higher-order veins) according to Ellis et al. (2009), Walls (2011). Firstly, cleaned fresh leaves were scanned using a scanner (LiDE 300, Canon, Vietnam), and leaf area and the length of 1° and 2° veins in each leaf were measured by ImageJ 18.0 (National Institutes of Health[1]). Secondly, all leaves were chemically cleared with 5% NaOH solution and boiled in a water bath with a constant temperature for 20–30 min. Then, 1-cm^2-sized samples (avoiding 1° and 2° veins as much as possible) were cut from symmetrical locations of the tip, middle, and bottom of the leaves (6 samples per leaf, 15 leaves per species, see **Supplementary Figure 1**) and bleached in 5% NaClO solution, then stained with an alcoholic solution of toluidine blue (3%) overnight. The above protocols were similar to other studies (Scoffoni et al., 2011; Sack et al., 2012; Petruzzellis et al., 2019). Finally, three images of each sample (a total of 18 images per leaf) were obtained with a digital camera (Leica, DFC7000 T, Germany) mounted on an optical microscope (Leica, DM6B Wetzlar, Germany) at 40 × magnification. Then, minor vein length was measured using the phenoVein software with manual correction (Bühler et al., 2015). The major and minor vein densities were calculated by dividing leaf area with vein length in major and minor veins, respectively. The ratio of major to minor vein density was obtained by the major vein length divided by the minor vein length.

[1]https://imagej.nih.gov/ij/

Leaf Vein Cell Wall Mass Analysis

One leaf on a sun-exposed branch from each of the same five individuals measured for vein architecture was collected for leaf vein cell wall mass measurements (cell wall mass denotes cell wall dry mass except where we specifically mentioned fresh mass). After scanning and measuring the leaf area, the leaves were chemically cleared with the same protocols as described above for vein systems. Then, the leaves were washed with deionized water and dried with absorbent paper. Then, 1°, 2°, and minor veins were separated from the cleared leaves with scissors and tweezers before the fresh mass was measured with an analytical balance (±0.1 mg, Mettler Toledo, XPE 205, Switzerland). For the leaf vein cell wall extraction, we used the same protocol as Wang et al. (2017). Briefly, the weighted fresh vein was transferred to a centrifuge tube that was injected with 75% ethanol, and the samples were ground to homogenate with a grinder (70 Hz, 2 min). Then, the homogenates were washed into a 50 ml centrifuge tube with 75% ethanol and kept in an ice-cold bath for 20 min. Later, the homogenates were centrifuged at 1,000 RPM for 10 min, and sediments were washed according to a sequence of 1:7 (vein fresh mass/volume) of ice-cold acetone, methanol-chloroform mixture (1:1, V/V), and methanol. The supernatant in each washing was discarded, and the final deposit was dried in an oven at 70°C for 48 h. The dry mass of the powder is the vein cell wall mass, hence the cell wall mass of 1°, 2°, and minor veins were separately obtained. Except for vein traits mentioned above, the other current-year leaves located on the third or fourth leaf positions of selected branches were collected. Then, the leaf area and leaf mass were obtained for calculation of (LMA).

Ideally, the vein cell wall mass and vein length should be measured at the same leaf area to get the vein cell mass per vein length. However, we used different leaves with different leaf areas for these two measurements. Hence, the vein cell wall mass was converted proportionally to the corresponding vein cell wall mass in the leaf area that was used for measuring vein length for each branch in each species. Based on the LMA values, the same proportional conversion was performed for obtaining the leaf mass of the same leaf area that was used for vein length measurements. In this way, all traits were obtained with the same leaf area that was measured for vein length in each species. For ensuring that the vein cell wall mass conversion was correct, we tested the scaling relationship of vein cell wall mass with leaf area across species. Since the scaling exponents were not different between original vein cell wall mass measurements and converted data with the same leaf area in the vein length measurements, we confirmed that the conversion was correct. The leaf area of each species in the two measurements was similar. Particularly, the points were on the 1:1 line, and the slope did not deviate from 1.0 (R^2 = 0.93).

Data Analyses

Preliminary regression analyses showed that all bivariate relationships were log-log linear. Thus, $\log_{10}$-transformed data were used in all statistical analyses for scaling relationships. The bivariate relationship was described by the equation $y = ax^b$, where x and y were two traits and a and b represented the intercept and slope of the linear relationship. We followed the other published papers on vein architecture and leaf trait studies in using ordinary least squares (OLS) or standard major axis (SMA) linear regression for fitting the data. They mainly depended on the calculation of the given trait and thus its relative level of measurement error (Niklas, 1994; Smith, 2009; Scoffoni et al., 2011; Price et al., 2012; Sack et al., 2012). The SMA is preferred for allometric scaling analyses, particularly when the measurement error in both variables is proportional and when there is no dependent variable (Warton et al., 2006). Furthermore, when measurement error in the ordinate variable is significantly higher than in the abscissa variable, the results analyzed by SMA are not as accurate as that in the OLS (Kimura, 1992; Sack et al., 2012). Therefore, for the scaling relationship of vein traits with leaf size, we used OLS, and alternatively, we used SMA. We noted that for most of the relationships, the directions of the relationships were not different regardless of using SMA or OLS, and the scaling exponents were similar when the correlation coefficients were high. The analysis of scaling relationships was conducted using Standardised Major Axis Tests and Routines (SMATR) (Falster et al., 2006), and confidence intervals for individual regression slopes were calculated following Pitman (1939). The common slops were obtained where homogeneity of slopes was demonstrated based on the methods of Warton and Weber (2002). Then, the differences in elevation of regression lines (y-intercept) were tested as in standard analysis of covariance (ANCOVA) (Wright and Westoby, 2002; Westoby and Wright, 2003; Yang et al., 2009).

Phylogenetically independent contrasts (PIC) were also performed for analyzing the correlation between functional traits throughout their phylogeny. The phylogenetic tree was constructed using PHYLOMATIC, which is based on the Angiosperm Phylogeny Group III classification of angiosperms (APG III[2]). The PIC analysis was conducted using the "ape" package (Paradis et al., 2004) in R 4.1.0 version.

To test trait differences between species groups of this study, the t-test was performed. The partial correlation analysis was performed for the intercorrelated relationship among the major vein density, the ratio of major to minor vein density, and leaf size across species, testing the relationship between two variables while holding the third variable constant (Scoffoni et al., 2011).

The global dataset (from Sack et al., 2012) was reanalyzed based on the same definition of major and minor veins as ours, so that the data are comparable. There were 485 species in the global dataset, including data from previous literature (36 species) and original data from their study, which had 410 of 449 species collected from the Daniel I. Axelrod cleared leaf image collection (Museum of Paleontology of the University of California, Berkeley, California). We extracted species in two ways. One contained detailed data of major and minor veins (63 species, called "Sack's data") to compare with our data. The other included all species from Axelrod, which accounted for most of the global dataset, including 1° and 2° but not more than 3° veins. Thus, we can get major vein data (401species) from Axelrod (called "Axelrod's data") to compare with ours or Sack's data. In addition, because there was no significant difference in the y-intercept of major vein density and the ratio of major to minor vein density vs. leaf area between evergreen and deciduous species within pinnate-veined species in our results, only venation type species were separately analyzed when comparing with Sack's data or Axelrod's data.

[2]http://phylodiversity.net/phylomatic/

RESULTS

Relationships Between Leaf Vein Density and Leaf Size

In the current study, the leaf size ranged from 7.69 to 196.00 cm^2, with a considerable range in total vein density from 52.04 to 122.54 cm^{-1}. Detailed functional traits can be found in **Supplementary Table 1**.

A strong negative correlation between the major vein density and leaf area in palmate-veined deciduous, pinnate-veined deciduous, and pinnate-veined evergreen species groups was found (all $R^2 > 0.824$), with a common slope of –0.525 [95% confidence interval (CI) –0.576, –0.450, $p = 0.158$], which did not differ significantly from –0.5 (**Figure 1A** and **Table 1**). The same result was found when leaf size was represented by lamina mass with a common slope of –0.453 (95% CI –0.561, –0.328, $p = 0.517$) (**Table 1**). These results indicated that the major vein density geometrically declined with leaf size. However, palmate-veined deciduous species had a significantly higher y-intercept than both the pinnate-veined deciduous and evergreen species ($p < 0.01$, **Figure 1A** and **Table 1**), suggesting that the palmate-veined species have a greater major vein density at the given leaf area than in the pinnate-veined species. However, deciduous and evergreen species showed no difference within the same pinnated-veined vein type. By contrast, the density of minor veins was independent of leaf size, as was the total vein density (**Figure 1B** and **Table 1**). The correlation between the major vein density and leaf size was also significant when expressed as correlated evolutionary divergences (**Table 2**).

Vein length was significantly and positively related to leaf area within each species group (all $R^2 > 0.827$). The slope of vein length vs. leaf area was not different among species groups, with the common slope 0.461 (95% CI 0.412, 0.545, $p = 0.072$) and 0.970 (95% CI 0.856, 1.053, $p = 0.202$) for major and minor veins, respectively (**Figures 1C,D** and **Table 1**). The palmate-veined deciduous species were significantly greater in the vein length than two pinnate-veined group species at the same leaf area ($p < 0.01$, y-intercept in **Figures 1C,D** and **Table 1**), indicating that the major and minor vein lengths were both significantly larger in palmate-veined species than in pinnate-veined species. The result of the PIC analysis also showed a positive correlation between correlated evolutionary divergences (**Table 2**).

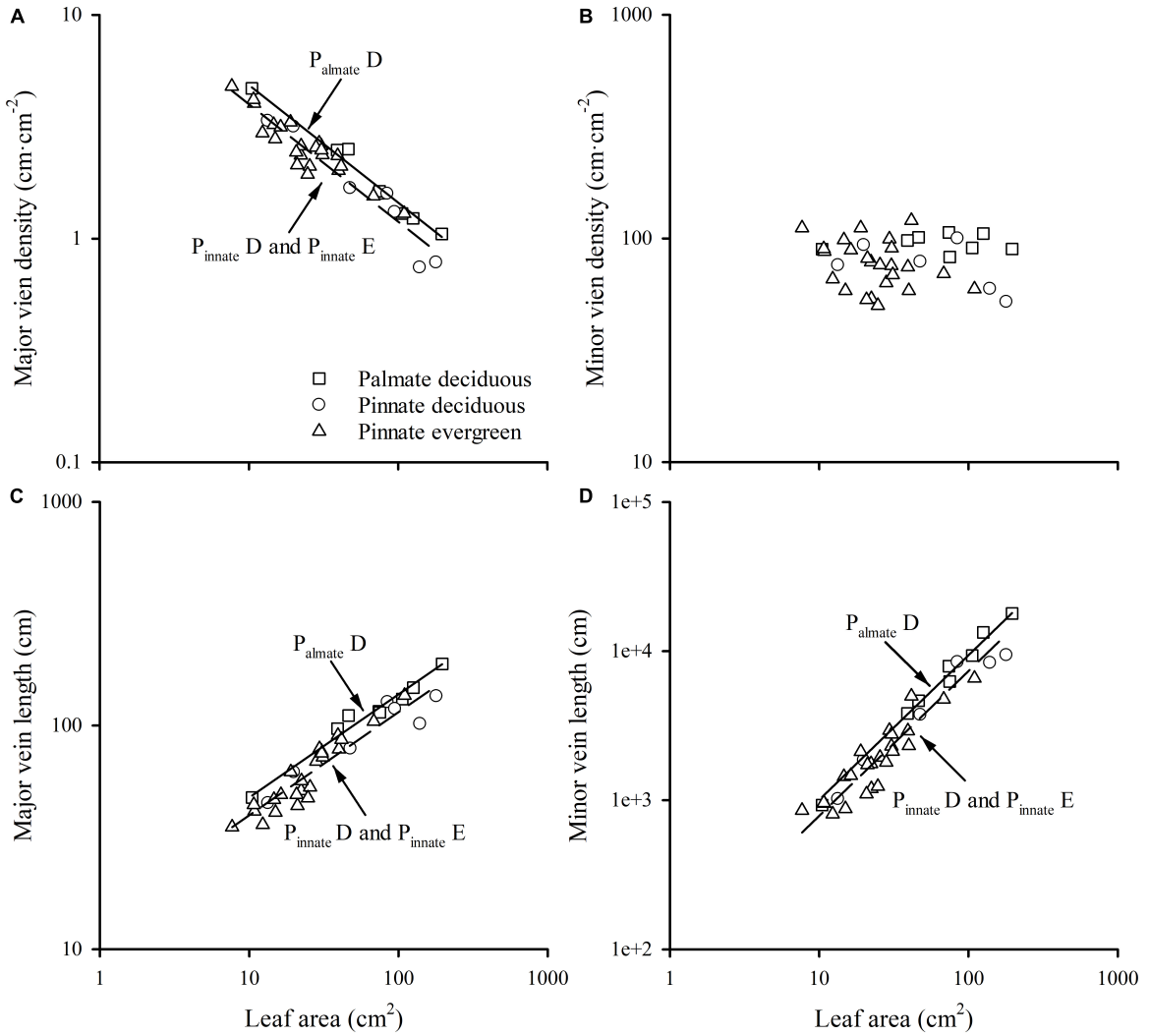

FIGURE 1 | The relationships of the major vein density **(A)**, the minor vein density **(B)**, the major vein length **(C)**, and minor vein length **(D)** with leaf area across different group species. P_{almate}D, plamate-veined deciduous species; P_{innate}D, pinnate-veined deciduous species; and P_{innate}E, pinnate-veined evergreen species.

Relationships Between Vein Cell Wall Mass per Length and Leaf Size

The major vein cell wall mass per length was significantly and positively related to leaf area in three groups (all $R^2 > 0.554$), with a common slope of 0.583 (95% CI 0.437, 0.721, $p = 0.919$), which did not significantly deviate from 0.5 (**Figure 2A** and **Table 1**). This was consistent with the positive relationship between correlated evolutionary divergences (**Table 2**). The difference in *y*-intercept was found to be significant between palmate-veined deciduous species and pinnate-veined (evergreen and deciduous) species ($p < 0.001$), but not significant between two pinnated-veined species groups ($p > 0.05$, **Table 1**). In contrast, minor vein cell wall mass per length was independent of leaf size (**Figure 2B** and **Table 1**).

In addition, there was a significantly negative correlation between the major vein cell wall mass per vein length and the major vein density within each species group (all $R^2 > 0.501$), with the common slope of −1.295 (95% CI −1.708, −1.048, $p = 0.355$), which marginally but significantly deviated from −1.0 (**Figure 2C** and **Table 1**). This suggested a tradeoff between the major vein density and the major vein cell wall biomass investment per unit vein length. The relationship was also strong when expressed as correlated evolutionary divergences (**Table 2**). However, there was no significant correlation between the minor vein cell wall mass per vein length and minor vein density in each species group (all $p > 0.05$).

The Scaling Relationship of the Ratio of Major to Minor Vein Density With Leaf Size

A significant scaling relationship was found between the ratio of major to minor vein density and leaf area within each species group (all $R^2 > 0.496$). Neither the slopes nor the intercepts of the ratio of major to minor vein density vs. leaf

TABLE 1 | Parameters for the scaling relationships of vein traits and leaf traits.

x	*y*		*b-Value* (95% CIs)			*a-value*		
		Method	**P_{almate} D**	**P_{innate} D**	**P_{innate} E**	**P_{almate} D**	**P_{innate} D**	**P_{innate} E**
Leaf area	*Vein length*, cm							
(cm^2)	Major vein	OLS		0.461(0.412, 0.545)		1.217a	1.134b	1.140b
			R^2: 0.969	0.887	0.879			
	Minor vein	OLS		0.970(0.856, 1.053)		2.032a	1.926b	1.923b
			R^2: 0.990	0.952	0.827			
	Total vein	OLS		0.958(0.846, 1.039)		2.064a	1.958b	1.955b
			R^2: 0.990	0.952	0.830			
	Vein density, cm cm^{-2}							
	Major vein	OLS		–0.525(–0.576, –0.450)		1.212a	1.122b	1.132b
			R^2: 0.979	0.935	0.824			
	Minor vein	OLS	ns	ns	ns	–	–	–
			R^2: 0.007	0.337	0.085			
	Total vein	OLS	ns	ns	ns	–	–	–
			R^2: 0.003	0.387	0.103			
	Vein cell wall mass per length, g cm^{-1}							
	Major vein	OLS		0.583(0.437, 0.721)		–4.968a	–4.702b	–4.614b
			R^2: 0.672	0.887	0.554			
	Minor vein	OLS	ns	ns	ns	–	–	–
			R^2: 0.001	0.390	0.021			
	Total vein	OLS	ns	ns	ns	–	–	–
			R^2: 0.001	0.397	0.049			
	MVD/M_iVD	OLS		–0.454(–0.554, –0.298)		–0.892a	–0.828a	–0.845a
			R^2: 0.950	0.592	0.496			
Lamina mass	MVD	OLS		–0.453(–0.561, –0.328)		0.158a	0.010a	0.156a
(g)			R^2: 0.764	0.734	0.635			
	MVD/M_iVD	OLS		–0.391(–0.509, –0.230)		–1.802a	–1.825a	–1.688b
			R^2: 0.682	0.843	0.376			
MVD	MVW/MVL	SMA		–1.295(–1.708, –1.048)		–3.575a	–3.422ab	–3.282b
			R^2: 0.638	0.814	0.501			
M_iVD	M_iVW/M_iVL	SMA	ns	ns	ns	–	–	–
			R^2: 0.191	0.003	0.017			
MVD	MVD/M_iVD	SMA		0.975 (0.820,1.130)		–1.967a	–1.865b	–1.868b
			R^2: 0.965	0.872	0.377			
Leaf area	Lamina mass	SMA		0.960 (0.839,1.103)		–1.964ab	–2.100a	–1.880b
			R^2: 0.721	0.862	0.872			

CIs, confidence intervals; OLS, ordinary linear regression; SMA, standard major axis; P_{almate}D, plamate-veined deciduous species; P_{innate}D, pinnate-veined deciduous species; and P_{innate}E, pinnate-veined evergreen species; MVD, major vein density, cm cm^{-2}; M_iVD, minor vein density, cm cm^{-2}; MVL, major vein length, cm; M_iVL, minor vein length, cm; MVD/M_iVD, the ratio of major to minor vein density; MVM/MVL, the cell wall mass per vein length of the major vein, g cm^{-1}; M_iVM/M_iVL, the cell wall mass per vein length of the minor vein, g cm^{-1}. b-value is the common slope among different species groups by ordinary linar regression (OLS) or standard major axis (SMA) method; a-value is the y-intercept based on the common slope; the small letter after the a-value is the significance test, different letters mean the significant difference; ns represented the scaling relationship was not significant. R^2 is the absolute coefficient of scaling relationship between two traits.

area relationships differed among the species groups, with a common slope of –0.454 (95% CI –0.554, –0.298, p = 0.064) that did not significantly deviate from –0.5 (**Figure 3A** and **Table 1**). A similar scaling relationship was also found when the leaf size was represented by lamina mass (**Table 1**). These results indicated that the leaf vein density distribution was tightly correlated with leaf size. Furthermore, the ratio of major to minor vein density was significantly related to the major vein density in each species group, with the common scaling exponent of 0.975 (95% CI 0.820, 1.130, p = 0.472) not being different from 1.0. Thus, these two venation traits have an isometrical relationship (**Figure 3B** and **Table 1**).

In addition, the relationships between the ratio of major to minor vein density and leaf size, and between the ratio of major to minor vein density and major vein density were also highly significant when expressed as correlated evolutionary divergences (**Table 2**).

TABLE 2 | The regression slopes between functional traits (log-log transformed data) of correlated evolutionary divergences for 39 subtropical woody plants in Tiantong National Forest Park, China.

Traits (*x*-axis–*y*-axis)	Slopes	R^2	*P*-value
LA–MVD	–0.428	0.914	<0.001
LA–MVL	0.574	0.953	<0.001
LA–M_iVL	0.994	0.960	<0.001
LA–MVM/MVL	0.433	0.638	<0.001
LA–MVD/M_iVD	–0.427	0.835	<0.001
LM–MVD	–0.432	0.701	<0.001
LM–MVD/M_iVD	–0.431	0.641	<0.001
MVD–MVW/MVL	–1.035	0.732	<0.001
MVD–MVD/M_iVD	0.942	0.814	<0.001

The OLS method on log-transformed variables was applied. All the regression lines were highly significant ($p < 0.001$). LA, leaf area; LM, lamina mass. For other abbreviations, see ***Table 1****.*

The Comparisons Between Our Results and the Global Dataset

The major vein density negatively scaled to leaf area in both this study and Sack's data (both $R^2 > 0.60$). Neither the slopes nor the intercepts of relationships differed between these two groups, with common slopes of –0.532 (95% CI –0.594, –0.454) and –0.496 (95% CI –0.553, –0.439) for palmate- and pinnated-veined species, respectively, which did not significantly deviate from –0.5 (**Figures 4A,B** and **Table 3**). However, the scaling exponent in the Axelrod's data (401 species) was significantly larger (less negative) than for this study and Sack's data, with exponents of –0.408 (95% CI –0.440, –0.375) and –0.427 (95% CI –0.447, –0.407) for palmate- and pinnated-veined species, respectively, both being significantly deviated from –0.5 (**Table 3**). Consequently, when we plot the scaling relationship for Axelrod's species, our data, and Sack's data, there was no common slope among them in both venation type species (**Figure 5A** and **Table 3**).

The ratio of major to minor vein density was significantly and negatively correlated with leaf area in both this study and Sack's data (both $R^2 > 0.39$), with common slopes of –0.509 (95% CI –0.602, –0.378) and –0.437 (95% CI –0.523, –0.347) for palmate- and pinnated-veined species, respectively, which did not differ from –0.5 (**Figures 4C,D** and **Table 3**). The *y*-intercept was also not different between this study and Sack's data in the palmate-veined species. However, the Sack's data had a significantly higher ratio of major to minor vein density than our data at a given leaf area in the pinnate-veined species. In addition, similar to Sack's global dataset, our data showed a considerable range in total vein density. The two datasets, both used high-resolution images, did not differ significantly (**Figure 5B**, $p = 0.231$ of *t*-test, **Supplementary Table 1**).

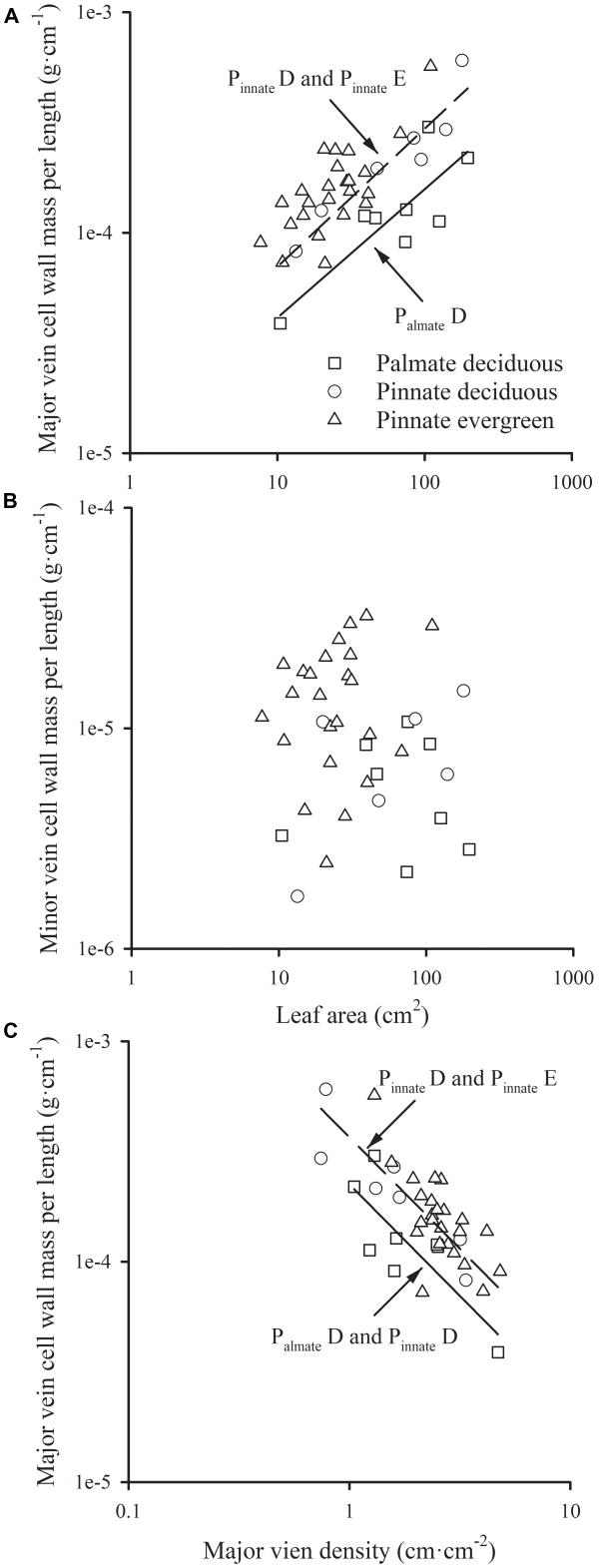

FIGURE 2 | The relationships of the cell wall mass per length of the major vein **(A)**, and that of the minor vein **(B)** with leaf area; the relationship of the cell wall mass per length of the major vein with the major vein density **(C)**. For abbreviations, see **Figure 1**.

DISCUSSION

Our results showed an extremely strong and consistent scaling relationship of leaf venation architecture with leaf size across species with different leaf habits (evergreen and deciduous) and leaf vein types (palmate-veined and pinnate-veined) within a

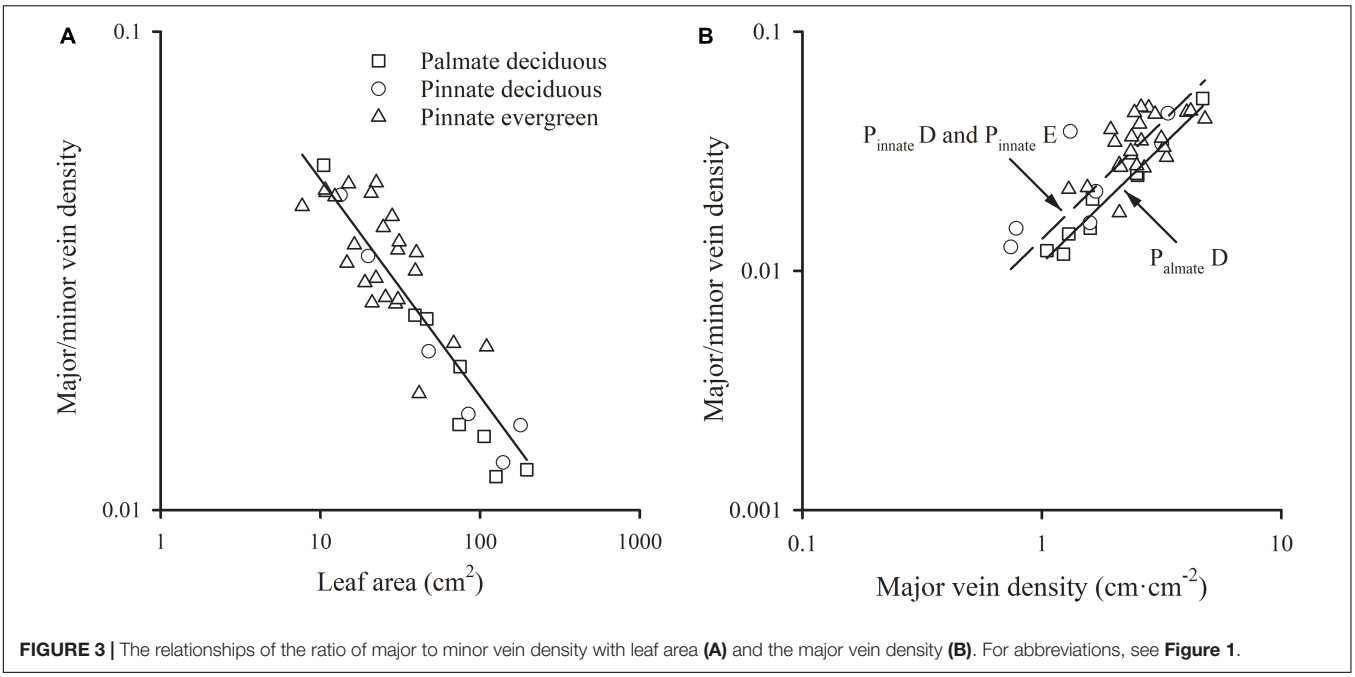

FIGURE 3 | The relationships of the ratio of major to minor vein density with leaf area **(A)** and the major vein density **(B)**. For abbreviations, see **Figure 1**.

community. The scaling relationship between leaf vein density and leaf size across species was the same as what was found in the global dataset (Sack et al., 2012). Additionally, we found that the leaf vein distribution (the ratio of major to minor vein density) and the major vein cell wall mass per length were significantly correlated with leaf size across species. Indeed, it is intriguing when different leaf habits and leaf vein types species have the same scaling relationships between leaf vein traits and leaf size. This pattern suggests that these leaf vein traits are of importance for leaf size and are governed by the law of physics or physiological requirements. These relationships are core discoveries in leaf structure and function, which have important ecological and biogeographic implications. These results also provide a new way to understand the optimization of leaf size.

The Scaling Relationship of Leaf Vein Density With Leaf Size

We found a strong negative correlation of major vein density with leaf size across 39 woody broad-leaved species within a community. However, minor vein density was independent of leaf size (**Figure 1**). Since total vein density was mainly determined by the minor vein length per area, which accounted for > 97% of the total vein length in this study (**Supplementary Table 1**), the total vein density was also not related to leaf size. This was consistent with findings from the previous global-scale dataset and small groups with no more than 10 species in previous studies (Sack et al., 2008, 2012; Dunbar-Co et al., 2009; Scoffoni et al., 2011).

These relationships were robust across different leaf habits and leaf vein types, with the common slope of major vein density with leaf size not different from –0.5 (**Figure 1** and **Table 1**). The consistent results when leaf size was represented with leaf area and lamina mass was because of the isometric relationship between leaf area and lamina mass (b = 0.96, 95% CI 0.84, 1.10, **Table 1**). This robust geometrical scaling of the major vein density with leaf size could be directly demonstrated from the scaling relationship between vein length and leaf area in the current study. The significant relationship between major vein length (MVL) and leaf area (A) among all groups showed a scaling slope not significantly different from 0.5 (b = 0.46; **Figure 1C** and **Table 1**), *i.e.*, MVL scaling with A was described as $MVL \propto A^{0.46}$, and the leaf area scaled with leaf area as $A \propto A^{1}$. Therefore, the major vein density was determined by $MVD = MVL/A \propto A^{-0.54}$, and the scaling exponent was not different from –0.5 (**Figure 1** and **Table 1**). Additionally, considering the geometric dimensions, geometric scaling predictions have been derived (Niklas, 1994) by treating each fundamental trait as an area (A) as a two-dimensional variable and length (L) as a one-dimensional variable. Hence, vein density is an $L/A \propto A^{-0.5}$. Thus, we can say that the major vein density geometrically declined with leaf size. However, the scaling of minor vein length (M_iVL) with leaf area was described as $M_iVL \propto A^{0.97}$, which was not different from 1.0 (**Table 1**). Thus, the minor vein density was determined by $M_iVD = M_iVL/A \propto A^{-0.03}$, suggesting that M_iVD did not change with leaf size. These trends can also be explained by the development mechanism of venation according to the synthetic model (Sack et al., 2012). With the leaf development, the 1° and 2° veins are formed during a "slow" limited expansion phase due to cell proliferation, and the vein density peaks as procambium forms and declines as leaves are pushed apart during subsequent rapid expansion. Thus, the major vein density would geometrically decline with increasing leaf size. In contrast, the 3° and other higher-order veins are principally formed during a "rapid" dramatic expansion phase mainly because of cell expansion, although cell divisions continue. Thus, the minor vein density stabilizes as their initiation, and is maintained during

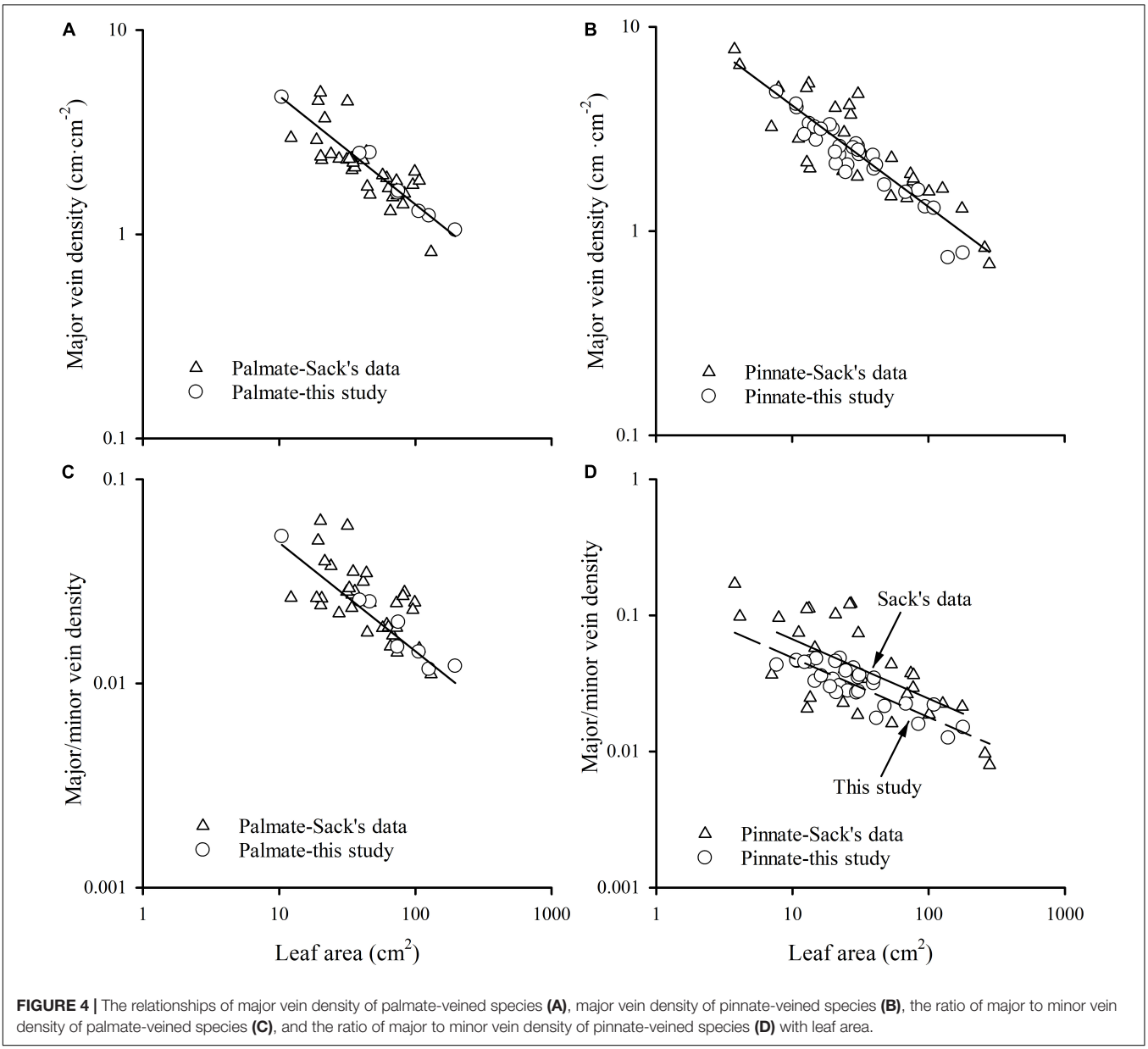

FIGURE 4 | The relationships of major vein density of palmate-veined species **(A)**, major vein density of pinnate-veined species **(B)**, the ratio of major to minor vein density of palmate-veined species **(C)**, and the ratio of major to minor vein density of pinnate-veined species **(D)** with leaf area.

leaf expansion (Sack et al., 2012). The declining trend of major vein density with leaf area was consistent among different leaf vein types and leaf habit groups. However, the palmate-veined species had higher major vein density than pinnate-veined species at a given leaf area (**Figure 1A**), which can be mainly ascribed from palmate-veined species having more midrib compared with pinnate-veined species (Sack et al., 2008; Scoffoni et al., 2011). Additionally, major vein length in palmate-veined species was significantly higher than in the pinnate-veined species at the same leaf area (**Figure 1C** and **Table 1**), which also contributed to the above difference. Even though evergreen species normally have smaller leaf area, photosynthesis efficiency, and higher LMA than for deciduous species (Zhang et al., 2013; Qi et al., 2021), major vein length and the major vein density were both insignificantly different between deciduous and evergreen species within the same leaf vein type in the current study ($p > 0.05$). Therefore, the *y*-intercept of scaling relationship in leaf vein density with leaf size was only impacted by vein type, not by leaf habit. Also, in the future, the evergreen and deciduous species could be combined within the same leaf vein type to study the scaling relationship of leaf venation architecture with leaf size.

The exponent of the geometrically scaling between major vein density and leaf area (no different from –0.5) in this study was different from that in the global dataset, which has the major vein density conservatively declined with leaf size (b = –0.341, 95% CI –0.360, –0.322) (Sack et al., 2012). This difference is not caused by different definitions of the major vein, but by the different range of leaf size of the studied species. When we reanalyzed the scaling relationship from the global dataset by recalculating major vein density based on the same

TABLE 3 | Parameters for the scaling of vein traits with leaf size analyzed by OLS method in this study, Sack's data, and Axelrod's data (Sack et al., 2012).

Vein type	Traits	Data source	N	R^2	b_1-value	b_2-value	a_2-value	Tests for differences between groups
					Slope (95% CIs)	Common slope (95% CIs)		*P*-value
Palmate	MVD	Sack's	34	0.607	–0.478(–0.616, –0.339)	–0.532 (–0.594, –0.454)	1.196	b_2: 0.434
	(cm cm^{-2})	This study	8	0.979	–0.544(–0.624, –0.464)		1.224	a_2: 0.211
	MVD/M_iVD	Sack's	34	0.391	–0.402(–0.583, –0.221)	–0.509 (–0.602, –0.378)	–0.765	b_2: 0.172
		This study	8	0.950	–0.545(–0.670, –0.420)		–0.792	a_2: 0.382
	MVD	Axelrod's	67	0.906	–0.408 (–0.440, –0.375)	–	–	b_2: 0.016
		This study	8	0.979	–0.544 (–0.624, –0.464)			–
		Sack's	34	0.607	–0.478 (–0.616, –0.339)			
Pinnate	MVD	Sack's	29	0.740	–0.442(–0.545, –0.339)	–0.496 (–0.553, –0.439)	1.137	b_2: 0.209
		This study	31	0.897	–0.519(–0.586, –0.453)		1.087	a_2: 0.069
	MVD/M_iVD	Sack's	29	0.513	–0.509(–0.704, –0.313)	–0.437 (–0.523, –0.347)	–0.738	b_2: 0.389
		This study	30	0.727	–0.415(–0.514, –0.317)		–0.876	a_2: 0.006
	MVD	Axelrod's	334	0.839	–0.427 (–0.447, –0.407)	–	–	b_2: 0.042
		This study	31	0.897	–0.519 (–0.586, –0.453)			–
		Sack's	29	0.740	–0.442 (–0.545, –0.339)			

CIs, confidence intervals; OLS, ordinary linear regression; MVD, major vein density, cm cm^{-2}; MVD/M_iVD, the ratio of major to minor vein density. Parameters for the scaling of vein traits, that is, of b value in the equation log (trait) = a + b log (leaf size), across species in different data sources. b_1-value is the slope of each data group, b_2-value is the common slope of two or three groups. a_2-value is the y-intercept based on the common slope. P-value is the test between groups for common slope b_2-value and y-intercept a_2-value, respectively.

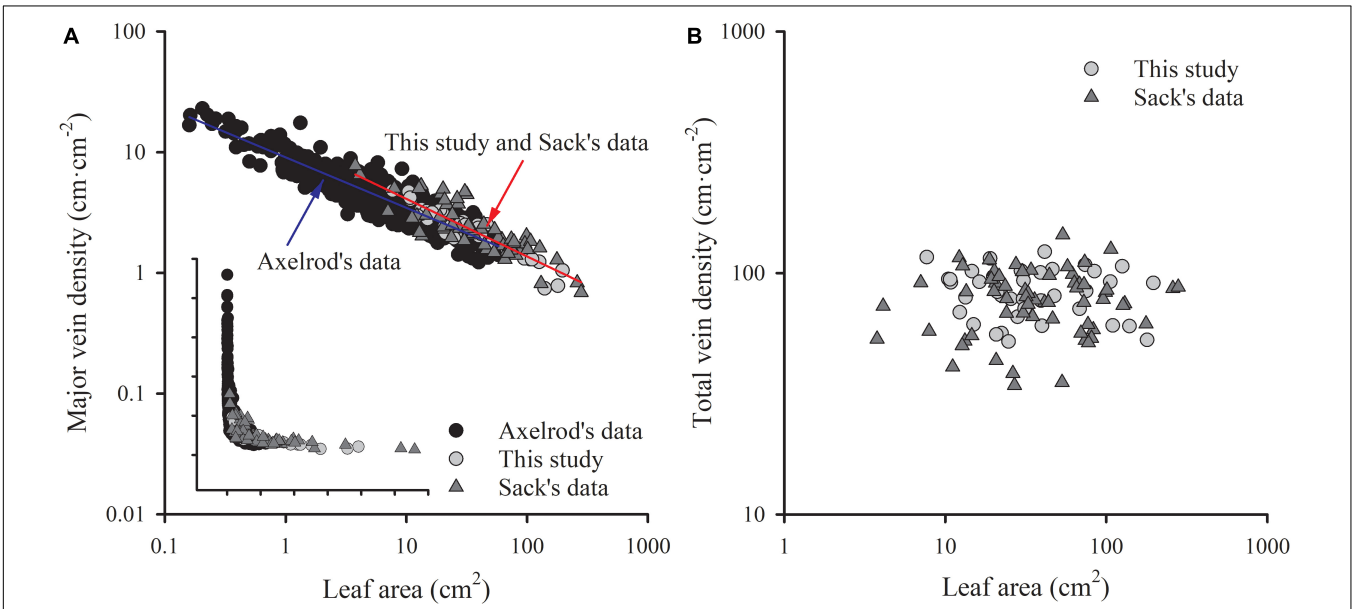

FIGURE 5 | The comparisons of the scaling relationship of major vein density with leaf area **(A)**, and the independence of total vein density from leaf area **(B)** in our study (39 woody species within subtropical forestry community), Sack's data (63 comprehensive species), and Axelrod's data. The red line is the common slope of this study and Sack's data, while the blue line is the slope of Axelrod's data. Inset in panel **(A)** is the same plot but with raw data.

definition of ours, the scaling exponent was still significantly larger than –0.5 (common slope of palmate- and pinnate-veined species, b = –0.405, 95% CI –0.383, –0.427), in agreement with original results reported in Sack et al. (2012). However, considering the data source, we found that the scaling exponent of Axelrod's data (401 species) was significantly larger than –0.5 (**Figure 5A** and **Table 3**), while the scaling exponent of Sack's data (63 species including major and minor veins) was not significantly different from –0.5, in agreement with our results (**Figures 4A,B** and **Table 3**). The conservative scaling exponent (>–0.5) found in the original global dataset was mainly determined by the Axelrod's data because Axelrod's species accounted for 85% of total species. The significant difference in scaling exponent between Axelrod's data and ours or Sack's data

might attribute to the source of species collected by Axelrod or their venation treatment. We noted that the leaf area of the species collected by Axelrod ranged from 0.16 to 57.67 cm^2, compared to 7.69 to 196.00 cm^2 in our study and 3.77 to 279.65 cm^2 in Sack's 63 species. Thus, most species collected by Axelrod were smaller than ours or Sack's, which could be related to the environment or climate condition. Therefore, we could say that within the same subtropical broad-leaved forest community, the major vein density was geometrically declined with leaf size, and this scaling exponent is consistent with another dataset that includes big leaves, but not with that including only small leaf species (Axelrod). The conserved scaling relationship between major vein density and leaf size may have important implications for understanding leaf size evolution, biogeography, physiological adaptation, and paleobiology. Further research work could be done to test whether the scaling exponent is related to the climate by studying different communities with different climate/environments. This will provide a new understanding of the species distribution based on the relationship between leaf venation structure and leaf size.

The Scaling Relationships of the Vein Cell Wall Dry Mass per Length With Leaf Size and Vein Density

Despite that the total dry mass of the cell wall of veins increased with leaf size across species in this study (in each group, $R^2 > 0.50$, $p < 0.001$), the cell wall mass per vein length was not fixed with the leaf growth, and the major and minor veins have different patterns. There was a significantly positive correlation between the cell wall mass per length and leaf size in major veins (**Figure 2A** and **Table 1**), but not in minor veins (**Figure 2B** and **Table 1**). As minor veins usually account for most of the total vein length, total vein cell wall mass per length was not significantly related to leaf size (**Table 1**). The above difference between major and minor veins could be caused by different diameter growth patterns of them during leaf development. The 1° and 2° veins have a prolonged diameter growth with the leaf development, and the power scaling exponent of vein diameter vs. leaf area was 0.452 (95% CI 0.426, 0.480) and 0.368 (95% CI 0.344, 0.394) for 1° and 2° veins, respectively (Sack et al., 2012). The thickening of major veins will lead to the increase of major vein volume per leaf area, resulting in the increase of cell wall biomass investment in the major vein (Niinemets et al., 2007; Niklas et al., 2007). However, minor veins (3° and higher-order) rapidly reach maximum diameter, and there is no correlation with leaf area (Sack et al., 2012). Hence, with the increase of leaf size, the cost of lengthening the major vein will increase, while the cost of that for the minor vein is relatively stable.

The results showed that the cell wall mass per unit length of major vein allometrically scaled with leaf area, with the scaling exponent not significantly different with 0.5 (**Figure 2A** and **Table 1**) across leaf habits and leaf vein types, indicating that the increase of cell wall mass per unit length of major vein could not keep up with the increase in leaf area. In other words, the leaf area that could be obtained by investing in the biomass of major vein cell wall per unit length increased with leaf area, *i.e.*, "increasing returns." Based on this allometrically relationship, it will be beneficial for the plant to increase the cell wall mass per unit length of the major vein. However, it is impossible for plants to infinitely increase their investment in the major vein cell wall mass per length, because the major vein density would decline with the increase of cell wall mass per unit vein length of major veins (**Figure 2C** and **Table 1**). Therefore, there is a trade-off between the length growth and thickness growth of the major vein at a given biomass investment for the major vein. For a leaf, the greatest mechanical stress occurs along its longitudinal axis (Anita et al., 2001), and the mechanical reinforcement is determined by its low-order veins (Kull and Herbig, 1995). With the increase of leaf size, the larger major veins are required to provide stronger mechanical support, and increasing the diameter of the major vein increases the hydraulic conductivity within the leaf, which is the premises to improve the water transport efficiency of the whole plant (McKown et al., 2010). Consequently, at the same major vein cell wall mass investment, plants will prefer increasing vein diameter but not extending the vein length, leading to a tradeoff between the major vein cell wall mass per length and major vein density. This might be one of the reasons for the continuous increase in thickness of the major vein, while the major vein density peaks as procambium forms during leaf growth.

The trade-off of cell wall mass per unit length of the major vein and major vein density was of great significance for the optimization of leaf size. Although a thicker major vein is more conducive to support a larger leaf size, it will limit the length of the major vein and shorten the water transport distance within the major vein, which would impact the whole leaf hydraulic conductance. In order to maintain the water transport efficiency, it is impossible to increase leaf area by infinitely increasing the cell wall mass per unit length of the major vein. Rather, plants reach a reasonable leaf size due to this trade-off.

The Ratio of Major to Minor Vein Density Scales With Leaf Size

In this study, the ratio of major to minor vein density was significantly scaled with leaf size among different species groups, which was consistent with a 10 species study (Scoffoni et al., 2011). This could be because the major and minor veins have different functions. For example, major veins (primary and secondary veins) act as the support and distribution network for leaves (Roth-Nebelsick et al., 2001; Ellis et al., 2009), while minor veins act as the sites of exchange between the mesophyll and the vascular system (Haritatos et al., 2000; Sack and Holbrook, 2006). Hence, the different distribution patterns of major and minor veins within a leaf would be preferred by different leaf sizes for adaption to the specific environment. In addition, this negative correlation could be ascribed to the slower speed of the increase in major vein length with leaf area compared to that of the minor vein. The scaling exponents were not far from 0.5 and 1.0 for major vein length and minor vein length, respectively (**Figures 1C,D** and **Table 1**). Thus, the ratio of major to minor vein density scaled with leaf area with an exponent not different from −0.5 (**Figure 3** and **Table 1**). The *y*-intercept of this scaling

relationship was not different between different leaf vein types or leaf habitats, although at the same leaf area major vein length was higher in palmate-veined species than in pinnate-veined species (**Figure 2** and **Table 1**). However, the same trend was found in the minor vein length vs. leaf area. Therefore, the *y*-intercept difference was offset during the major vein length divided by the minor vein length to analyze the scaling relationship between the ratio of major to minor vein density and leaf area. The above results demonstrated that the scaling relationship between the ratio of major to minor vein density and leaf area was robust, approximately –0.5, regardless of palmate- or pinnate-veined species and evergreen or deciduous species.

The ratio of major to minor vein density was scaled with leaf area in our study and Sack's data (63 species). This stable scaling relationship indicated that the ratio of major to minor vein density was another key venation trait linked with leaf area that maintained the same scaling exponent –0.5, which could be used for explaining the evolution of leaf size and adaptation to the environment. Also, the ratio of major to minor vein density was isometrically related to the major vein density [SMA results: $b = 0.975$ (95% CI 0.820, 1.130)] in our data (**Table 1**). However, within the subtropical community, we found that the evergreen species have higher mean values in the ratio of major to minor vein density and smaller leaf area compared to deciduous species within the same pinnate-veined species (**Figure 3**, both $p < 0.05$ by *t*-test). These trends are beneficial for species with small leaf areas because the higher the ratio of major to minor vein density, the smaller leaf area and more tolerance to leaf xylem cavitation (Scoffoni et al., 2011). This can be extended to the global scale species, of which small leaf species can survive unfavorable situations with a higher ratio of major to minor vein density.

The dramatic linkage between venation architecture (including major vein density and the ratio of major to minor vein density) and leaf size in the subtropical forest community or at the global scale (**Figures 1**, **3**, **4**) provides a hydraulic mechanism for explaining the ecological or biogeographical distribution of leaf size. Small leaves are predominant in drier and more exposed habitats (Givnish, 1987; Peppe et al., 2011; Sack et al., 2012), while large leaves in moister and/or shaded habitats (Givnish, 1987; Fonseca et al., 2000). A spatially explicit model showed that the greatest impact for the increase of K_{leaf} in the reticulate hierarchy system was from increases in major vein conductivity and in the minor vein density (McKown et al., 2010). Hence, the major veins normally have long and wide conduits (Choat et al., 2005), which in turn have higher vulnerability to cavitation (Choat et al., 2005; Blackman et al., 2010; Scoffoni et al., 2011). Because of this, higher major vein density in small leaves provides redundant hydraulic "superhighways," *i.e.*, pathways around embolized major veins (Sack et al., 2008, 2012; Scoffoni et al., 2011). Both a high major vein density and a high ratio of major to minor density could reduce hydraulic vulnerability (Scoffoni et al., 2011). This study showed that small leaves generally have higher major vein density and ratio of major to minor vein density across leaf habits and leaf vein types (**Figures 1**, **3**). Therefore, the hydraulic mechanism in providing the benefit of small leaves in dry and exposed habitats are the tight scaling relationships between leaf major vein density and leaf area, and between the ratio of major to minor vein density and leaf area. With a partial correlation analysis, the relationship of the ratio of major to minor vein density with leaf area was still significant after partialing out major vein density ($r = -0.585$, $p < 0.01$), and the correlation of major vein density with leaf area was also significant after partialing out the ratio of major to minor vein density ($r = -0.778$, $p < 0.01$) for pooled data of our study. These results indicated that the major vein density and the ratio of major to minor vein density both played a key role in leaf size distribution. Small leaves would have a lower hydraulic vulnerability that is preferred in dry habitats (Ackerly et al., 2002; Bragg and Westoby, 2002; McDonald et al., 2003; Sack et al., 2012). This provides an explanation for the fact that leaf size declines as annual temperature and precipitation decrease (McDonald et al., 2003).

In conclusion, we found strong correlations of the major vein density and the ratio of major to minor vein density with leaf size, and the isometrical relationship between the major vein density and the ratio of major to minor vein density across 39 species within a subtropical forest. These findings were confirmed by reanalyzing the global dataset. However, these relationships were not found in small leaf species collected by Axelrod, thereby asking for further studies to test this scaling exponent in different ecosystems with leaf size ranges. Interestingly, our results also demonstrated that these trends were robust in different vein types and leaf habits. However, palmate-veined species have higher major vein density and ratio of major to minor vein density at the given leaf size than pinnate-veined species, which was mainly due to a more uniform distribution of large veins in palmate-veined leaves (Niinemets et al., 2007). In contrast, evergreen and deciduous species have similar venation architecture at a certain leaf area. The linkages of the major vein density, the ratio of major to minor vein density with leaf size, and the negative relationship between the major vein density and the cell wall mass per vein length of major vein could have important implications in the optimization of leaf size, niche differentiation of coexisting species, plant drought tolerance, and species distribution.

DATA AVAILABILITY STATEMENT

The original contributions presented in the study are included in the article/**Supplementary Material**, further inquiries can be directed to the corresponding author/s.

AUTHOR CONTRIBUTIONS

DY and GP conceived the research plans, supervised the experiments, analyzed the data, and wrote the manuscript. GP performed most of the experiments. YX, MY, and XW performed the leaf vein length measurements. WZ and ZC performed the leaf vein cell wall mas measruments. Y-JZ helped to revise the manuscript. All authors contributed to the article and approved the submitted version.

FUNDING

This research was supported by grants from the National Natural Science Foundation of China (No. 31770647), the Zhejiang Provincial Natural Science Foundation of China (LY19C150007), and the Ten Thousand Talents Program of Zhejiang Province (2019R52014).

ACKNOWLEDGMENTS

We thank Kailu Wei, Sili Zhu, Zhiwen Song, Ningjing Zheng, Xiangxiang Tang, Jiahe Xu, and Hongru Geng for their field and laboratory assistance with vein traits measurements and samples collections. We also thank Yaxin Li for helping draw the illustration of sampling positions for minor veins within a leaf, and thank workers of Zhejiang Tiantong Forest Ecosystem National Observation and Research Station.

SUPPLEMENTARY MATERIAL

The Supplementary Material for this article can be found online at: https://www.frontiersin.org/articles/10.3389/fpls.2022.873036/full#supplementary-material

REFERENCES

Ackerly, D. (2004). Adaptation, niche conservatism, and convergence: comparative studies of leaf evolution in the California chaparral. *Am. Nat.* 163, 654–671. doi: 10.1086/383062

Ackerly, D., Knight, C., Weiss, S., Barton, K., and Starmer, K. (2002). Leaf size, specific leaf area and microhabitat distribution of chaparral woody plants: contrasting patterns in species level and community level analyses. *Oecologia* 130, 449–457. doi: 10.1007/s004420100805

Anita, R. N., Dieter, U., Volker, M., and Hans, K. (2001). Evolution and function of leaf venation architecture: a review. *Ann. Bot.* 87, 553–566. doi: 10.1006/anbo.2001.1391

Blackman, C. J., Brodribb, T. J., and Jordan, G. J. (2010). Leaf hydraulic vulnerability is related to conduit dimensions and drought resistance across a diverse range of woody angiosperms. *New Phytol.* 188, 1113–1123. doi: 10.1111/j.1469-8137.2010.03439.x

Bragg, J. G., and Westoby, M. (2002). Leaf size and foraging for light in a sclerophyll woodland. *Funct. Ecol.* 16, 633–639. doi: 10.1046/j.1365-2435.2002.00661.x

Brodribb, T. J., Feild, T. S., and Jordan, G. J. (2007). Leaf maximum photosynthetic rate and venation are linked by hydraulics. *Plant Physiol.* 144, 1890–1898. doi: 10.1104/pp.107.101352

Bühler, J., Rishmawi, L., Pflugfelder, D., Huber, G., Scharr, H., Hülskamp, M., et al. (2015). PhenoVein-a tool for leaf vein segmentation and analysis. *Plant Physiol.* 169, 2359–2370. doi: 10.1104/pp.15.00974

Cavender-Bares, J., and Holbrook, N. M. (2001). Hydraulic properties and freezing-induced xylem cavitation in evergreen and deciduous oaks with contrasting habitats. *Plant Cell Environ.* 24, 1243–1256. doi: 10.1046/j.1365-3040.2001.00797.x

Choat, B., Lahr, E. C., Melcher, P. J., Zwieniecki, M. A., and Holbrook, N. M. (2005). The spatial pattern of air seeding thresholds in mature sugar maple trees. *Plant Cell Environ.* 28, 1082–1089. doi: 10.1111/j.1365-3040.2005.01336.x

Cochard, H., Nardini, A., and Coll, L. (2004). Hydraulic architecture of leaf blades: where is the main resistance? *Plant Cell Environ.* 27, 1257–1267. doi: 10.1111/j.1365-3040.2004.01233.x

Dunbar-Co, S., Sporck-Koehler, M. J., and Sack, L. (2009). Leaf trait diversification and design in seven rare taxa of the Hawaiian Plantago Radiation. *Int. J. Plant Sci.* 170, 61–75. doi: 10.1086/593111

Ellis, B., Daly, D. C., Hickey, L. J., Johnson, K. R., Mitchell, J. D., Wilf, P., et al. (2009). *Manual of Leaf Architecture*. New York, NY: Cornell University Press.

Evert, R. F. (2006). *Esau's Plant Anatomy: Meristems, Cells, and Tissues of the Plant Body: Their Structure, Function, and Development*, 3rd Edn. Hoboken, NJ: Wiley-Interscience.

Falster, D. S., Warton, D. I., and Wright, I. J. (2006). *User's guide to SMATR: Standardised Major Axis Tests and Routines Version 2.0*.

Fauset, S., Freitas, H. C., Galbraith, D. R., Sullivan, M. J. P., Aidar, M. P. M., Joly, C. A., et al. (2018). Differences in leaf thermoregulation and water use strategies between three co-occurring Atlantic forest tree species. *Plant Cell Environ.* 41, 1618–1631. doi: 10.1111/pce.13208

Fonseca, C. R., Overton, J. M., Collins, B., and Westoby, M. (2000). Shifts in trait combinations along rainfall and phosphorus gradients. *J. Ecol.* 88, 964–977. doi: 10.1007/s00442-011-2112-z

Givnish, T. J. (1987). Comparative studies of leaf form: assessing the relative roles of selective pressures and phylogenetic constraints. *New Phytol.* 106, 131–160. doi: 10.1111/j.1469-8137.1987.tb04687.x

Givnish, T. J., and Vermeij, G. J. (1976). Sizes and shapes of liane leaves. *Am. Nat.* 110, 743–778. doi: 10.1086/283101

Haritatos, E., Ayre, B. G., and Turgeon, R. (2000). Identification of phloem involved in assimilate loading in leaves by the activity of the galactinol synthase promoter. *Plant Physiol.* 123, 929–937. doi: 10.1104/pp.123.3.929

Kimura, D. K. (1992). Symmetry and scale dependence in functional-relationship regression. *Syst. Biol.* 41, 233–241. doi: 10.2307/2992523

Kull, U., and Herbig, A. (1995). Das blattadersystem der angiospermen: form und evolution. *Naturwissenschaften* 82, 441–451. doi: 10.1007/bf01131595

Li, Y., Reich, P., Schmid, B., Shrestha, N., Feng, X., Lyu, T., et al. (2020). Leaf size of woody dicots predicts ecosystem primary productivity. *Ecol. Lett.* 23, 1003–1013. doi: 10.1111/ele.13503

McDonald, P. G., Fonseca, C. R., Overton, J. M., and Westoby, M. (2003). Leaf-size divergence along rainfall and soil-nutrient gradients: is the method of size reduction common among clades? *Funct. Ecol.* 17, 50–57. doi: 10.1046/j.1365-2435.2003.00698.x

McKown, A., Cochard, H., and Sack, L. (2010). Decoding leaf hydraulics with a spatially explicit model: principles of venation architecture and implications for its evolution. *Am. Nat.* 175, 447–460. doi: 10.1086/650721

Michaletz, S. T., Cheng, D., Kerkhoff, A. J., and Enquist, B. J. (2014). Convergence of terrestrial plant production across global climate gradients. *Nature* 512, 39–43. doi: 10.1038/nature13470

Niinemets, U., Portsmuth, A., and Tobias, M. (2007). Leaf shape and venation pattern alter the support investments within leaf lamina in temperate species: a neglected source of leaf physiological differentiation? *Funct. Ecol.* 21, 28–40.

Niklas, K. J. (1994). *Plant Allometry: the Scaling of Plant form and Process*. Chicago, IL: University of Chicago Press.

Niklas, K. J. (1999). A mechanical perspective on foliage leaf form and function. *New Phytol.* 143, 19–31. doi: 10.1046/j.1469-8137.1999.00441.x

Niklas, K. J., Cobb, E. D., Niinemets, U., Reich, P. B., Sellin, A., Shipley, B., et al. (2007). "Diminishing returns" in the scaling of functional leaf traits across and within species groups. *PNAS* 104, 8891–8896. doi: 10.1073/pnas.0701135104

Paradis, E., Claude, J., and Strimmer, K. (2004). APE: analyses of phylogenetics and evolution in R language. *Bioinformatics*. 20, 289–290. doi: 10.1093/bioinformatics/btg412

Parkhurst, D. F., and Loucks, O. L. (1972). Optimal leaf size in relation to environment. *J. Ecol.* 60, 505–537. doi: 10.2307/2258359

Peppe, D. J., Royer, D. L., et al. (2011). Sensitivity of leaf size and shape to climate: global patterns and paleoclimatic applications. *New Phytol.* 190, 724–739. doi: 10.1111/j.1469-8137.2010.03615.x

Petruzzellis, F., Peng, G., Tyree, M. T., Tonet, V., and Nardini, A. (2019). Plasticity of functional traits of tree of heaven is higher in exotic than in native habitats. *Trees* 33, 411–420. doi: 10.1007/s00468-018-1787-8

Pitman, E. J. G. (1939). A note on normal correlation. *Biometrika* 31, 9–12. doi: 10.2307/2334971

Price, C. A., Wing, S., and Weitz, J. S. (2012). Scaling and structure of dicotyledonous leaf venation networks. *Ecol. lett.* 15, 87–95. doi: 10.1111/j.1461-0248.2011.01712.x

Qi, J. H., Fan, Z. X., Fu, P. L., Zhang, Y. J., and Sterck, F. (2021). Differential determinants of growth rates in subtropical evergreen and deciduous juvenile trees: carbon gain, hydraulics and nutrient-use efficiencies. *Tree Physiol.* 41, 12–23. doi: 10.1093/treephys/tpaa131

Roth-Nebelsick, A., Uhl, D., Mosbrugger, V., and Kerp, H. (2001). Evolution and function of leaf venation architecture: a review. *Ann. Bot.* 87, 553–566.

Sack, L., and Frole, K. (2006). Leaf structural diversity is related to hydraulic capacity in tropical rain forest trees. *Ecology* 87, 483–491. doi: 10.1890/05-0710

Sack, L., and Holbrook, N. M. (2006). Leaf hydraulics. *Annu. Rev. Plant Biol.* 57, 361–381. doi: 10.1146/annurev.arplant.56.032604.144141

Sack, L., and Scoffoni, C. (2013). Leaf venation: structure, function, development, evolution, ecology and applications in the past, present and future. *New Phytol.* 198, 983–1000. doi: 10.1111/nph.12253

Sack, L., Dietrich, E. M., Streeter, C. M., Sánchez-Gómez, D., and Holbrook, N. M. (2008). Leaf palmate venation and vascular redundancy confer tolerance of hydraulic disruption. *PNAS* 105, 1567–1572. doi: 10.1073/pnas.0709333105

Sack, L., Scoffoni, C., John, G. P., Poorter, H., Mason, C. M., Mendez-Alonzo, R., et al. (2013). How do leaf veins influence the worldwide leaf economic spectrum? review and synthesis. *J. Exp. Bot.* 64, 4053–4080. doi: 10.1093/jxb/ert316

Sack, L., Scoffoni, C., McKown, A. D., Frole, K., Rawls, M., Havran, J. C., et al. (2012). Developmentally based scaling of leaf venation architecture explains global ecological patterns. *Nat. Commun.* 3:837. doi: 10.1038/ncomms1835

Sack, L., Tyree, M. T., and Holbroo, N. M. (2005). Leaf hydraulic architecture correlates with regeneration irradiance in tropical rainforest trees. *New Phytol.* 167, 403–413. doi: 10.1111/j.1469-8137.2005.01432.x

Scoffoni, C., Rawls, M., McKown, A., Cochard, H., and Sack, L. (2011). Decline of leaf hydraulic conductance with dehydration: Relationship to leaf size and venation architecture. *Plant Physiol.* 156, 832–843. doi: 10.1104/pp.111.173856

Smith, R. J. (2009). Use and misuse of the reduced major axis for line-fitting. *Am. J. Phys. Anthropol.* 140, 476–486. doi: 10.1002/ajpa.21090

Walls, R. L. (2011). Angiosperm leaf vein patterns are linked to leaf functions in a global scale data set. *Am. J. Bot.* 98, 244–253. doi: 10.3732/ajb.1000154

Wang, S. Y., Yuan, S. L., Su, L. T., Lv, A. M., Zhou, P., and An, Y. (2017). Aluminum toxicity in alfalfa (Medicago sativa) is alleviated by exogenous foliar IAA inducing reduction of Al accumulation in cell wall. *Environ. Exp. Bot.* 139, 1–13. doi: 10.1016/j.envexpbot.2017.03.018

Warton, D. I., and Weber, N. C. (2002). Common slope tests for bivariate errors in-variables models. *Biometrical J.* 44, 161–174. doi: 10.1002/1521-4036(200203)44:2<161::aid-bimj161>3.0.co;2-n

Warton, D. I., Wright, I. J., Falster, D. S., and Westoby, M. (2006). Bivariate line-fitting methods for allometry. *Biol. Rev.* 81, 259–291. doi: 10.1017/S1464793106007007

Westoby, M., and Wright, I. J. (2003). The leaf size-tgwig size spectrum and its relationship to other important spectra of variation among species. *Oecologia* 135, 621–628. doi: 10.1007/s00442-003-1231-6

Wright, I. J., and Westoby, M. (2002). Leaves at low versus high rainfall: coordination of structure, lifespan and physiology. *New Phytol.* 155, 403–416. doi: 10.1046/j.1469-8137.2002.00479.x

Wright, I. J., Reich, P. B., Westoby, M., Ackerly, D. D., Baruch, Z., Bongers, F., et al. (2004). The worldwide leaf economics spectrum. *Nature* 428, 821–827.

Yang, D. M., Li, G. Y., and Sun, S. C. (2008). The generality of leaf size versus number trade-off in temperate woody species. *Ann. Bot.* 102, 623–629. doi: 10.1093/aob/mcn135

Yang, D. M., Li, G. Y., and Sun, S. C. (2009). The effects of leaf size, leaf habit, and leaf form on leaf/stem relationships in plant twigs of temperate woody species. *J. Veg. Sci.* 20, 359–366. doi: 10.1111/j.1654-1103.2009.05573.x

Zhang, Y. J., Meinzer, F. C., Qi, J. H., Goldstein, G., and Cao, K. F. (2013). Midday stomatal conductance is more related to stem rather than leaf water status in subtropical deciduous and evergreen broadleaf trees. *Plant Cell Environ.* 36, 149–158. doi: 10.1111/j.1365-3040.2012.02563.x

Conflict of Interest: The authors declare that the research was conducted in the absence of any commercial or financial relationships that could be construed as a potential conflict of interest.

Publisher's Note: All claims expressed in this article are solely those of the authors and do not necessarily represent those of their affiliated organizations, or those of the publisher, the editors and the reviewers. Any product that may be evaluated in this article, or claim that may be made by its manufacturer, is not guaranteed or endorsed by the publisher.

frontiers | Frontiers in Plant Science

ORIGINAL RESEARCH
published: 19 May 2022
doi: 10.3389/fpls.2022.881282

Variations in Plant Water Use Efficiency Response to Manipulated Precipitation in a Temperate Grassland

*Xuying Hai[1], Jianping Li[2], Jiwei Li[3], Yulin Liu[3], Lingbo Dong[1], Xiaozhen Wang[1], Wenwen Lv[1], Zhenhong Hu[1], Zhouping Shangguan[1] and Lei Deng[1,3]**

[1] State Key Laboratory of Soil Erosion and Dryland Farming on the Loess Plateau, Northwest A&F University, Yangling, China, [2] School of Agriculture, Ningxia University, Yinchuan, China, [3] Institute of Soil and Water Conservation, Chinese Academy of Sciences and Ministry of Water Resources, Yangling, China

Water use efficiency (WUE) plays important role in understanding the interaction between carbon and water cycles in the plant-soil-atmosphere system. However, little is known regarding the impact of altered precipitation on plant WUE in arid and semi-arid regions. The study examined the effects of altered precipitation [i.e., ambient precipitation (100% of natural precipitation), decreased precipitation (DP, −50%) and increased precipitation (IP, +50%)] on the WUE of grass species (*Stipa grandis* and *Stipa bungeana*) and forb species (*Artemisia gmelinii*) in a temperate grassland. The results found that WUE was significantly affected by growth stages, precipitation and plant species. DP increased the WUE of *S. grandis* and *S. bungeana* generally, but IP decreased WUE especially in *A. gmelinii*. And the grasses had the higher WUE than forbs. For different growth stages, the WUE in the initial growth stage was lower than that in the middle and late growth stages. Soil temperature, available nutrients (i.e., NO_3^-, NH_4^+, and AP) and microorganisms under the altered precipitations were the main factors affecting plant WUE. These findings highlighted that the grasses have higher WUE than forbs, which can be given priority to vegetation restoration in arid and semi-arid areas.

Keywords: climate change, grassland, precipitation, soil microbe, soil nutrients, soil temperature, water use efficiency

OPEN ACCESS

Edited by:
Daniel Johnson,
University of Georgia, United States

Reviewed by:
Romà Ogaya,
Ecological and Forestry Applications Research Center (CREAF), Spain
Yuanxin Liu,
Capital Normal University, China

***Correspondence:**
Lei Deng
leideng@ms.iswc.ac.cn

Specialty section:
This article was submitted to Plant Physiology, a section of the journal Frontiers in Plant Science

Received: *22 February 2022*
Accepted: *28 March 2022*
Published: *19 May 2022*

Citation:
Hai X, Li J, Li J, Liu Y, Dong L, Wang X, Lv W, Hu Z, Shangguan Z and Deng L (2022) Variations in Plant Water Use Efficiency Response to Manipulated Precipitation in a Temperate Grassland. Front. Plant Sci. 13:881282. doi: 10.3389/fpls.2022.881282

INTRODUCTION

Precipitation patterns are important environmental factors that affect the structure and process of terrestrial ecosystems and the key drivers of biological activity in semi-arid and arid ecosystems (Nielsen and Ball, 2015). With the intensification of climate change, the global precipitation pattern has undergone enormous changes, and the frequency of extreme manipulation events has been increasing (Sponseller, 2010). This affects the structure and function of plants and microbial communities, which in turn influences the water, energy and nutrient cycles of terrestrial ecosystems (Weltzin et al., 2003).

Water use efficiency (WUE) is the ratio of carbon (C) assimilation to water losses, which reflects the interaction between the C and water cycles for the plant-soil-atmosphere system (Bai et al., 2020). Moreover, it is also an important indicator to explore the adaptability of plants to

environmental change and to predict the impact of global change (Nielsen and Ball, 2015). At the leaf scale, WUE is the ratio of photosynthetic rate to transpiration rate (Bai et al., 2020). C isotope fractionation is highly correlated with the ratio of photosynthetic C assimilation and transpiration rate, and C isotope fractionation is also highly correlated with plant WUE (Latif et al., 2014). Stable C isotope technology is used globally to determine WUE, and the main principle of this technology is that there is a strong correlation between the stable C isotope ratio ($^{13}C/^{12}C$, $\delta^{13}C$) or stability C isotope discrimination coefficient (Δ) and WUE of C3 plants, thus can be used it as an indicator of WUE (Latif et al., 2014). It is an effective method to study the long-term WUE of plants and reflects the use of water and adaptation of plants to water stress over time (Chen et al., 2011).

The factors affecting plant WUE mainly including plant species, environmental and regional factors, especially, soil moisture (SM) is one of the most direct factors (Law et al., 2010). Under limited soil water conditions, plants can control water losses and increase their WUE by reducing stomatal conductance, which varies among plant species and depends on water availability and carbon dioxide concentration in the atmosphere (Latif et al., 2014; Silva, 2015). Precipitation deficiency is frequently recorded as a result of global warming, and affects the terrestrial C and water cycles by reducing the C sequestration ability and aggravating the evaporation rate of plants (Battipaglia et al., 2014), which further influences the WUE of plants. However, one study reported that plant WUE also decrease with drought in semi-arid regions (Yang et al., 2016). Moreover, previous studies paid more attentions on the precipitation changes effect on WUE at the community scale, little information at the plant species scale. Furthermore, plant species is the key factor determined the WUE under the changes in precipitation patterns. Therefore, it is necessary to explore the variation tendency in plant WUE at the species scale, which are crucial for predicting the impact of future climatic change on plant C and water cycling processes.

The grassland area of the world is approximately 50 million km^2, accounting for approximately 33.5% of global land area (Kang et al., 2007). As an important subsystem of terrestrial ecosystems, grasslands play a key role in global change and ecosystem function. Considering the background of global climate change, alterations in precipitation patterns will affect water utilization in plants directly and the functions and processes of grassland ecosystems indirectly. However, most of the previous studies had only focused on short-term (at the day scale) WUE of plants, a single plant species or single growth period responded to altered precipitation (Karatassiou and Noitsakis, 2010; Sensuła, 2015; Han et al., 2020). Therefore, this study first to explore the effect of altered precipitation on WUE among functional groups (two grasses and one forbs) following the whole growth period, and further to identify the key abiotic and biotic factors effecting on the dynamic of WUE in temperate grasslands. It would be useful to better understand the changes and the response mechanisms of WUE to altered precipitation patterns in grassland ecosystems.

MATERIALS AND METHODS

Study Area

This study was conducted at the national fixed grassland monitoring point (106°17′49.2″E, 36°16′44.5″N, 1,963 m a.s.l.) in the Yunwu Mountains on the Loess Plateau of China, where has a temperate continental climate and is located inland. The mean annual temperature is 7.12°C. The mean annual precipitation of 439.3 mm and where has a strong rainfall seasonality (mainly occurring between June and September). The soil types were gray cinnamonic soil and loessial soil. The study area is a typical temperate grassland, and the main vegetation types are *Stipa. grandis*, *Stipa. bungeana*, *Artemisia. gmelinii*, *Agropyron cristatum*, and *Heteropappus altaicus* et al.

Experimental Design and Sampling

The experiment platform was built in 2017 where as a randomized complete block design with five replicate blocks in the grassland. In each block, three 6 m × 6 m plots were established with a 1 m buffer zone between each plot. A transparent plastic rain sheltering rack (the uniformly laid rain shelter was constructed with PVC with a length of 5 m, a groove width of 30 cm, and a light transmittance of 95%) was adopted to support the collecting bucket and the artifact drip irrigation system to realize real-time collection and redistribution of the natural precipitation in the plots. Rain shelters intercepted half of the ambient precipitation (control) to form a reduced precipitation treatment (DP). The intercepted water was piped to an adjacent plot to form an increased precipitation manipulated (IP). To prevent the interference of soil moisture from the outside, 1-m deep PVC boards were embedded around the perimeter to prevent the surface soil moisture from seeping sideways (**Figure 1**).

The terminology of Allen et al. (2011) was used as the basis to divide all the plants into the two functional groups: grass (plant species of the *Poaceae* family) and forb (herbaceous, dicotyledonous broad-leaved plant). Based on a field survey, we found that there had three dominant species that are *S. grandis*, *S. bungeana*, and *A. gmelinii*, which were typical zonal vegetation and the main constructive species in the hilly and gully region on Loess Plateau. The three plants can be divided into two functional groups: grass species (*S. grandis* and *S. bungeana*) and forb species (*A. gmelinii*).

During the initial (May), middle (July), and final (September) stages of the growing season of 2019, we harvested the aboveground biomass of individuals in these plots, the biomass was mixed to form a composite sample, stored in ice boxes, and brought back to the laboratory to measure relevant indexes. The plant $\delta^{13}C$ were analyzed by isotope ratio mass spectrometer (IRMS, Thermo-Fisher Scientific, Bremen, Germany) after the samples were dried at 60°C for 72 h. After removing the litter layer, soil samples were collected from each quadrat. In each plot, three soil cores (5 cm diameter) were randomly collected with an "S" shape using a soil drilling sampler (9 cm inner diameter), and the soils were combined to provide one composite soil sample per plot. The soil samples were passed through a 2 mm sieve to

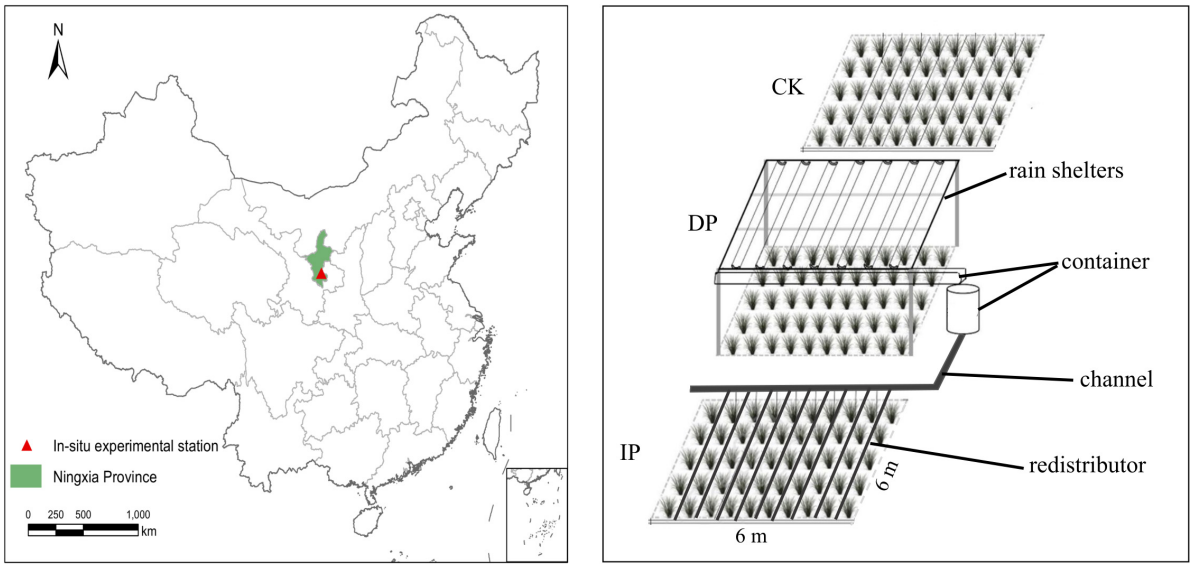

FIGURE 1 | Schematic diagramof study area and experiment design.

remove roots and stones. Then, all soil samples were separated into two parts; one part was used for the determination of soil properties (air-dried and stored at 25°C) and the other part was utilized for soil microbial biomass (stored at 4°C).

Measurement of the Abiotic and Biotic Properties

Soil moisture (%) and soil temperature (ST, °C) were measured using a soil moisture meter (Takeme-10, Mianyang, China). The soil organic carbon content (SOC) was analyzed using exothermic heating and oxidation using the potassium dichromate method (Nelson and Sommers, 1982). The soil total nitrogen content (TN) was determined using the Kjeldahl method (Bremner, 1996). The soil available nitrogen content (AN) was determined using the alkali-hydrolyzed diffusion method (Stanford, 1982). Soil total phosphorus (TP) and available phosphorus (AP) were determined using melted molybdenum, antimony, and scandium colorimetry (Olsen and Sommers, 1982). Soil nitrate nitrogen (NO_3^-–N) and ammoniacal nitrogen content (NH_4^+–N) were measured using a continuous flow analytical system (Autoanalyzer 3, Bran and Luebbe, Germany).

Microbial biomass for carbon (MBC), nitrogen (MBN), and phosphorus (MBP) concentrations were analyzed using the chloroform fumigation extraction method (Vance et al., 1987). The specific experimental methods referred to Li J. W. et al. (2019).

Calculation of Carbon Isotope Discrimination and Water Use Efficiency

The isotopic discrimination in photosynthesis can be described by the model proposed by Farquhar et al. (1989):

$$\triangle^{13}C(‰) = a + \left(b - a\right) C_i/C_a \quad (1)$$

Where C_i is the intercellular CO_2 concentration, C_a is the ambient CO_2 concentration, a (4.4‰) represents the fractionation effect that occurs during CO_2 diffusion through the stomata, and b (27‰) represents the discrimination associated with carboxylation. The leaf conductivity used for water vapor loss (g_{H2O}) and CO_2 absorption (g_{CO2}) has the following relationship:

$$g_{H_2O} = 1.6 g_{co_2} g \quad (2)$$

In addition, the net photosynthetic rate (A) of the plant has the following relationship with gCO_2 (Hietz et al., 2005):

$$\mathrm{A} = g_{H_2O}(C_a - C_i) \quad (3)$$

Combined with the above formula, WUE (A/gH_2O) can be determined by Δ^{13}C:

$$\triangle^{13}C\,(‰) = a + (b - a)(1 - \frac{1.6A}{C_a} g_{H_2O}) \quad (4)$$

So,

$$\mathrm{WUE} = \frac{\mathrm{A}}{g_{H_2O}} = (b - \triangle^{13}C)/1.6(b - a) \quad (5)$$

where A is the net photosynthesis, g is the stomatal conductance, and 1.6 is the ratio of diffusivities of water and CO_2 in air.

Statistical Analyses

Two-way ANOVA were performed to test the main effects of precipitation manipulated, growth stages, and their interactive effects on WUE, soil properties and ecological stoichiometry characteristics of the microbial biomass. Significance was evaluated at the 0.05 level ($P < 0.05$). We have carried out normality analysis and the test of homogeneity of variance before ANOVA analysis. When significance was observed at the $P < 0.05$ level, Post Hoc Duncan's multiple range test was used to carry

out the multiple comparisons. Pearson correlation analysis was used to determine the relationship between WUE and abiotic and biotic properties in the soil. Furthermore, a stepwise regression model was applied to detect the main factors affecting soil and microbial properties that affected plant WUE. The structural equation modeling framework was performed using Amos 22.0 to estimate the direct and indirect effects of environmental variables on plant WUE.

RESULTS

Response of Plant Water Use Efficiency to Precipitation Manipulation at Different Growth Stages

Plant WUE was significantly affected by growth stage, precipitation treatment, and their interaction ($P < 0.001$; **Table 1**). For *S. grandis* and *S. bungeana*, the WUE of the DP was

TABLE 1 | ANOVA (*P*-value) analysis of the effects of growth stages and precipitation manipulation on plant WUE, soil properties, and microbial biomass ecological stoichiometry characteristics.

Factor	WUE	SM	ST	SOC	TN	TP	SOC:TN	SOC:TP	TN:TP	NH_4^+–N	NO_3^-–N	AHN	AP	MBC	MBN	MBP	MBC:MBN	MBC:MBP	MBN:MBP
Growing stages	0.00***	0.00***	0.00***	0.00***	0.03*	0.92	0.00***	0.00***	0.07	0.00***	0.00***	0.21	0.00***	0.00***	0.00***	0.38	0.13	0.00***	0.01*
Treatments	0.00***	0.00***	0.00***	0.23	0.10	0.52	0.63	0.23	0.08	0.05	0.00***	0.28	0.21	0.00***	0.26	0.03*	0.36	0.32	0.40
Growing stages × Treatments	0.00***	0.18	0.01*	0.98	0.66	0.42	0.41	0.72	0.38	0.28	0.00***	0.58	0.00***	0.53	0.00***	0.36	0.61	0.61	0.52

*CK, ambient precipitation; DP, decrease precipitation (50%); IP, increase precipitation (50%); SM, soil moisture; ST, soil temperature; SOC, soil organic carbon; TN, soil total nitrogen; TP, soil total phosphorus; SOC:TN, SOC:TN ratio; SOC:TP, SOC:TP ratio; TN:TP, TN:TP ratio; NH_4^+–N, soil NH_4^+–N content; NO_3^-–N, soil NO_3^-–N content; AN, soil available nitrogen content; AP, soil available phosphorus content; MBC, microbial biomass carbon; MBN, microbial biomass nitrogen; MBP, microbial biomass phosphorus; MBC:MBN, MBC:MBP, MBC:MBP ratio; MBC:MBP, MBN:MBP ratio. *$P < 0.05$; ***$P < 0.001$.*

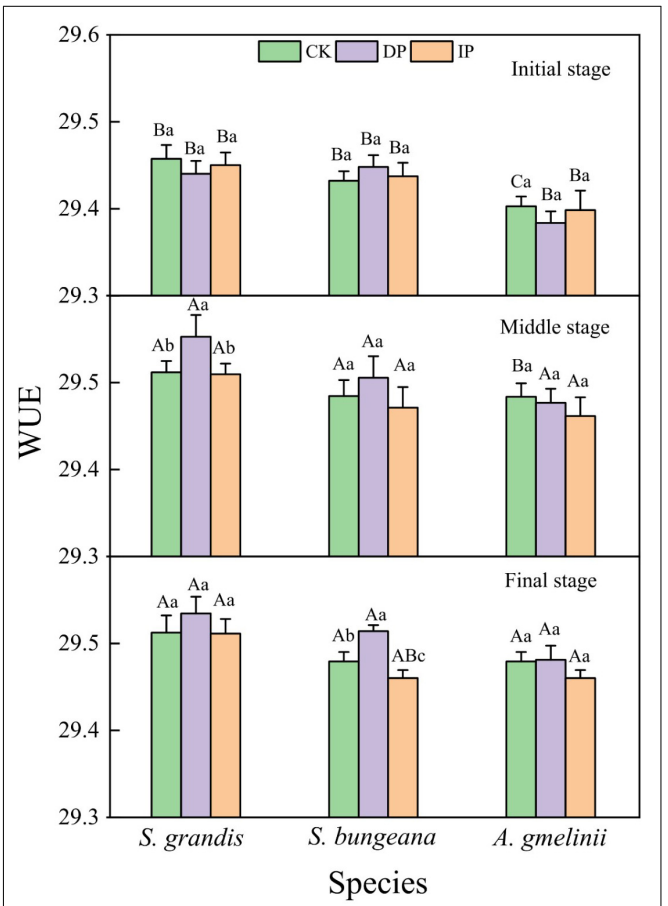

FIGURE 2 | Response of plant WUE to precipitation manipulation at different growth stages. CK, ambient precipitation; DP, decrease precipitation (–50%); IP, increase precipitation (+50%); WUE, water use efficiency. Different small letters mean significant difference among different treatments at the 0.05 level; different capital letters mean significant difference among different growing stages at the 0.05 level.

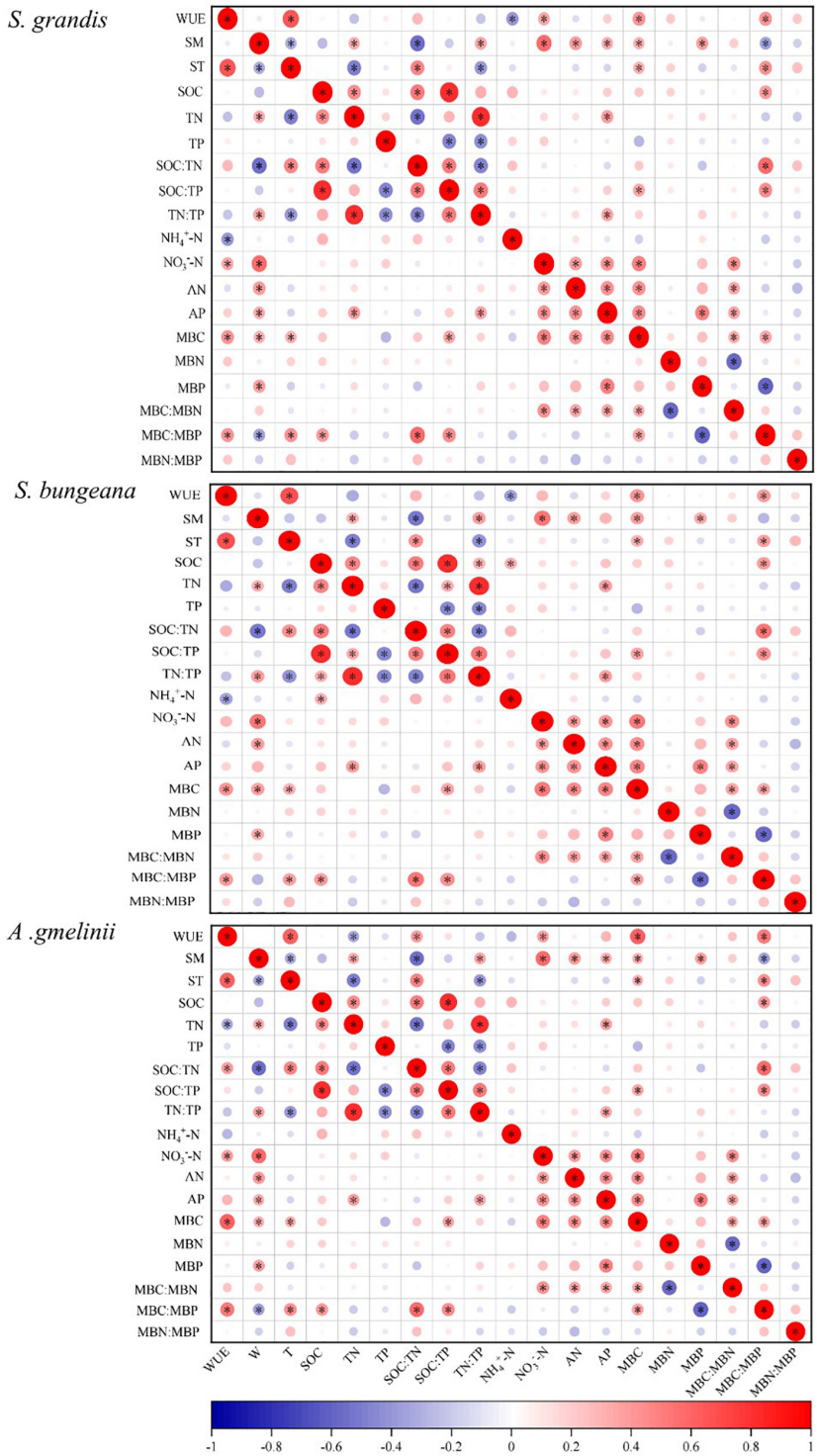

FIGURE 3 | Correlation analysis of factors affecting WUE with precipitation manipulation. CK, ambient precipitation; DP, decrease precipitation (–50%); IP, increase precipitation (+50%). WUE, water use efficiency; SM, soil moisture; ST, soil temperature; SOC, soil organic carbon; TN, soil total nitrogen; TP, soil total phosphorus; SOC:TN, SOC:TN ratio; SOC:TP, SOC:TP ratio; TN:TP, TN:TP ratio; NH_4^+–N, soil NH_4^+–N content; NO_3^-–N, soil NO_3^-–N content; AN, soil available nitrogen content; AP, soil available phosphorus content; MBC, microbial biomass carbon; MBN, microbial biomass nitrogen; MBP, microbial biomass phosphorus; MBC:MBN, MBC:MBN ratio; MBC:MBP, MBC:MBP ratio; MBN:MBP, MBN:MBP ratio. Red indicates positive correlation and blue indicates negative correlation. The larger the circle, the greater the absolute value of the correlation coefficient. $^*P \leq 0.05$.

higher than ambient precipitation and IP generally, among them, significant differences were found in the middle growth stage of *S. grandis* and in the final growth stage of *S. bungeana*. However, IP decreased WUE, especially in *S. bungeana* and *A. gmelinii* (**Figure 2**). Among the different growth stages, the WUE of the *S. grandis*, *S. bungeana*, and *A. gmelinii* in the initial growth stage was lower than that in the other growth stages.

Correlation Analysis of Factors Affecting Water Use Efficiency With Precipitation Manipulation

For *S. grandis*, the factors that were significantly related to WUE were ST, NH_4^+−N, NO_3^-–N, MBC, and MBC:MBP. For *S. bungeana*, ST, NH_4^+–N, MBC, and MBC:MBP were significantly correlated with WUE. The WUE of *A. gmelinii* was significantly correlated with ST, TN, SOC:TN, NO_3^-–N, MBC, and MBC:MBP (**Figure 3**). Moreover, the stepwise regression models detected that the WUE of *S. grandis* was mainly influenced by NO_3^-–N and NH_4^+–N, ST, NO_3^-–N, and NH_4^+–N had strong effects on WUE of *S. bungeana*, and the influencing factors for *A. gmelinii* were ST, MBC:MBP, NO_3^-–N, AP, and TN (**Table 2**).

Structural Equation Model of Soil Properties and Microbial Biomass Ecological Stoichiometry Characteristics Affecting Water Use Efficiency With Precipitation Manipulation

The final structural equation model accurately fitted the data describing the interaction pathways among WUE, soil properties, and microbial biomass ecological stoichiometry in response to altered precipitation (**Figure 4**).

The main factors associated with the WUE of *S. grandis* and *S. bungeana* were NO_3^-–N, NH_4^+–N, ST, MBC, and MBC:MBP, and the final model explained 63 and 56% of the variation in WUE of *S. grandis* and *S. bungeana,* respectively. In addition, ST, TN, SOC:TN, AP, NO_3^-–N, MBC, and MBC:MBP played a critical role in the WUE of *A. gmelinii*, and the final model explained 62% of the variation in WUE. As a driving force, SM indirectly affects WUE by having positive or negative effects on other factors.

DISCUSSION

Effects of Precipitation Manipulation on Plant Water Use Efficiency

Higher WUE indicates generally more dry matter production or C uptake per water loss (Gao et al., 2009). Generally, DP increased WUE and IP decreased WUE (**Figure 2**). Plants have higher WUE under drought, mainly because the stomatal conductance and transpiration rate of leaves decrease, but the change in net photosynthetic rate is relatively small (Latif et al., 2014). However, it is different in increasing photosynthesis and stomatal conductance of plants when higher SM under the IP conditions.

TABLE 2 | Multiple regression equation between WUE and soil properties and microbial biomass ecological stoichiometry characteristics.

Species	Multi-regression equation	*P*-value
S. grandis	$y = 0.006 + 0.005NO_3^-–N - 0.007NH_4^+–N$	0.00***
S. bungeana	$y = 29.376 + 0.005ST - 0.005NH_4^+–N + 0.002NO_3^-–N$	0.00***
A. gmelinii	$y = 29.403 + 0.004ST + 0.001MBC:MBP + 0.004NO_3^-–N + 0.01AP - 0.07TN$	0.00***

ST, soil temperature; TN, soil total nitrogen; NH_4^+–N, soil NH_4^+–N content; NO_3^-–N, soil NO_3^-–N content; MBC:MBP, MBC:MBP ratio.
****$P < 0.001$.*

The same increase in precipitation will greatly increase the amount of water available for evaporation, but which has little effect on promoting the photosynthetic rate of plants (Tian et al., 2010), thus reducing the WUE of plants.

Certain studies have reported that plants of different functional group are characterized by diversities in ecological strategies (Davison et al., 2020). Such variable strategies make plants to regulate the ability of resource absorption, utilization and transformation under changing environments, indicating mutable phenotypic plasticity of different function groups (Davison et al., 2020). The unique biological characteristics of grasses and forbs have adopted an underground strategy for storing in infertile soils potentially (Chapin, 1980). In our study, the WUE of *A. gmelinii* under different precipitation treatments showed no obvious change trend (**Figure 2**), and generally the WUE was higher in grasses than forbs given its larger leaf area. Although leaves are beneficial for intercepting the maximum light resources, it also means more water loss. Therefore, plant controls water loss through stomatal regulation resulting in a reduction in photosynthetic rate per unit area and thus leading to lower WUE, which showed a trade-off between different functional groups to maximize access to light and control water loss (Reich et al., 1997) and indicated that future vegetation restoration can be dominated by the functional groups with high resource competitiveness and WUE such as grasses in arid and semi-arid regions.

Plants WUE is synchronized with the total primary productivity, which is lower at the beginning and the end of the growing period, but higher at the growth peak (Tang et al., 2015), suggesting WUE varied with plant growth. However, our study showed that the WUE of the plants in the middle and final growth stages was significantly higher than that at the initial stage of growth (**Figure 2**). The reasons may be that in the middle and final growth stages when the temperature, amount of water evapotranspiration and the water demand of plants is high, the imbalance between water loss caused by vegetation evapotranspiration and the amount of SM replenishment will make the available water more and more short (Reynolds et al., 2004) and increase the plant WUE.

Effects of Soil Hydrothermal Conditions on Plant Water Use Efficiency

The SM is the main determinant of plant WUE (Law et al., 2010). However, our study found that SM could not adequately explain the change in WUE (**Figures 3**, **4**), indicating that

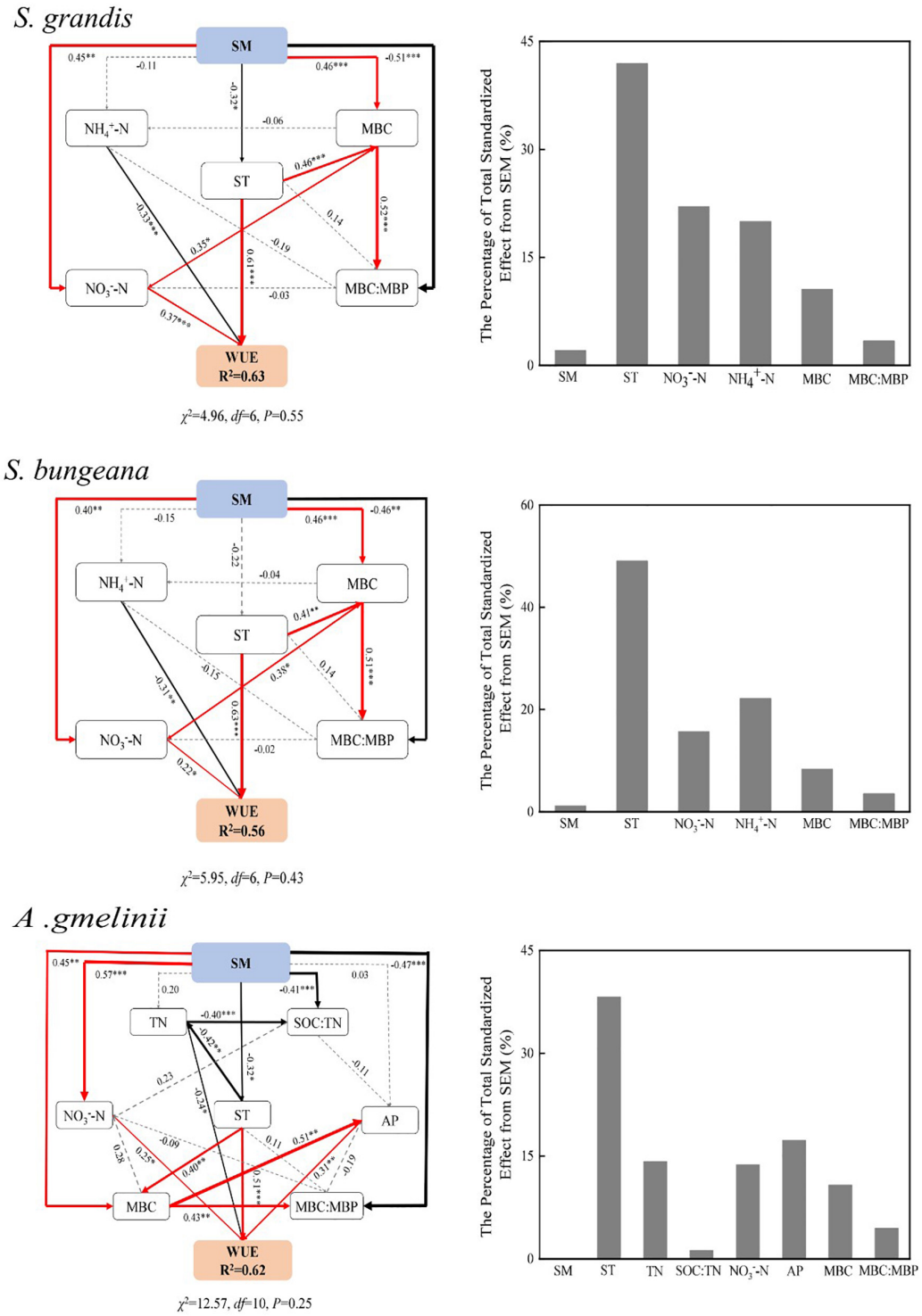

FIGURE 4 | Structural equation model of the effect of soil properties and microbial biomass ecological stoichiometry on WUE with precipitation manipulation. SM, soil moisture; ST, soil temperature; TN, soil total nitrogen; SOC:TN, soil organic carbon: soil total nitrogen; NH_4^+–N, soil NH_4^+–N content; NO_3^-–N, soil NO_3^-–N content; AP, soil available phosphorus content; MBC, microbial biomass carbon; MBN, microbial biomass nitrogen; MBP, microbial biomass phosphorus; MBC:MBN, MBC:MBN ratio; MBC:MBP, microbial biomass carbon: microbial biomass phosphorus ratio. The final model fit the data well: *S. grandis* (χ^2 = 4.96, *df* = 6, *P* = 0.55); *S. bungeana* (χ^2 = 5.95, *df* = 6, *P* = 0.43); *A. gmelinii* (χ^2 = 12.57, *df* = 10, *P* = 0.25). Numbers at arrows are standardized path coefficients. Width of the arrows indicates the strength of the relationships. The red lines indicate positive and significant, the black lines indicate negative significant, and the dashed lines indicate insignificant, respectively; R^2 values indicate the proportion of the variance explained for each endogenous variable; result for goodness-of-fit tests are also reported underneath each plot (*P* > 0.05 indicates a good fit); **P* < 0.05; ***P* < 0.01; ****P* < 0.001.

TABLE 3 | Response of soil physical-chemical properties to precipitation manipulation at different growth stages.

Growing stages	Treatments	SM (%)	ST (°C)	SOC (g/kg)	TN (g/kg)	TP (g/kg)	SOC:TN	SOC:TP	TN:TP	NH_4^+–N (mg/kg)	NO_3^-–N (mg/kg)	AN (mg/kg)	AP (mg/kg)
Initial stage	CK	8.76 ± 1.57Bb	21.5 ± 2.07Cb	20.56 ± 0.8Ba	2.23 ± 0.10Aab	1.42 ± 0.03Aa	9.24 ± 0.52Ba	14.51 ± 0.56Ba	1.57 ± 0.07ABab	11.65 ± 2.13Aa	4.29 ± 1.07Bb	144.55 ± 11.32Aa	2.66 ± 0.38Bb
	DP	5.4 ± 1.6Bc	25.4 ± 5.11Ba	20.36 ± 1.09Ba	2.15 ± 0.08Ab	1.41 ± 0.06Aa	9.46 ± 0.45Ba	14.44 ± 0.86Ba	1.53 ± 0.07Ab	10.78 ± 2.17Aa	3.51 ± 0.85Bb	152.25 ± 3.91Aa	2.63 ± 0.46Bb
	IP	10.75 ± 1.34Ba	23.0 ± 3.32Cb	21.01 ± 1.85Aa	2.30 ± 0.11Aa	1.42 ± 0.02Aa	9.11 ± 0.55Ba	14.86 ± 1.28Aa	1.63 ± 0.07Aa	11.28 ± 2.00ABa	5.45 ± 1.53Ba	158.11 ± 8.73Aa	5.39 ± 1.51Aa
Middle stage	CK	12.68 ± 2.24Aa	27.6 ± 3.03Ba	20.09 ± 0.97Ba	2.27 ± 0.34Aa	1.37 ± 0.04Ba	8.96 ± 0.93Ba	14.65 ± 0.80Ba	1.66 ± 0.25Aa	9.52 ± 1.63Ba	5.75 ± 0.58Ab	160.13 ± 4.71Aa	4.42 ± 0.67Aa
	DP	10.44 ± 2.74Ab	27.4 ± 2.64Ba	19.97 ± 0.76Ba	2.15 ± 0.09Aa	1.46 ± 0.17Aa	9.30 ± 0.30Ba	13.90 ± 1.62Ba	1.50 ± 0.17Aa	9.10 ± 1.45Aa	11.18 ± 2.01Aa	155.40 ± 9.45Aa	4.18 ± 0.93Aa
	IP	14.22 ± 4.4Aa	26.7 ± 2.27Ba	20.68 ± 1.33Aa	2.23 ± 0.11Aa	1.40 ± 0.12Aa	9.28 ± 0.44Ba	14.88 ± 1.19Aa	1.61 ± 0.15Aa	9.52 ± 0.97Ba	10.06 ± 1.07Aa	159.83 ± 8.25Aa	3.70 ± 0.92Ba
Final stage	CK	6.86 ± 1.37Cb	29.4 ± 2.14Ab	22.19 ± 1.12Aa	2.09 ± 0.09Aa	1.40 ± 0.05ABa	10.62 ± 0.51Aa	15.88 ± 1.10Aa	1.49 ± 0.07Ba	11.19 ± 2.01ABab	5.28 ± 0.92Ab	151.42 ± 8.24Aa	3.81 ± 0.91Bab
	DP	2.89 ± 0.94Cc	31.9 ± 3.13Aa	21.80 ± 1.08Aa	2.10 ± 0.12Aa	1.40 ± 0.06Aa	10.40 ± 0.37Aa	15.59 ± 0.70Aa	1.50 ± 0.08Aa	9.82 ± 1.15Ab	3.51 ± 0.61Bc	144.90 ± 14.27Aa	3.49 ± 0.56Bb
	IP	8.66 ± 1.26Ca	28.5 ± 0.99Ab	22.22 ± 1.88Aa	2.16 ± 0.25Aa	1.42 ± 0.07Aa	10.34 ± 0.76Aa	15.67 ± 1.27Aa	1.52 ± 0.16Aa	12.62 ± 2.56Aa	8.47 ± 2.86Aa	155.75 ± 9.42Aa	4.51 ± 0.75ABa

CK, ambient precipitation; DP, decrease precipitation (50%); IP, increase precipitation (50%); SM, soil moisture; ST, soil temperature; SOC, soil organic carbon; TN, soil total nitrogen; TP, soil total phosphorus; SOC:TN, SOC:TN ratio; SOC:TP, SOC:TP ratio; TN:TP, TN:TP ratio; NH_4^+–N, soil NH_4^+–N content; NO_3^-–N, soil NO_3^-–N content; AN, soil available nitrogen content; AP, soil available phosphorus content.
Different small letters mean significant difference between different treatments at the 0.05 level; different capital letters mean significant difference between different growing stages at the 0.05 level.

small precipitation events do not effectively replenish the water available to plants in the arid area (Wright et al., 2001). At the same time, the weak correlation between WUE and soil water content may also be caused by the fact that the ecohydrological process mainly depends on the amount of water available in the phenological period, and the supplementation of SM through precipitation does not necessarily coincide with plant demand (Dong et al., 2011). In addition, precipitation has a delayed effect, which means that the effect of supplementation of SM on plants growth and community structure is a cumulative process (Sala et al., 2012; Bunting et al., 2017). Therefore, the effects of precipitation change on plant community may not be reflected if only did one growing season's study. Therefore, long-term observation data are urgently needed to explore the effects of precipitation changes on the structure and function for plants.

Temperature is also an important factor affecting plant C isotope fractionation, which affect C isotope fractionation by regulating C_i/C_a (Liu and Li, 2007), and affect plant WUE by causing a photosynthetic carboxylase reaction directly. Previous studies have found that WUE decreases with an increase in temperature due to high temperatures limit the stomatal conduction of plants (Ponton et al., 2006). With increasing temperature, the water vapor pressure difference between the inside and outside of the leaves increases and the transpiration of plants becomes intense, leading to a drop of leaf water potential that intensifies the change in transpiration and decreases WUE accordingly. However, our study found that ST had a significant positive effect on WUE (**Figure 4**), which may be supported by reduced stomatal conductance and high internal resistance of the thick epidermis (Latif et al., 2014). Our results also showed that ST affects plant WUE by affecting soil microbes [i.e., MBC ($P < 0.05$) and MBC:MBP] indirectly and positively. Soil microbes can form parasitic, symbiotic, or saprophytic relationships with plants directly or by promoting the decomposition of SOM, nutrient transformation, oxidation, nitration and the N biogeochemical processes of soil (van der Heijden et al., 2008). The rise of ST increased the activity of soil microbes, which affected the extracellular enzymes involved in SOM decomposition (Li et al., 2022), the regulation of nutrient cycling and thus affecting plant WUE.

Effects of Soil Nutrients Conditions on Plant Water Use Efficiency

Soil moisture is one of the crucial factors affecting soil nutrient cycling both directly and indirectly. Plants consume excessive amounts of soil water content and nutrients during periods of rapid growth and reproduction, leading to plant growth being gradually limited by N and P (Deng et al., 2021). Our results showed that altered precipitation had a significant effect on TN and TN:TP positively at the initial growth stage (**Table 3**), because SM accelerates the decomposition of SOM with an increase in precipitation, and leading to the accumulation of soil TN (Cui et al., 2019; Deng et al., 2021). In our study, there was a significant negative correlation between WUE and soil TN of *A. gmelinii* (**Figure 4**). More C is often fixed by plants in low-N soil and more biomass per unit of N is produced (high N use efficiency, NUE)

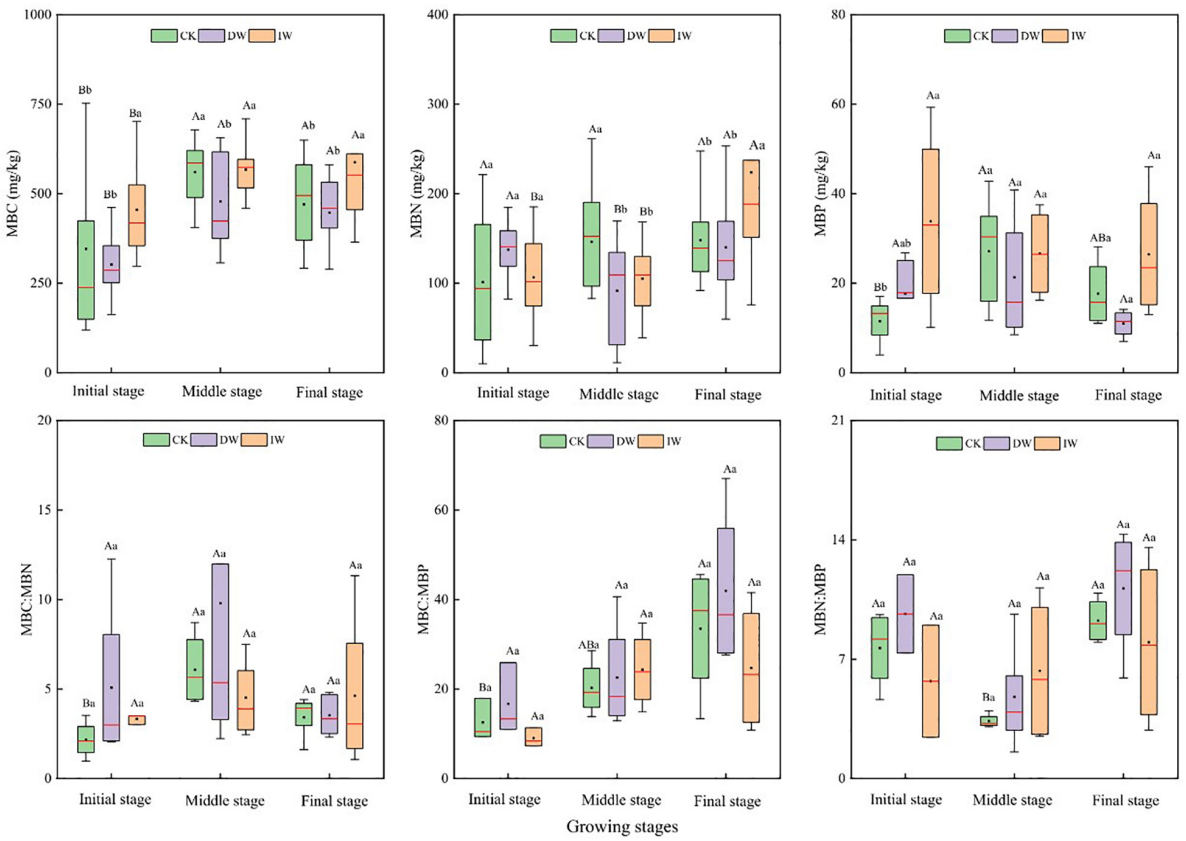

FIGURE 5 | Response of soil microbial biomass C, N, P ecological stoichiometry characteristics to precipitation manipulation at different growth stages. CK, ambient precipitation; DP, decrease precipitation (–50%); IP, increase precipitation (+50%); MBC, microbial biomass carbon; MBN, microbial biomass nitrogen; MBP, microbial biomass phosphorus; MBC:MBN, MBC:MBN ratio; MBC:MBP, MBC:MBP ratio; MBN:MBP, MBN:MBP ratio. Different small letters mean significant difference among different treatments at the 0.05 level; different capital letters mean significant difference among different growing stages at the 0.05 level.

(Aerts and Chapin, 2000). Some studies have shown that there is a trade-off between plant WUE and NUE, where plants often decrease their WUE with the increase in NUE (Gong et al., 2011). Physiological constraints in the leaf have been used to explain the trade-off when plants increase intercellular CO_2 concentration of leaves by opening their stomata, which increases photosynthesis per unit of N in leaves. However, it will increase transpiration and reducing WUE (Gong et al., 2011). Therefore, reduced WUE by greater water availability frequently increases NUE. Similarly, N in leaf tissue increases when N availability increases (NUE decreases), which promotes the photosynthetic capacity of leaves, thereby increasing WUE (Ripullone et al., 2004).

Soil inorganic N mainly resulted from the ammonification and nitrification activities of soil microorganisms, which transform soil organic N into NH_4^+–N and NO_3^-–N (Chapin et al., 2011). In our study, the NH_4^+–N and NO_3^-–N showed a decreasing trend under DP conditions (**Table 3**), which may be related to the reduction in ammonification and nitrification rate. In addition, NH_4^+–N played a negatively critical role in WUE, but NO_3^-–N had a significant positive effect on WUE (**Figure 4**). Giese et al. (2011) observed that the pools of NO_3^-–N and NH_4^+–N were controlled by precipitation. When the precipitation is low, NH_4^+–N is the main form of inorganic N available, and the content of NO_3^-–N increases with an increase in precipitation. However, NH_4^+–N is an effective N that is converted from soil organic N by microbial mineralization, which can be absorbed by soil but not easily leached and can be directly absorbed and utilized by plants. Moreover, NO_3^-–N is negatively charged and is not easily absorbed by soil colloids, and as it is easily lost because of leaching with an increase in precipitation, it results in a large loss of N (Deluca et al., 2002). Soil NH_4^+–N and NO_3^-–N can be absorbed and utilized by plants and affecting the WUE directly.

Soil AP is an important indicator for evaluating the ability of soil to provide P. In our study, AP content increased with increasing precipitation (**Table 3**). This is because that increased precipitation can improve the utilization rate of P by plants, promote the growth of plant roots, enhances the osmotic regulation ability of plants, and maintain the balance between water absorption and water loss (Gutiérrez-Boem and Thomas, 1998). Moreover, increased precipitation will enhance soil microbial activity and thus accelerate the P cycle rate, which may lead to an increase in AP content. Our results also showed that soil AP had a significant positive effect on the WUE of

A. gmelinii, and the reason is probably that AP can improve the water relationship of plants to a certain extent and significantly affect the growth status of plants. In addition, P plays a very important role in the improvement of photosynthesis as it is an important player in the photosynthetic process, and can affect the catalytic rate of Rubisco carboxylase either directly or indirectly, and promote photosynthesis in plants (Pieters et al., 2001).

Effects of Soil Microbial Biomass Ecological Stoichiometry Characteristics on Plant Water Use Efficiency

Changes in precipitation patterns may affect soil microbial biomass and its community structure by changing SM, ST, nutrient, and SOM input from aboveground and underground plant residues either directly or indirectly (Hawkes et al., 2011). Soil microbes are the driving force of SOM decomposition, which are closely related to C, N, and P cycling in soil (Xu et al., 2013). The ratios of microbe C:N:P can be used to determine the nutritional status and limitations of microbial growth (Zhou et al., 2019). In our study, soil microbial biomass was negatively affected by DP treatment generally (**Figure 5**), suggesting that the decrease in precipitation inhibited the proliferation and turnover of soil microorganisms (Wang et al., 2015). The consumer-driven nutrient cycling theory highlights that the biogeochemical cycle of nutrients can be promoted by microorganisms when these nutrients are required to meet their own needs (Elser and Urabe, 1999). Therefore, a high MBC represents high microbial activities, which reflects the strong ability of material circulation and promote plant growth and development of the ecosystem.

The MBC:MBP reflects the potential of soil microorganisms to regulate soil P availability (Li P. et al., 2019). A low MBC:MBP indicates that P is relatively abundant compared with soil SOC. At the time, microorganisms mineralize SOM to supplement the soil P pool, which further increases the restriction of soil C on microorganisms. A high MBC:MBP indicates that the soil is relatively rich in SOC and limited in P. At this time, microorganisms need to assimilate more P and maintain their normal growth and development, which shows that the ability of P fixation is improved. In our study, MBC and MBC:MBP affected WUE indirectly by affecting soil available nutrients (NH_4^+–N, NO_3^-–N, and AP). The higher MBC and the greater population of microorganisms influence the content of AN in soil through their N fixation and nitrification activities positively (Leff et al., 2015). Moreover, the release of extracellular enzymes and the decomposition of substrates by microorganisms also affect the supply of nutrients such as AP in the soil (Makino et al., 2010). However, a low MBC:MBP indicates that soil microorganisms have a greater potential to release P through circulation and thus play a significant role in replenishing the soil effective P pool.

CONCLUSION

Changes in precipitation patterns had significant effects on the WUE of two functional groups in the grassland ecosystem. DP increased the WUE of grass species (*S. grandis* and *S. bungeana*) generally, but IP decreased WUE especially in forb species (*A. gmelinii*). The WUE was higher in grasses than forbs. Moreover, soil hydrothermal conditions, soil nutrients (i.e., NO_3^-–N, NH_4^+–N, and AP) and soil microbial activities were the main factors affecting the WUE of plants. Among them, ST played a key role. SM affected WUE through changes in ST, soil nutrients, and microbes indirectly. These results suggested that SM is not the main factor determining the change in WUE, but soil available nutrients play a critical role in affecting plant WUE in arid grassland ecosystems. In addition, the functional groups with high resource competitiveness and WUE such as grass species can be selected for vegetation restoration in arid and semi-arid areas. These findings provide a better understanding of the change and response process of plants WUE in grassland ecosystems to altered precipitation pattern, which will reveal the drivers and underlying mechanisms of WUE are crucial to predicting the impact of future climatic change on plant C and water cycling processes.

DATA AVAILABILITY STATEMENT

The raw data supporting the conclusions of this article will be made available by the authors, without undue reservation.

AUTHOR CONTRIBUTIONS

LDe, JPL, ZS, and ZH conceived the ideas and designed the study. XH, JWL, YL, LDo, XW, and WL measured soil nutrients and soil microbial biomass. XH wrote the first draft of the manuscript. All authors contributed critically to the drafts and gave final approval for publication.

FUNDING

This study was supported by the National Natural Science Foundation of China (41730638), the Science and Technology Innovation Program of Shaanxi Academy of Forestry Sciences (SXLK2021-0206), the Major Basic Research Development Program of Shaanxi Province, China (2021ZDLSF05-02), the Funding of Top Young talents of Ten Thousand talents Plan in China (2021), the Funding of Special Support Plan of Young Talents Project of Shaanxi Province (2018) and National Forestry and Grassland Administration in China (20201326015).

REFERENCES

Aerts, R., and Chapin, F. (2000). The mineral nutrition of wild plants revisited: a re-evaluation of processes and patterns. *Adv. Ecol. Res.* 30, 1–67. doi: 10.1016/S0065-2504(08)60016-1

Allen, V. D., Batello, C., Berretta, E. J., Hodgson, J., Kothmann, M., Li, X., et al. (2011). An international terminology for grazing lands and grazing animals. *Grass Forage Sci.* 66, 2–28. doi: 10.1111/j.1365-2494.2010.00780.x

Bai, Y. J., Zha, T. S., Bourque, C. P. A., Jia, X., Ma, J. Y., Liu, P., et al. (2020). Variation in ecosystem water use efficiency along a southwest-to-northeast

aridity gradient in China. *Ecol. Indic.* 110:105932. doi: 10.1016/j.ecolind.2019.105932

Battipaglia, G., Micco, V. D. E., Brand, W. A., Saurer, M., Aronne, G., Linke, P., et al. (2014). Drought impact on water use efficiency and intra-annual density fluctuations in *Erica arborea* on Elba (Italy). *Plant Cell Environ*. 37, 382–391. doi: 10.1111/pce.12160

Bremner, J. (1996). Chloroform fumigation and the release of soil nitrogen: a rapid direct extraction method to measure microbial biomass nitrogen in soil - ScienceDirect. *Soil Biol. Biochem*. 17, 837–842. doi: 10.1016/0038-0717(85)90144-0

Bunting, E. L., Munson, S. M., and Villarreal, M. L. (2017). Climate legacy and lag effects on dryland plant communities in the south western U.S. *Ecol. Indic.* 74, 216–229. doi: 10.1016/j.ecolind.2016.10.024

Chapin, F. S. (1980). The mineral nutrition of wild plants. *Annu. Rev. Ecol. Syst*. 11, 233–260. doi: 10.1146/annurev.es.11.110180.001313

Chapin, F. S., Matson, P. A., and Mooney, H. A. (2011). *Principles of Terrestrial Ecosystem Ecology*. Berlin: Springer.

Chen, J., Chang, S. X., and Anyia, A. O. (2011). The physiology and stability of leaf carbon isotope discrimination as a measure of water-use efficiency in Barley on the Canadian Prairies. *J. Agron. Crop Sci*. 197, 1–11. doi: 10.1111/j.1439-037X.2010.00440.x

Cui, Y. X., Fang, L. C., Deng, L., Guo, X. B., Han, F., Ju, W. L., et al. (2019). Patterns of soil microbial nutrient limitations and their roles in the variation of soil organic carbon across a precipitation gradient in an arid and semi-arid region. *Sci. Total Environ.* 658, 1440–1451. doi: 10.1016/j.scitotenv.2018.12.289

Davison, J., Garcia de Leon, D., Zobel, M., Moora, M., Bueno, C. G., Barcelo, M., et al. (2020). Plant functional groups associate with distinct arbuscular mycorrhizal fungal communities. *N. Phytol.* 226, 1117–1128. doi: 10.1111/nph.16423

Deluca, T., Nilsson, M. C., and Zackrisson, O. (2002). Nitrogen mineralization and phenol accumulation along a fire chronosequence in northern Sweden. *Oecologia* 133, 206–214. doi: 10.1007/s00442-002-1025-2

Deng, L., Peng, C. H., Li, J. W., Liu, Y. L., Hai, X. Y., Liu, Q. Y., et al. (2021). Effects of droughts on soil carbon and nitrogen dynamics in natural ecosystems. *Earth Sci Rev*. 214:103501. doi: 10.1016/j.earscirev.2020.103501

Dong, G., Guo, J. X., Chen, J. Q., Sun, G., Gao, S., Hu, L. J., et al. (2011). Effects of spring drought on carbon sequestration, evapotranspiration and water use efficiency in the Songnen meadow steppe in northeast China. *Ecohydrology* 4, 211–224. doi: 10.1002/eco.200

Elser, J. J., and Urabe, J. (1999). The stoichiometry of consumer-driven nutrient recycling: theory, observations, and consequences. *Ecology* 80, 735–751. doi: 10.1890/0012-9658(1999)080[0735:tsocdn]2.0.co;2

Farquhar, G. D., Ehleringer, J. R., and Hubick, K. T. (1989). Carbon isotope discrimination and photosynthesis. *Annu. Rev. Plant Phys.* 40, 503–537. doi: 10.1146/annurev.pp.40.060189.002443

Gao, L., Yang, J., and Liu, R. X. (2009). Effects of soil moisture levels on photosynthesis, transpiration, and moisture use efficiency of female and male plants of *Hippophae rhamnoides* ssp.sinensis. *Acta Ecol. Sin.* 29, 6025–6034.

Giese, M., Gao, Y. Z., Lin, S., and Brueck, H. (2011). Nitrogen availability in a grazed semi-arid grassland is dominated by seasonal rainfall. *Plant Soil* 340, 157–167. doi: 10.1007/s11104-010-0509-9

Gong, X. Y., Chen, Q., Lin, S., Brueck, H., Dittert, K., Taube, F., et al. (2011). Tradeoffs between nitrogen- and water-use efficiency in dominant species of the semiarid steppe of inner Mongolia. *Plant Soil* 340, 227–238. doi: 10.1007/s11104-010-0525-9

Gutiérrez-Boem, F. H., and Thomas, G. W. (1998). Phosphorus nutrition affects wheat response to water deficit. *Agron J*. 90, 166–171. doi: 10.2134/agronj1998.00021962009000020008x

Han, T., Ren, H., Wang, J., Lu, H., Song, G., and Chazdon, R. L. (2020). Variations of leaf eco-physiological traits in relation to environmental factors during forest succession. *Ecol Indic*. 117:106511. doi: 10.1016/j.ecolind.2020.106511

Hawkes, C. V., Kivlin, S. N., Rocca, J. D., Huguet, V., Thomsen, M. A., and Suttle, K. B. (2011). Fungal community responses to precipitation. *Glob. Change Biol.* 17, 1637–1645. doi: 10.1111/j.1365-2486.2010.02327.x

Hietz, P., Wanek, W., and Dunisch, O. (2005). Long-term trends in cellulose delta ^{13}C and water-use efficiency of tropical Cedrela and Swietenia from Brazil. *Tree Physiol*. 25, 745–752. doi: 10.1093/treephys/25.6.745

Kang, L., Han, X., Zhang, Z., and Sun, O. J. (2007). Grassland ecosystems in China: review of current knowledge and research advancement. *Philos Trans R Soc Lond B Biol. Sci.* 362, 997–1008. doi: 10.1098/rstb.2007.2029

Karatassiou, M., and Noitsakis, B. (2010). Changes of the photosynthetic behaviour in annual C-3 species at late successional stage under environmental drought conditions. *Photosynthetica* 48, 377–382. doi: 10.1007/s11099-010-0049-9

Latif, A. A., Olivier, N., Stephane, M. O., Langlade, N. B., Thierry, L., Philippe, G., et al. (2014). Genetic control of water use efficiency and leaf carbon isotope discrimination in Sunflower (*Helianthus annuus* L.) subjected to two drought scenarios. *PLoS One* 9:e101218. doi: 10.1371/journal.pone.0101218

Law, B. E., Anthoni, P. M., and Aber, J. D. (2010). Measurements of gross and net ecosystem productivity and water vapour exchange of a *Pinus ponderosa* ecosystem, and an evaluation of two generalized models. *Glob. Change Biol.* 6, 155–168. doi: 10.1046/j.1365-2486.2000.00291.x

Leff, J. W., Jones, S. E., Prober, S. M., Barberán, A., Borer, E. T., Firn, J. L., et al. (2015). Consistent responses of soil microbial communities to elevated nutrient inputs in grasslands across the globe. *Proc. Natl. Acad. Sci. U.S.A*. 112, 10967–10972. doi: 10.1073/pnas.1508382112

Li, J. W., Dong, L. B., Liu, Y. L., Wu, J. Z., Wang, J., Shangguan, Z. P., et al. (2022). Soil organic carbon variation determined by biogeographic patterns of microbial carbon and nutrient limitations across a 3, 000-km humidity gradient in China. *Catena* 209:105849. doi: 10.1016/j.catena.2021.105849

Li, J. W., Liu, Y. L., Hai, X. Y., Shangguan, Z. P., and Deng, L. (2019). Dynamics of soil microbial C:N:P stoichiometry and its driving mechanisms following natural vegetation restoration after farmland abandonment. *Sci. Total Environ*. 693:133613. doi: 10.1016/j.scitotenv.2019.133613

Li, P., Muledeer, T., Tian, D., and Feng, Z. Z. (2019). Seasonal dynamics of soil microbial biomass carbon, nitrogen and phosphorus stoichiometry across global forest ecosystems. *Chin. J. Plant Ecol*. 43, 532–542. doi: 10.17521/cjpe.2019.0075

Liu, H. Y., and Li, J. Y. (2007). Application of carbon isotope in revealing environment changes. *Chin. Agricult. Sci. Bull*. 23, 217–221. doi: 10.3969/j.issn.1000-6850.2007.06.049

Makino, W., Cotner, J. B., Sterner, R. W., and Elser, J. J. (2010). Are bacteria more like plants or animals? Growth rate and resource dependence of bacterial C:N:P stoichiometry. *Funct. Ecol.* 17, 121–130. doi: 10.1046/j.1365-2435.2003.00712.x

Nelson, D. W., and Sommers, L. E. (1982). "Total carbon, organic carbon and organic matter," in *Methods of Soil Analysis, Part 2*, eds A. L. Page, R. H. Miller, and D. R. Keeney (Madison, WI: American Society of Agronomy), 539–579. doi: 10.2134/agronmonogr9.2.2ed.c29

Nielsen, U. N., and Ball, B. A. (2015). Impacts of altered precipitation regimes on soil communities and biogeochemistry in arid and semi-arid ecosystems. *Glob. Change Biol*. 21, 1407–1421. doi: 10.1111/gcb.12789

Olsen, S. R., and Sommers, L. E. (1982). "Phosphorus: phosphorus soluble in sodium bicarbonate," in *Methods of Soil Analysis, Part 2, Chemical and Microbiological Properties*, 2nd Edn, eds A. L. Page, R. H. Miller, and D. R. Keeney (Madison, WI: American Society of Agronomy), 421–422.

Pieters, A. J., Paul, M. J., and Lawlor, D. W. (2001). Low sink demand limits photosynthesis under Pi deficiency. *J. Exp. Bot*. 52, 1083–1091. doi: 10.1093/jexbot/52.358.1083

Ponton, S., Flanagan, L. B., Alstad, K. P., Johnson, B. G., Morgenstern, K., Kljun, N., et al. (2006). Comparison of ecosystem water use efficiency among Douglasfir forest, aspen forest, and grassland using eddy covariance and carbon isotope techniques. *Glob. Change Biol.* 12, 294–310. doi: 10.1111/j.1365-2486.2005.01103.x

Reich, P. B., Walters, M. B., and Ellsworth, D. S. (1997). From tropics to tundra: global convergence in plant functioning. *Proc. Natl. Acad. Sci. U.S.A*. 94, 13730–13734. doi: 10.1073/pnas.94.25.13730

Reynolds, J. F., Kemp, P. R., Ogle, K., and Fernández, R. J. (2004). Modifying the 'Pulse-Reserve' paradigm for deserts of North America: precipitation pulses, soil water, and plant responses. *Oecologia* 141, 194–210. doi: 10.1007/s00442-004-1524-4

Ripullone, F., Lauteri, M., Grassi, G., Amato, M., and Borghetti, M. (2004). Variation in nitrogen supply changes water use efficiency of *Pseudotsuga menziesii* and Populus x euroamericana; a comparison of three approaches to determine water-use efficiency. *Tree Physiol.* 24, 671–679. doi: 10.1093/treephys/24.6.671

Sala, O. E., Gherardi, L. A., Reichmann, L., Jobbágy, E., and Peters, D. (2012). Legacies of precipitation fluctuations on primary production: theory and data synthesis. *Philos Trans. R. Soc. B.* 367, 3135–3144. doi: 10.1098/rstb.2011.0347

Sensuła, B. M. (2015). Spatial and short-temporal variability of $\delta^{13}C$ and $\delta^{15}N$ and water-use efficiency in pine needles of the three forests along the most industrialized part of Poland. *Water Air Soil Poll.* 226:362. doi: 10.1007/s11270-015-2623-z

Silva, L. C. R. (2015). From air to land: understanding water resources through plant-based multidisciplinary research. *Trends Plant Sci.* 20, 399–401. doi: 10.1016/j.tplants.2015.05.007

Sponseller, R. A. (2010). Precipitation pulses and soil CO_2 flux in a Sonoran Desert ecosystem. *Glob. Change Biol.* 13, 426–436. doi: 10.1111/j.1365-2486.2006.01307.x

Stanford, G. (1982). "Assessment of soil nitrogen availability," in *Nitrogen in Agricultural Soils*, ed. F. J. Stevenson. doi: 10.2134/agronmonogr22.c17

Tang, X. G., Li, H. P., Griffis, T. J., Xu, X. B., Ding, Z., and Liu, G. H. (2015). Tracking ecosystem water use efficiency of cropland by exclusive use of MODIS EVI data. *Remote Sens.* 7, 11016–11035. doi: 10.3390/rs70911016

Tian, H. Q., Chen, G. S., Liu, M. L., Zhang, C., Sun, G., Lu, C. Q., et al. (2010). Model estimates of net primary productivity, evapotranspiration, and water use efficiency in the terrestrial ecosystems of the southern United States during 1895–2007. *For. Ecol. Manag.* 259, 1311–1327. doi: 10.1016/j.foreco.2009.10.009

van der Heijden, M. G. A., Bardgett, R. D., and van Straalen, N. M. (2008). The unseen majority: soil microbes as drivers of plant diversity and productivity in terrestrial ecosystems. *Ecol. Lett.* 11, 296–310. doi: 10.1111/j.1461-0248.2007.01139.x

Vance, E. D., Brooke, P. C., and Jenkinson, D. S. (1987). An extraction method for measuring soil microbial biomass C. *Soil Biol. Biochem.* 19, 703–707. doi: 10.1016/0038-0717(87)90052-6

Wang, N., Wang, M. J., Li, S. L., Wang, N. N., Feng, F. J., and Han, S. J. (2015). Effects of precipitation variation on growing seasonal dynamics of soil microbial biomass in broadleaved Korean pine mixed forest. *Chin. J. Appl. Ecol.* 26, 1297–1305. doi: 10.13287/j.1001-9332.201503.02.015

Weltzin, J. F., Loik, M. E., Schwinning, S., Williams, D. G., Fay, P. A., Haddad, B. M., et al. (2003). Assessing the response of terrestrial ecosystems to potential changes in precipitation. *Bioscience* 53, 941–952. doi: 10.1641/0006-3568(2003)053[0941:atrote]2.0.co;2

Wright, I. J., Reich, P. B., and Westoby, M. (2001). Strategy shifts in leaf physiology, structure and nutrient content between species of high- and low-rainfall and high- and low-nutrient habitats. *Funct. Ecol.* 15, 423–434. doi: 10.1046/j.0269-8463.2001.00542.x

Xu, X., Thornton, P. E., and Post, W. M. (2013). A global analysis of soil microbial biomass carbon, nitrogen and phosphorus in terrestrial ecosystems. *Glob. Ecol. Biogeogr.* 22, 737–749. doi: 10.1111/geb.12029

Yang, Y., Guan, H., Batelaan, O., McVicar, T. R., Long, D., Piao, S., et al. (2016). Contrasting responses of water use efficiency to drought across global terrestrial ecosystems. *Sci. Rep.* 6:23284. doi: 10.1038/srep23284

Zhou, X., Sun, H., Pumpanen, J., Sietiö, O., Heinonsalo, J., Köster, K., et al. (2019). The impact of wildfire on microbial C:N:P stoichiometry and the fungal-to-bacterial ratio in permafrost soil. *Biogeochemistry* 142, 1–17. doi: 10.1007/s10533-018-0510-6

Conflict of Interest: The authors declare that the research was conducted in the absence of any commercial or financial relationships that could be construed as a potential conflict of interest.

Publisher's Note: All claims expressed in this article are solely those of the authors and do not necessarily represent those of their affiliated organizations, or those of the publisher, the editors and the reviewers. Any product that may be evaluated in this article, or claim that may be made by its manufacturer, is not guaranteed or endorsed by the publisher.

Advantages of publishing in Frontiers

OPEN ACCESS
Articles are free to read for greatest visibility and readership

FAST PUBLICATION
Around 90 days from submission to decision

HIGH QUALITY PEER-REVIEW
Rigorous, collaborative, and constructive peer-review

TRANSPARENT PEER-REVIEW
Editors and reviewers acknowledged by name on published articles

Frontiers
Avenue du Tribunal-Fédéral 34
1005 Lausanne | Switzerland

Visit us: www.frontiersin.org
Contact us: frontiersin.org/about/contact

REPRODUCIBILITY OF RESEARCH
Support open data and methods to enhance research reproducibility

DIGITAL PUBLISHING
Articles designed for optimal readership across devices

FOLLOW US
@frontiersin

IMPACT METRICS
Advanced article metrics track visibility across digital media

EXTENSIVE PROMOTION
Marketing and promotion of impactful research

LOOP RESEARCH NETWORK
Our network increases your article's readership